Norwegian University of Life Sciences
Faculty of Veterinary Medicine
Department of Companion Animal Clinical Sciences

Philosophiae Doctor (PhD)
Thesis 2020:28

NDRG1 and PrP^C in peripheral nerve myelin maintenance: Insights from morphological studies in two unique animal models

NDRG1 og PrP^C i perifert myelinvedlikehold: Innsikt fra morfologiske studier i to unike dyremodeller

Fredrik Strebel Skedsmo

NDRG1 and PrP^C in peripheral nerve myelin maintenance:

Insights from morphological studies in two unique animal models

NDRG1 og PrP^C i perifert myelinvedlikehold:

Innsikt fra morfologiske studier i to unike dyremodeller

Philosophiae Doctor (PhD) Thesis

Fredrik Strebel Skedsmo

Norwegian University of Life Sciences

Faculty of Veterinary Medicine

Department of Companion Animal Clinical Sciences

Adamstuen 2020

Thesis number 2020:28

ISSN 1894-6402

ISBN 978-82-575-1691-8

"The study of things caused must precede the study of the causes of things"
John Hughlings Jackson

Contents

Acknowledgements

The work presented in this thesis was conducted at the Norwegian University of Life Sciences, Faculty of Veterinary Medicine, as a collaboration between Department of Companion Animal Clinical Sciences and Department of Preclinical Sciences and Pathology. It was funded by Agria och SKK Forskningsfond (paper I, II) and the Research Council of Norway (paper III). I highly appreciate the opportunity I have been given by NMBU and would also like to acknowledge the committee for evaluating this thesis.

I would like to express my sincere gratitude to my supervisors Karin, Arild and Michael. Thank you for good discussions, your encouragement, guidance and valuable feedback. Your open doors are a welcoming sight in the life of a PhD student.

A special thanks to Kaspar, for sharing your knowledge about peripheral neuropathies, for welcoming me to your lab and teaching me how to prepare nerve samples for microscopy. I would also like to thank Gjermund, for introducing the Schwann cell cultures to the project, and Giulia, for nice collaboration on paper III. Thanks to Lene and Hilde at the Imaging Centre, for introducing me to the world of electron microscopy. I would also like to acknowledge all my co-authors for their contributions to the papers, this thesis would not have been possible without you. Also, thanks to the library at NMBU for all help during the project.

To my colleagues at the Pathology unit, Biochemistry unit and Small animal clinic - I have enjoyed working with you all! A special thanks to Mari and Susan for your patience when teaching me laboratory techniques, to Maren, Mette and Aleksandra for shared coffee breaks, and to Josefin for nice company at neurology conferences.

To my family and friends, thank you for always being there for me! A special thanks to my mom and dad, for your unlimited support, encouragement and helpful advice, and to Karoline and Jan Alexander, for evenings with fun discussions, good food and wine, and great holidays together.

Finally, to my four-legged friend Sniff, for always being by my side.

Abbreviations

ACP	Acute Canine Polyradiculoneuritis
AEC	3-amino-9-ethylcarbazole
AIDP	Acute Inflammatory Demyelinating Polyradiculoneuropathy
AMP	Alaskan Malamute Polyneuropathy (also called Hereditary Polyneuropathy of Alaskan Malamutes)
BioID	Proximity-dependent biotin identification
BLAST	Basic local alignment search tool
BSE	Bovine spongiform encephalopathy
CIPD	Chronic Inflammatory Demyelinating Polyradiculoneuropathy
CMAP	Compound muscle action potential
CMT	Charcot-Marie-Tooth disease
CNS	Central nervous system
CWD	Chronic wasting disease
DAB	3,3'diaminobenzidine tetrachloride
DRG	Dorsal root ganglion
EMG	Electromyography
FGD4	FYVE, RhoGEF and PH domain-containing protein 4 (also called FRABIN)
FRABIN	FGD1-related F-actin binding protein
GBS	Guillain-Barré syndrome
GFAP	Glial fibrillary acidic protein
GJB1	Gap junction beta 1 (also called connexin 32)
GAPDH	Glyceraldehyde 3-phosphate dehydrogenase
HNPP	Hereditary neuropathy with pressure palsies
Iba1	Ionized calcium-binding adapter molecule 1
IF	Immunofluorescence
IHC	Immunohistochemistry
IMSN	Inherited motor and sensory neuropathy
LDL	Low-density lipoprotein
MAF	Minimum allele frequency
MAG	Myelin-associated glycoprotein

MBP	Myelin basic protein
MNCV	Motor nerve conduction velocity
MFN2	Mitofuscin 2
MPZ	Myelin protein zero
MTMR	Myotubularin-related protein
NDRG1	N-myc downstream-regulated gene 1 (protein)
NDRG1	N-myc downstream-regulated gene 1 (gene)
Ndrg1	N-myc downstream-regulated gene 1 (gene, mouse and rat)
NDRG1$^{mut/mut}$	Alaskan Malamutes homozygous for missense mutation (p.Gly98Val) in *NDRG1*
NDRG1$^{wt/wt}$	Alaskan Malamutes homozygous for wild-type NDRG1 allele
Ndrg1 KO	*Ndrg1* knock-out; Mouse model expressing low levels of normal NDRG1 protein
NVH	Norges Veterinærhøgskole (Norwegian School of Veterinary Science)
NMBU	Norges miljø- og biovitenskapelige universitet (Norwegian University of Life Sciences)
PMP22	Peripheral myelin protein 22
pNDRG1	Phosphorylated NDRG1 (threonine 346)
PNS	Peripheral nervous system
PRNP	Prion protein gene
Prnp	Prion protein gene (mouse and rat)
Prnp$^{-/-}$	PrP^{C}-deficient mice
PRNP$^{+/+}$	Goats homozygous for the wild-type *PRNP* allele
PRNP$^{Ter/Ter}$	PrP^{C}-deficient goats; Goats homozygous for the codon 32 nonsense (termination) mutation
PrP^{C}	Cellular prion protein
PrP^{Sc}	Misfolded (scrapie) form of the prion protein
PtdIns	Phosphatidylinositol
RIN	RNA integrity number
RT-qPCR	Reverse transcriptase quantitative polymerase chain reaction
Sgk1	Serum glucocorticoid kinase 1

SLC	Schmidt-Lanterman cleft (synonym: Schmidt-Lanterman incisure)
Str	Stretcher; NDRG1-deficient mice
TEM	Transmission electron microscopy
WB	Western blotting

Summary

Peripheral nerves transmit signals between peripheral tissue and the central nervous system, essential for normal motor and sensory function. To enable this, the integrity of both the axon and Schwann cell is crucial. The Schwann cell forms a myelin sheath around large diameter axons, necessary for rapid nerve conduction and axonal survival. Neuropathies, diseases affecting peripheral nerves, have diverse etiologies and may cause severe clinical signs in both human and animals. Some neuropathies are caused by inherited deficiencies in proteins necessary for normal axonal function or formation/maintenance of the myelin sheath. In this work, we have investigated how deficiencies in NDRG1 or PrP^C affect peripheral nerve myelin maintenance by using morphological studies in two unique, spontaneous animal models.

The hereditary polyneuropathy of Alaskan Malamutes is associated with a mutation in *N-myc downstream-regulated gene 1* (*NDRG1*). Other mutations in the same gene cause polyneuropathies in humans, rodent models and Greyhound show dogs. However, the function of NDRG1 in peripheral nerves is largely unknown and the pathomorphological changes described in *NDRG1*-associated neuropathies of different species diverge. Whereas the human disease, denominated Charcot-Marie-Tooth disease type 4D, is considered a primary demyelinating disease with secondary axonal loss, axonal degeneration dominated in the polyneuropathy of Greyhounds. A detailed mapping of NDRG1 in canine tissues and cells presented in this thesis revealed high NDRG1 expression in epithelia and myelinating Schwann cells. A phosphorylated isoform of the protein localized to the centrosomes and cleavage furrow in a primary canine Schwann cell culture. Phosphorylated NDRG1 was restricted to the abaxonal cytoplasm of myelinating Schwann cells in control dogs, but this signal was not observed in an affected Alaskan Malamute. Ultrastructural studies and teased fiber preparations of nerves from neuropathic Alaskan Malamutes uncovered a demyelinating neuropathy associated with accumulation of actin in the Schwann cell and prominent myelin infoldings. The latter ultimately segregated the axon into pockets with aggregates of organelles, suggestive of early axonal degeneration. We therefore suggest that impaired NDRG1 function in the myelinating Schwann cells of

affected Alaskan Malamutes results in deranged myelin maintenance, demyelination and secondary axonal degeneration.

The cellular prion protein (PrP^{C}) has been studied extensively because of its role in the development of transmissible spongiform encephalopathies in several species, such as Creutzfeldt-Jakobs disease in humans, bovine spongiform encephalopathy ("mad cow disease") in cattle and scrapie in small ruminants. In these diseases, a misfolded isoform of the protein, PrP^{Sc}, accumulates in the brain and ultimately results in neuronal death. The normal functions of PrP^{C} are not fully understood. Some of the phenotypes reported from transgenic mice lacking PrP^{C} have later been ascribed to other genes, but recent reports have suggested that PrP^{C} is important in dampening pro-inflammatory signaling and in myelin maintenance. We have used a nontransgenic, spontaneous model to investigate the latter; a line of Norwegian dairy goats lacking PrP^{C}. Morphological studies revealed a demyelinating neuropathy with infiltration of macrophages and lymphocytes, vacuolated fibers and paranodal myelin outfoldings. Peripheral nerve lipid composition of adult goats lacking PrP^{C} was significantly different from controls, while no difference was observed in young goats, suggesting a progressive disease. In conclusion, this is the first report of a demyelinating polyneuropathy caused by loss of PrP^{C} in a nontransgenic mammal, supporting that PrP^{C} has a vital role in peripheral nerve myelin maintenance.

Sammendrag (summary in Norwegian)

Perifere nerver overfører nerveimpulser mellom perifert vev og sentralnervesystemet, og er derfor essensielle for normal motorisk og sensorisk funksjon. For opprettholdelse av denne funksjonen, er både aksonet og den Schwannske cellen viktige. Aksonet er en utløper fra nervecellen og sørger for overføring av nerveimpulser. Den Schwannske cellen danner en myelinskjede rundt større aksoner. Dette er nødvendig for rask nerveledningshastighet og aksonal overlevelse. Nevropatier, sykdommer i perifere nerver, har ulik etiologi og kan forårsake alvorlige kliniske tegn både hos mennesker og dyr. Noen nevropatier er forårsaket av arvelige forstyrrelser i proteiner som er nødvendig for normal aksonal funksjon eller dannelse/vedlikehold av myelinskjeden. I dette arbeidet har vi undersøkt hvordan mangel på NDRG1 eller PrP^C påvirker myelinvedlikehold i perifere nerver ved å bruke morfologiske studier i to unike, spontane dyremodeller.

Arvelig polynevropati hos alaskan malamute er assosiert med en mutasjon i *N-myc downstream-regulated gene 1* (*NDRG1*). Andre mutasjoner i samme genet forårsaker polynevropatier hos menneske, gnagermodeller og utstillingslinjer av greyhound. Funksjonen til NDRG1 i perifere nerver er imidlertid ukjent, og de patomorfologiske forandringene ved *NDRG1*-assosierte nevropatier hos ulike arter divergerer. Mens den humane nevropatien, Charcot-Marie-Tooths sykdom type 4D, er ansett for å være en primær demyeliniserende sykdom med sekundært aksonalt tap, dominerte aksonal degenerasjon ved polynevropati hos greyhound. En detaljert kartlegging av NDRG1 i celler og vev fra hund presentert i denne avhandlingen viser høye nivåer av NDRG1 i epitel og myeliniserende Schwannske celler. En fosforylert isoform av proteinet ble lokalisert i centrosomer og kløyvingsfuren hos Schwannske celler isolert fra hund. Fosforylert NDRG1 var begrenset til abaksonale cytoplasma i myeliniserende Schwannske celler i kontrollhunder, men dette signalet ble ikke observert i en syk alaskan malamute. Ultrastrukturelle studier og teased nerve fibers av nerver fra affiserte alaskan malamuter avslørte en demyeliniserende nevropati assosiert med aktinaggregater i de myeliniserende Schwannske cellene og uttalte innfoldinger av myelin. Innfoldingene delte stedvis aksonene inn i atskilte lommer med aggregater av organeller, forenelig med tidlig aksonal degenerasjon. Resultatene tyder på at svekket

NDRG1-funksjon i myeliniserende Schwannske celler hos affiserte alaskan malamuter fører til forstyrret vedlikehold av myelin, demyelinisering og sekundær aksonal degenerasjon.

Det cellulære prionproteinet (PrP^C) har blitt grundig studert på grunn av sin rolle i utvikling av overførbare spongiforme encefalopatier, eller prionsykdommer, hos flere arter, for eksempel Creutzfeldt-Jakobs sykdom hos menneske, bovin spongiform encefalopati («kugalskap») hos storfe og skrapesjuke hos små drøvtyggere. Ved disse sykdommene vil en misfoldet isoform av proteinet, PrP^{Sc}, akkumulere i hjernen og tilslutt resultere i nevronal celledød. Normalfunksjonen til PrP^C er ikke fullstendig forstått, og forståelsen av denne kan være viktig for å belyse den molekylære patogenesen ved prionsykdommer. Noen fenotyper rapportert fra transgene mus uten PrP^C ble senere vist å skyldes andre gener, men nylige rapporter foreslår at PrP^C er viktig for å dempe proinflammatorisk signalering og myelinvedlikehold. Vi har brukt en ny, ikke-transgen, spontan modell - en linje av norske melkegeiter som mangler PrP^C - til å undersøke om denne modellen kan bekrefte tidligere studier fra transgene mus som har vist myelinskader. Morfologiske studier hos geiter uten PrP^C avslørte en demyeliniserende nevropati med infiltrasjon av makrofager og lymfocytter, vakuoliserte nervefibre og paranodale myelinutfoldinger. Lipidsammensetningen i perifere nerver hos voksne geiter uten PrP^C var signifikant forskjellig fra kontrollene, mens ingen forskjell ble observert hos unge dyr, noe som tyder på en progredierende sykdom. Dette er den første rapporten av en demyeliniserende polynevropati forårsaket av PrP^C-mangel hos et ikke-transgent pattedyr, og støtter at PrP^C har en viktig rolle i myelinvedlikehold.

List of papers

Paper I:

Fredrik S. Skedsmo, Michael A. Tranulis, Arild Espenes, Kristian Prydz, Kaspar Matiasek, Gjermund Gunnes, Lene C. Hermansen, Karin H. Jäderlund. **Cell and context-dependent sorting of neuropathy-associated protein NDRG1 – insights from canine tissues and primary Schwann cell cultures**. BMC Veterinary Research 2019;15(1):121. https://doi.org/10.1186/s12917-019-1872-2

Paper II:

Fredrik S. Skedsmo, Arild Espenes, Michael A. Tranulis, Kaspar Matiasek, Gjermund Gunnes, Inge Bjerkås, Lars Moe, Susan Skogtvedt Røed, Mette Berendt, Merete Fredholm, Cecilia Rohdin, G. Diane Shelton, Per Bruheim, Marit H. Stafsnes, Zdenka Bartosova, Lene C. Hermansen, Øyvind Stigen, Karin H. Jäderlund. **Impaired NDRG1 functions in Schwann cells cause demyelinating neuropathy with focally folded myelin in a dog model of Charcot-Marie-Tooth type 4D**. Manuscript

Paper III:

Fredrik S. Skedsmo, Giulia Malachin, Dag Inge Våge, Mie Marie Hammervold, Øyvind Salvesen, Cecilie Ersdal, Birgit Ranheim, Marit H. Stafsnes, Zdenka Bartosova, Per Bruheim, Karin H. Jäderlund, Kaspar Matiasek, Arild Espenes, Michael A. Tranulis. **Demyelinating polyneuropathy in goats lacking prion protein**. The FASEB Journal. 2020; 00: 1– 17. https://doi.org/10.1096/fj.201902588R

Introduction

Background

In the late 1970s, a previously unidentified neurological disorder in Alaskan Malamutes was diagnosed for the first time at the Norwegian School of Veterinary Science (NVH) (now Norwegian University of Life Sciences (NMBU)) (1). The dominating clinical signs at presentation were exercise intolerance, dysphonia, inspiratory stridor and pelvic limb ataxia, progressing to paraparesis, and in some cases, tetraparesis (2). Neurological status, including decreased postural reactions and spinal reflexes, suggested a disease affecting the peripheral nervous system, a polyneuropathy. Based on pedigree studies and test mating, an autosomal recessive inheritance was suspected and the disease was thereafter called "hereditary polyneuropathy of Alaskan Malamutes" (AMP) (1) .

After advice from the researchers, the Norwegian Alaskan Malamute breeders' club initiated a breeding program and no new cases were diagnosed in Norway for more than 20 years. However, several new cases have been examined during the last decade. By using a candidate gene approach and the known association between degenerative neuropathies and mutations in *N-myc downstream-regulated gene 1* (*NDRG1*) in human patients with Charcot-Marie-Tooth disease type 4D (CMT4D) (3) and Greyhound show dogs (4), a missense mutation in *NDRG1* was found in the affected Alaskan Malamute dogs (2). In a recent study, both the historical and recent AMP cases were shown to carry the same mutation causing a Gly98Val substitution in the NDRG1 protein (5). In total, almost 25 Alaskan Malamutes with AMP have been examined by veterinarians in our Scandinavian research group.

CMT4D is defined as a primary demyelinating disease (3, 6-8), and nerves of rodent models with *NDRG1* mutations show Schwann cell abnormalities (7). In line with this, degenerative changes in the myelin sheath were described in reports from the first AMP cases in the 1980s (1). Conversely, the polyneuropathy in Greyhounds is classified as a mixed or predominantly axonal disease (4), and axonal degeneration was also described from recent AMP cases (2).

Through the work with this thesis, the demyelinating changes in the nerves from AMP cases became increasingly evident. Thus, the affected Alaskan Malamutes clearly emerged as a model with a demyelinating phenotype caused by impaired NDRG1 function. These results opened up the opportunity to include exploration of the myelin-related functions of another protein – the cellular prion protein (PrP^C) that recently was suggested to serve in myelin maintenance, demonstrated in studies of transgenic mice lacking PrP^C (9). After the discovery of goats naturally lacking prion protein (10), this unique, nontransgenic animal model has been used by researchers at NMBU to study the functions of the cellular prion protein (PrP^C) (11-14), but until now the peripheral nerves of the goats have not been examined.

Before introducing NDRG1 and PrP^C, I will give an overview of the structure of the nervous system, general pathological reactions in peripheral nerves and neuropathies.

Overview of the nervous system

Topographically, the nervous system is divided into the central and the peripheral nervous system. An alternative classification is based on functionality and distinguish e.g. the somatic and autonomic nervous system. The autonomic nervous system innervates viscera, vessels and glands, functions largely unconsciously and involuntarily (15), and will not be discussed further in this thesis. The central nervous system (CNS), consisting of the brain and the spinal cord, is enclosed by the cranium and the vertebral column, respectively, and surrounded by the three meningeal layers, dura mater, arachnoid and pia mater. The subarachnoid space is filled with cerebrospinal fluid and communicates with the ventricular system of the brain and the central canal in the spinal cord through apertures in the fourth ventricle. The ventricular system and the central canal are lined by ependymal epithelium. Twelve pairs of cranial nerves emerge from the brain and more than 30 pairs of spinal nerves emerge from the spinal cord.

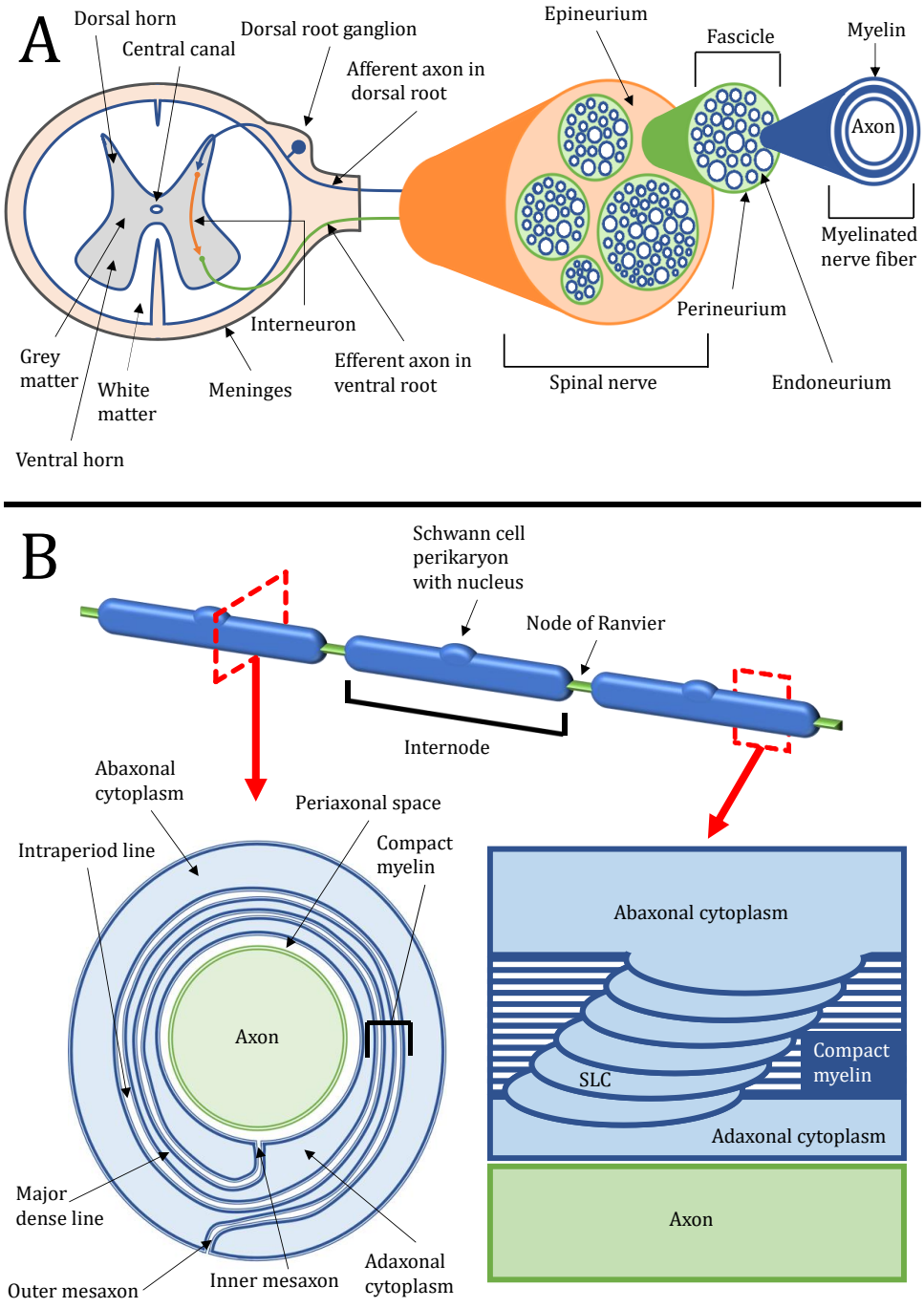

Figure 1. Schematic overview of (A) the spinal cord and spinal nerve and (B) microanatomy of a myelinated nerve fiber. SLC = Schmidt-Lanterman cleft. For details see main text.

Histologically, the CNS is divided into grey and white matter. The grey matter mainly consists of neuronal cell bodies, dendrites and glial cells, while the white matter largely consists of axons (16). Many of these axons are surrounded by myelin sheaths, responsible for the white appearance of the tissue macroscopically. In the CNS, the myelin is produced by oligodendrocytes. In contrast to the situation in the peripheral nervous system (PNS), each oligodendrocyte can myelinate segments of several axons. In the spinal cord, the grey matter is found centrally, in the dorsal and ventral horns. The ventral horns contain motor neurons, whose efferent axons leave the spinal cord through the ventral roots. The dorsal horns receive afferent sensory nerve fibers via the dorsal roots. The white matter of the spinal cord is divided into funiculi, containing ascending and descending nerve fibers. Most of these fibers are grouped together in fasciculi containing fibers with a common destination, origin and function . A schematic overview of spinal cord, spinal nerve and myelinated nerve fiber is shown in Fig. 1.

The PNS include the cranial nerves, the spinal nerves with their roots and ramifications, the peripheral nerves and the peripheral component of the autonomic nervous system (17). At the intervertebral foramen, the dorsal and ventral root from the spinal cord unite to form a spinal nerve. The dorsal root ganglion (DRG), containing the cell body of the afferent neurons, is found close to the point where the roots combine. Outside the vertebral column, the spinal nerve divides into dorsal and ventral branches (rami). The dorsal branch supplies the back, while the ventral branch supplies the limbs and ventrolateral part of the body wall. In the cervicothoracic and lumbosacral region, the ventral branches combine to form plexa, from which the major nerves to the limbs arise.

The peripheral nerves are enveloped by epineurium, a dense connective tissue, which also fills the space between the fascicles (16) (Fig. 1A). Each fascicle is surrounded by a layer of flattened polygonal cells, the perineurium, while the intrafascicular connective tissue is called endoneurium (18). The large majority, up to 90% of the intrafascicular cells are Schwann cells, 10% are fibroblast (19) and 2-4% are macrophages (20). Mast cells and lymphocytes also occur (21). The extracellular component of the endoneurium consists of collagen, elastic fibrillin fibers, water and various macromolecules (21).

Myelinated and unmyelinated nerve fibers are dispersed within the endoneurium. Throughout this thesis the term “nerve fiber” will be used to denote an axon with its associated glia cell. Large diameter axons (most axons exceeding 2 µm (22)) are enveloped by a myelin sheath, consisting of a series of cylindrical myelin segments. The myelin sheath is essential for rapid, saltatory nerve conduction. Each segment of the sheath is called an internode and produced by a single Schwann cell, while the node of Ranvier is the space between consecutive Schwann cells (Fig. 1B). In the myelination process, the Schwann cell extends its cytoplasm and plasma membrane in a spiral around the axon and the intervening cytoplasm is eliminated to form a multilamellated structure (22, 23). The major dense line represent the apposition of the cytoplasmic leaflets of the Schwann cell plasma membrane, whereas the outer leaflets form the intraperiod line (24). The Schwann cell structures and cytoplasm that remain outside the compact myelin are abaxonal, whereas the minor portion of cytoplasm internal to the compact myelin, close to the axon, is called the adaxonal cytoplasm. The Schwann cell nucleus is situated abaxonally, approximately in the middle of the internode (25). Schmidt-Lanterman clefts (SLC) are cytoplasmic channels spanning through the compact myelin, connecting the ab- and adaxonal cytoplasm (24). Unmyelinated nerve fibers are found in Remak bundles, where several unmyelinated axons are invaginated into a single Schwann cell (23).

In early life, the internodal length is approximately 300 µm in humans (23), and a comparable “minimal” internodal length is found in other species (26-28). During body growth, the length of the nerves increases and, as the number of internodes along the axon remains constant, the internodal length increases (23, 27). Consequently, the nerves in the body parts growing most in length, such as the limbs, will have the longest internodes in adult animals (27, 29). Furthermore, large diameter axons are myelinated at an earlier stage than small diameter axons, causing axons with the largest diameters to have the longest internodes (23). In the sciatic nerve of an adult dog, the myelin sheaths of the largest axons had internodal lengths close to two mm (28).

In the early 20th century, several peaks of voltage were detected when the electrical activity in a nerve was recorded following stimulation (30). The peaks represented groups of nerve fibers with different nerve conduction velocities and formed the basis

for their classification. Even though nerve fibers were originally classified according to nerve conduction velocity, the classification also has morphological implications, as large myelinated fibers have higher nerve conduction velocity than small myelinated fibers and unmyelinated fibers (22, 23, 30). One of the classification systems distinguish between class A, B and C fibers: Class A fibers are somatic afferent and efferent myelinated fibers with diameters of up to 20 µm, class B fibers are myelinated autonomic preganglionic fibers with diameters up to 3 µm, while class C are unmyelinated autonomic postganglionic and somatic afferent fibers (23). Most peripheral nerves are mixed, containing both motor (efferent) and sensory (afferent) nerve fibers (31).

The myelin sheath is a modification of the Schwann cell membrane and is composed of approximately 75% lipids and 25% proteins in dry weight (22, 32, 33). For comparison, the hepatocyte plasma membrane contains 34% lipids (33). There are no myelin-specific lipids, but some lipid classes, for example cholesterol and glycolipids, are enriched in myelin compared with other plasma membranes (32-34). In contrast, certain proteins, such as P_0, periaxin, myelin basic protein (MBP) and myelin-associated glycoprotein (MAG), are specific for the myelin sheath (32, 35). In a recent study, these proteins constituted 22%, 16%, 8% and 0.28%, respectively, of the myelin proteins in mouse peripheral nerves (36). The characteristic composition of the myelin is considered necessary for proper wrapping of the membrane in the myelin sheath and for providing electrical insulation to the axon (32, 33).

General pathology in peripheral nerves

Wallerian degeneration, distal axonopathy and segmental demyelination are common changes in diseased peripheral nerves. In the following paragraphs, I will give an overview of these processes.

Wallerian degeneration

Wallerian degeneration means changes occurring in the distal stump of a myelinated axon following an acute focal crush or transection injury (37). Multifocal axonal swellings with degenerating organelles occur within 24 hours (37-39). Myelin retracts from the nodes of Ranvier and there is widening of the SLC (40). The Schmidt-Lanterman clefts serve as constriction sites for the fragmentation of the internode into

ellipsoids, containing axon fragments centrally surrounded by degenerating myelin. Actin polymerization in the cleft was necessary for this process (41). Initially, Schwann cell phagocytose and degrade some of the myelin (37, 38). Later, macrophages invade the nerve and phagocytose debris (42).

If the neuronal cell body is uninjured, there is potential for regeneration. Schwann cells proliferate, forming Büngner bands, in the space where the distal stump resided. Several axonal sprouts grow from the proximal end of the transected axon and give rise to a regenerative cluster, a group of small myelinated fibers encircled by a common basal lamina (38). With time, one sprout is selected to complete the reinnervation (37). The remyelinated internodes are short, comparable to the 300 μm length they have at birth, and exhibit thin myelin sheaths. While the thickness of the myelin sheath gradually increase to near-normal thickness, the internodes along the regenerated axon remain uniformly short as no elongation due to body growth occurs (27, 38, 42).

Although the term Wallerian degeneration is reserved for the synchronous changes occurring after crush or transection, similar changes occur in other neuropathies. However, in these cases, axonal degeneration and regeneration are often seen concurrently (42).

Distal axonopathy

Distal axonopathy denotes axonal degeneration starting in the distal part of the long axons, progressing in a proximal direction. This pattern of changes, also called “dying-back” of the axon, can be found in metabolic, toxic and inherited neuropathies (22, 37, 43). Some examples are acrylamide (44) and organophosphate toxicity (37). The classical theory behind this distribution of changes is that many essential substances are supplied from the neuronal cell body (42), and in situations of metabolic deficiencies or impaired axonal transport, the distal part of the axon suffers first (43). The changes observed are usually non-specific (42), and include focal axonal swellings (spheroids) with accumulation of neurofilaments, mitochondria and other degenerating organelles (37, 42). As Schwann cells remove axonal debris through axon-Schwann cell networks, these networks can be prominent in distal axonopathies (43, 45). In a healthy nerve, axon-Schwann cell networks are only found in low

numbers paranodally (42). The axonal changes may progress to breakdown of the distal fiber in a Wallerian-like process (45), and subsequent attempts of regeneration (37).

Segmental demyelination

In segmental demyelination there is loss of myelin from scattered internodes along the nerve fiber (37, 46). Most commonly, this is a result of defects in or damage to the Schwann cell or myelin sheath (primary demyelination) (22, 24), but may also occur secondary to axonal atrophy in primary axonal disorders (24). Segmental demyelination was first described in lead intoxication, but occurs in both inherited and acquired neuropathies (38, 46). The first change observed is usually retraction of myelin from the nodes. If the nodal gap is less than 40 µm, a single Schwann cell may remyelinate the demyelinated segment. The remyelinated segments are called intercalated internodes. If the paranodal demyelination extends to involve more than half of the internode, myelin breakdown along the whole internode occurs (38). This segment is remyelinated by several Schwann cells, forming short and thinly myelinated intercalated internodes intermingling with internodes of normal length and thickness (38, 46). This contrasts with the remyelination seen after axonal regeneration, where the internodes along the regenerated axon are uniformly short and thin (38) (Fig. 2).

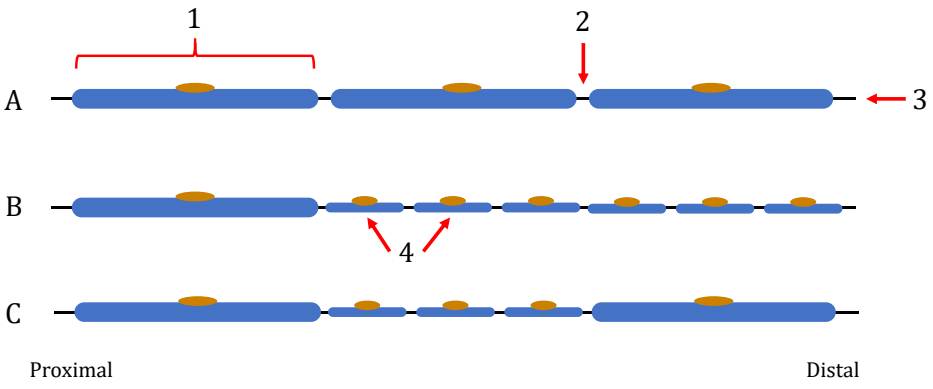

Figure 2. Schematic illustration of changes in teased fiber preparations. A. Normal nerve fiber. B. After axonal degeneration and regeneration with subsequent remyelination of regenerated segment. Remyelinated internodes are short and initially exhibit a thinner myelin sheath than normal internodes. C. After segmental demyelination and subsequent remyelination, intercalated internodes are present between normal internodes. 1=Internode. 2=Node of Ranvier. 3=Axon. 4=Intercalated internodes.

In neuropathies with recurrent demyelination and remyelination, “onion bulbs” can be found. During the remyelination process, the Schwann cells proliferate, leading to the production of more Schwann cells than needed for the remyelination (22). The supernumerary Schwann cells are displaced peripherally, resulting in an onion-like structure with a central, remyelinated axon surrounded by concentric layers of Schwann cell processes (22, 24). The Schwann cells can be distinguished from other endoneurial cells by the presence of a basal lamina (47).

While demyelination, remyelination and onion bulb formation are quite unspecific changes, more specific findings are found in certain neuropathies. Macrophage-mediated myelin stripping is considered a hallmark for immune-mediated demyelinating polyradiculoneuropathies, such as the human Acute Inflammatory Demyelinating Polyradiculoneuropathy (AIDP, a demyelinating form of Guillain-Barré syndrome (GBS)) and Chronic Inflammatory Demyelinating Polyradiculoneuropathy (CIPD) (48). In this process, macrophages penetrate the basal lamina of a morphologically intact nerve fiber and extend its processes along the intraperiod line (38, 48), causing destruction of the myelin sheath and segmental demyelination (24).

Axon-Schwann cell interaction

The proper functioning of each party of the axon-glia axis is heavily dependent on the other, highlighted by the fact that primary demyelinating diseases cause secondary axonal degeneration and vice versa (49). One example is axonal expression of Neuregulin 1 (NRG1), in particular the membrane-bound isoform NRG1 type III, which binds to its receptor ErbB2/3 on the Schwann cell. This signaling triggers myelination and ensures optimal thickness of the myelin sheath relative to axonal size (reviewed in (50, 51)). Furthermore, stimulation of the G protein coupled receptor GPR126 on Schwann cells, resulting in increased intracellular cAMP levels, promote myelination (50). Axonal PrP^{C}-signaling has been proposed to participate in maintenance of the myelin sheath (9) by activating this receptor (52). On the other hand, the function of the Schwann cell is not restricted to provide passive insulation of the axon (49, 53). The Schwann cell has been suggested to supply ribosomes, proteins, mRNA and metabolic substrates to the axon, and is proposed to form a functional syncytium with the axon (reviewed in (53), (54)). Furthermore, the Schwann cell participates in maintenance of axonal integrity by removing damaged organelles through axon-

Schwann cell networks (45), as described previously. On one hand it may therefore seem artificial to distinguish between demyelinating and axonal neuropathies. However, knowing which cell type is primarily affected is important for understanding the function of a protein and why its deficiency causes neuropathy.

Neuropathies

Diseases affecting several nerves are called polyneuropathies. Based on etiology, the polyneuropathies are usually divided into inherited and acquired forms. The latter group is further subdivided into toxic and metabolic, infectious and inflammatory, neoplastic and paraprotein-associated polyneuropathies (55). In the developed world, metabolic and toxic causes account for more than 50% of the human neuropathies, inflammatory and genetic for 10-20% each, neoplasia for 5-10%, while 10-20% are idiopathic (55).

Acquired neuropathies

A great variety of etiologies can cause acquired neuropathies both in humans and animals (55-57), for example hypothyroidism, diabetes mellitus (31, 56), and intoxication with lead or organophosphates (22, 31). Chemotherapeutic agents can cause toxic neuropathy as side effect (31, 58). One of these, paclitaxel, is used in the treatment of human breast cancer. Interestingly, one study identified an increased risk of paclitaxel-induced neuropathy in patients with low NDRG1 expression in peripheral nerves (59).

Immune-mediated polyradiculoneuropathies are triggered by autoimmunity against the peripheral nervous system (60). The main subtypes in humans are GBS and CIPD (48), while Acute Canine Polyradiculoneuritis (ACP, also called coonhound paralysis) is considered the canine counterpart of GBS (61). Although the pathogenetic mechanisms are not completely known, an immune response targeting proteins or glycolipids in the myelin sheath or axonal membrane has been suggested (61). In both GBS and ACP, the immune reaction is thought to result from molecular mimicry following exposure to antigens for example during infection or vaccination (48, 56).

Prion-related peripheral neuropathy resides at the boundary between acquired and genetically determined neuropathies, as it has been described in both sporadic (62)

and familial prion diseases in humans (63). The patients have clinical and electrophysiological signs of polyneuropathy (62, 63) and axonal degeneration has been noticed in nerve biopsies (62). The misfolded isoform of the prion protein (PrP^{Sc}) was detected in the peripheral nerves (62).

Inherited neuropathies: Charcot-Marie-Tooth disease and Inherited motor and sensory neuropathies

Most inherited neuropathies are classified as Charcot-Marie-Tooth disease (CMT) in humans, while the canine counterparts are called Inherited Motor and Sensory Neuropathies (IMSN) (64). Mutations in more than 80 genes have been found as causative of different types of CMT (65), and during the last ten years some of the inherited neuropathies in dogs have been linked to specific mutations (2, 4, 66, 67). CMT has a prevalence of 1 per 1214 persons in Norway (68, 69), and, although severity and age of onset may vary, most patients display a "classical" CMT phenotype characterized by distal muscle atrophy and weakness, sensory loss, foot deformities and absent ankle reflexes with onset of clinical signs during the first two decades of life (70).

CMT has traditionally been classified into subtypes based on clinical and pathological phenotype, inheritance mode, nerve conduction velocity and causative gene (summarized in Table 1). Both CMT1 and CMT2 are inherited in an autosomal dominant manner, and nerve conduction velocity (NCV) is used to separate between them clinically (71). Patients with CMT1 have a NCV of less than 38 m/s (71, 72), and the nerve changes are dominated by extensive demyelination, remyelination, onion bulb formation and secondary axonal loss (71, 73). In contrast, CMT2 patients have normal or almost normal conduction velocity (72, 73), but reduced amplitudes because of axonal loss (71). In the nerves, there is axonal degeneration without obvious segmental demyelination (73). Furthermore, there is loss of myelinated fibers, especially large fibers, and frequent regenerative clusters (71). CMT forms with NCV in the 25-45 m/s range, and a combination of demyelination and axonal degeneration ("mixed") in nerve biopsies, are denoted "intermediate" (74).

Table 1. Overview of main CMT subtypes. See text for references. Please note that the table is not exhaustive.

CMT subtypes	Disease features, inheritance, phenotypes and pathology
CMT1	• Autosomal dominant inheritance. • Nerve conduction velocity (NCV) <38 m/s. • Primary demyelinating neuropathy with segmental demyelination, remyelination and onion bulb formation. • Examples of mutated genes: Duplication of ***PMP22*** (CMT1A), point mutations in ***MPZ*** (CMT1B), mutations in ***SIMPLE*** (CMT1C) and in ***EGR*** (CMT1D).
CMT2	• Typically autosomal dominant inheritance (designated AR CMT2 if autosomal recessive). • NCV >38 m/s, reduced amplitudes. • Primary axonal neuropathy with axonal loss and regenerative clusters. • Examples of mutated genes: ***MFN2*** (CMT2A), ***RAB7*** (CMT2B), ***NEFL*** (CMT2E), ***MPZ*** (CMT2I and CMT2J).
Dejerine-Sottas syndrome (DSS, formely CMT3)	• Autosomal dominant or recessive inheritance. • Severe, early-onset demyelinating polyneuropathy. • Mutations in the same genes as in CMT1, thus nowadays often placed in the CMT1 subgroup.
CMT4	• Autosomal recessive inheritance. • NCV < 38 m/s. • Primary demyelinating neuropathy. Focally folded myelin in CMT4B and CMT4H, see discussion part of thesis. • Examples of mutated genes: ***MTMR2*** and ***MTMR13*** (CMT4B1 and CMT4B2), ***NDRG1*** (CMT4D), ***FRABIN*** (CMT4H).
CMTX	• X-linked inheritance. • NCV intermediate between demyelinating and axonal CMT. • Both axonal and demyelinating changes (mixed). • Mutation in ***GJB1***.
Hereditary Neuropathy with Pressure Palsies (HNPP)	• Autosomal dominant inheritance. • Recurrent episodes of mononeuropathy following compression of the nerve. • "Tomacula" formation, i.e. focal thickening of the myelin sheath resulting in "sausage-like" appearance in teased nerve fiber preparations. • Deletion in ***PMP22***.

Several other subtypes of CMT exists. CMT forms with autosomal recessive inheritance are classified as CMT4 if they are demyelinating and AR CMT2 if they are axonal (75). Dejerine-Sottas syndrome, formerly denominated CMT3, is an early-onset form of demyelinating neuropathy of either autosomal dominant or autosomal recessive inheritance (76), while CMTX is X-linked (77). Hereditary neuropathy with pressure palsies (HNPP) is characterized by recurrent episodes with mononeuropathy clinically and prominent focal myelin thickenings histologically (71).

The main CMT forms are further divided into subtypes based on genetic abnormality, such as CMT1A and CMT1B. However, the increasing number of mutations identified has complicated the current classification. This is further accentuated by the recognition that different mutations in the same gene might cause different CMT forms (76). To simplify the classification, a new categorization, where the CMT forms are denominated according to inheritance, phenotype and gene, was recently suggested (76). In this thesis, the traditional classification is used, as this is most commonly used in the literature.

Despite the large number of mutated genes in different CMT subtypes (65), mutations in the four genes *PMP22*, *GJB1*, *MPZ* and *MFN2* account for more than 90% of CMT cases with molecular diagnoses. A duplication in *PMP22* cause CMT1A, while a deletion in the gene cause HNPP. PMP22 is a transmembrane protein in compact myelin, but the normal function of the protein and exactly how the gene defects cause disease is unclear (71, 78). *MPZ* is mutated in the demyelinating CMT1B, while other mutations in the gene cause the axonal neuropathies CMT2I and CMT2J. The gene encodes P_0, which is a transmembrane protein necessary for myelin compaction (78). It is not well understood why particular mutations in the gene cause predominantly demyelinating neuropathy and others axonal neuropathy (79), but it is hypothesized that the mutation disrupts Schwann cell-axon interactions (80). Mutations in *GJB1* cause X-linked CMT. *GJB1* encodes the gap junction protein connexin 32, which is located at the nodes of Ranvier and SLC. The gap junctions facilitate transfer of ions and small molecules across the compact myelin to the adaxonal part of the myelin sheath, and, possibly, the axon (77). Mitofuscin 2, encoded by *MFN2*, is present in the outer mitochondrial membrane and regulate mitochondrial fusion. Mutations in *MFN2* cause CMT2A (81).

In contrast to the situation in humans, most of the canine IMSNs have an autosomal recessive inheritance (64, 82). Furthermore, only a few of the canine IMSNs are described as demyelinating (64), while demyelinating neuropathies form the majority of CMTs in humans. The clinical signs in neuropathic dogs are usually nonspecific (57, 64, 82). Paresis, decreased spinal reflexes and neurogenic muscle atrophy usually start distally in the pelvic limbs and may progress to involve the thoracic limbs as well (31, 64). Some giant breeds, such as Leonberger dogs (83), develop a characteristic high-stepping pelvic limb gait to compensate for atrophy and dysfunction of the cranial tibial muscle (64). Typical sensory signs are ataxia, proprioceptive deficits and decreased sensation (57, 64). Furthermore, dysfunction of the recurrent laryngeal nerve might lead to laryngeal paralysis and megaesophagus (31, 64). IMSN have been described in at least 22 dog breeds, but the associated mutations have only been identified in a few, such as Greyhound show dogs (4), Alaskan Malamutes (2), Leonberger dogs (66, 84) and Miniature Schnauzer (67).

NDRG1-associated neuropathies

Charcot-Marie-Tooth type 4D was first identified in a Gypsy community in Lom, Bulgaria, and originally called "hereditary motor and sensory neuropathy-Lom" (HMSNL) (85). The disease has later been diagnosed from patients in several countries in Europe and Asia (86-91). A causative *R148X* mutation in *NDRG1* was originally found (3), but later at least seven different mutations in the gene have been described from human CMT4D patients (86, 91-94). Nerve biopsy findings consist of demyelination and remyelination, onion bulb formation in young individuals, dyscompaction of the inner part of the myelin sheath, accumulation of pleomorphic material in the adaxonal Schwann cell cytoplasm and nerve fiber loss (6, 8, 76, 88-90, 95, 96). Clinically, signs from the lower limbs are observed during the first decade of life, upper limb weakness presents in the second decade and some patients develop deafness in the third decade (6, 8, 88-90, 95-97).

In 2010, an inherited polyneuropathy with autosomal recessive inheritance in Greyhound show dogs was described (4). The clinical signs appeared as early as three months of age in some of the dogs, and the affected dogs developed tetraparesis, ataxia, decreased spinal reflexes and postural reactions, muscle atrophy in distal limbs and laryngeal paresis. No animals survived longer than 10 months after appearance of

clinical signs, as they were euthanized on humane grounds due to disease severity. A deletion in *NDRG1* was found in the affected dogs, causing a decrease in NDRG1 mRNA and a lack of NDRG1 protein in the peripheral nerves. The neuropathy was classified as mixed or predominantly axonal based on the finding of axonal dystrophy in biopsies (4).

The Alaskan Malamutes with *NDRG1* mutations have clinical signs of polyneuropathy similar to the neuropathic Greyhounds (2), but the clinical signs appeared later (median 13.5 months) in the affected Alaskan Malamutes (2). Morphological descriptions from neuropathic Alaskan Malamutes are differing (1, 2), however, in-depth studies of nerves from affected dogs have not been performed yet.

NDRG1 protein

NDRG1 was first described as a gene that is up-regulated by homocysteine (98), during cellular differentiation (99) and a few years later, as mentioned, as the mutated gene in human and canine neuropathies (2-4). Furthermore, much research has focused on its role in cancer (99-105).

NDRG1 encodes a 43-kDa protein, consisting of 394 and 384 amino acids in humans (106) and dogs, respectively, and is highly conserved between species (106-108). The NDRG1 protein is a member of the NDRG protein family (109, 110), comprising NDRG1, 2, 3 and 4, which have 53-65% similarity in amino acid sequences (106). NDRG1 belongs to the alfa/beta hydrolase superfamily, but reportedly lack the catalytic site required to exert enzymatic activity (111). Within the alfa/beta hydrolase fold, there is a predicted phosphopantetheine attachment motif (98, 99). NDRG1 harbors a C-terminal tandem repeat, where the sequence GTRSRSHTSE, is repeated two or three times, in the canine and human protein, respectively. This sequence is unique to NDRG1 in the NDRG family (106). The protein undergoes complex posttranslational processing, including phosphorylation at several phosphorylation sites (108, 112, 113), SUMOylation (114) and proteolytic cleavage (115, 116).

A wide range of processes, chemicals and compounds regulate the expression of NDRG1 [reviewed in (106)]. NDRG1 is upregulated during cellular differentiation (99, 104). Furthermore, NDRG1 levels are increased by cellular stress, such as hypoxia

(117, 118), hypoxia-mimicking agents (119), heavy metals (120) and P53, which activate cell-cycle arrest and induce apoptosis following DNA damage (121). In contrast, NDRG1 is downregulated by N-myc and C-myc (122), and during cellular proliferation (123) and malignant transformation (99)

NDRG1 is ubiquitously expressed in human (117) and murine tissues (116), with especially high levels in the peripheral nerves (116) and epithelial cells, while the protein was not found in mesenchymal cells (117). Cellular, cytoplasmic and nuclear localizations have been observed (117, 119), and, at the ultrastructural level, NDRG1 localized to the plasma membrane, mitochondrial inner membrane and adherens junctions (117). The localization is dynamic, for instance hypoxia caused redistribution of NDRG1 from the cytoplasm to the cell nucleus, plasma membrane and ER in human trophoblasts (119) and differentiation provoked a membranous localization in human colon adenocarcinoma cells (99).

NDRG1 is considered a metastasis-suppressor (100, 101, 104, 122, 124), and the expression is downregulated in several malignancies, for instance those derived from the colon (99), prostate (100) and breast (101). Reduced NDRG1 level is mostly associated with a poor prognosis (100, 125, 126), but the opposite pattern was reported from hepatocellular carcinomas (103) and cervical adenocarcinomas (127). The exact mechanisms by which NDRG1 mediate these effects are not known.

Although numerous reports have implicated NDRG1 in a diverse set of cellular processes [reviewed in (106, 108, 109)], a definite function has not been assigned. Several studies have suggested a role in vesicular transport (118), and more specifically as a RAB4a effector molecule necessary for recycling of E-cadherin (128). Furthermore, NDRG1 is involved in formation of intracellular lipid droplets (129, 130), and interacted with the apolipoproteins A-I and A-II (131). Silencing of NDRG1 caused an increased level of cholesteryl esters in cultured hepatocytes (130) and breast cancer cells (129), while NDRG1-deficient epithelial cells had reduced uptake of low-density lipoprotein (LDL) and reduced level of cholesteryl esters as a result of disturbed recycling of the LDL receptor (132). NDRG1 is also recognized as a microtubule-associated protein (MAP). The protein localizes to centrosomes (105,

121), participates in formation of the mitotic spindle (105) and regulation of centrosome numbers (121).

In human (116, 117) and rodent (116, 133, 134) peripheral nerves, NDRG1 is present in the cytoplasm of myelinating Schwann cells. A student thesis from NMBU suggested a similar expression in dogs (135). NDRG1 was also present in the Schwann cell nucleus of rodents during remyelination after nerve crush (134). In one report, neuronal expression was found in human peripheral nerves (117). NDRG1 is upregulated during myelination and the expression follows myelin-related genes, such as PMP22 (116, 134). However, the protein seems dispensable for initial myelination, as changes in the nerves were first observed at five weeks of age in rodents lacking NDRG1. This rather pointed towards a role in myelin maintenance (133).

Prion protein

The cellular prion protein, PrP^{C}, has been extensively studied after the discovery that its misfolded isoform, PrP^{Sc}, causes transmissible spongiform encephalopathies. PrP^{C} is encoded by the *PRNP* gene, located on chromosome 20 in humans and 13 in goats. The protein consists of an ordered C-terminal globular domain and a N-terminal unstructured domain. A glycosylphosphatidylinositol (GPI)-anchor binds the protein to the cell membrane, and PrP^{C}-derived peptides might be released by proteolytic cleavage (136).

During the development of prion diseases, PrP^{Sc} interacts with PrP^{C} and converts it to PrP^{Sc}, leading to aggregates in the CNS. The diseases may be infectious, inherited or spontaneous (137). An overview of prion diseases and their etiologies is provided in Table 2.

Table 2. Overview of prion diseases and their etiologies.

Host	Disease	Etiology
Human	Creutzfeldt-Jakob disease	Spontaneous
	Variant Creutzfeldt-Jakob disease	Infectious (BSE-contaminated food)
	Familial Creutzfeldt-Jakob disease	Germline *PRNP* mutation
	Iatrogenic Creutzfeldt-Jakob disease	Surgical and medical treatments
	Kuru	Infectious (cannibalism)
	Fatal familial insomnia	Germline *PRNP* mutation
	Gerstmann-Sträussler-Scheinker syndrome	Germline *PRNP* mutation
Cattle	Classical bovine spongiform encephalopathy (BSE)	Infectious
	Atypical BSE	Spontaneous
Sheep and goat	Classical scrapie	Infectious
	Atypical scrapie (Nor98)	Spontaneous
Cervids	Chronic wasting disease (CWD)	Infectious
	Atypical CWD	Under investigation
Cat	Feline spongiform encephalopathy	Infectious (BSE-contaminated food)
Mink	Transmissible mink encephalopathy	Infectious
Camelids	Camelid prion disease	Infectious

Demyelinating neuropathy in mice lacking prion protein

Several lineages of transgenic mice lacking PrP^C, have been generated to investigate the physiological role of the protein (138-142) as results from such studies could give clues to whether the cell damage during prion diseases is caused by "loss of function" or "gain of toxicity" through aberrant stimulation of PrP^C-mediated cell signalling (143). Apart from being prion disease resistant, only minor abnormalities were initially observed in these mice under resting conditions. The first phenotype observed was ataxia and Purkinje cell degeneration in the Nagasaki knock-out mice (140, 144). This phenotype was later shown to be caused by the ectopic expression of Doppel (145, 146), but the authors also reported vacuolation in the spinal cord and demyelination in the peripheral nerves. The latter finding was also observed in the nonataxic Zurich I mice (144). Thus, it was suggested that PrP^C serves important roles in myelin formation and/or maintenance in both the central and peripheral nervous

system (144). More recently this has been investigated in several *Prnp*$^{-/-}$ mouse lineages and has led to the hypothesis that axonal PrP^{C} is important for maintenance of the myelin sheath (9, 142). Specifically, it was proposed that proteolytic liberation of PrP^{C}-derived peptides from axons could diffuse to Schwann cell receptors (52) to provide signalling for myelin maintenance (52), and that absence of such signalling gradually would lead to demyelination (9).

Goats lacking PrP^{C}

In 2012, a unique lineage of Norwegian Dairy Goats, spontaneously lacking PrP^{C} was discovered. These goats carry a point mutation in *PRNP*, resulting in a premature stop codon that terminates translation (10). To the best of our knowledge, this is the only naturally PrP^{C}-deficient animal reported. The goats appear normal and are considered healthy, however, a more pronounced sickness behavior (12) and lung damage (13) were observed when subjected to endotoxin challenge.

Animal models

Searching for phenotypes in knock-out animals, is a commonly used tool to investigate the physiological function of a specific protein. This is often accomplished by using transgenic rodent models. Rodents offer advantages such as rapid breeding cycles, short life span, availability of transgenic techniques and they are easily housed in experimental animal facilities (147). While giving valuable information, rodent models are often not able to fully reproduce the conditions observed in humans (147), also when it comes to peripheral neuropathies (7, 148, 149), suggesting a need for other animal models.

Domestic animals, such as dogs and goats, are valuable models for research of several reasons. In terms of their size, they have an anatomy more similar to humans when compared to rodents (147). This is especially relevant when investigating neuropathies, where length-dependent axonal degeneration is often observed. Dogs and goats also have a longer life-time expectancy and live in a more natural environment than laboratory rodents. Additionally, the use of animals with naturally occurring, spontaneous mutations to address a research question is preferable in the context of the 3Rs (replacement, reduction, refinement). Also, the study of biological

processes in several and evolutionally distant species generally will provide expanded knowledge compared with studies in one species only.

Furthermore, to achieve certain desirable traits in domestic animals, a restricted number of individuals have been bred and disease-causing mutations have been enriched in the same process. This is particularly pronounced for dogs, where each dog breed may be considered a partially inbred genetic isolate (150), and within most breeds there are specific inherited diseases, often with an autosomal recessive inheritance. Thus, CMT4D, which is a severe, but relatively rare human disease, may be more easily studied in canines with *NDRG1* mutations simply because the disease occurs with higher frequency.

On the other hand, spontaneous non-rodent models also impose some limitations, such as restricted access to material. For example, the Alaskan Malamutes studied in this thesis are privately owned companion animals. As sampling has been performed as part of the routine diagnostic procedures or postmortem examinations, samples from all sites are not available from all the dogs. Furthermore, many of the methods used in this thesis are dependent on specialized tissue preparation techniques, thus, in some instances it was necessary to prioritize which method to employ when the number of nerve samples from an individual was limited.

A general problem when trying to associate a mutation in a certain gene with a trait, is that also the genes surrounding the mutation show more similarity in the mutated animals than in the general population. The "flanking gene problem" is when a phenotype is falsely attributed to a mutation in a specific gene but actually caused by a closely linked gene (151). For example, PrP^C was suggested to regulate phagocytosis in a transgenic rodent model (152), but this phenotype was later shown to be caused by polymorphism in a linked gene encoding SIRP-α (153). The possibility of linked mutations has been addressed earlier for Alaskan Malamutes with *NDRG1* mutations by considering the function of surrounding genes (2). However, for the goats lacking PrP^C, this question is discussed later in the thesis.

Aims of the thesis

In the peripheral nervous system, Schwann cells form a biologically active, multilamellar myelin sheath around large diameter axons. Myelination is important for rapid signal conduction, axonal function and survival. Several debilitating diseases of peripheral nerves, known as polyneuropathies, occur in both humans and animals. In order to prevent or ameliorate these diseases, it is essential to understand in molecular detail how specific proteins contribute to myelin homeostasis or normal axonal function. Furthermore, the morphological and molecular changes observed may be relevant for a wider range of neuropathies. In this work, we have taken advantage of two unique, spontaneous animal models to investigate NDRG1 and PrP^C in peripheral nerves. While *NDRG1* mutations are known to cause neuropathies in several species, PrP^C has been hypothesized to participate in myelin maintenance from studies in transgenic mice.

Therefore, the overall aim of the project was to **investigate how deficiencies in NDRG1 or PrP^C affect peripheral nerves by using morphological studies in dogs and goats with and without mutations in the respective encoding genes.**

More specifically:

- **Determine and interpret the localization of NDRG1 in canine tissues and cells (paper I)**. Knowing the normal distribution of NDRG1 in canine peripheral nerves was a prerequisite to understand its role in maintenance of normal nerve structure, and a detailed mapping in different cells and tissues might give clues about possible functions.
- **Describe and analyze in detail the morphology, including ultrastructural changes, of AMP nerves and discuss these changes in relation to the cell biology of NDRG1 (paper II).**
- **Investigate whether goats without PrP^C develop a demyelinating disease and discuss the changes in relation to changes described in transgenic rodents and the cell biology of PrP^C (paper III).**

Summary of papers

Paper I

Cell and context-dependent sorting of neuropathy-associated protein NDRG1 – insights from canine tissues and primary Schwann cell cultures

The NDRG1 distribution has been studied in humans and rodents, but not in dogs. In paper I we performed a detailed analysis of NDRG1 localization in canine tissues and primary Schwann cell cultures, with emphasis on peripheral nerves. The signals were compared to a polyneuropathy-affected Alaskan Malamute homozygous for the missense mutation in *NDRG1*.

Although NDRG1 was present in several cell types, strong NDRG1 signal was observed in Schwann cells. A phosphorylated isoform of the protein was present in the abaxonal cytoplasm of myelinating Schwann cells of *NDRG1*$^{wt/wt}$ Alaskan Malamutes, but this signal was not observed in the *NDRG1*$^{mut/mut}$ Alaskan Malamute. Furthermore, no signal was observed in axons. In epithelial cells, cytosolic, basolateral and granular signals were present. In some cells, NDRG1 localized to centrosomes, and in developing spermatids, NDRG1 was present in the midpiece.

We concluded that canine NDRG1 shows a cell and context-dependent localization. Some of the observed localizations point towards interaction with the microtubule cytoskeleton. The subcellular localization of NDRG1 is affected by signaling events causing phosphorylation of the protein. We proposed that disease-causing mutations in *NDRG1* can disrupt signaling in myelinating Schwann cells, affecting myelin homeostasis and axonal-glial cross talk, leading to polyneuropathy.

Paper II

Impaired NDRG1 functions in Schwann cells cause demyelinating neuropathy with focally folded myelin in a dog model of Charcot-Marie-Tooth type 4D

Mutations in *NDRG1* cause a primary demyelinating polyneuropathy, CMT4D, in humans. In contrast, axonal changes dominated in *NDRG1*-associated polyneuropathy in Greyhounds and a previous report of Alaskan Malamute polyneuropathy, albeit the latter has not been studied in detail. Therefore, in paper II, a detailed morphological

analysis of changes in nerves of Alaskan Malamutes with polyneuropathy was performed. Additionally, levels of NDRG1 mRNA and protein in nerves were assessed by RT-qPCR and Western blotting, respectively, and lipidomics were performed to investigate the lipid composition of AMP nerves.

NDRG1$^{mut/mut}$ Alaskan Malamutes do not have a total lack of NDRG1, but significantly reduced levels of NDRG1 protein in the peripheral nerves. In contrast, the levels of NDRG1 mRNA were not significantly different from controls. In teased nerve fibers, demyelinated segments and intercalated internodes intermingled with longer internodes of normal myelin thickness, consistent with a primary demyelinating disease. Supporting this, onion bulbs and thinly myelinated fibers were present in semithin sections. Ultrastructurally, filamentous material, consisting of actin, was found in the adaxonal cytoplasm and disrupted SLC. Furthermore, infoldings and outfoldings of the myelin sheath were present.

The changes in Alaskan Malamute polyneuropathy is consistent with a primary demyelinating disease, in accordance with reports from humans and rodents with *NDRG1* mutations. However, we also report changes not previously described in CMT4D, such as prominent myelin infoldings dividing the axon. Our data suggests that the low levels of mutant NDRG1 protein in nerves of affected Alaskan Malamutes are insufficient to support Schwann cells in maintaining the myelin sheath.

Paper III

Polyneuropathy in Goats lacking Prion protein

Mice lacking the cellular prion protein, PrP^C, develop a progressive demyelinating polyneuropathy, suggesting a role for PrP^C in myelin maintenance. In paper III, we investigated this in a unique lineage of dairy goats that, due to a naturally occurring nonsense mutation, lack PrP^C.

Teased nerve fibre preparations showed a demyelinating pathology in goats devoid of PrP^C, and paranodal outfoldings were often present adjacent to the remyelinated internodes. Ultrastructurally, vacuolated nerve fibres, shrunken axons and onion bulbs were present. Increased numbers of macrophages (Iba1+ cells) and T cells (CD3+ cells) were found in affected nerves. While the peripheral nerve lipid composition of young

goats was not significantly different between the genotypes, a difference was found in adult goats, suggestive of a progressive neuropathy. Haplotype analysis showed that the homozygous region only comprises 2.5 Mb of genomic DNA around the *PRNP* gene.

This is the first report of a sub-clinical demyelinating polyneuropathy caused by loss of PrP^C function in a human-sized mammal. The results presented strongly indicates that PrP^C functions in myelin maintenance.

Methodological considerations

All materials and methods are fully described in the papers, and an overview of the methods used is presented in Table 3. In this section, I will go through some important considerations regarding the materials and methods used.

Table 3. Overview of methods used in the study.

Methods	Paper I	Paper II	Paper III
Western blotting	X	X	X
Immunohistochemistry (IHC)	X	X	X
Immunofluorescence (IF)	X	X	X
Isolation and culturing of primary Schwann cells	X		
Nerve fiber teasing		X	X
Electron microscopy		X	X
Morphometry		X	X
Electrophysiology		X	X*
RT-qPCR		X	
Lipid composition analysis*		X	X
Haplotype analysis*			X

*External methods performed in collaboration with other laboratories.

Light and electron microscopy: Processing and assessment

Fixation

The purpose of fixation is to preserve the structure of living tissue, thus it must protect the tissue from autolysis as well as disruption during the embedding and further procedures (154). As both the fixatives and tissues have varied properties, the choice of fixation protocol must be adjusted to the tissue and the downstream analyses. All samples used in this thesis were fixed by immersion, as it allows parts from the same tissue to be fixed by different methods – thus allowing different analyses to be performed on the same tissue. An overview of the fixation methods used is shown in Table 4.

Table 4. Overview of fixatives applied for different methods in the study.

	Formalin	Glutar-aldehyde	Osmium tetroxide	Liquid nitrogen
Paraffin-embedding (IHC, IF in paper I and II)	X			
Resin-embedding (semithin, ultrathin sections)		X	X	
Nerve fiber teasing		X	X	
Cryosections (IF in paper III)				X
Western blotting				X
RT-qPCR				X
Lipidomics				X

Formalin, a solution containing formaldehyde (154), is a commonly used fixative for histology and immunohistochemistry. Formaldehyde mainly preserves proteins, by reacting with amino groups in the tissue. During this process, reactive hydroxylmethyl groups are formed, which again react with hydrogen groups to produce cross-links between the proteins (155). Formaldehyde penetrates the tissue about five times faster than glutaraldehyde, and the fixation achieved is to some extent reversible (155), which is relevant for antigen retrieval during immunohistochemistry (discussed later).

Glutaraldehyde have two terminal aldehyde groups that reacts with amino groups and cross-link proteins irreversibly. Additionally, glutaraldehyde reacts with carbohydrates, lipids and nucleic acids to some degree (154). As it stabilizes structures very effectively, glutaraldehyde is commonly used for ultrastructural studies. However, glutaraldehyde penetrates the tissue slowly, especially if the tissue contains multiple layers of membranes, such as the myelin sheaths in peripheral nerves.

Osmium tetroxide reacts with lipids in the tissue. By oxidizing fatty acids and at the same time being reduced to metallic osmium, osmium tetroxide both fix lipids and add contrast to the sample (154), and is therefore used as a secondary fixative when samples are prepared for resin-embedding and nerve fiber teasing.

In this work, formalin fixation and subsequent paraffin-embedding were used for tissue destined for immunohistochemistry and immunofluorescence (paper I and II). However, as the lipids of the myelin sheath are not well preserved by formalin fixation and dissolved by the xylene during paraffin-embedding (156), resin-embedded nerves and teased nerve fibers were used for assessment of morphological changes. For these analyses, the samples were fixed in 2.5% glutaraldehyde and post-fixed in osmium tetroxide.

Peripheral nerves are lipid-rich tissues. Therefore, to obtain an efficient penetration of the fixative and the chemicals used during the embedding procedure, the epineurial fat was removed and the nerve separated into individual fascicles less than 1 mm in diameter before fixation. Nerves are susceptible to artefacts produced by crush and stretching, necessitating a careful handling of the samples during processing. During the first minutes of the fixation, the nerve fascicle was fixed attached to a piece of paper. This was to avoid contraction, which would have caused a wavy appearance of the nerve in sections and teased fiber preparations.

Resin-embedding

Resin-embedded nerves can be sectioned at 0.5 µm (semithin section) and stained with toluidine blue and safranin-O. Semithin sections can be assessed in the light microscope, allowing evaluation of features such as the number of myelinated nerve fibers, myelin thickness, onion bulbs and axonal swelling. Furthermore, regions of interest can be chosen, the block trimmed accordingly and sectioned at 50-70 nm (ultrathin section). After enhancing contrast in the sample by staining with uranyl acetate (stains nucleic acids and proteins) and lead citrate (stains many cellular components) (157), the sections were studied in a transmission electron microscope. In the electron microscope, it is possible to study the unmyelinated nerve fibers, which are not adequately visualized by light microscopy (158). Additionally, subcellular details can be studied, such as accumulation of mitochondria within the axons.

Epoxy resin was used as embedding medium in this work. This is a commonly used resin for morphological studies. After fixation with glutaraldehyde and osmium tetroxide, the samples were dehydrated by an ascending acetone series. The samples were incubated with a mixture of epoxy and acetone, and epoxy infiltration of the

samples was achieved by using a gradually increasing epoxy/acetone ratio. After orientation of the samples, the epoxy polymerized by incubation at 60 °C for 48 hours.

Morphometry

Morphometry, the quantitative evaluation of size or shape, was used in this work for two purposes. First, it allows a more objective evaluation of nerve changes than morphological assessment alone. Second, by combining measurements from many nerve fibers, it is possible to detect changes that are not readily visualized by inspection alone. A semi-automated approach was used for morphometrical analyses: Images from semithin sections were converted into black and white. Thereafter, the color segmentation tool in Image-Pro Plus software was used to outline the myelin sheaths and the areas of the whole nerve fiber and axon were measured.

Several different methods are used to estimate nerve fiber diameter and myelin thickness (159). As many of the nerve fibers have a flattened or crenated shape, measuring the diameter directly is difficult. In this work, the diameter was calculated by the formula $D = 2\sqrt{(Area/\pi)}$, assuming the measured area to be that of a circle. This method is reported to provide the best precision and accuracy (159). As differences in sampling site, tissue processing and measurement method (159, 160) between laboratories may affect the results, the measurements in this work were only compared to our own samples that have been processed the same way.

Mixed motor and sensory nerves, such as the tibial and common fibular nerves, normally consist of a mixture of large and small diameter fibers, as mentioned in the introduction, and the fiber diameter histogram is used to assess the presence of these. The g-ratio (axonal diameter divided by the diameter of the whole nerve fiber) is used to measure the thickness of the myelin sheaths. As remyelinated internodes have a slightly thinner myelin sheath than normal, an increased g-ratio suggests demyelination/remyelination or axonal regeneration. In contrast, hypermyelination and axonal atrophy result in decreased g-ratio (161).

Nerve fiber teasing

Nerve fiber teasing is a method used to evaluate the consecutive internodes along a nerve fiber. Even though this is also possible to observe in longitudinal semithin

sections, changes are more easily detected in preparations from teased fibers. After fixation with glutaraldehyde and osmium tetroxide, the nerve is separated into individual nerve fibers under a dissection microscope. Paranodal demyelination can be detected by a widening of the node of Ranvier, while short and thinly myelinated internodes suggest previous segmental demyelination and remyelination. If all the internodes along the nerve fibers are short, this suggests remyelination after axonal regeneration (38).

The suggested number of fibers to be evaluated varies widely between different references, from 50 (162) to more than 500 (159, 163). When assessing the effect of a variable on nerves, it is suggested to rather increase the number of nerves evaluated than to increase the number of teased fibers from a single nerve (159). In this work, at least 25-30 fibers from each nerve were evaluated, and, if available, several nerves from each individual were assessed. Some age-related changes are expected, therefore teased fiber preparations from cases were compared to controls and, for the dogs, published data about age-related changes (164). Furthermore, changes observed in teased fibers were correlated to findings in semithin and ultrathin sections.

Protein detection

Immunohistochemistry and immunofluorescence

Immunohistochemistry (IHC) and immunofluorescence (IF) are methods used to localize antigens in tissues or cells by using specific antibodies (155). In IHC, the binding of antibody to antigen is detected by production of a colored product through a histochemical reaction. In IF, the antibody is conjugated to a fluorochrome with specific absorption and emission spectra. In IHC, the slides can be assessed by bright-field light microscopy, while IF requires a fluorescence microscope.

Only indirect immunolabeling was used in this thesis. This is a two-step process where the primary antibody binds to the antigen of interest and a secondary antibody binds to the primary antibody. As several molecules of the secondary antibody binds to every molecule of the primary antibody, the signal is amplified through the indirect technique. Further signal amplification is achieved by having multiple molecules of enzyme bound to every secondary antibody (used in the Envision method) or adding an amplification step based on the interaction between streptavidin and biotin (used

in the ABC PO method) (155). Horseradish peroxidase is one of the most commonly used enzymes, which produces a colored product when incubated with substrates such as 3-amino-9-ethylcarbazole (AEC) or 3,3′diaminobenzidine tetrachloride (DAB).

Immunofluorescence is often used to label several antigens in the same section. This is achieved by adding primary antibodies of different isotypes or produced in different species, combined with secondary antibodies conjugated to different fluorochromes. To avoid crosstalk (i.e. the signal from one of the fluorochromes extending into the other channel) it is important to use fluorochromes with non-overlapping emission spectra. In this thesis, fluorochromes with emission maxima at 525 nm and 617 nm were combined.

Immunohistochemistry and immunofluorescence were used in this thesis to localize NDRG1 and PrP^C in tissues and cells. Furthermore, immunohistochemistry and immunofluorescence against antigens with known localization were used to ascertain the identity of specific cell types, as summarized in Table 5.

Table 5. Overview of markers used to identify specific cell types in the study.

Antigen	Marker for
CD3	T lymphocytes
CD79	B lymphocytes
Iba1 (ionized calcium-binding adapter molecule 1)	Microglia and macrophages
GFAP (glial fibrillary acidic protein)	Astrocytes and immature Schwann cells
Neurofilament	Axons

To maximize signal-to-noise ratio, the labeling protocols were optimized for the antibodies used. Optimal antibody concentration was determined from initial titration runs. Fixation alters the tertiary structure of proteins and may mask epitopes. Therefore, antigen retrieval with heat (all antibodies used except Iba) or enzymes (Iba1) was used to expose antigens. In paper III, cryosections were used to avoid masking of epitopes from formalin fixation. Furthermore, background staining as a result of hydrophobic interactions between the antibody and macromolecules in the tissue (155) were reduced by blocking the slides with bovine serum albumin and/or serum from the same species as the secondary antibody. The slides were also

incubated with hydrogen peroxide in methanol, which inhibits endogenous peroxidase activity in the tissue, to avoid false positive results.

The NDRG1 antibodies used in paper I and II had not been tested previously in canine tissues. Even though the amino acid sequence is highly conserved across species (122), several antibodies targeting different epitopes were used in parallel to ensure specific labeling of the protein in dogs. The PrP^{C} antibody in paper III has been tested in goat tissues previously (13). Slides, where the primary antibody was omitted, were used as negative controls. In the immunofluorescence protocols, unlabeled slides were used to assess autofluorescence. Furthermore, in paper III, tissue from *PRNP*$^{Ter/Ter}$ goats were used to verify the specificity of the antibody, as these animals lack PrP^{C} completely.

Western blotting

Western blotting was used in the thesis to assess the level of protein expression in tissues. The tissue is homogenized, and the proteins separated by gel electrophoresis. Subsequently, the proteins are blotted to a membrane, blocked with dry milk and labeled with primary and secondary antibodies. The secondary antibodies used in this thesis were conjugated to alkaline phosphatase, which produce a fluorescent product when ECF substrate is added. As Western blotting is a technique for immunolabeling, many of the principles mentioned for immunohistochemistry and immunofluorescence, is also applicable here. However, in contrast to immunohistochemistry and immunofluorescence, the proteins are denatured before separation in Western blotting.

The total protein concentration in the lysates were measured by spectrophotometry to ensure that an equal amount of total protein was loaded from all the samples. This was further controlled by staining the gels (shown in paper III) and/or membranes (shown in paper II) for total proteins. In paper II, NDRG1 levels for the different genotypes were quantified relative to total protein levels.

Electrophysiology

The nervous system is specialized for propagation of electrical impulses. By recording these impulses with specialized equipment, which is the basis for electrophysiological testing, the function of the nervous system can be assessed. Many of the tests are

sensitive for functional disturbance, but the results are usually not characteristic for specific diseases (31). Motor nerve conduction velocity (MNCV) and electromyography (EMG) were used in paper II.

To measure MNCV a nerve impulse is evoked by placing an electrode close to a nerve, and depolarization of the innervated muscle is recorded. The latency is defined as the time from stimulation of the nerve to a compound muscle action potential (CMAP) is produced (31). The latency includes both the nerve conduction time and the time required for neuromuscular transmission. Therefore, it is necessary to stimulate the nerve at two different sites to obtain the MNCV. The MNCV is calculated by the distance between the stimulation points divided by the difference in latencies between the sites.

In healthy dog nerves, the MNCV should be higher than 50 m/s (165). The MNCV of dogs reaches adult values before one year of age and is considered to be stable until the age of seven years. All recordings were performed on dogs within this age interval, except for one of the dogs where serial measurements were performed. In dogs older than 10 years, an age-related reduction in MNCV might occur (165). Basically, reduction in MNCV indicates demyelination, while reduction in the amplitude of CMAP is usually caused by axonal loss or severe muscle disease (31). In human medicine, a cut-off value at 38 m/s has been used to separate axonal from demyelinating neuropathies (71, 72). However, a similar distinction cannot be made in veterinary medicine, as even dogs with neuropathies considered to be primary axonal have had MNCV in the range of 10-20 m/s (64).

Electromyography evaluates the electrical activity in the muscle. When a needle is inserted into a muscle, myofibers depolarize and produce insertion activity. A healthy, resting muscle, quickly turn electrically silent again. In contrast, denervated muscles or muscles affected by myopathies, may show prolonged insertional activity or abnormalities produced by spontaneous depolarization of myofibers (such as fibrillation potentials, positive sharp waves and complex repetitive discharges) (31).

Electrophysiological measurements of the nociceptive withdrawal reflex were done in paper III. This reflex is a polysynaptic spinal reflex responsible for withdrawal of the limb from potentially harmful stimuli. It was chosen because it can be performed in

unsedated, standing animals (166). The reflex was evoked by electrical stimulation on the distal part of the forelimb and the response measured by electromyography in the deltoid muscle. Experimentally, measurement of this reflex is used when testing the effects of antinociceptive drugs, where decreased reflex response or increased reflex threshold following administration of the drug indicate an antinociceptive effect. While this experimental setup made it possible to measure latency, MNCV cannot be calculated as neither the synaptic delay in the spinal cord nor transmission at the neuromuscular junction are eliminated in the nociceptive withdrawal reflex. Measurement of MNCV is a more sensitive method for detection of demyelination, and, therefore, in hindsight, would have been more suited to assess the effect of demyelination in the goats lacking prion protein.

RT-qPCR

RT-qPCR was used in paper II, to compare the levels of *NDRG1* mRNA in nerves from *NDRG1*$^{mut/mut}$ and *NDRG1*$^{wt/wt}$ Alaskan Malamutes. As mRNA is rapidly degraded, all nerve samples were snap-frozen in liquid nitrogen shortly after euthanasia and stored at -80 °C until analysis. After homogenization and extraction, the purity of the total RNA was assessed by a Nanodrop spectrophotometer. Furthermore, the quality of the total RNA was investigated on a Bioanalyzer, which gives an RNA integrity number (RIN) based on the intactness of the 18S and 28S rRNA.

cDNA was produced from the total RNA with random primers, as described in paper II. In the next step, sequence-specific primers were used to amplify *NDRG1* cDNA. The PCR products are detected by binding of a fluorescent reporter, for example SYBR Green I. As SYBR Green I emits light when it binds to DNA, the fluorescence increases with the levels of PCR product during the PCR reaction. The cycle quantification value (C_q) is the cycle where the fluorescence exceeds a certain threshold value and is detected by the system. As C_q is directly related to the amount of template initially present in the sample, the amount of *NDRG1* mRNA in the sample could be calculated by using a standard curve, produced by serial dilution of the template. The results were normalized against an internal reference gene, *GAPDH*, to account for differences between the samples, for example related to tissue homogenization, nucleic acid quality or cDNA synthesis. Furthermore, the specificity of the primers was verified by BLAST (basic local alignment sequence search tool) search against the canine genome,

as well as sequencing of the PCR product. Melting curves and controls without template were assessed to control for unspecific amplifications.

Results and discussion

The peripheral nerves are structures highly specialized for rapid propagation of nerve impulses. This is vital to the organism, enabling fast transmission of impulses from sensory organs to the CNS and impulses from the brain and spinal cord to target organs, for example to allow coordinated contractions of the musculature. To perform this task, the two main cell types in the peripheral nerve – the neuron and the Schwann cell - have adapted in a remarkable manner through evolution. The impulses are conducted in an axonal process extending for up to several meters from the neuronal soma, making the neuron the longest cell type in the body and highlighting the need for an effective transport machinery to support the distal part of the axon. For example, the axons of the recurrent laryngeal nerves of giraffes may measure five meters in length (167). The fastest propagating nerve fibers are enveloped by myelin sheaths. The myelin sheath reduces the energy required for impulse transmission and increase conduction velocity in the axon. Additionally, the Schwann cell provide metabolic support to the axon (49, 54). The sheath of the largest canine nerve fibers consisted of more than 150 lamellae and one Schwann cell contributed with myelin along two mm of the nerve fiber (28). Thus, the formation and maintenance of a myelin sheath put an enormous pressure on the Schwann cell – in terms of cytoskeleton to support the complex structure, lipid and protein synthesis, as well as intracellular transport (7, 168).

Polyneuropathies are caused by disturbance in the normal function of either the neuron, the Schwann cell or both. In this thesis, we have studied two ubiquitous proteins, NDRG1 and PrP^{C}, where mutations in the encoding genes cause polyneuropathies. Several functions have been proposed for both, but a precise function in the peripheral nerves has not been assigned.

NDRG1

To understand possible roles of NDRG1 in polyneuropathies, we first decided to study the localization of the protein in canine tissues. This was triggered by the apparent disagreement between pathomorphological changes observed in CMT4D and canine *NDRG1*-associated neuropathies, suggesting species differences in the cell biology of NDRG1. Furthermore, a broad overview of NDRG1 expression in different tissues and

cell types might give clues to possible protein functions. We concluded that the localization was cell- and context-dependent. NDRG1 was found in all examined tissues, and several isoforms were present. The expression level and localization varied between the cells (illustrated schematically in Fig. 3 and summarized in Table 1 in paper I). Briefly, diffuse cytoplasmic signals were present in a wide range of cells, while distinct and strong signals from NDRG1 isoforms were observed in highly polarized cells, such as epithelia (basolateral signal), myelinating Schwann cells (abaxonal cytoplasm) and spermatids (signal from midpiece). Furthermore, signal from centrosomes and cleavage furrow were present in cells undergoing mitosis.

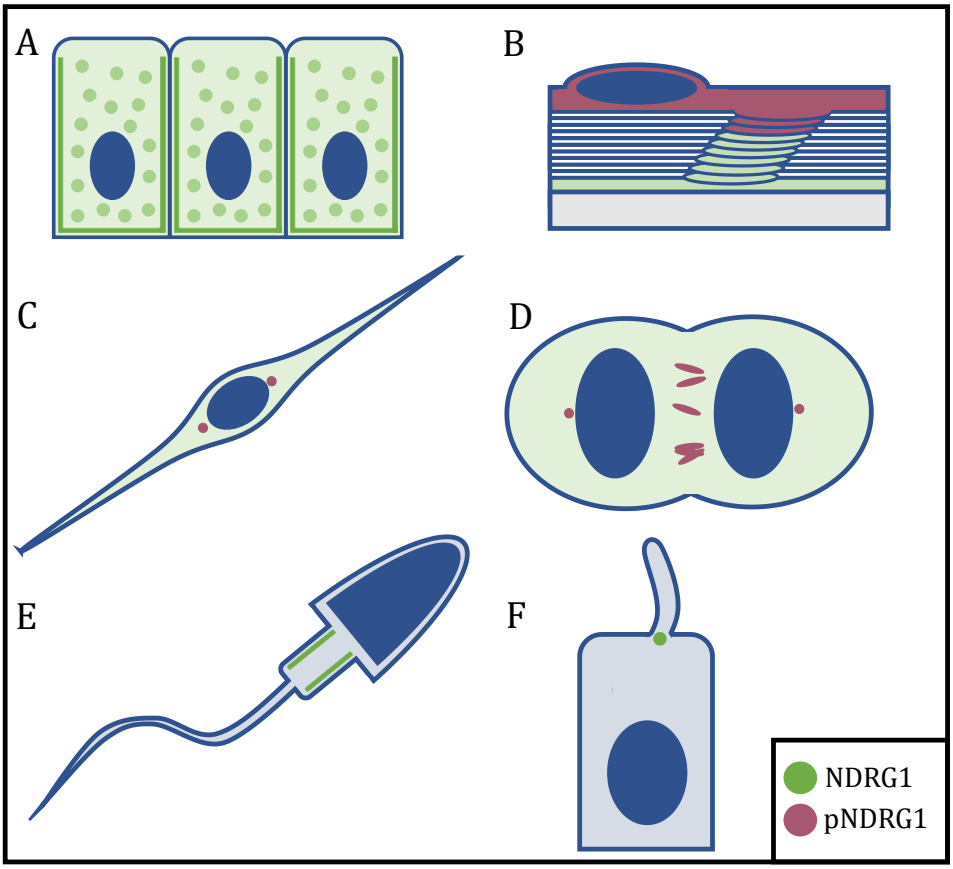

Figure 3. Schematic illustration of NDRG1 localization, based on our own results from paper I (A-E) and reported in (169) (F). Note that NDRG1 was also present in the red areas. A. Diffuse and granular cytoplasmic NDRG1 signals were observed in many cells, while strong basolateral signal was present in epithelia. B. In myelinating Schwann cells, pNDRG1 was present in the abaxonal cytoplasm and outer part of SLC, while NDRG1 was found throughout the Schwann cell cytoplasm. C, D. pNDRG1 localized to centrosomes (C) and cleavage furrow (D) in dividing cells. E. Strong signals were present in the midpiece of developing spermatids. F. NDRG1 is also reported from the transition zone of the primary cilium.

A granular signal was observed in several cell types (for example bile duct epithelium, Fig. 3a, see also Fig. 3C in paper I). Based on the close link between NDRG1 and intracellular trafficking (118, 128-132), this signal may derive from intracellular vesicles. More specifically, NDRG1 is reported as a RAB4a effector protein, interacting with active, membrane-bound RAB4a (128). RAB4a is a marker for recycling endosomes, and NDRG1 is recruited to these by binding to the phosphoinositide phosphatidylinositol 4-phosphate (PtdIns(4)P) (128). By giving identity to membranes and attracting specific effector proteins, both RAB proteins and phosphoinositides are important regulators of membrane trafficking in the cell (170). Among the recruited effectors are the Rho GTPase activators, responsible for regulating actin polymerization (171). Phosphatidylinositol 4-phosphate is enriched in the membranes of the Golgi apparatus, endosomes and the primary cilium, but is also present at the plasma membrane (170, 172, 173). Considering the Golgi apparatus as a central hub where proteins and lipids from various cellular compartments are exchanged, PtdIns(4)P plays an important role in the cellular trafficking machinery. Furthermore PtdIns(4)P serves as a precursor for the synthesis of other phosphoinositides (174).

Particularly, PtdIns(4)P is required for transport from the Golgi to the plasma membrane (174). Bearing in mind that NDRG1 participates in recycling of E-cadherin (128) and the LDL receptor (132) to the plasma membrane, the strong basolateral signal we observed in epithelial cells (Fig. 3a, see also Fig. 3A, B and E in paper I) could be explained by vesicle-mediated trafficking of lipids and proteins to this cellular domain. Polarized cells, such as epithelia and myelinating Schwann cells, are characterized by membrane domains with distinct lipid and protein composition (reviewed in (26)). For example PtdIns(3,4,5)P_3 is associated with the basolateral membrane in epithelia and the basolateral-like abaxonal membrane in myelinating Schwann cells, while PtdIns(4,5)P_2 is present in the apical membrane of epithelia and in the apical-like adaxonal membrane and SLC of myelinating Schwann cells (175, 176). To maintain this polarized phenotype, correct targeting of intracellular vesicles is crucial (176, 177), exemplified by the fact that myelinating Schwann cells sorted proteins destined for compact myelin, non-compact myelin and abaxonal plasma membrane into separate vesicles in the trans-Golgi network. Although vesicles were transported by microtubules abaxonally along the internode, the microtubules did not

target them for specific sites, and it was suggested that ligand-receptor binding ensure fusion of vesicles with correct target membrane (177).

Taking into account the epithelial-like polarization of myelinating Schwann cells, the distinct distribution of NDRG1 isoforms we observed in the Schwann cell (Fig. 3B) might be explained by the same association as discussed for epithelia, i.e. NDRG1 associating with vesicles intended for specific membrane domains: While pNDRG1 was present in the outer part of the SLC and the abaxonal cytoplasm in myelinating Schwann cells, total NDRG1 localized to both the ad- and abaxonal parts. Unfortunately, attempts at localizing pNDRG1 in non-neural tissues were unsuccessful. Although the phospho-specific antibody gave strong signals from cultured Schwann cells and myelinating Schwann cells in paraffin sections, no signal was detected in other tissues by immunofluorescence (unpublished observations). As shown by Western blotting (Fig. 1 in paper I), the pNDRG1 levels in these tissues were low compared to the peripheral nerves. Thus, further optimization of the immunofluorescence protocol might be needed to localize the relatively low levels in non-neural tissues. Also note that the NDRG1 antibody used probably detect pNDRG1 to some extent, as discussed in paper I.

In cultured dog Schwann cells, pNDRG1 localized to centrosomes (Fig. 3C and D, see also Fig. 11 and 12 in paper I). The centrosome is the major microtubule-organizing center in the cell and mature into spindle poles during mitosis (178, 179). Cells lacking NDRG1 failed to form mitotic spindles (105) and developed centrosome amplification (121), thus NDRG1 exerts an important function at these sites. By proximity-ligation assay, NDRG1 was shown to associate with γ-tubulin and it was speculated if the protein sequesters γ-tubulin, by unknown mechanisms, to ensure that only the proper amount is available to synthesize the required number of centrosomes (121). The exact functions of NDRG1 related to the microtubule cytoskeleton remains to be determined, however, by interacting with γ-tubulin, NDRG1 might take part in nucleation of microtubules, e.g. serving as tracks for intracellular transport of vesicles.

Interestingly, emerging evidence indicates an important role for vesicular transport in the formation of spindle poles during mitosis (180). For example, RAB11-positive recycling endosomes bring microtubule-nucleating components, including γ-tubulin, to

the spindle poles (reviewed in (180, 181)). When the mitosis progresses, the recycling endosomes redistribute from the spindle pole to the cleavage furrow and contribute with membranes and proteins necessary for abscission during cytokinesis (180). The localization of RAB4a in the spindle poles and cleavage furrow (182) together with the presence of PtdIns(4)P-enriched organelles in the cleavage furrow and midbody (183, 184), may indicate some association between these molecules and NDRG1, which we also observed in these structures (Fig. 3C and D, see also Fig. 11 in paper I and (112)).

In many differentiating cells, the centrosome moves to the apical domain as the cell enters G_0, giving rise to a primary cilium (185). Here, the centrioles are called basal bodies and generate an axoneme (186). While the primary cilium is a non-motile structure, some cell types have evolved specialized structures deriving from the basal bodies, such as motile flagella in spermatozoa (186) and the light absorbing outer segment of retinal photoreceptors (187). Interestingly, a strong NDRG1 signal was present in the midpiece of developing spermatids (Fig. 3E, see also Fig. 5a in paper I). Triggered by the apparent association between NDRG1 and centrioles/basal bodies, we searched through a protein interaction library of the centrosome-cilium interface, generated by proximity-dependent biotin identification (BioID) (169). Remarkably, NDRG1 was among the proteins present in the transition zone of the centrosome, in both ciliated and non-ciliated cells (169). The transition zone is the proximal part of the axoneme and serves as a gate, controlling lipid and protein transport into the primary cilium (172, 188) (Fig. 3F). PtdIns(4)P is enriched in the plasma membrane of the primary cilium, and an association between NDRG1 and this phosphoinositide could potentially serve functional roles also in the transition zone.

NDRG1 is reported as a microtubule-associated protein (MAP) (105, 112). However, to the best of our knowledge, the microtubule-binding domain of the protein is not known. By comparing the protein sequence of NDRG1 to sequence motifs of known MAPs, we found the sequence RSH (189). This sequence is found in the C-terminal tandem repeats of NDRG1. As the phosphorylation site threonine 346 is within the tandem repeats, the phosphorylation status of the protein could conceivably influence the microtubule-binding properties of the protein. Supporting this, it was the phosphorylated form of the protein that we localized to centrosomes in cultured Schwann cells. Importantly, binding to microtubules does not exclude a vesicle-

associated role, as NDRG1 have several protein domains (119) and intracellular vesicles are transported along microtubules (177).

One of the aims of this study was to investigate whether AMP is a primary demyelinating or primary axonal neuropathy. Interestingly, no NDRG1 signal was observed in the axons or the neuronal cell bodies in the spinal cord and DRG. This was surprising, as axonal changes dominated in reports from *NDRG1*-associated neuropathy in Greyhounds (4) and a report from recent Alaskan Malamutes cases (2). In paper two, we performed a detailed investigation of changes in nerves and musculature from affected Alaskan Malamute dogs. Indeed, axonal loss was evident in semithin sections from all nerves examined and was reflected in denervation atrophy present in muscle biopsies. However, many of the remaining nerve fibers had thin myelin sheaths in relation to axonal size and were occasionally surrounded by small onion bulbs. Furthermore, in teased nerve fibers, intercalated internodes were present multifocally. These were spread along the nerve fibers and intermingled with longer internodes with thicker myelin sheaths. Wallerian-like axonal degeneration with fragmentation of the myelin sheath was only observed in a few fibers in a minority of examined nerves. Although onion bulbs can be observed in primary axonal neuropathies (24) and regenerated axons have short internodes, a neuropathy primarily affecting the Schwann cell and causing secondary axonal loss seems most likely based on the pattern of changes. This conclusion is further supported by the strong NDRG1 expression in Schwann cells and apparent lack of NDRG1 in axons by IHC.

Ultrastructurally, filamentous aggregates in the SLC and adaxonal cytoplasm were present, resembling inclusions observed in CMT4D in humans (8, 88, 96) and rodents with *NDRG1* mutations (7). Morphological appearance and previous reports suggested that the aggregates contained actin, and immunofluorescence supported this. The segmental actin aggregates in AMP nerves differed from the sparse amount of F-actin normally present in SLC (Fig. 9 in paper II). In humans, several publications report that actin-accumulations are specific for 4D subtype of CMT (75, 96). In dogs, accumulations of actin have also been reported from the adaxonal cytoplasm and inner part of SLC in nerves of Tibetan Mastiffs with Inherited Hypertrophic Neuropathy (22,

190, 191), and it would therefore be interesting to study if *NDRG1* is involved in the neuropathy of this breed as well.

Furthermore, focally folded myelin was often found in the AMP nerves. The term "tomacula" is frequently used to describe focal thickenings of the myelin sheath, giving a sausage-like appearance in teased fiber preparations, most commonly observed in HNPP (192). Although focally folded myelin, for example in CMT4B and CMT4B models (67), is sometimes described as tomaculae, we have chosen to use "focally folded myelin" about the changes present in AMP nerves, as they neither have the length nor the smooth external contour of typical tomacula (193). The folds were observed both external and internal to the myelin sheath, and often associated with SLC or paranodes (Fig. 7 in paper II).

In some instances, the folds derived from the inner part of the myelin sheath, and by intruding into the axon, seemingly divided the axon into several pockets. This resulted in the appearance of several axonal structures within one myelin sheath, separated by thin myelin septa (Fig. 8 in paper II). Aggregates of mitochondria were present in the axon in these segments, suggestive of disrupted axonal transport and early axonal degeneration (38). As the axonal diameters in the segments with focally folded myelin (Fig. 8 in paper II) and actin aggregates (Fig. 9 in paper II) were reduced, the axonal degeneration might be caused by constriction in a mechanism similar to the "demyelinative internal strangulation" observed in HNPP (71, 194). Although myelin outfoldings have been observed in CMT4D (4), the division of the axon into several pockets is not reported from human patients with *NDRG1* mutations, but was present in Greyhounds lacking NDRG1 (4).

Interestingly, intrusions from the filamentous regions of the Schwann cell caused subdivision of the axon in the neuropathic Tibetan Mastiffs mentioned previously (22), a change highly resembling that observed in AMP nerves. In contrast, several axonal pockets within one myelin sheath were described as axonal outfoldings in the recurrent laryngeal nerve of horses with laryngeal neuropathy (195). The equine recurrent laryngeal neuropathy is considered a distal axonopathy and the axonal outfoldings were suggested to be caused by disturbance in axonal transport (195, 196). Based on the other findings presented in this thesis, e.g. the focally folded myelin

and the localization of NDRG1, we consider it most likely that the division of the axon into pockets in AMP nerves is formed by infoldings from the Schwann cell and not the opposite, i.e. axonal outfoldings.

Focally folded myelin is present in several neuropathies caused by mutations in genes encoding phosphoinositide-associated proteins, such as *MTMR2*, *MTMR13, MTMR5, Pten* and *FGD4* (148, 149, 197-199). Mutations in the phosphoinositide 3-phosphatases *MTMR2* (myotubularin-related protein 2) and *MTMR13* (myotubularin-related protein 13) cause CMT4B1 and CMT4B2, respectively, in humans (200). Additionally, mutation in *MTMR13* was recently shown to cause a demyelinating neuropathy with abnormally folded myelin in Miniature Schnauzers (67). PTEN (phosphatase and tensin homologue) is a phosphatase that dephosphorylates PtdIns(3,4,5)P_3 to PtdIns(4,5)P_2 and PtdIns(3,4)P_2 to PtdIns(4)P (170), and knock-out of the protein in mice causes polyneuropathy. FGD4/FRABIN is a Cdc42-specific guanine nucleotide exchange factor (GEF), and mutations in the encoding gene are responsible for CMT4H (149). In general, the myelin folds usually arise from SLC and paranodes, which are considered the main sites of membrane addition (148, 149, 199). Furthermore, myelin fold formation is considered to represent a defect in myelin homeostasis rather than just initial myelination, as knock-out of FGD4 (149) or PTEN (199) in myelinated nerves of adult mice were sufficient for their formation. The myelin folds in the neuropathies mentioned above are hypothesized to be caused by dysregulated phosphoinositide levels in noncompact myelin, resulting in abnormal signaling and uncontrolled growth of the Schwann cell membranes (175, 199). As previously discussed, the different phosphoinositides are under strict spatial and temporal regulation as they participate in signaling pathways and recruit effector molecules (170, 176, 199). PtdIns(3,4,5)P_3 are known to promote actin polymerization by recruiting a variety of proteins necessary for F-actin assembly (reviewed in (171)). Thus, when PtdIns(3,4,5)P_3 is ectopically inserted into the apical membrane of epithelial cells, actin-rich membrane protrusions are formed (176). Similarly, in the *Pten*-mutant, abnormal PtdIns(3,4,5)P_3 level in the apical-like adaxonal domains of the myelinating Schwann cell led to actin-rich membrane protrusion as an initial step in the formation of myelin folds.

What could be the origin of the actin aggregates in the SLC and adaxonal cytoplasm of mutant Alaskan Malamute nerves? In contrast to PtdIns(3,4,5)P_3, the link between

actin polymerization and PtdIns(4)P is not well established (201). However, in a recent paper, mice lacking phosphatidylinositol 4-kinase alpha (PI4KA), one of the kinases responsible for production of PtdIns(4)P, developed thinly myelinated nerve fibers and focally folded myelin. Furthermore, aggregates of actin were present in the nerves (201). Therefore, spatial and temporal regulation of PtdIns(4)P also seems important to avoid aberrant actin polymerization and formation of myelin folds. Thus, we speculate if the actin-aggregates observed in AMP nerves represent an early step in the events leading to focally folded myelin. Based on the interaction between NDRG1 and PtdIns(4)P, deranged PtdIns(4)P levels in the apical-like membrane domains of adaxonal cytoplasm and SLC could lead to the actin aggregates and uncontrolled membrane growth (Fig. 4) through a mechanism similar to that observed in the *Pten*-mutant.

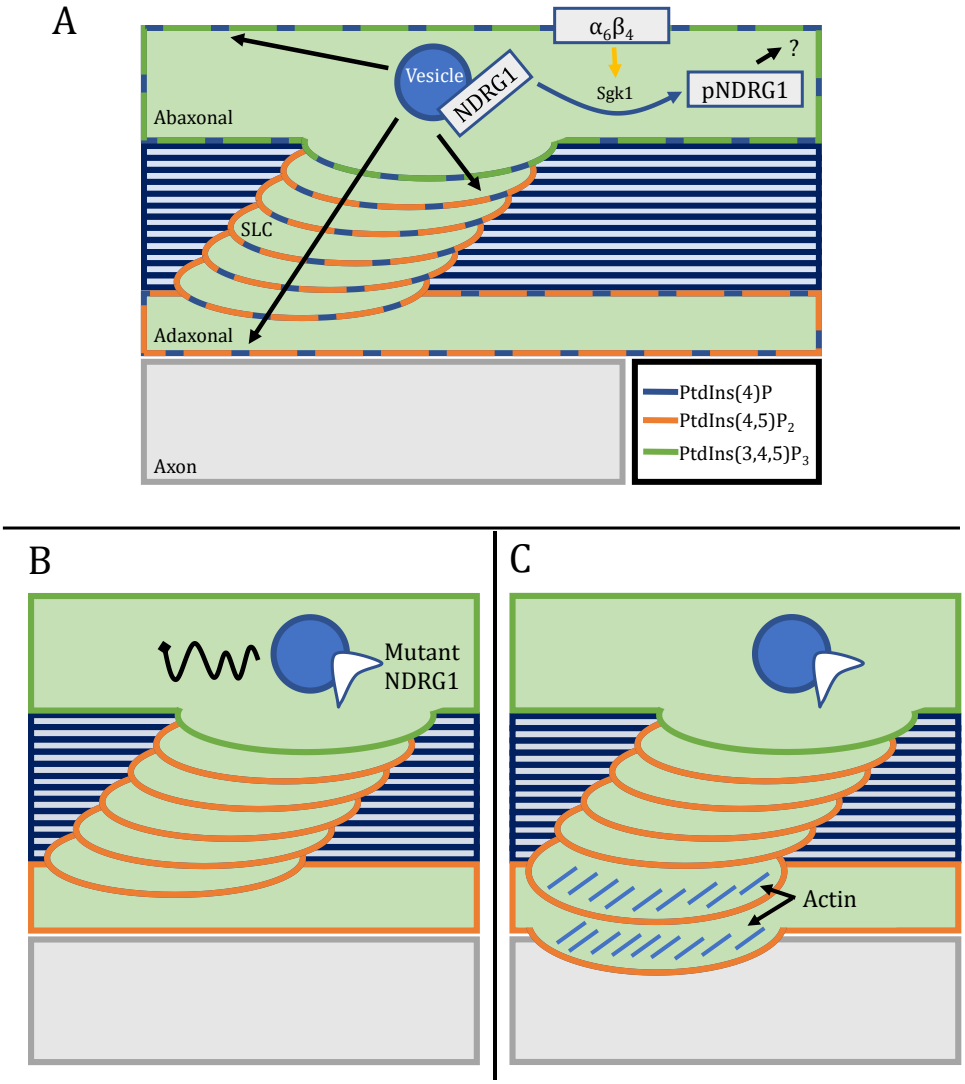

Figure 4. Hypothesis for the formation of actin aggregates and myelin infoldings in AMP nerves, for details see text. (A) In healthy nerves, NDRG1 binds to PtdIns(4)P in the membrane of recycling endosomes and participates in vesicular transport to the plasma membrane. (B) In AMP nerves, normal vesicular recycling is disrupted. (C) This leads to changes in the normal membrane domain composition, including reduction in PtdIns(4)P levels in the plasma membrane. The deranged phosphoinositide levels trigger actin polymerization, formation of actin-rich membrane protrusions, and, eventually, formation of myelin folds.

Focally folded myelin represents focal hypermyelination. Interestingly, mice lacking serum glucocorticoid kinase 1 (Sgk1), the kinase responsible for phosphorylation of NDRG1 at threonine 346, exhibited diffusely hypermyelinated nerves. While the role of NDRG1 in this process was not investigated, it was speculated that the

hypermyelination could be caused by reduced phosphorylation of NDRG1 (202). The signaling cascade activating Sgk1 in Schwann cells is stimulated by abaxonal laminin-integrin signaling (202), consistent with the abaxonal enrichment of pNDRG1 that we observed (Fig. 8 and 9 in paper I). As discussed in paper II, we did not observe decreased g-ratios in AMP nerves, as would be expected from diffuse hypermyelination. However, this does not rule out focal hypermyelination, as most fibers with focally folded myelin are represented in a transverse section as a fiber with normal myelination. Thus, one possibility that needs further investigation is whether the *NDRG1* mutation disrupts signaling in the Schwann cells by affecting the phosphorylation of the protein, either directly (mutant NDRG1 fails to interact properly with Sgk1) or indirectly (reduced levels of pNDRG1 as a result of the overall reduced NDRG1 levels), eventually resulting in the focal hypermyelination observed.

The nerves of *NDRG1*$^{mut/mut}$ Alaskan Malamutes had significantly reduced levels of NDRG1 and pNDRG1 compared to controls, while the mRNA levels were not significantly altered. In contrast, Greyhounds with *NDRG1*-associated neuropathy had decreased mRNA levels and no NDRG1 protein was detected (4). Could this explain differences in phenotype between the breeds? In human CMT4D patients, two individuals with different missense mutations in the gene had a later age of onset compared to those with nonsense mutations (91), and in rodent models even low levels of normal NDRG1 protein (*Ndrg1* KO) gave a less severe phenotype than total NDRG1 deficiency (*str* mice) (7). Thus, the earlier age of onset and predominantly axonal changes at the time of biopsy in Greyhounds (2, 4), might reflect a more rapid Schwann cell degeneration and onset of axonal degeneration compared to the Alaskan Malamutes. Furthermore, other mutations causing amino acid substitutions in the α/β hydrolase fold of NDRG1 resulted in direct functional changes (91). Therefore, combined functional changes and low NDRG1 levels, resulting from regulation at the translational level or posttranslational degradation, probably contribute to the pathogenesis in AMP. Both proteasomal and autophagic pathways were involved in the degradation of the mutant NDRG1 protein in CMT4D caused by missense mutations (91).

Even though NDRG1 is found in a wide range of tissues, changes reported from humans, dogs and rodents with *NDRG1* mutations is restricted to the peripheral (2, 4,

7, 8), and to a lesser degree, the central nervous system (94, 97). One explanation for this is functional redundancy, whereby other proteins compensate for the loss of NDRG1 function. For example, it was suggested that NDRG4 could compensate for loss of central nervous, but not peripheral, NDRG1 (203). Secondly, both production and maintenance of the myelin sheath are metabolic challenges (168). During myelination, each oligodendrocyte synthesizes 1500 protein molecules and several thousand new lipid molecules per second (168). Little information is available regarding myelin turnover in the peripheral nervous system, but it is assumed to be substantial (168). With the increased internodal length concurring with somatic growth, resulting in internodal lengths near two millimeters, the myelinating Schwann cells must have an efficient machinery for intracellular transport, conceivably making the Schwann cell extremely vulnerable to aberrations in intracellular trafficking. This is further highlighted by defects in vesicular transport as a common disease mechanism in several demyelinating neuropathies (reviewed in (200)). Last, but not least, the close relationship between the Schwann cell and axon, enabling the cells to have a remarkable physiology and anatomy in health, also means that defects at either side in disease will affect the other. It is suggested that "no myelin is better than bad myelin" (204). Thus, defective NDRG1 function in Schwann cells results in demyelination, secondary axonal degeneration, and eventually, nerve fiber loss and overt clinical signs of neuropathy.

Prion protein

In paper III, we investigated the peripheral nerves of goats lacking PrP^C. In contrast to the Alaskan Malamutes, the basis for the study was not clinical signs of neuropathy, but rather studies from *Prnp*$^{-/-}$ mice suggesting a role for PrP^C in myelin maintenance (9, 144).

Indeed, a demyelinating neuropathy was found in goats lacking PrP^C. In teased nerve fibers from *PRNP*$^{Ter/Ter}$ goats, intercalated internodes were found frequently and demyelinated segments were also observed. As some age-related changes are expected in older animals, we quantified the changes and found statistically significant differences between the genotypes. Most of the intercalated internodes were single, remyelinated internodes between two internodes of normal thickness and length, probably resulting from remyelination secondary to paranodal demyelination.

Furthermore, long paranodal outfoldings were present around some of these intercalated internodes, resembling sites of focally folded myelin observed in mice lacking PrP^C (9). The paranodal demyelination and paranodal outfoldings, with less frequent breakdown of the whole internode, suggest a problem in maintaining the integrity of the paranodes. At the ultrastructural level, intramyelinic edema and splitting along the intraperiod line, as well as swelling of the cytoplasm of the Schwann cells, were found. A similar change, vacuolated fibers with thin myelin sheaths were observed in *Prnp*$^{-/-}$ mice (144).

As discussed earlier, focally folded myelin is associated with disrupted myelin maintenance, and usually arise from the noncompact myelin in paranodes and SLC. In contrast to the myelin folds in AMP nerves, focally folded myelin was only detected paranodally in the nerves of *PRNP*$^{Ter/Ter}$ goats. Furthermore, some of the paranodal outfoldings included both the myelin sheath and axon, and thus differed from those present in AMP nerves. As mentioned, disturbance in the membrane domains of the Schwann cell has been hypothesized as one mechanism for formation of myelin folds (199). In an analysis of myelin proteins from mice lacking PrP^C, an increased abundance of septin 9 was found compared to wild type mice (36). Furthermore, septin 9, associated with membranous structures and intracellular vesicles, was restricted to the abaxonal cytoplasm in the wild type mice, but also present in the SLC of mutant mice. This is interesting, as septins form barriers that prevent diffusion of membrane proteins between different membrane domains (205) and therefore participate in separation of myelin compartments, such as compact and noncompact myelin (206). Therefore, disturbance in the membrane domains of the Schwann cell could conceivably be relevant for the myelin folds in goats lacking PrP^C as well. In paper III, we also discussed the possible involvement of membrane junctions. As PrP^C was necessary for the stability of cell junctions (reviewed in (207)), PrP^C deficiency could result in destabilization of autotypic adherens junctions in the paranodes and SLC. Another possibility could be an immune-mediated event aggravating the neuropathy, seen in some hereditary neuropathies (208), as molecules present in the node of Ranvier are frequent targets in inflammatory neuropathies (48) and dysmorphic paranodes were observed in immune-mediated polyradiculoneuropathies (61).

An increased number of both Iba1+ macrophages and CD3+ T-lymphocytes were present in the endoneurium of goats lacking PrP^C. In *Prnp*$^{-/-}$ mice, an increased number of macrophages, phagocytosing myelin debris, was present in the nerves, but no increase in CD3 staining was observed (9). Infiltration and/or proliferation of macrophages are expected in neuropathies (21), but we questioned whether the lymphocytes we observed were simply attracted by the disease process or actually a part of the pathogenesis. We did not detect macrophage-mediated myelin stripping, a hallmark of inflammatory demyelinating neuropathies (48). Intriguingly, in the neuropathic Alaskan Malamutes, increased Iba1 staining, but not CD3, were observed. As a systemic immunological imbalance has been observed in both mice and goats lacking PrP^C (reviewed in (136)), it cannot be ruled out that the leukocytes observed participate in the disease process. However, further investigations are needed, for example, by examining nerves from younger goats to see if infiltration of leukocytes precedes the demyelination.

It was suggested that axonal, and not Schwann cell-expressed, PrP^C was necessary for maintenance of the myelin sheath (9). By immunofluorescence, we detected PrP^C in the Schwann cell cytoplasm and compact myelin, and not the axon. This could be due to the axonal levels being below the detection threshold in the method used. However, from our data it cannot be ruled out that PrP^C expressed in the Schwann cell is important for myelin maintenance.

Some phenotypes observed in mice initially ascribed to lack of PrP^C were later shown to be caused by genetic confounders. To address this issue, we investigated the *PRNP*^{Ter} haplotype. The *PRNP*$^{Ter/Ter}$ goats are completely homozygous in a region consisting of 2.5 MB surrounding the *PRNP* gene. Furthermore, reduced MAF (minimum allele frequency) is found in a region consisting of 6.3 MB, meaning that genes located in this wider region have increased linkage to the *PRNP*^{Ter} allele. *SIRP-α* is located outside this region, thus the demyelinating phenotype in *PRNP*$^{Ter/Ter}$ goats is not caused by defects in this gene. This is interesting as one phenotype observed in *Prnp*$^{-/-}$ mice was later shown to be caused by polymorphisms in the *SIRP-α* gene (153).

No overt clinical or electrophysiological signs of neuropathy were observed, even though, as discussed earlier, the electrophysiological methods employed might not

have been sensitive enough. The neuropathy was progressive, as the changes were most pronounced in the oldest goats. Although the goats were old when compared to normal husbandry practice, a goat can get much older. Thus, it would be interesting to see if electrophysiological and clinical signs of neuropathy arise when they get even older.

In the work presented in this thesis, we have investigated the roles of NDRG1 and PrP^C in maintaining healthy peripheral nerves by using Alaskan Malamutes with *NDRG1* mutations and goats devoid of PrP^C. Both proteins have been extensively studied, but their functions are still largely unknown. Interestingly, both NDRG1 and PrP^C are ubiquitously expressed, but the major phenotype described from different species lacking (or with severely reduced levels of) the proteins is a demyelinating neuropathy. Based on the morphological studies presented in this thesis, we suggest that both NDRG1 and PrP^C are important for maintaining the polarized phenotype of myelinating Schwann cells, and disruption of these functions causes demyelination with focally folded myelin. This hypothesis might serve as a basis for further investigations to clarify more in detail the functions of these enigmatic proteins.

Conclusions

- The localization of NDRG1 varies between cell types and is influenced by signaling events causing phosphorylation of the protein.
- The localization of NDRG1 is consistent with its reported role in intracellular vesicular trafficking, but the protein also localizes to microtubular structures in the centrosomes, primary cilium and spermatid flagellum.
- NDRG1 is expressed in the Schwann cells in peripheral nerves of dogs. Phosphorylated NDRG1 is restricted to the abaxonal cytoplasm and outer part of SLC. No signal was detected in the axon.
- The missense mutation in *NDRG1* results in low levels of NDRG1 and pNDRG1 in the nerves of affected Alaskan Malamutes (by WB). In contrast, the levels of *NDRG1* mRNA were not significantly different between the genotypes (by RT-qPCR), suggesting that the low protein levels in mutant dogs is due to regulation at the translational level or posttranslational degradation. The abaxonal pNDRG1 signal was not observed in an affected Alaskan Malamute (by IF), indicating that the mutation might disrupt signaling in myelinating Schwann cells.
- The changes in the AMP nerves are consistent with a primary demyelinating polyneuropathy and characterized by actin aggregates and focally folded myelin, with secondary axonal degeneration. We have hypothesized that these changes arise following aberrant vesicular trafficking resulting in disrupted maintenance of membrane domains.
- Goats lacking PrP^{C} develop a demyelinating polyneuropathy, and the homozygous region surrounding the *PRNP*^{Ter} allele is short compared to those observed in some *Prnp*$^{-/-}$ mice. This strongly suggests a role for PrP^{C} in myelin maintenance.
- While the peripheral nerve lipid composition of young goats was not significantly different between the genotypes, a difference was found in adult goats, suggestive of a progressive neuropathy.
- Paranodal outfoldings and vacuolated nerve fibers with myelin splitting were found in the nerves of goats lacking PrP^{C}. Similar changes have been observed in rodent models. We have suggested that these could result from disrupted

PrP^C function in membrane junctions or barriers separating membrane domains in myelinating Schwann cells.

Future perspectives

- The subcellular localization of NDRG1 is highly dynamic and complex. To get a better understanding of the function of this protein, it would be interesting to study its interaction partners in different situations, for example during the cell cycle, by BioID (proximity-dependent biotin identification).
- Investigate in primary Schwann cell culture if distribution of RAB4a-positive endosomes differs between cultures derived from *NDRG1*$^{wt/wt}$ and *NDRG1*$^{mut/mut}$ Alaskan Malamutes. By using Schwann cell-DRG cocultures, this can be further assessed in myelinating Schwann cells.
- To get a better understanding of the function of NDRG1 and PrP^{C} in myelinating Schwann cells, the protein localization could be assessed by cryo-immunoelectron microscopy.
- To assess the functionality of mutant NDRG1, uptake of LDL in cell cultures can be investigated.
- To understand how the mutant NDRG1 is degraded, cell cultures could be treated with MG132 and 3-methyladenine, which inhibits the proteasome and autophagy, respectively.
- X-ray crystallography of the mutant NDRG1-protein could be used to investigate if the mutation affects the three-dimensional structure of the protein.
- Oligodendrocytes also have a massive production of lipids and proteins to the myelin sheath. By MRI, white matter changes were described in two case reports from human CMT4D patients (94, 97). No abnormalities were found in an MRI study of one affected Alaskan Malamute (unpublished observations). However, it would be interesting to see if histopathological changes are evident in the CNS of affected Alaskan Malamutes and goats lacking PrP^{C}, respectively.
- Differences in the lipid composition of peripheral nerves were observed in Alaskan Malamutes of the two genotypes. To investigate if some of the differences are directly related to NDRG1, the lipid composition in homozygous mutant and wild type Schwann cell cultures, respectively, could be assessed.

- To further address the role of immune cells in demyelination caused by lack of prion protein, one could examine the nerves of younger goats to see if the infiltration precedes demyelination.
- Furthermore, older goats could be examined to see if the neuropathy progresses into a clinical detectable neuropathy.
- Both NDRG1 and PrP^{C} have been suggested to participate in signaling pathways in Schwann cells: pNDRG1 in laminin-integrin signaling abaxonally, PrP^{C} in signaling between the axon and Schwann cell adaxonally. This signaling could be investigated in Schwann cell-DRG cocultures. For example, by coculturing DRGs from *PRNP*$^{Ter/Ter}$ goats with Schwann cells from *PRNP*$^{+/+}$ goats and vice versa. Furthermore, the stimuli leading to phosphorylation of NDRG1 in Schwann cells could be explored by culturing Schwann cells in dishes with and without laminin-coating.

References

1. Moe L. Hereditary polyneuropathy of Alaskan malamutes. In: Kirk R, Bonagura J, editors. Kirks Current Veterinary Therapy. XI ed. St. Louis, Missouri: Saunders 1992. p. 1038-9.
2. Bruun CS, Jaderlund KH, Berendt M, Jensen KB, Spodsberg EH, Gredal H, et al. A Gly98Val mutation in the N-Myc downstream regulated gene 1 (NDRG1) in Alaskan Malamutes with polyneuropathy. PLoS One. 2013;8(2):e54547.
3. Kalaydjieva L, Gresham D, Gooding R, Heather L, Baas F, de Jonge R, et al. N-myc downstream-regulated gene 1 is mutated in hereditary motor and sensory neuropathy-Lom. Am J Hum Genet. 2000;67(1):47-58.
4. Drogemuller C, Becker D, Kessler B, Kemter E, Tetens J, Jurina K, et al. A deletion in the N-myc downstream regulated gene 1 (NDRG1) gene in Greyhounds with polyneuropathy. PLoS One. 2010;5(6):e11258.
5. Jäderlund KH, Rohdin C, Berendt M, Stigen Ø, Fredholm M, Espenes A, et al. Re-emergence of hereditary polyneuropathy in Scandinavian Alaskan malamute dogs—old enemy or new entity? A case series. Acta Vet Scand. 2017;59(1):26.
6. Kalaydjieva L, Nikolova A, Turnev I, Petrova J, Hristova A, Ishpekova B, et al. Hereditary motor and sensory neuropathy--Lom, a novel demyelinating neuropathy associated with deafness in gypsies. Clinical, electrophysiological and nerve biopsy findings. Brain. 1998;121 (Pt 3):399-408.
7. King RH, Chandler D, Lopaticki S, Huang D, Blake J, Muddle JR, et al. Ndrg1 in development and maintenance of the myelin sheath. Neurobiol Dis. 2011;42(3):368-80.
8. King RH, Tournev I, Colomer J, Merlini L, Kalaydjieva L, Thomas PK. Ultrastructural changes in peripheral nerve in hereditary motor and sensory neuropathy-Lom. Neuropathol Appl Neurobiol. 1999;25(4):306-12.
9. Bremer J, Baumann F, Tiberi C, Wessig C, Fischer H, Schwarz P, et al. Axonal prion protein is required for peripheral myelin maintenance. Nat Neurosci. 2010;13(3):310-8.
10. Benestad SL, Austbo L, Tranulis MA, Espenes A, Olsaker I. Healthy goats naturally devoid of prion protein. Vet Res. 2012;43:87.
11. Malachin G, Reiten MR, Salvesen Ø, Aanes H, Kamstra JH, Skovgaard K, et al. Loss of prion protein induces a primed state of type I interferon-responsive genes. PLoS One. 2017;12(6):e0179881.
12. Salvesen Ø, Reiten MR, Espenes A, Bakkebo MK, Tranulis MA, Ersdal C. LPS-induced systemic inflammation reveals an immunomodulatory role for the prion protein at the blood-brain interface. J Neuroinflammation. 2017;14(1):106.
13. Salvesen Ø, Reiten MR, Kamstra JH, Bakkebo MK, Espenes A, Tranulis MA, et al. Goats without prion protein display enhanced proinflammatory pulmonary signaling and extracellular matrix remodeling upon systemic lipopolysaccharide challenge. Front Immunol. 2017;8:1722.
14. Reiten MR, Bakkebo MK, Brun-Hansen H, Lewandowska-Sabat AM, Olsaker I, Tranulis MA, et al. Hematological shift in goat kids naturally devoid of prion protein. Front Cell Dev Biol. 2015;3:44.
15. Brodal P. Det autonome nervesystemet. Sentralnervesystemet. 5th ed. Oslo: Universitetsforlaget; 2013. p. 435.

16. Junqueira LC, Carneiro J. Nerve Tissue & the Nervous System. Basic Histology. 11 ed. New York: McGraw-Hill; 2005. p. 153-81.
17. Gardner E, Bunge RP. Gross Anatomy of the Peripheral Nervous System. In: Dyck PJ, Thomas PK, Lambert EH, Bunge R, editors. Peripheral neuropathy. vol. 1. 2nd ed. Philadelphia: WB Saunders; 1984. p. 11-38.
18. Thomas PK, Olsson Y. Microscopic Anatomy and Function of the Connective Tissue Components of Peripheral Nerve. In: Dyck PJ, Thomas PK, Lambert EH, Bunge R, editors. Peripheral neuropathy. vol. 1. 2nd ed. Philadelphia: WB Saunders; 1984. p. 97-120.
19. Ochoa J, Mair WG. The normal sural nerve in man. I. Ultrastructure and numbers of fibres and cells. Acta Neuropathol. 1969;13(3):197-216.
20. Oldfors A. Macrophages in peripheral nerves. Acta Neuropathol. 1980;49(1):43-9.
21. Bilbao JM, Schmidt RE. Normal Anatomy of the Peripheral (Sural) Nerve. Biopsy Diagnosis of Peripheral Neuropathy. Cham: Springer International Publishing; 2015. p. 21-41.
22. Summers BA, Cummings JF, DeLahunta A. Diseases of the Peripheral Nervous System. Veterinary Neuropathology. St. Louis, Mo: Mosby; 1995. p. 402-501.
23. Weller RO, Cervós-Navarro J. Normal Peripheral Nerves. Pathology of Peripheral Nerves. London: Butterworths; 1977. p. 30-60.
24. Bilbao JM, Schmidt RE. Schwann Cells and Myelin in the Peripheral Nervous System. Biopsy Diagnosis of Peripheral Neuropathy. Cham: Springer International Publishing; 2015. p. 85-109.
25. Thomas PK, Ochoa J. Microscopic Anatomy of Peripheral Nerve Fibers. In: Dyck PJ, Thomas PK, Lambert EH, Bunge R, editors. Peripheral neuropathy. vol. 1. 2nd ed. Philadelphia: WB Saunders; 1984. p. 39-96.
26. Tricaud N. Myelinating Schwann Cell Polarity and Mechanically-Driven Myelin Sheath Elongation. Front Cell Neurosci. 2017;11:414.
27. Vizoso AD, Young JZ. Internode length and fibre diameter in developing and regenerating nerves. J Anat. 1948;82(Pt 1-2):110-34.1.
28. Friede RL, Bischhausen R. The precise geometry of large internodes. J Neurol Sci. 1980;48(3):367-81.
29. Vizoso AD. The relationship between internodal length and growth in human nerves. J Anat. 1950;84(4):342-53.
30. Manzano GM, Giuliano LM, Nobrega JA. A brief historical note on the classification of nerve fibers. Arq Neuropsiquiatr. 2008;66(1):117-9.
31. Lorenz MD, Coates JR, Kent M. Tetraparesis, Hemiparesis, and Ataxia. In: Lorenz MD, Coates JR, Kent M, editors. Handbook of Veterinary Neurology. 5th ed. Saint Louis: W.B. Saunders; 2011. p. 162-249.
32. Garbay B, Heape AM, Sargueil F, Cassagne C. Myelin synthesis in the peripheral nervous system. Prog Neurobiol. 2000;61(3):267-304.
33. Chrast R, Saher G, Nave K-A, Verheijen M. Lipid metabolism in myelinating glial cells: Lessons from human inherited disorders and mouse models. J Lipid Res. 2010;52:419-34.
34. Nave KA, Werner HB. Myelination of the nervous system: mechanisms and functions. Annu Rev Cell Dev Biol. 2014;30:503-33.
35. Kursula P. Structural properties of proteins specific to the myelin sheath. Amino Acids. 2008;34(2):175-85.

36. Patzig J, Jahn O, Tenzer S, Wichert SP, de Monasterio-Schrader P, Rosfa S, et al. Quantitative and integrative proteome analysis of peripheral nerve myelin identifies novel myelin proteins and candidate neuropathy loci. J Neurosci. 2011;31(45):16369-86.
37. Cantile C, Youssef S. Nervous System. In: Maxie MG, editor. Jubb, Kennedy & Palmer's Pathology of Domestic Animals. vol. 1. 6th ed. Edinburgh: W.B. Saunders; 2016. p. 250-406.
38. Weller RO, Cervós-Navarro J. General Pathology of Peripheral Nerves. Pathology of Peripheral Nerves. London: Butterworths; 1977. p. 61-89.
39. Ballin RHM, Thomas PK. Changes at the Nodes of Ranvier during Wallerian Degeneration: an Electron Microscope Study. Acta Neuropathol. 1969;14(3):237-49.
40. Williams PL, Hall SM. Prolonged in vivo observations of normal peripheral nerve fibres and their acute reactions to crush and deliberate trauma. J Anat. 1971;108(Pt 3):397-408.
41. Jung J, Cai W, Lee HK, Pellegatta M, Shin YK, Jang SY, et al. Actin polymerization is essential for myelin sheath fragmentation during Wallerian degeneration. J Neurosci. 2011;31(6):2009-15.
42. Bilbao JM, Schmidt RE. The Axon: Normal Structure and Pathological Alterations. Biopsy Diagnosis of Peripheral Neuropathy. Cham: Springer International Publishing; 2015. p. 51-84.
43. Spencer PS, Schaumburg HH. Experimental Models of Primary Axonal Disease Induced by Toxic Chemicals. In: Dyck PJ, Thomas PK, Lambert EH, Bunge R, editors. Peripheral neuropathy. vol. 1. 2nd ed. Philadelphia: WB Saunders; 1984. p. 636-49.
44. Fullerton PM, Barnes JM. Peripheral neuropathy in rats produced by acrylamide. Br J Ind Med. 1966;23(3):210-21.
45. Spencer PS, Thomas PK. Ultrastructural studies of the dying-back process II. The sequestration and removal by Schwann cells and oligodendrocytes of organelles from normal and diseased axons. J Neurocytol. 1974;3(6):763-83.
46. Windebank AJ, Dyck PJ. Lead Intoxication As a Model of Primary Segmental Demyelination. In: Dyck PJ, Thomas PK, Lambert EH, Bunge R, editors. Peripheral neuropathy. vol. 1. 2nd ed. Philadelphia: WB Saunders; 1984. p. 650-65.
47. Vallat J-M, Anthony D, de Girolami U. Pathology of Peripheral Nerve. In: Escourolle R, Gray Fo, De Girolami U, Gray Fo, Duyckaerts C, editors. Escourolle & Poirier's Manual of Basic Neuropathology. 5th. Oxford: Oxford University Press; 2014. p. 313-42.
48. Bilbao JM, Schmidt RE. The Inflammatory Demyelinating Neuropathies. Biopsy Diagnosis of Peripheral Neuropathy. Cham: Springer International Publishing; 2015. p. 161-96.
49. Nave KA. Myelination and the trophic support of long axons. Nat Rev Neurosci. 2010;11(4):275-83.
50. Taveggia C. Schwann cells-axon interaction in myelination. Curr Opin Neurobiol. 2016;39:24-9.
51. Simons M, Trotter J. Wrapping it up: the cell biology of myelination. Curr Opin Neurobiol. 2007;17(5):533-40.
52. Küffer A, Lakkaraju AK, Mogha A, Petersen SC, Airich K, Doucerain C, et al. The prion protein is an agonistic ligand of the G protein-coupled receptor Adgrg6. Nature. 2016;536(7617):464.
53. Lopez-Leal R, Alvarez J, Court FA. Origin of Axonal Proteins: Is the Axon-Schwann Cell Unit a Functional Syncytium? Cytoskeleton. 2016;73(10):629-39.

54. Ohno N, Sakoh T, Saitoh Y, Terada N, Ohno S. Schwann Cell–Axon Interactions: The Molecular and Metabolic Link Between Schwann Cells and Axons. In: Sango K, Yamauchi J, editors. Schwann Cell Development and Pathology. Tokyo: Springer Japan; 2014. p. 47-67.
55. Bilbao JM, Schmidt RE. Peripheral Neuropathy and the Role of Nerve Biopsy. Biopsy Diagnosis of Peripheral Neuropathy. Cham: Springer International Publishing; 2015. p. 1-20.
56. Cuddon PA. Acquired canine peripheral neuropathies. Vet Clin North Am Small Anim Pract. 2002;32(1):207-49.
57. Faissler D, Jurina K, Cauzinille L, Gaschen F, Adamo F, Jaggy A. Peripheral Nervous System and Musculature. In: Jaggy A, Platt SR, editors. Small animal neurology: an illustrated text. Hannover: Schlütersche Verlagsgesellschaft mbH & Co. KG; 2010. p. 271-331.
58. Bilbao JM, Schmidt RE. Toxic Neuropathies. Biopsy Diagnosis of Peripheral Neuropathy. Cham: Springer International Publishing; 2015. p. 355-74.
59. Sundar R, Jeyasekharan AD, Pang B, Soong RC, Kumarakulasinghe NB, Ow SG, et al. Low Levels of NDRG1 in Nerve Tissue Are Predictive of Severe Paclitaxel-Induced Neuropathy. PLoS One. 2016;11(10):e0164319.
60. Fadia M, Shroff S, Simpson E. Immune-Mediated Neuropathies. Curr Treat Options Neurol. 2019;21(6):28.
61. Gross S, Fischer A, Rosati M, Matiasek L, Corlazzoli D, Cappello R, et al. Nodo-paranodopathy, internodopathy and cleftopathy: Target-based reclassification of Guillain-Barré-like immune-mediated polyradiculoneuropathies in dogs and cats. Neuromuscul Disord. 2016;26(12):825-36.
62. Baiardi S, Redaelli V, Ripellino P, Rossi M, Franceschini A, Moggio M, et al. Prion-related peripheral neuropathy in sporadic Creutzfeldt-Jakob disease. J Neurol Neurosurg Psychiatry. 2019;90(4):424-7.
63. Mead S, Gandhi S, Beck J, Caine D, Gallujipali D, Carswell C, et al. A novel prion disease associated with diarrhea and autonomic neuropathy. N Engl J Med. 2013;369(20):1904-14.
64. Granger N. Canine inherited motor and sensory neuropathies: an updated classification in 22 breeds and comparison to Charcot-Marie-Tooth disease. Vet J. 2011;188(3):274-85.
65. Timmerman V, Strickland AV, Zuchner S. Genetics of Charcot-Marie-Tooth (CMT) Disease within the Frame of the Human Genome Project Success. Genes. 2014;5(1):13-32.
66. Becker D, Minor KM, Letko A, Ekenstedt KJ, Jagannathan V, Leeb T, et al. A GJA9 frameshift variant is associated with polyneuropathy in Leonberger dogs. BMC Genomics. 2017;18(1):662.
67. Granger N, Lujan Feliu-Pascual A, Spicer C, Ricketts S, Hitti R, Forman O, et al. Charcot-Marie-Tooth type 4B2 demyelinating neuropathy in miniature Schnauzer dogs caused by a novel splicing SBF2 (MTMR13) genetic variant: a new spontaneous clinical model. PeerJ. 2019;7:e7983.
68. Barreto LCLS, Oliveira FS, Nunes PS, de França Costa IMP, Garcez CA, Goes GM, et al. Epidemiologic Study of Charcot-Marie-Tooth Disease: A Systematic Review. Neuroepidemiology. 2016;46(3):157-65.
69. Braathen GJ, Sand JC, Lobato A, Hoyer H, Russell MB. Genetic epidemiology of Charcot-Marie-Tooth in the general population. Eur J Neurol. 2011;18(1):39-48.

70. Saporta ASD, Sottile SL, Miller LJ, Feely SME, Siskind CE, Shy ME. Charcot-Marie-Tooth disease subtypes and genetic testing strategies. Ann Neurol. 2011;69(1):22-33.
71. Bilbao JM, Schmidt RE. Genetically Determined Neuropathies. Biopsy Diagnosis of Peripheral Neuropathy. Cham: Springer International Publishing; 2015. p. 375-428.
72. Harding AE, Thomas PK. The clinical features of hereditary motor and sensory neuropathy types I and II. Brain. 1980;103(2):259-80.
73. Harding AE, Thomas PK. Genetic aspects of hereditary motor and sensory neuropathy (types I and II). J Med Genet. 1980;17(5):329-36.
74. Bradley WG, Madrid R, Davis CJF. The peroneal muscular atrophy syndrome: Clinical, genetic, electrophysiological and nerve biopsy studies part 3. Clinical, electrophysiological and pathological correlations. J Neurol Sci. 1977;32(1):123-36.
75. Tazir M, Hamadouche T, Nouioua S, Mathis S, Vallat J-M. Hereditary motor and sensory neuropathies or Charcot–Marie–Tooth diseases: An update. J Neurol Sci. 2014;347(1):14-22.
76. Mathis S, Goizet C, Tazir M, Magdelaine C, Lia AS, Magy L, et al. Charcot-Marie-Tooth diseases: an update and some new proposals for the classification. J Med Genet. 2015;52(10):681-90.
77. Bergoffen J, Scherer SS, Wang S, Scott MO, Bone LJ, Paul DL, et al. Connexin mutations in X-linked Charcot-Marie-Tooth disease. Science. 1993;262(5142):2039-42.
78. Niemann A, Berger P, Suter U. Pathomechanisms of mutant proteins in Charcot-Marie-Tooth disease. Neuromolecular Med. 2006;8(1-2):217-42.
79. Shy ME, Patzko A. Axonal Charcot-Marie-Tooth disease. Curr Opin Neurol. 2011;24(5):475-83.
80. Shy ME. Charcot-Marie-Tooth disease: an update. Curr Opin Neurol. 2004;17(5):579-85.
81. Züchner S, Mersiyanova IV, Muglia M, Bissar-Tadmouri N, Rochelle J, Dadali EL, et al. Mutations in the mitochondrial GTPase mitofusin 2 cause Charcot-Marie-Tooth neuropathy type 2A. Nat Genet. 2004;36(5):449-51.
82. Coates JR, O'Brien DP. Inherited peripheral neuropathies in dogs and cats. Vet Clin North Am Small Anim Pract. 2004;34(6):1361-401.
83. Shelton GD, Podell M, Poncelet L, Schatzberg S, Patterson E, Powell HC, et al. Inherited polyneuropathy in Leonberger dogs: a mixed or intermediate form of Charcot-Marie-Tooth disease? Muscle Nerve. 2003;27(4):471-7.
84. Ekenstedt KJ, Becker D, Minor KM, Shelton GD, Patterson EE, Bley T, et al. An ARHGEF10 Deletion Is Highly Associated with a Juvenile-Onset Inherited Polyneuropathy in Leonberger and Saint Bernard Dogs. PLoS genetics. 2014;10(10):e1004635.
85. Kalaydjieva L, Hallmayer J, Chandler D, Savov A, Nikolova A, Angelicheva D, et al. Gene mapping in Gypsies identifies a novel demyelinating neuropathy on chromosome 8q24. Nat Genet. 1996;14(2):214-7.
86. Chen B, Niu S, Chen N, Pan H, Wang X, Zhang Z. A novel homozygous NDRG1 mutation in a Chinese patient with Charcot-Marie-Tooth disease 4D. J Clin Neurosci. 2018;53:231-4.
87. Merlini L, Villanova M, Sabatelli P, Trogu A, Malandrini A, Yanakiev P, et al. Hereditary motor and sensory neuropathy Lom type in an Italian Gypsy family. Neuromuscul Disord. 1998;8(3-4):182-5.
88. Baethmann M, Göhlich-Ratmann G, Schröder JM, Kalaydjieva L, Voit T. HMSNL in a 13-year-old Bulgarian girl. Neuromuscul Disord. 1998;8(2):90-4.

89. Butinar D, Zidar J, Leonardis L, Popovic M, Kalaydjieva L, Angelicheva D, et al. Hereditary auditory, vestibular, motor, and sensory neuropathy in a Slovenian Roma (Gypsy) kindred. Ann Neurol. 1999;46(1):36-44.
90. Colomer J, Iturriaga C, Kalaydjieva L, Angelicheva D, King RHM, Thomas PK. Hereditary Motor and Sensory Neuropathy-Lom (HMSNL) in a Spanish family: clinical, electrophysiological, pathological and genetic studies. Neuromuscul Disord. 2000;10(8):578-83.
91. Li LX, Liu GL, Liu ZJ, Lu C, Wu ZY. Identification and functional characterization of two missense mutations in NDRG1 associated with Charcot-Marie-Tooth disease type 4D. Hum Mutat. 2017;38(11):1569-78.
92. Hunter M, Bernard R, Freitas E, Boyer A, Morar B, Martins IJ, et al. Mutation screening of the N-myc downstream-regulated gene 1 (NDRG1) in patients with Charcot-Marie-Tooth Disease. Hum Mutat. 2003;22(2):129-35.
93. Okamoto Y, Goksungur MT, Pehlivan D, Beck CR, Gonzaga-Jauregui C, Muzny DM, et al. Exonic duplication CNV of NDRG1 associated with autosomal-recessive HMSN-Lom/CMT4D. Genet Med. 2014;16(5):386-94.
94. Piscosquito G, Magri S, Saveri P, Milani M, Ciano C, Farina L, et al. A novel NDRG1 mutation in a non-Romani patient with CMT4D/HMSN-Lom. J Peripher Nerv Syst. 2017;22(1):47-50.
95. Luigetti M, Taroni F, Milani M, Del Grande A, Romano A, Bisogni G, et al. Clinical, electrophysiological and pathological findings in a patient with Charcot-Marie-Tooth disease 4D caused by the NDRG1 Lom mutation. J Neurol Sci. 2014;345(1-2):271-3.
96. Ricard E, Mathis S, Magdelaine C, Delisle MB, Magy L, Funalot B, et al. CMT4D (NDRG1 mutation): genotype-phenotype correlations. J Peripher Nerv Syst. 2013;18(3):261-5.
97. Echaniz-Laguna A, Degos B, Bonnet C, Latour P, Hamadouche T, Levy N, et al. NDRG1-linked Charcot-Marie-Tooth disease (CMT4D) with central nervous system involvement. Neuromuscul Disord. 2007;17(2):163-8.
98. Kokame K, Kato H, Miyata T. Homocysteine-respondent genes in vascular endothelial cells identified by differential display analysis. GRP78/BiP and novel genes. J Biol Chem. 1996;271(47):29659-65.
99. van Belzen N, Dinjens WN, Diesveld MP, Groen NA, van der Made AC, Nozawa Y, et al. A novel gene which is up-regulated during colon epithelial cell differentiation and down-regulated in colorectal neoplasms. Lab Invest. 1997;77(1):85-92.
100. Bandyopadhyay S, Pai SK, Gross SC, Hirota S, Hosobe S, Miura K, et al. The Drg-1 gene suppresses tumor metastasis in prostate cancer. Cancer Res. 2003;63(8):1731-6.
101. Bandyopadhyay S, Pai SK, Hirota S, Hosobe S, Takano Y, Saito K, et al. Role of the putative tumor metastasis suppressor gene Drg-1 in breast cancer progression. Oncogene. 2004;23(33):5675-81.
102. Bandyopadhyay S, Pai SK, Hirota S, Hosobe S, Tsukada T, Miura K, et al. PTEN up-regulates the tumor metastasis suppressor gene Drg-1 in prostate and breast cancer. Cancer Res. 2004;64(21):7655-60.
103. Cheng J, Xie HY, Xu X, Wu J, Wei X, Su R, et al. NDRG1 as a biomarker for metastasis, recurrence and of poor prognosis in hepatocellular carcinoma. Cancer Lett. 2011;310(1):35-45.
104. Guan RJ, Ford HL, Fu Y, Li Y, Shaw LM, Pardee AB. Drg-1 as a differentiation-related, putative metastatic suppressor gene in human colon cancer. Cancer Res. 2000;60(3):749-55.

105. Kim KT, Ongusaha PP, Hong YK, Kurdistani SK, Nakamura M, Lu KP, et al. Function of Drg1/Rit42 in p53-dependent mitotic spindle checkpoint. J Biol Chem. 2004;279(37):38597-602.
106. Ellen TP, Ke Q, Zhang P, Costa M. NDRG1, a growth and cancer related gene: regulation of gene expression and function in normal and disease states. Carcinogenesis. 2008;29(1):2-8.
107. Kräuter-Canham R, Bronner R, Evrard J-L, Hahne G, Friedt W, Steinmetz A. A transmitting tissue- and pollen-expressed protein from sunflower with sequence similarity to the human RTP protein. Plant Sci. 1997;129(2):191-202.
108. Sun J, Zhang D, Bae DH, Sahni S, Jansson P, Zheng Y, et al. Metastasis suppressor, NDRG1, mediates its activity through signaling pathways and molecular motors. Carcinogenesis. 2013;34(9):1943-54.
109. Melotte V, Qu X, Ongenaert M, van Criekinge W, de Bruine AP, Baldwin HS, et al. The N-myc downstream regulated gene (NDRG) family: diverse functions, multiple applications. FASEB J. 2010;24(11):4153-66.
110. Schonkeren SL, Massen M, van der Horst R, Koch A, Vaes N, Melotte V. Nervous NDRGs: the N-myc downstream-regulated gene family in the central and peripheral nervous system. Neurogenetics. 2019;20(4):173-86.
111. Shaw E, McCue LA, Lawrence CE, Dordick JS. Identification of a novel class in the alpha/beta hydrolase fold superfamily: the N-myc differentiation-related proteins. Proteins. 2002;47(2):163-8.
112. McCaig C, Potter L, Abramczyk O, Murray JT. Phosphorylation of NDRG1 is temporally and spatially controlled during the cell cycle. Biochem Biophys Res Commun. 2011;411(2):227-34.
113. Sugiki T, Murakami M, Taketomi Y, Kikuchi-Yanoshita R, Kudo I. N-myc downregulated gene 1 is a phosphorylated protein in mast cells. Biol Pharm Bull. 2004;27(5):624-7.
114. Lee JE, Kim JH. SUMO modification regulates the protein stability of NDRG1. Biochem Biophys Res Commun. 2015;459(1):161-5.
115. Ghalayini Mohammad K, Dong Q, Richardson Des R, Assinder Stephen J. Proteolytic cleavage and truncation of NDRG1 in human prostate cancer cells, but not normal prostate epithelial cells. Biosci Rep. 2013;33(3):e00042.
116. Berger P, Sirkowski EE, Scherer SS, Suter U. Expression analysis of the N-Myc downstream-regulated gene 1 indicates that myelinating Schwann cells are the primary disease target in hereditary motor and sensory neuropathy-Lom. Neurobiol Dis. 2004;17(2):290-9.
117. Lachat P, Shaw P, Gebhard S, van Belzen N, Chaubert P, Bosman FT. Expression of NDRG1, a differentiation-related gene, in human tissues. Histochem Cell Biol. 2002;118(5):399-408.
118. Askautrud HA, Gjernes E, Gunnes G, Sletten M, Ross DT, Borresen-Dale AL, et al. Global gene expression analysis reveals a link between NDRG1 and vesicle transport. PLoS One. 2014;9(1):e87268.
119. Shi XH, Larkin JC, Chen B, Sadovsky Y. The expression and localization of N-myc downstream-regulated gene 1 in human trophoblasts. PLoS One. 2013;8(9):e75473.
120. Zhou D, Salnikow K, Costa M. Cap43, a novel gene specifically induced by Ni2+ compounds. Cancer Res. 1998;58(10):2182-9.
121. Croessmann S, Wong HY, Zabransky DJ, Chu D, Mendonca J, Sharma A, et al. NDRG1 links p53 with proliferation-mediated centrosome homeostasis and genome stability. Proc Natl Acad Sci U S A. 2015;112(37):11583-8.

122. Fang BA, Kovacevic Z, Park KC, Kalinowski DS, Jansson PJ, Lane DJ, et al. Molecular functions of the iron-regulated metastasis suppressor, NDRG1, and its potential as a molecular target for cancer therapy. Biochim Biophys Acta. 2014;1845(1):1-19.
123. Piquemal D, Joulia D, Balaguer P, Basset A, Marti J, Commes T. Differential expression of the RTP/Drg1/Ndr1 gene product in proliferating and growth arrested cells. Biochim Biophys Acta. 1999;1450(3):364-73.
124. Kovacevic Z, Richardson DR. The metastasis suppressor, Ndrg-1: a new ally in the fight against cancer. Carcinogenesis. 2006;27(12):2355-66.
125. Sharma A, Mendonca J, Ying J, Kim HS, Verdone JE, Zarif JC, et al. The prostate metastasis suppressor gene NDRG1 differentially regulates cell motility and invasion. Mol Oncol. 2017;11(6):655-69.
126. Mao Z, Sun J, Feng B, Ma J, Zang L, Dong F, et al. The metastasis suppressor, N-myc Downregulated gene 1 (NDRG1), is a prognostic biomarker for human colorectal cancer. PLoS One. 2013;8(7):e68206.
127. Nishio S, Ushijima K, Tsuda N, Takemoto S, Kawano K, Yamaguchi T, et al. Cap43/NDRG1/Drg-1 is a molecular target for angiogenesis and a prognostic indicator in cervical adenocarcinoma. Cancer Lett. 2008;264(1):36-43.
128. Kachhap SK, Faith D, Qian DZ, Shabbeer S, Galloway NL, Pili R, et al. The N-Myc down regulated Gene1 (NDRG1) Is a Rab4a effector involved in vesicular recycling of E-cadherin. PLoS One. 2007;2(9):e844.
129. Sevinsky CJ, Khan F, Kokabee L, Darehshouri A, Maddipati KR, Conklin DS. NDRG1 regulates neutral lipid metabolism in breast cancer cells. Breast Cancer Res. 2018;20(1):55.
130. Schweitzer CJ, Zhang F, Boyer A, Valdez K, Cam M, Liang TJ. N-Myc Downstream-Regulated Gene 1 Restricts Hepatitis C Virus Propagation by Regulating Lipid Droplet Biogenesis and Viral Assembly. J Virol. 2018;92(2):e01166-17.
131. Hunter M, Angelicheva D, Tournev I, Ingley E, Chan DC, Watts GF, et al. NDRG1 interacts with APO A-I and A-II and is a functional candidate for the HDL-C QTL on 8q24. Biochem Biophys Res Commun. 2005;332(4):982-92.
132. Pietiainen V, Vassilev B, Blom T, Wang W, Nelson J, Bittman R, et al. NDRG1 functions in LDL receptor trafficking by regulating endosomal recycling and degradation. J Cell Sci. 2013;126(Pt 17):3961-71.
133. Okuda T, Higashi Y, Kokame K, Tanaka C, Kondoh H, Miyata T. Ndrg1-deficient mice exhibit a progressive demyelinating disorder of peripheral nerves. Mol Cell Biol. 2004;24(9):3949-56.
134. Hirata K, Masuda K, Morikawa W, He JW, Kuraoka A, Kuwano M, et al. N-myc downstream-regulated gene 1 expression in injured sciatic nerves. Glia. 2004;47(4):325-34.
135. Bjerke K, Molteberg T. Polynevropati hos Alaskan Malamute : patologiske forandringer og immunhistokjemisk lokalisering av NDRG1 i nervevev hos hunder som er homozygote og heterozygote for en Gly98Val mutasjon i NDRG1 [Fordypningsoppgave Smådyrdifferensiering]. Oslo: Norwegian University of Life Sciences; 2014.
136. Salvesen O, Tatzelt J, Tranulis MA. The prion protein in neuroimmune crosstalk. Neurochem Int. 2019;130:104335.
137. Atkinson CJ, Zhang K, Munn AL, Wiegmans A, Wei MQ. Prion protein scrapie and the normal cellular prion protein. Prion. 2016;10(1):63-82.

138. Manson J, Clarke A, Hooper M, Aitchison L, McConnell I, Hope J. 129/Ola mice carrying a null mutation in PrP that abolishes mRNA production are developmentally normal. Mol Neurobiol. 1994;8(2-3):121-7.
139. Büeler H, Fischer M, Lang Y, Bluethmann H, Lipp H-P, DeArmond SJ, et al. Normal development and behaviour of mice lacking the neuronal cell-surface PrP protein. Nature. 1992;356(6370):577-82.
140. Sakaguchi S, Katamine S, Nishida N, Moriuchi R, Shigematsu K, Sugimoto T, et al. Loss of cerebellar Purkinje cells in aged mice homozygous for a disrupted PrP gene. Nature. 1996;380(6574):528-31.
141. Rossi D, Cozzio A, Flechsig E, Klein MA, Rülicke T, Aguzzi A, et al. Onset of ataxia and Purkinje cell loss in PrP null mice inversely correlated with Dpl level in brain. EMBO J. 2001;20(4):694-702.
142. Nuvolone M, Hermann M, Sorce S, Russo G, Tiberi C, Schwarz P, et al. Strictly co-isogenic C57BL/6J-Prnp−/− mice: A rigorous resource for prion science. J Exp Med. 2016;213(3):313-27.
143. Linden R. The Biological Function of the Prion Protein: A Cell Surface Scaffold of Signaling Modules. Front Mol Neurosci. 2017;10:77.
144. Nishida N, Tremblay P, Sugimoto T, Shigematsu K, Shirabe S, Petromilli C, et al. A mouse prion protein transgene rescues mice deficient for the Prion protein gene from Purkinje cell degeneration and demyelination. Lab Invest. 1999;79(6):689-97.
145. Moore RC, Lee IY, Silverman GL, Harrison PM, Strome R, Heinrich C, et al. Ataxia in prion protein (PrP)-deficient mice is associated with upregulation of the novel PrP-like protein doppel. J Mol Biol. 1999;292(4):797-817.
146. Weissmann C, Aguzzi A. Perspectives: neurobiology. PrP's double causes trouble. Science. 1999;286(5441):914-5.
147. Eaton SL, Wishart TM. Bridging the gap: large animal models in neurodegenerative research. Mamm Genome. 2017;28(7-8):324-37.
148. Bolino A, Bolis A, Previtali SC, Dina G, Bussini S, Dati G, et al. Disruption of Mtmr2 produces CMT4B1-like neuropathy with myelin outfolding and impaired spermatogenesis. J Cell Biol. 2004;167(4):711-21.
149. Horn M, Baumann R, Pereira JA, Sidiropoulos PN, Somandin C, Welzl H, et al. Myelin is dependent on the Charcot-Marie-Tooth Type 4H disease culprit protein FRABIN/FGD4 in Schwann cells. Brain. 2012;135(Pt 12):3567-83.
150. Matiasek K, Drogemuller C. Charcot-Marie-Tooth disease: inherited neuropathies revisited. Vet J. 2011;188(3):254-5.
151. Crusio WE. Flanking gene and genetic background problems in genetically manipulated mice. Biol Psychiatry. 2004;56(6):381-5.
152. de Almeida CJ, Chiarini LB, da Silva JP, PM ES, Martins MA, Linden R. The cellular prion protein modulates phagocytosis and inflammatory response. J Leukoc Biol. 2005;77(2):238-46.
153. Nuvolone M, Kana V, Hutter G, Sakata D, Mortin-Toth SM, Russo G, et al. SIRPalpha polymorphisms, but not the prion protein, control phagocytosis of apoptotic cells. J Exp Med. 2013;210(12):2539-52.
154. Bozzola JJ, Russell LD. Specimen preparation for transmission electron microscopy. Electron microscopy: principles and techniques for biologists. Boston: Jones & Bartlett Publishers; 1992. p. 14-38.
155. Ramos-Vara JA. Technical aspects of immunohistochemistry. Vet Pathol. 2005;42(4):405-26.

156. Jortner BS. Preparation and analysis of the peripheral nervous system. Toxicol Pathol. 2011;39(1):66-72.
157. Knight DP. Cytological staining methods in electron microscopy. In: Lewis PR, Knight DP, editors. Staining methods for sectioned material. Practical methods in electron microscopy. Amsterdam: North-Holland; 1977. p. 25-76.
158. Sommer CL, Brandner S, Dyck PJ, Harati Y, LaCroix C, Lammens M, et al. Peripheral Nerve Society Guideline on processing and evaluation of nerve biopsies. J Peripher Nerv Syst. 2010;15(3):164-75.
159. Dyck PJ, J. K, Lais A, Lofgren EP, Stevens JC. Pathologic alterations of the peripheral nervous system of humans. In: Dyck PJ, Thomas PK, Lambert EH, Bunge R, editors. Peripheral neuropathy. vol. 1. 2nd ed. Philadelphia: WB Saunders; 1984. p. 790-3.
160. Braund KG, McGuire JA, Lincoln CE. Age-related changes in peripheral nerves of the dog. II. A morphologic and morphometric study of cross-sectional nerve. Vet Pathol. 1982;19(4):379-98.
161. Bilbao JM, Schmidt RE. Quantitative Techniques. Biopsy Diagnosis of Peripheral Neuropathy. Cham: Springer International Publishing; 2015. p. 43-50.
162. Mendell J, Erdem S, Agamanolis D. The role of peripheral nerve and skin biopsies. In: Mendell JR, Cornblath DR, Kissel JT, editors. Diagnosis and management of peripheral nerve disorders. vol. 59. New York: Oxford University Press; 2001. p. 90-128.
163. Weis J, Brandner S, Lammens M, Sommer C, Vallat J-M. Processing of nerve biopsies: a practical guide for neuropathologists. Clin Neuropathol. 2012;31(1):7-23.
164. Braund KG, McGuire JA, Lincoln CE. Age-related changes in peripheral nerves of the dog. I. A morphologic and morphometric study of single-teased fibers. Vet Pathol. 1982;19(4):365-78.
165. Srenk P, Flühmann G, Muhle A, Bergamasco L, Jaggy A. Electrodiagnostics. In: Jaggy A, Platt SR, editors. Small animal neurology: an illustrated text. Hannover: Schlütersche Verlagsgesellschaft mbH & Co. KG; 2010. p. 153-70.
166. Risberg AI, Spadavecchia C, Ranheim B, Hendrickson EH, Lervik A, Haga HA. Antinociceptive effect of buprenorphine and evaluation of the nociceptive withdrawal reflex in foals. Vet Anaesth Analg. 2015;42(3):329-38.
167. Wedel MJ. A Monument of Inefficiency: The Presumed Course of the Recurrent Laryngeal Nerve in Sauropod Dinosaurs. Acta Palaeontol Pol. 2011;57:251-6.
168. Figlia G, Gerber D, Suter U. Myelination and mTOR. Glia. 2018;66(4):693-707.
169. Gupta GD, Coyaud É, Gonçalves J, Mojarad BA, Liu Y, Wu Q, et al. A Dynamic Protein Interaction Landscape of the Human Centrosome-Cilium Interface. Cell. 2015;163(6):1484-99.
170. Jean S, Kiger AA. Coordination between RAB GTPase and phosphoinositide regulation and functions. Nat Rev Mol Cell Biol. 2012;13(7):463-70.
171. Wu CY, Lin MW, Wu DC, Huang YB, Huang HT, Chen CL. The role of phosphoinositide-regulated actin reorganization in chemotaxis and cell migration. Br J Pharmacol. 2014;171(24):5541-54.
172. Gonçalves J, Pelletier L. The Ciliary Transition Zone: Finding the Pieces and Assembling the Gate. Mol Cells. 2017;40(4):243-53.
173. Dickson E. Recent advances in understanding phosphoinositide signaling in the nervous system. F1000Res. 2019;8(278).
174. De Craene J-O, Bertazzi DL, Bär S, Friant S. Phosphoinositides, Major Actors in Membrane Trafficking and Lipid Signaling Pathways. Int J Mol Sci. 2017;18(3):634.

175. Pereira JA, Lebrun-Julien F, Suter U. Molecular mechanisms regulating myelination in the peripheral nervous system. Trends Neurosci. 2012;35(2):123-34.
176. Gassama-Diagne A, Yu W, ter Beest M, Martin-Belmonte F, Kierbel A, Engel J, et al. Phosphatidylinositol-3,4,5-trisphosphate regulates the formation of the basolateral plasma membrane in epithelial cells. Nat Cell Biol. 2006;8(9):963-70.
177. Trapp BD, Kidd GJ, Hauer P, Mulrenin E, Haney CA, Andrews SB. Polarization of myelinating Schwann cell surface membranes: role of microtubules and the trans-Golgi network. J Neurosci. 1995;15(3 Pt 1):1797-807.
178. Bettencourt-Dias M, Hildebrandt F, Pellman D, Woods G, Godinho SA. Centrosomes and cilia in human disease. Trends Genet. 2011;27(8):307-15.
179. Vertii A, Hehnly H, Doxsey S. The Centrosome, a Multitalented Renaissance Organelle. Cold Spring Harb Perspect Biol. 2016;8(12).
180. Jongsma ML, Berlin I, Neefjes J. On the move: organelle dynamics during mitosis. Trends Cell Biol. 2015;25(3):112-24.
181. Das S, Hehnly H, Doxsey S. A new role for Rab GTPases during early mitotic stages. Small GTPases. 2014;5.
182. Bielli A, Thörnqvist P-O, Hendrick AG, Finn R, Fitzgerald K, McCaffrey MW. The Small GTPase Rab4A Interacts with the Central Region of Cytoplasmic Dynein Light Intermediate Chain-1. Biochem Biophys Res Commun. 2001;281(5):1141-53.
183. Dyer N, Rebollo E, Domínguez P, Elkhatib N, Chavrier P, Daviet L, et al. Spermatocyte cytokinesis requires rapid membrane addition mediated by ARF6 on central spindle recycling endosomes. 2007;134(24):4437-47.
184. Gulluni F, Martini M, Hirsch E. Cytokinetic Abscission: Phosphoinositides and ESCRTs Direct the Final Cut. J Cell Biochem. 2017;118(11):3561-8.
185. Satir P, Pedersen LB, Christensen ST. The primary cilium at a glance. J Cell Sci 2010;123(4):499-503.
186. Carvalho-Santos Z, Azimzadeh J, Pereira-Leal JB, Bettencourt-Dias M. Evolution: Tracing the origins of centrioles, cilia, and flagella. J Cell Biol. 2011;194(2):165-75.
187. Molday RS, Moritz OL. Photoreceptors at a glance. J Cell Sci 2015;128(22):4039-45.
188. Palander O, El-Zeiry M, Trimble WS. Uncovering the Roles of Septins in Cilia. Front Cell Dev Biol. 2017;5:36.
189. Zhou Y, Yang S, Mao T, Zhang Z. MAPanalyzer: a novel online tool for analyzing microtubule-associated proteins. Database. 2015;2015.
190. Cooper BJ, Duncan I, Cummings J, de Lahunta A. Defective Schwann cell function in canine inherited Hypertrophic Neuropathy. Acta Neuropathol. 1984;63(1):51-6.
191. Cummings JF, Cooper BJ, de Lahunta A, van Winkle TJ. Canine inherited hypertrophic neuropathy. Acta Neuropathol. 1981;53(2):137-43.
192. Schenone A. Principles of pathology and nerve biopsy. In: Kuhlenbäumer G, Stögbauer F, Ringelstein EB, Young P, editors. Hereditary Peripheral Neuropathies. Darmstadt: Steinkopff; 2005. p. 41-70.
193. Ellezam B. Hereditary neuropathy with liability to pressure palsy. In: Vallat J-M, Weis J, editors. Peripheral nerve disorders. Oxford: International Society of Neuropathology; 2014. p. 126-30.
194. Dyck PJ, Dyck PJB, Engelstad J. Pathologic Alterations of Nerves. In: Dyck PJ, Thomas PK, editors. Peripheral Neuropathy. 4th ed. Philadelphia: W.B. Saunders; 2005. p. 733-829.

195. Duncan ID, Hammang JP. Ultrastructural observations of organelle accumulation in the equine recurrent laryngeal nerve. J Neurocytol. 1987;16(2):269-80.
196. Draper ACE, Piercy RJ. Pathological classification of equine recurrent laryngeal neuropathy. J Vet Intern Med. 2018;32(4):1397-409.
197. Robinson DC, Mammel AE, Logan AM, Larson AA, Schmidt EJ, Condon AF, et al. An In Vitro Model of Charcot-Marie-Tooth Disease Type 4B2 Provides Insight Into the Roles of MTMR13 and MTMR2 in Schwann Cell Myelination. ASN Neuro. 2018;10.
198. Murakami T, Sunada Y. Schwann Cell and the Pathogenesis of Charcot–Marie–Tooth Disease. In: Sango K, Yamauchi J, Ogata T, Susuki K, editors. Myelin: Basic and Clinical Advances. Singapore: Springer Singapore; 2019. p. 301-21.
199. Goebbels S, Oltrogge JH, Wolfer S, Wieser GL, Nientiedt T, Pieper A, et al. Genetic disruption of Pten in a novel mouse model of tomaculous neuropathy. EMBO Mol Med. 2012;4(6):486-99.
200. Bucci C, Bakke O, Progida C. Charcot-Marie-Tooth disease and intracellular traffic. Prog Neurobiol. 2012;99(3):191-225.
201. Alvarez-Prats A, Bjelobaba I, Aldworth Z, Baba T, Abebe D, Kim YJ, et al. Schwann-Cell-Specific Deletion of Phosphatidylinositol 4-Kinase Alpha Causes Aberrant Myelination. Cell Rep. 2018;23(10):2881-90.
202. Heller BA, Ghidinelli M, Voelkl J, Einheber S, Smith R, Grund E, et al. Functionally distinct PI 3-kinase pathways regulate myelination in the peripheral nervous system. J Cell Biol. 2014;204(7):1219-36.
203. Okuda T, Kokame K, Miyata T. Differential expression patterns of NDRG family proteins in the central nervous system. J Histochem Cytochem. 2008;56(2):175-82.
204. Nave KA. Myelination and support of axonal integrity by glia. Nature. 2010;468(7321):244-52.
205. Mostowy S, Cossart P. Septins: the fourth component of the cytoskeleton. Nat Rev Mol Cell Biol. 2012;13(3):183-94.
206. Buser AM, Erne B, Werner HB, Nave KA, Schaeren-Wiemers N. The septin cytoskeleton in myelinating glia. Mol Cell Neurosci. 2009;40(2):156-66.
207. Petit CSV, Besnier L, Morel E, Rousset M, Thenet S. Roles of the cellular prion protein in the regulation of cell-cell junctions and barrier function. Tissue barriers. 2013;1(2):e24377-e.
208. Martini R, Toyka KV. Immune-mediated components of hereditary demyelinating neuropathies: lessons from animal models and patients. Lancet Neurol. 2004;3(8):457-65.

Enclosed papers I-III

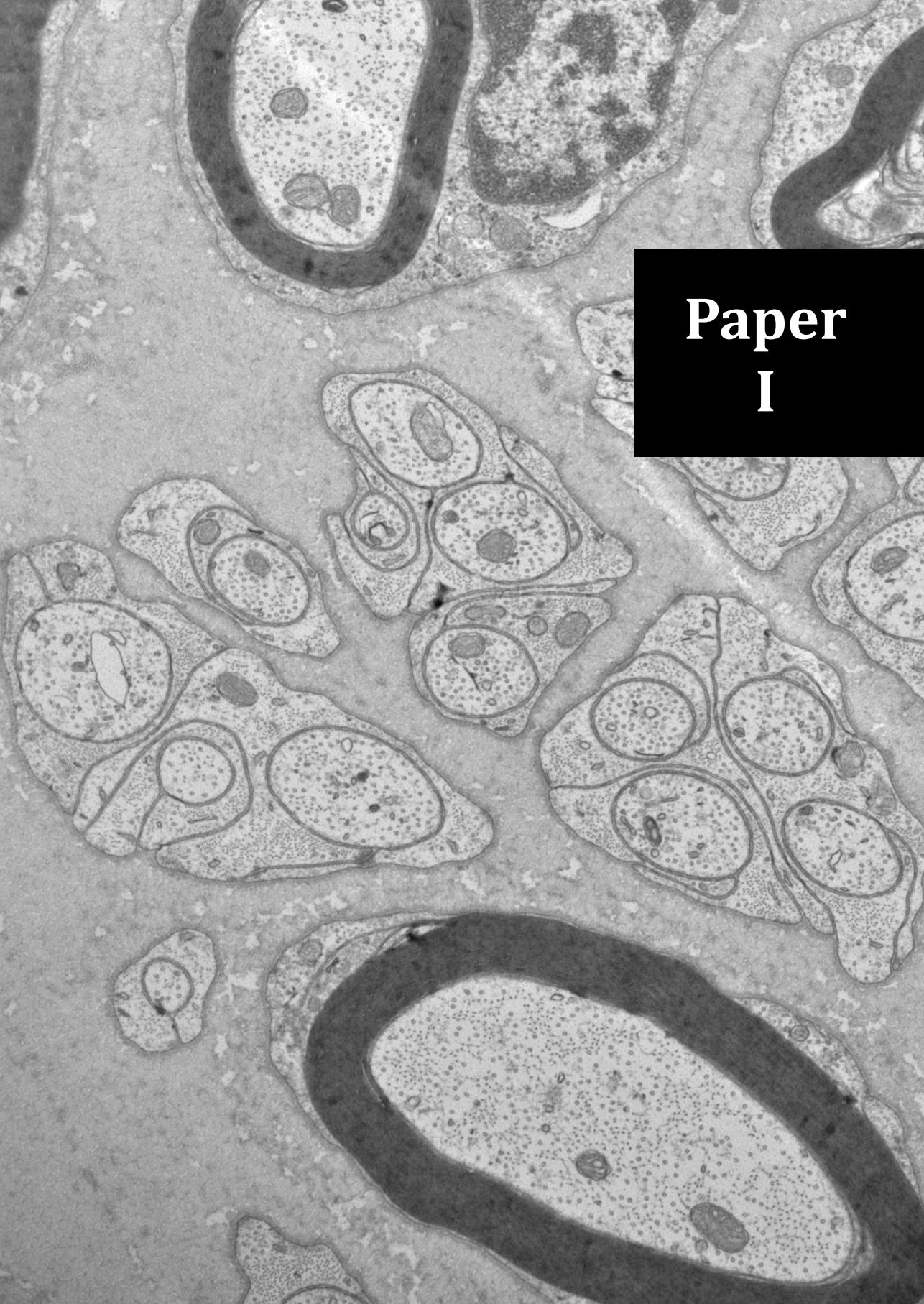
Paper
I

Skedsmo et al. BMC Veterinary Research (2019) 15:121
https://doi.org/10.1186/s12917-019-1872-2

BMC Veterinary Research

RESEARCH ARTICLE Open Access

Cell and context-dependent sorting of neuropathy-associated protein NDRG1 – insights from canine tissues and primary Schwann cell cultures

Fredrik S. Skedsmo[1], Michael A. Tranulis[2], Arild Espenes[2], Kristian Prydz[3], Kaspar Matiasek[4], Gjermund Gunnes[2], Lene C. Hermansen[5] and Karin H. Jäderlund[1*]

Abstract

Background: Mutations in the *N-myc downstream-regulated gene 1* (*NDRG1*) can cause degenerative polyneuropathy in humans, dogs, and rodents. In humans, this motor and sensory neuropathy is known as Charcot-Marie-Tooth disease type 4D, and it is assumed that analogous canine diseases can be used as models for this disease. NDRG1 is also regarded as a metastasis-suppressor in several malignancies. The tissue distribution of NDRG1 has been described in humans and rodents, but this has not been studied in the dog.

Results: By immunolabeling and Western blotting, we present a detailed mapping of NDRG1 in dog tissues and primary canine Schwann cell cultures, with particular emphasis on peripheral nerves. High levels of phosphorylated NDRG1 appear in distinct subcellular localizations of the Schwann cells, suggesting signaling-driven rerouting of the protein. In a nerve from an Alaskan malamute homozygous for the disease-causing *Gly98Val* mutation in *NDRG1*, this signal was absent. Furthermore, NDRG1 is present in canine epithelial cells, predominantly in the cytosolic compartment, often with basolateral localization. Constitutive expression also occurs in mesenchymal cells, including developing spermatids that are transiently positive for NDRG1. In some cells, NDRG1 localize to centrosomes.

Conclusions: Overall, canine NDRG1 shows a cell and context-dependent localization. Our data from peripheral nerves and primary Schwann cell cultures suggest that the subcellular localization of NDRG1 in Schwann cells is dynamically influenced by signaling events leading to reversible phosphorylation of the protein. We propose that disease-causing mutations in *NDRG1* can disrupt signaling in myelinating Schwann cells, causing disturbance in myelin homeostasis and axonal-glial cross talk, thereby precipitating polyneuropathy.

Keywords: Polyneuropathy, Charcot-Marie-tooth disease (CMT), Dog, Greyhound, Alaskan malamute, Microtubules, Microtubule-associated protein (MAP), Myelin

Background

The *N-myc downstream-regulated gene 1* (*NDRG1*) was first described as a gene that is up-regulated by homocysteine [1] and during cellular differentiation [2], and later identified as the mutated gene in an inherited demyelinating neuropathy, Charcot-Marie-Tooth type 4D (CMT4D), in humans [3]. Subsequently, mutations in *NDRG1* were observed in Greyhound show dogs [4] and Alaskan malamutes [5] suffering from inherited peripheral neuropathy. *NDRG1* encodes a 43-kDa protein in humans, which is expressed in many tissues, predominantly epithelial cells [6]. High levels of NDRG1 have been found in human and murine peripheral nerves, where the protein was expressed in the myelinating Schwann cells [7] and constituted 0.09% of total myelin proteins in the peripheral nervous system [8].

Furthermore, NDRG1 expression is downregulated in several malignancies, for instance those originating from

* Correspondence: karinhultin.jaderlund@nmbu.no
[1]Department of Companion Animal Clinical Sciences, Norwegian University of Life Sciences, Oslo, Norway
Full list of author information is available at the end of the article

the prostate and colon in humans [2, 9–13]. Decreased NDRG1 levels in these neoplasms is associated with a poor prognosis [9, 11–13], possibly explained by the ability of NDRG1 to inhibit epithelial-mesenchymal transition (EMT) [14]. At the molecular level, NDRG1 has been linked to vesicular transport [15], as a Rab4a-effector involved in recycling of E-cadherin [16] and being involved in the uptake of low-density lipoproteins (LDL) [17]. In line with the wide range of reported functions, NDRG1 can undergo substantial post-translational modifications by proteolytic cleavage [18], SUMO 2/3-modification [19] and phosphorylation [20–22].

Despite the ubiquitous expression of NDRG1 in the epithelium of different tissues, the pathologic changes reported from humans, rodents, and dogs with *NDRG1*-associated neuropathies are restricted to the peripheral nervous system [3–5, 7], and, to a lesser degree, the central nervous system [23]. This suggests that a comparative study of NDRG1 in different cell types from dogs with and without mutation in NDRG1 is required to understand the many facets of this protein.

In both humans and mice with *NDRG1* mutations, the degeneration of the nerves is described as a primary demyelination [24]. In contrast, the polyneuropathies of Greyhounds and Alaskan malamutes were dominated by axonal changes [4, 5]. Greyhounds, humans and mice with *NDRG1* mutations all have a total NDRG1 deficiency [24], suggesting that NDRG1 is involved in axonal-glial cross talk and that disruption of NDRG1 function may affect either side of the communication axis. A detailed mapping of the cellular and subcellular distribution of NDRG1, as well as post-translational modifications of the protein in peripheral nerves of dogs, is one prerequisite for deciphering NDRG1's roles in neuropathies. Studies of NDRG1 in the highly specialized Schwann cells can also have broader implications and contribute to our understanding of NDRG1 in other tissues during physiological conditions, as well as in malignancies.

In comparison with laboratory rodents, dogs offer significant advantages as models for human diseases. Dogs have a life expectancy and body size more similar to humans [4], and, as companion animals, they are exposed to the same environmental factors as their human counterparts. In addition, they have naturally occurring *NDRG1* mutations. Thus, the aim of this study was to describe and interpret the immunolocalization of NDRG1 isoforms in tissues and cells from control dogs and an Alaskan malamute dog homozygous for a disease-causing *Gly98Val* mutation in *NDRG1* (hereafter called *NDRG1*$^{mut/mut}$ Alaskan malamute). The results of this should aid in our understanding of *NDRG1*-associated diseases in dogs, humans, and rodents.

Results

Levels of NDRG1 isoforms vary significantly between tissues

Western blotting with four antibodies recognizing different epitopes of NDRG1 revealed several isoforms and dissimilarities between the analyzed tissues. The schematic structure of the protein and the antibody epitopes are summarized in Fig. 1a. The 42 kDa band, corresponding to the canine full-length protein, is recognized by all antibodies (Fig. 1b), albeit with different strengths. One of the phospho-specific antibodies, recognizing phosphorylation at threonine 346 (Thr346), revealed a band with molecular mass of 45–47 kDa, prominently present in nerve tissue preparations, Schwann cell culture, and testicle, but almost undetectable in the other tissue lysates. The reduced electrophoretic mobility of the phosphorylated protein is mainly caused by an increased size and bulkiness compared to the unphosphorylated isoform. Several, but not identical bands of lower molecular mass, ranging from 30 to 37 kDa were present at different levels in all the lysates, including the Schwann cell culture, suggesting that NDRG1 undergoes complex and tissue-specific proteolytic processing and/or degradation. The weak band from the prostate reflects low abundance of NDRG1 compared with the high levels of total protein. However, as shown immunohistochemically (Fig. 3e), there is strong expression of NDRG1 in the prostate.

Specificity of the antibodies

To ascertain the specificity of the NDRG1 antibodies used, we performed an immunoprecipitation from peripheral nerve lysate with the polyclonal anti-NDRG1 antibody produced in rabbit, and a subsequent Western blot with the monoclonal anti-NDRG1 antibody produced in mouse (Fig. 1c). The presence of bands corresponding to full-length protein, phosphorylated protein, and proteolytically processed NDRG1 with this method, supports that the detection of these NDRG1 isoforms is specific, as they are recognized by both antibodies. The presence of the 45–47 kDa band indicated that the antibodies also recognize the phosphorylated form of the protein to some extent.

For the immunohistochemical analysis of canine tissues, three different NDRG1 antibodies were used in parallel. The signals from these antibodies were similar, as shown in Fig. 2, indicating a specific detection of NDRG1 by immunohistochemistry. However, the monoclonal anti-NDRG1 antibody produced in mouse (Fig. 2a) consistently yielded a stronger signal than the two others (Fig. 2b-c).

Immunoreactivity was strong in epithelial cells

Immunohistochemistry of canine tissues showed that epithelial cells have strong expression of NDRG1 protein, in all the investigated digestive, urinary, and

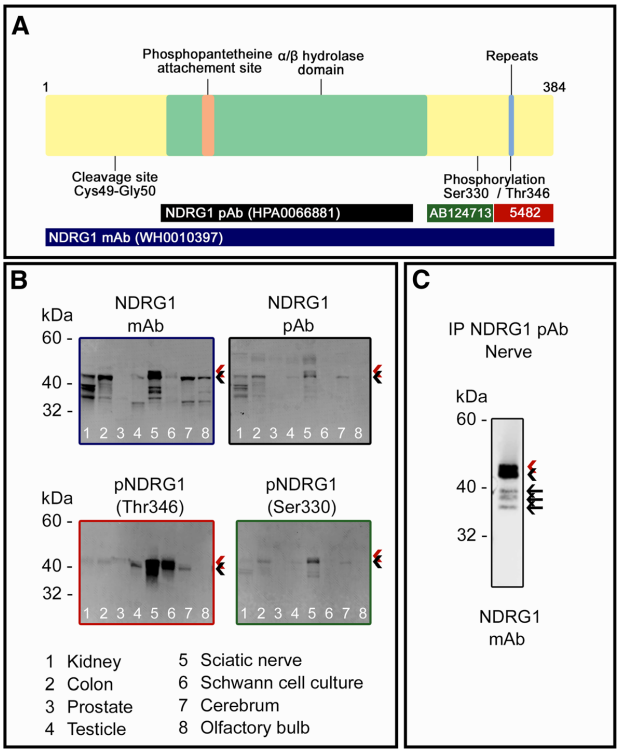

Fig. 1 Western blot analysis of canine tissues from control dogs. **a** Schematic structure of the canine NDRG1 protein and the epitopes of the NDRG1 antibodies used in the analyses. Note that the epitope of the NDRG1 mAb is not known. **b** Western blotting of lysate from canine tissues. **c** Western blotting after immunoprecipitation from peripheral nerve lysate. Full-length protein and phosphorylated protein are indicated by black and red arrowhead, respectively. In C, black arrows mark the truncated isoforms

reproductive organs. However, the staining pattern differed between the epithelial tissues. The distribution of NDRG1 in all the investigated tissues is summarized in Table 1. In addition to the control dogs, tissues from one *NDRG1*$^{mut/mut}$ Alaskan malamute were immunostained. Micrographs from this dog are shown for some tissues. In general, the staining pattern and intensity were similar to what was observed for the control dog, unless otherwise stated. In the colon (Fig. 3a) and jejunum (Fig. 3b), the epithelium of the mucosa, including the intestinal glands, stained strongly throughout. The immunoreactivity was predominantly localized to the basolateral region. The acinar cells of the exocrine pancreas showed a cytoplasmic staining pattern, which again was most pronounced basolaterally (not shown). In the liver, the hepatocytes did not show any signal, but a granular signal was detectable in the cytoplasm of the bile duct epithelium in the majority of the dogs (Fig. 3c). There was no signal from the bile duct epithelium of the *NDRG1*$^{mut/mut}$ Alaskan malamute. However, as this signal was not consistently present in the control dogs, this could be an incidental finding rather than an effect of the genotype.

In the urinary and reproductive organs, the most notable finding was a strong immunoreactivity in the epithelium of the proximal convoluted tubules of the kidney (Fig. 2a-c). Here, a moderate, homogenous cytoplasmic staining was found in addition to a stronger signal basolaterally. The immunoreactivity in the cells of the proximal tubules was clearly stronger than in the distal convoluted tubules (Fig. 2b). In the ovaries, an intense basolateral signal was observed in the granulosa cells of the follicles, while the cells of the corpus luteum showed a weaker, slightly granular signal from the cytoplasm (not shown). There was diffuse cytoplasmic staining in the epithelium of the endometrium and the endometrial glands (Fig. 3d). In the prostate, the secretory epithelium showed basolateral immunoreactivity, similar to the epithelium in the

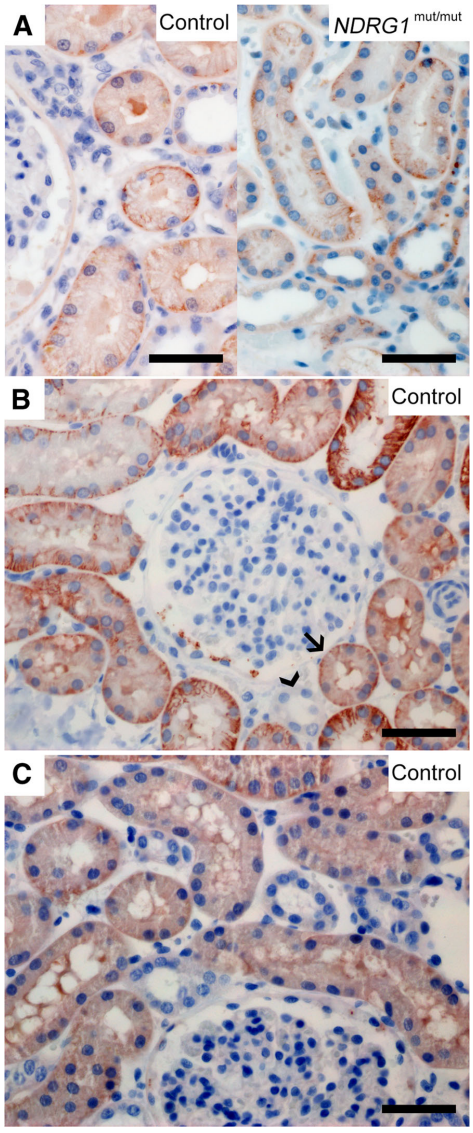

Fig. 2 Expression of NDRG1 in the kidney. NDRG1 is expressed in the epithelium of the proximal convoluted tubules in the kidneys (**a-c**). The figure compares the signal from the three different antibodies against NDRG1 used in the immunohistochemical analysis (**a**: mAb produced in mouse, **b**: pAb produced in goat, **c**: pAb produced in rabbit). In A, the NDRG1 signal from the *NDRG1*$^{mut/mut}$ Alaskan malamute is similar to the control. In B, the proximal and distal convoluted tubules are indicated by arrow and arrowhead, respectively. Bar 50 μm

intestine, but there was also some diffuse cytoplasmic signal (Fig. 3e).

The bronchiolar epithelium in the lungs showed a cytoplasmic signal and a slightly increased intensity basolaterally. Around 10–20% of the cells had a marked increase in signal intensity compared to the others (Fig. 3f). These cells lacked cilia and had a slightly granulated cytoplasm, and were therefore assumed to be club cells. In lung tissue (Fig. 3f), as well as in the other tissues (not shown), the endothelial cells stained strongly.

In some cells of the intestinal mucosa, the pancreas, the prostate, and the seminiferous tubules, one or two distinct structures close to, or overlying the nucleus, stained strongly (Fig. 4a-d). As described for the Schwann cell culture (see below), these punctate structures most probably represent centrosomes. Additionally, a fine granular nuclear signal was observed in some of these cells, most prominently in the seminiferous tubules. However, the centrosomal and nuclear signals were not present in all cells, suggesting that NDRG1 localizes to these structures at distinct phases of the cell cycle.

Some NDRG1 expression was also observed in developing spermatids and mesenchymal cells

In the testis, as described, centrosomal and nuclear signals were present in the developing spermatogonia (Fig. 4d). Additionally, intense NDRG1 signals were observed in the developing spermatids in the testicle, localized to a short, circular structure in the midpiece of the spermatids (Fig. 5a). Moreover, NDRG1 was observed in myoepithelial cells surrounding the seminiferous tubules.

NDRG1 was also present in other mesenchymal cells. In lymphatic organs, NDRG1 was present in several cell types. In the spleen, there was signal in macrophages present in the wall of the ellipsoids (Fig. 5b), and a cytoplasmic staining in a subpopulation of leukocytes in the red pulp. In the subcapsular sinus and follicles of the lymph node cortex (not shown), the follicles (Fig. 5c) and periarteriolar lymphocyte sheaths of the spleen (not shown), as well as in the lymphoid tissue of the Peyer's patches (Fig. 5d), dendritic cells, projecting interdigitating processes between surrounding lymphocytes, showed a prominent cytoplasmic and granular nuclear NDRG1 signal.

A weak and diffuse cytoplasmic NDRG1 staining was present in smooth muscle cells in both the intestinal and uterine wall, as well as in the wall of arterioles. A similar signal was observed in fibrocytes in several organs (not shown).

NDRG1 was strongly expressed in Schwann cells

In the nervous system, NDRG1 was expressed in the cerebellar Purkinje cells (Fig. 6a), satellite cells surrounding the neurons in the dorsal root ganglia of the spinal

Table 1 Distribution of NDRG1 protein in canine tissues and cells

Organ	Cell type	Epithelial (E) Mesenchymal (M) Neural (N)	NDRG1 staining pattern			
			Cytoplasmic[a]	Basolateral	Nuclear	Centrosomal
Kidney	Epithelium, proximal tubules	E	+	+		
Jejunum, colon	Epithelium	E		+	+	+
	Smooth muscle cells	M	+			
Lung	Epithelium, bronchioles	E	+	+		
	Club cells	E	+			
Liver	Epithelium, bile ducts	E	+			
Pancreas	Acinar cells	E	+	+	+	+
Ovary	Granulosa cells	E		+		
	Cells of the corpus luteum	E	+			
Uterus	Epithelium of the endometrium	E	+			
	Smooth muscle cells of the myometrium	M	+			
Testicle	Spermatogonia	M			+	
	Spermatids	M	Midpiece			
Prostate	Secretory epithelium	E	+	+	+	+
Lungs	Epithelium of the bronchioles	E	+	+		
Spleen, lymph nodes	Dendritic cells	M	+		+	
	Macrophages in the wall of ellipsoids	M	+			
Blood vessels	Endothelium	E	+			
	Smooth muscle cells	M	+			
Cerebral cortex	Oligodendrocytes	N	+		+	
Cerebellum	Purkinje neurons	N	+			
	Oligodendrocytes	N	+		+	
Spinal cord	Oligodendrocytes	N	+		+	
Peripheral nerves	Schwann cells	N	+		+	
Schwann cell culture		N	+		+	+

[a]The cytoplasmic staining was mostly diffuse, but in some tissues, a distinct granular pattern was observed, such as the bile ducts and cells of the corpus luteum
Note: All the different cell types in a tissue were evaluated. Only positively stained cells are included in the table

cord (Fig. 6b), Schwann cells in the peripheral nerves (Fig. 6c), and the submucosal (Fig. 6d) and myenteric nerve plexus in the intestinal wall. There was no signal in neuronal cell bodies, nuclei (Fig. 6b) or axons (Fig. 6c). NDRG1 was also strongly expressed in the oligodendrocytes (Fig. 7b). Serial sections from the spinal cord labeled with the astrocyte-marker GFAP (glial fibrillary acidic protein, Fig. 7a), NDRG1 (Fig. 7b), and the microglia-marker Iba1 (ionized calcium binding adaptor molecule 1, Fig. 7c) showed that the NDRG1-positive cells are not positive for GFAP or Iba1, and therefore rather represent oligodendrocytes. In both oligodendrocytes and Schwann cells there were diffuse nuclear signals (Fig. 7b, 6c and 9a). In the ependymal cells, a cytoplasmic signal with increased staining intensity basolaterally was observed (not shown).

To follow up on the strong expression of both total and phosphorylated NDRG1 in Western blots from peripheral nerve lysates, we further investigated the distribution of total NDRG1 and phosphorylated NDRG1 (pNDRG1 Thr346) in the peripheral nerves by immunofluorescence. Interestingly, while total NDRG1 (Fig. 8a) was present in both the adaxonal and abaxonal cytoplasm of the Schwann cells, as well as throughout the Schmidt-Lanterman clefts, phosphorylated NDRG1 (Fig. 8b) localized exclusively to the outer aspects of the Schmidt-Lanterman clefts and the abaxonal cytoplasm. In contrast, there was no detectable immunoreactivity in the compact myelin, neither against total nor phosphorylated NDRG1. In the nerve from the *NDRG1*$^{mut/mut}$ Alaskan malamute, total NDRG1 was found both in the adaxonal and abaxonal Schwann cell cytoplasm (Fig. 9e), similar to the control (Fig. 9a). However, phosphorylated NDRG1 was absent (Fig. 9f).

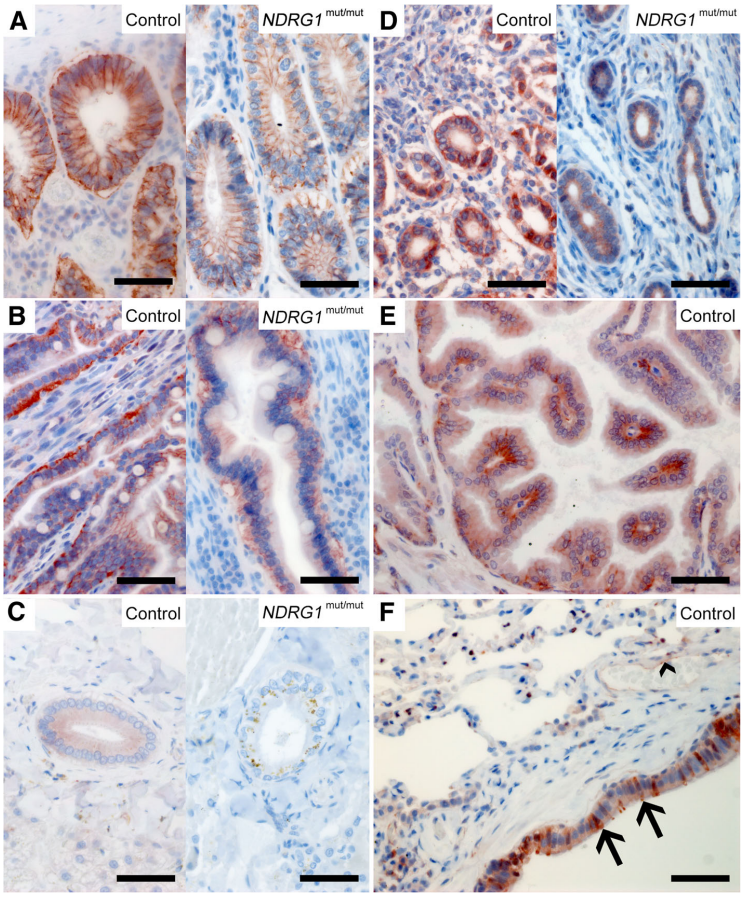

Fig. 3 Expression of NDRG1 in epithelia. Strong signal is present in the epithelium of the colon (**a**) and jejunum (**b**) of both the control and *NDRG1*$^{mut/mut}$ Alaskan malamute, whereas NDRG1 staining in the epithelial cells of the bile ducts in the liver was only detected in the control dog (**c**). NDRG1 is also present in the endometrium (**d**) and the epithelium of the prostate (**e**). In the lungs (**f**), the club cells (arrows) of the bronchiolar epithelium display a more intense signal than the surrounding epithelial cells. In addition, signal from the endothelium (arrowhead) can be seen. Note that except for the lack of signal in the bile ducts, the NDRG1 staining in the *NDRG1*$^{mut/mut}$ Alaskan malamute is similar to the controls. The extensive yellow-brown granules in the bile ducts of the *NDRG1*$^{mut/mut}$ Alaskan malamute is interpreted as pigment deposits. Bar 50 μm

Phosphorylated NDRG1 was present in the nucleus of cultured, immature Schwann cells

As there was a marked difference in the expression of the NDRG1 isoforms in Western blots from canine tissues, we next assessed the distribution of NDRG1 in primary Schwann cell culture. The cell culture consisted of canine Schwann cells and fibroblasts. Morphologically, the Schwann cells had a characteristic spindle shape, and stained strongly for GFAP (Fig. 10b). NDRG1 was present in both the Schwann cells and fibroblasts, albeit with a much weaker signal from the latter. In the cultured Schwann cells, total NDRG1 was present in both the cytoplasm and the nucleus (Fig. 11a). Whereas NDRG1 phosphorylated at Ser330 was present in both the cytoplasm and the nuclei of Schwann cells (not shown), similarly to total NDRG1, NDRG1 phosphorylated at Thr346 was primarily found in the nuclei (Fig. 11b). In some cells, punctate, juxta-nuclear structures, probably centrosomes, stained intensely for pNDRG1 Although these structures were often observed in the nuclear area, they were, in fact, localized in the cytoplasm close to the nuclear membrane (Fig. 12b).

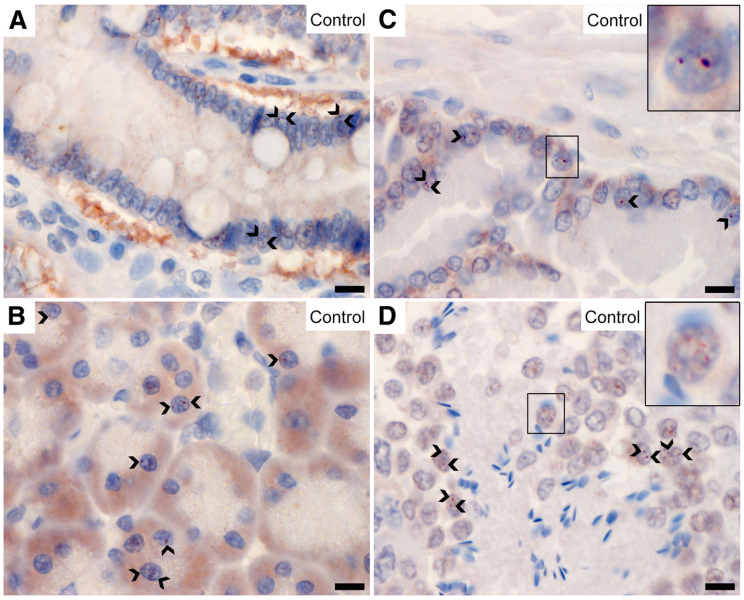

Fig. 4 Centrosomal and nuclear localization of NDRG1. NDRG1 localized to one or two distinct structures (arrowheads) in the jejunal (**a**), pancreatic (**b**) and prostatic (**c**) epithelium, as well as the developing spermatogonia (**d**). The inset in C shows a magnified image of these punctate structures. Note that this signal is not present in all the cells. The inset in D shows a magnified image of the granular nuclear signal in the seminiferous tubules. Bar 10 μm

Additionally, in some of the cells a granular nuclear signal was observed (Fig. 12b).

Discussion

Loss of NDRG1 functions causes degenerative polyneuropathy and increases malignancy of several human cancers. For instance, in colorectal cancer, NDRG1 counteracts EMT [14], thereby reducing metastatic potential. In both humans and dogs, specific mutations affecting *NDRG1* cause progressive polyneuropathies, classified as CMT4D in the former. Elucidating the normal subcellular localization and post-translational modifications of NDRG1 in diverse tissues holds one key to understanding its roles in both neuropathies and malignancies. Our data show that the subcellular localization of NDRG1 differs between canine tissues and that it varies dynamically through the cell cycle. Some of these fundamental features appear to be linked to post-translational modifications, such as phosphorylation. These observations also provide important clues as to how the cellular components, with which NDRG1 associates, exert their functions.

In this study, NDRG1 is detected in a variety of canine tissues, but most prominently in myelinating Schwann cells. The axons, however, appeared negative. In other organs, epithelial localization was mainly observed, as previously reported from human tissues [6]. However, there appears to be some marked differences between dogs and humans in the distribution of NDRG1. For example, no signal was detected in canine hepatocytes, but has been reported from human hepatocytes [6]. While we observed signal from canine mesenchymal cells, endothelia, and certain cells in the testicle and lymph nodes, no signal was observed in these tissues from humans by immunohistochemistry, although in testicle NDRG1 was detected by Western blotting [6]. Furthermore, all cell types in the human brain were negative [6], in contrast to the canine central nervous system where oligodendrocytes and Purkinje cells express NDRG1, a finding supported by Western blotting. Whereas epithelial cells mainly showed a prominent basolateral signal, NDRG1 had a more diffuse cytoplasmic distribution in the mesenchymal cells.

Western blot analysis revealed tissue-specific post-translational modifications of NDRG1, including proteolytic processing. Studies of prostate cancer cells [18] and healthy kidney tissue [7] have identified truncated isoforms of NDRG1, with molecular masses varying from 35 to 40 kDa. Our data strongly resembles this,

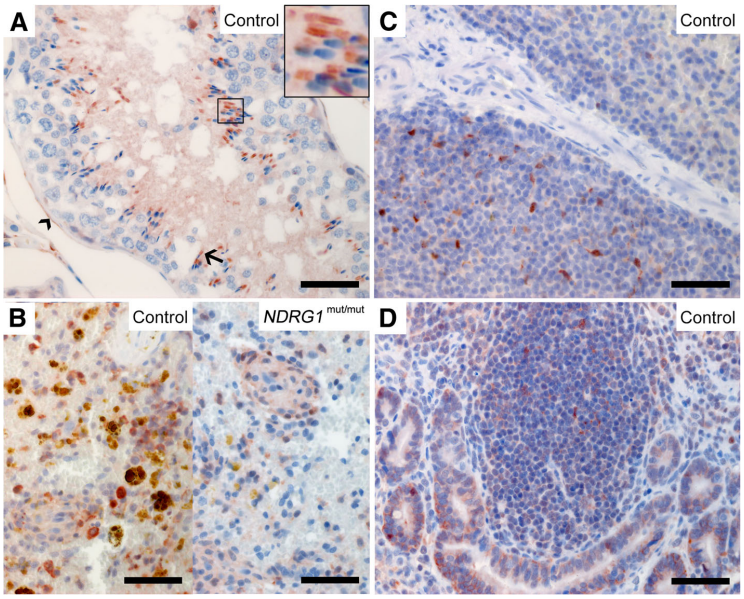

Fig. 5 Expression of NDRG1 in developing spermatids and mesenchymal cells. NDRG1 is present in the midpiece (arrow and inset) of the spermatids and the myoepithelial cells (arrowhead) surrounding the seminiferous tubules (**a**), the ellipsoids and a subpopulation of the leukocytes in the spleen (**b**), follicles in the spleen (**c**) and the intestinal Peyer's patches (**d**). The NDRG1 localization in the spleen of the *NDRG1*$^{mut/mut}$ Alaskan malamute is similar to the control (**c**). Note the extensive hemosiderin deposits (yellow-brown granules) in the spleen of the control dog. Bar 50 μm

suggesting that these processing events are specific and functionally important. A proteolytic cleavage site between Cys49 and Gly50 has been suggested for prostate cancer cells [18] and would lead to an approximately 5 kDa decrease in the molecular mass of the protein. A detailed fragment analysis has not been performed here, however, we have identified strong expression of phosphorylated NDRG1 in the testicle, peripheral nerves, and Schwann cell culture. Clearly, the subcellular sorting and posttranslational processing of NDRG1 is complex and variable between tissues. Mutations in *NDRG1*, however, appear to solely precipitate pathology in the nervous system. This suggest that NDRG1 serves critically important, non-redundant roles in myelinating Schwann cells. Therefore, detailed studies of NDRG1 isoforms in Schwann cells are particularly important.

Based on our observation of high levels of phosphorylated NDRG1 in the peripheral nerves, this post-translational regulatory mechanism must be important for the physiological function of NDRG1 in nervous tissue. The NDRG1 protein is reported to be involved in several signaling pathways [25]. In the peripheral nerves, NDRG1 has been shown to be a target in the phosphoinositide 3-kinase (PI3-K)/Akt-pathway and is mainly phosphorylated by the serum and glucocorticoid-regulated kinase 1 (Sgk1) and Akt1 [20]. Although total NDRG1 was present throughout the cytoplasm of the myelinating Schwann cells, phosphorylated NDRG1 (Thr346) was restricted to the abaxonal cytoplasm of the control dogs. This finding suggests a phosphorylation-driven rerouting of the protein in Schwann cells. In mice, NDRG1 phosphorylation was shown to be dispensable for myelination in early life [20], but, to our knowledge, the importance of phosphorylated NDRG1 in peripheral nerves of animals later in life has not been addressed. The lack of phosphorylated NDRG1 in the nerve from the *NDRG1*$^{mut/mut}$ Alaskan malamute could indicate that the mutation disrupts signaling in the Schwann cell. However, it could also be an unspecific result of the nerve pathology, so further studies are needed to elucidate the role of phosphorylated NDRG1 in the pathogenesis of neuropathies.

Although the predominant pathologic findings in dogs with *NDRG1*-associated neuropathies were reported to be axonal [4, 5], no NDRG1 signal was detected in the axons. This is in accordance with previous findings in peripheral nerves from humans and rodents [7]. As such, when our result of immunolocalization of NDRG1

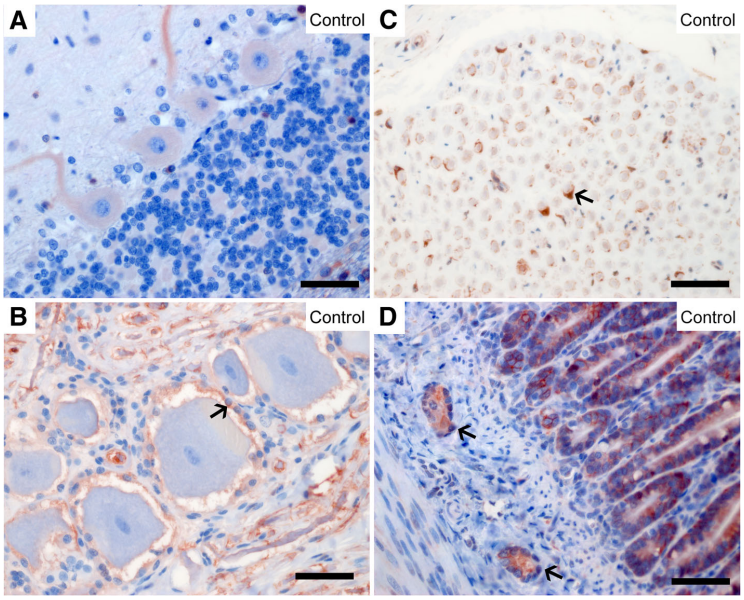

Fig. 6 Expression of NDRG1 in the nervous system. NDRG1 is present in the Purkinje cells in the cerebellum (**a**), the satellite cells (arrow) surrounding the neurons in the dorsal root ganglia (**b**), the Schwann cells (arrow) in the peripheral nerves (**c**) and the submucosal nerve plexus of the enteric nervous system (**d**). Bar 50 μm

to the Schwann cell cytoplasm is combined with the previously reported pathology of the polyneuropathies of Greyhounds and Alaskan malamutes, it seems that the expression of NDRG1 in Schwann cells is indispensable for both the Schwann cell and the axon. However, the fact that primary pathology in the axon leads to secondary changes in the Schwann cell, and vice versa, highlights the intimate relationship between the Schwann cell and the axon. The apparent divergence between the pathologic changes in dogs versus humans and rodents could, therefore, be more artefactual than real, and either caused by inter-species differences in the temporal progression of axonal atrophy [24] or the peripheral nerves being examined at different stages in the disease process.

Our observations of NDRG1 localizing to centrosomes, the midpiece of spermatids and basolateral cellular domains, clearly suggest that one or more isoforms of NDRG1 temporarily associate with microtubules or microtubule-organizing centers (MTOC). This is in accordance with a previous report, where NDRG1 was found to co-localize with gamma-tubulin in the centrosomes in colon cancer cells [21]. NDRG1 has been proposed to regulate centrosome number [26] and seems important for the formation of spindle fibers [27]. The midpiece of the spermatid contains the proximal and distal centrioles, and the latter extends distally as the axoneme [28]. The distal centriole degenerates during maturation of the spermatids and is not found in mature spermatozoa [28], which might explain why NDRG1 signal was not observed in all the seminiferous tubules. Although the basolateral NDRG1 signal in epithelia has been shown to originate from adherens junctions [6], this finding might actually support a tubulin-associated role for NDRG1, as the minus ends of the apico-basal microtubules are anchored to adherens junctions [29].

Microtubule-associated proteins (MAPs) bind directly to microtubules or tubulin via specific sequence elements, of which RSH is one [30]. Interestingly, the C-terminal tandem repeat of NDRG1 (GTRS**RSH**TSE) harbors this element. The tandem-repeat sequence is unique to NDRG1 in the NDRG family [31], and is repeated two and three times in the canine and human NDRG1 proteins, respectively. Therefore, we hypothesize that NDRG1 is a MAP that interacts with microtubules or tubulin through its C-terminal repeats. This enables NDRG1 to interact with other molecules through its N-terminal region, such as the phosphopantetheine attachment site and α/β hydrolase domain. The centrosomal signals in the Schwann cell cultures were only observed with the antibody against phosphorylated NDRG1 (Thr346). This phosphorylation site is located

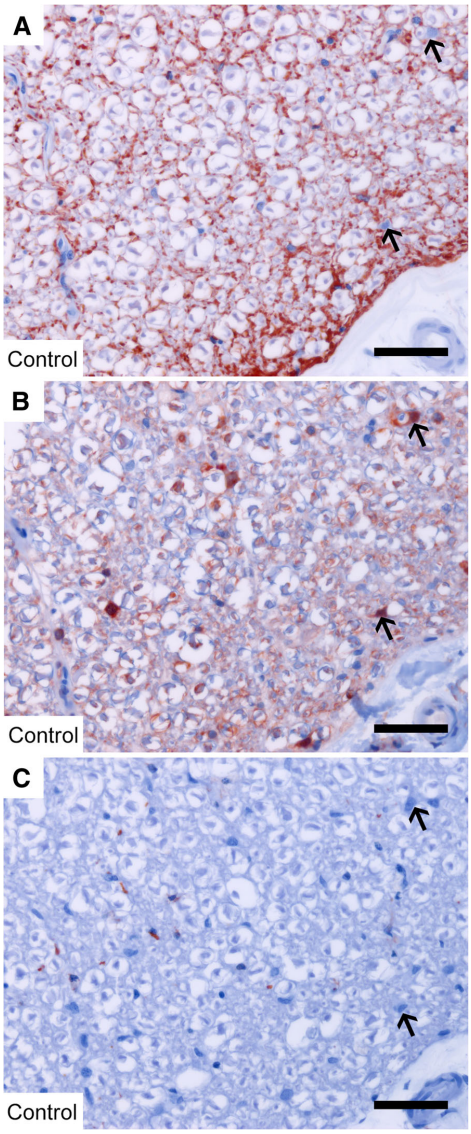

Fig. 7 Immunohistochemistry against GFAP (**a**), NDRG1 (**b**) and Iba1 (**c**) on spinal cord white matter from control dogs Note that the NDRG1-positive cells (arrows) are not positive for GFAP or Iba1. Bar 50 μm

close to the putative microtubule-binding sequence of NDRG1 and could therefore affect the tubulin-binding properties of the protein. Phosphorylated NDRG1 is regulated through the cell cycle and has been suggested to play a role in microtubule organization and successful mitosis [21]. However, the exact mechanisms and functions of this phosphorylation, as well as interactions between NDRG1 and microtubules, remain to be clarified.

A granular nuclear signal was observed in the epithelium of the prostate, the pancreas, the intestinal crypts, dendritic cells in lymphatic tissues, spermatocytes, and cultured Schwann cells. These findings support the fact that NDRG1 shuttles between the cytoplasm and the nucleus, as previously reported from the epithelium of the prostate [6], in human trophoblasts exposed to hypoxia [32], and in Schwann cells during myelination [33]. The nuclear translocation of NDRG1 is puzzling, as no nuclear-targeting sequence has been identified in the protein [6]. Neither the nuclear nor centrosomal signal was present in all cells, suggesting that NDRG1 is redistributed during the cell cycle. In myelinating Schwann cells and oligodendrocytes, as well as cultured Schwann cells, a weak and diffuse nuclear staining was observed, indicating that NDRG1 is present in the nucleus in the G_0 phase as well. During interphase and mitosis, NDRG1 concentrates at specific structures in the nucleus, centrosomes, and midbody.

Conclusions

In conclusion, our results show a cell and context-dependent sorting of NDRG1. Our data from peripheral nerves and primary cultures of Schwann cells suggest that NDRG1 is highly dynamic in these cells, and most probably influenced by signaling events leading to reversible phosphorylation of the protein. Based on the lack of pNDRG1 signal in a nerve from the *NDRG1*$^{mut/mut}$ Alaskan malamute, we propose that disease-causing mutations in *NDRG1* can disrupt signaling events in myelinating Schwann cells, leading to disturbance in the myelin homeostasis and axonal-glial cross talk, thereby precipitating polyneuropathy.

Methods

Animals

Samples were retrieved from the archive of the pathology laboratory, Norwegian University of Life Sciences. From control dogs, tissues from diseased organs were omitted from the analysis. Dogs of any breed, age, and gender were included. Alaskan Malamute dogs included as controls in the analyses were homozygous for the wild type *NDRG1* allele, while the neuropathic Alaskan malamute was homozygous for the *Gly98Val* mutation in *NDRG1*. Details on the individuals are summarized in Table 2.

Tissue sampling

Tissues from the following organs were sampled shortly after pentobarbital-euthanasia; skeletal muscle, myocardium, lung, liver, colon, jejunum, pancreas, spleen,

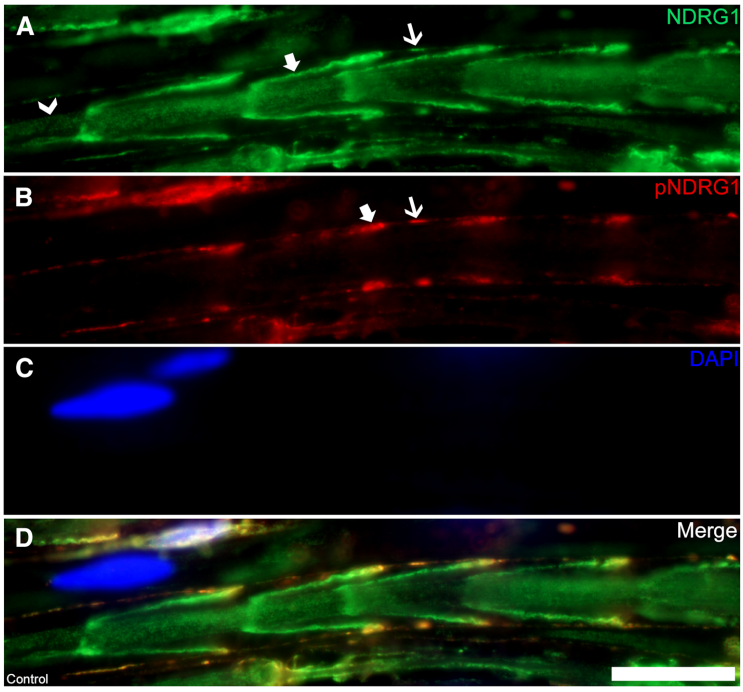

Fig. 8 Immunofluorescence of total NDRG1 (green) and phosphorylated NDRG1 (Thr346) (red) in Schwann cell cytoplasm. Longitudinal (**a-d**) sections from a control dog. Total NDRG1 (**a**) is present in the adaxonal cytoplasm (arrowhead), the Schmidt-Lanterman clefts (bold arrow), and abaxonal cytoplasm (arrow), while pNDRG1 (**b**) is restricted to the outer parts of the Schmidt-Lanterman cleft (bold arrow) and abaxonal cytoplasm (arrow). DAPI (blue) labels nuclei (**c**). Bar 20 μm

lymph node, kidney, uterus, ovary, testicle, prostate, peripheral nerves, cerebellum, cerebrum and spinal cord. Samples for immunohistochemistry were fixed in 10% buffered formalin and subsequently paraffin embedded. Samples for Western blotting were snap frozen in isopentane, transferred to liquid nitrogen, and stored at −80 °C until analysis.

Antibodies

Five different antibodies against NDRG1 were used in the analyses; Mouse monoclonal anti-NDRG1 antibody (catalog number WH0010397, Sigma-Aldrich, Merck, Darmstadt, Germany), goat polyclonal anti-NDRG1 antibody (catalog number PA5–18109, Invitrogen, Thermo Fisher Scientific, Massachusetts, United States), rabbit polyclonal anti-NDRG1 antibody (catalog number HPA006881, Sigma-Aldrich, Merck), rabbit monoclonal phospho-specific anti-NDRG1 (Thr346) (catalog number 5482, Cell Signaling Technology, Leiden, Netherlands), and a rabbit monoclonal phospho-specific anti-NDRG1 (Ser330) (catalog number ab124713, Abcam, Cambridge, United Kingdom). Additionally, antibodies against glial fibrillary acidic protein (GFAP) (catalog number Z0334, Dako, California, United States) and Iba1 (catalog number 019–19741, Fujifilm Wako Chemicals, Neuss, Germany) were used as markers for glial cells. Details on the antibodies are summarized in Table 3.

Western blotting

The samples were thawed, and the nerve tissue was freed from the epineurial fat. The tissue samples were lysed in homogenization buffer (50 mM Tris HCl, 150 mM NaCl, 1 mM EDTA, 0.25% DOC, 1% NP40, pH 7.4) supplemented with protease inhibitor cocktail (Roche complete, Roche Holding AG, Basel, Switzerland) and anti-phosphatase (Halt™ Phosphatase Inhibitor Cocktail, Thermo Fisher Scientific). Protein concentrations were measured using Protein assay (Bio-Rad, Hercules, California, United States).

25 μg protein from individual samples were separated by sodium dodecyl sulfate (SDS) polyacrylamide gel electrophoresis (12% Criterion™ XT-Bis-Tris, Bio-Rad), and

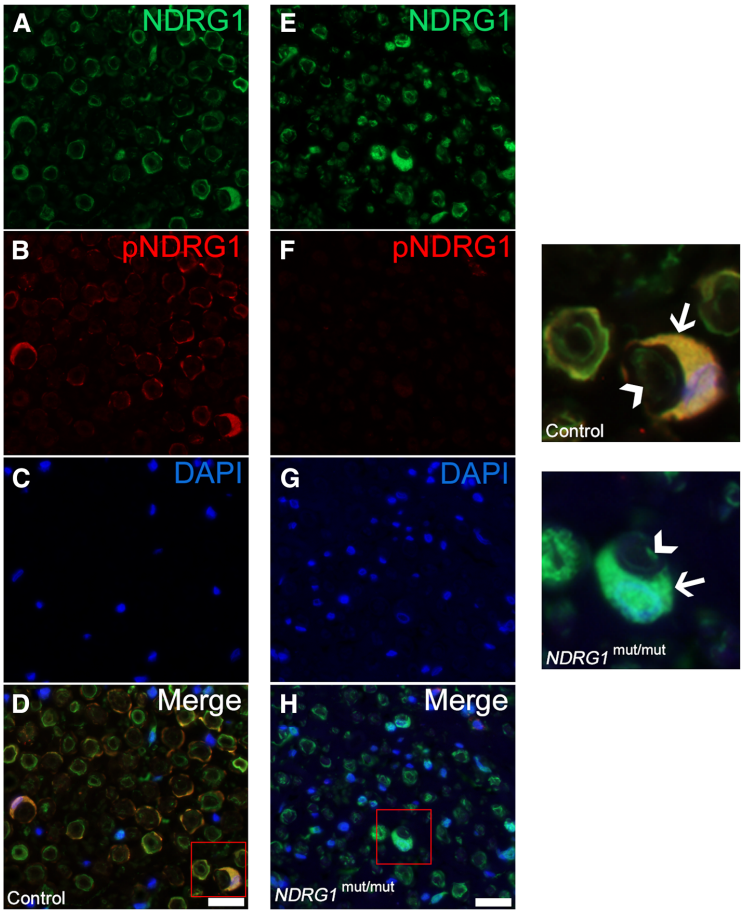

Fig. 9 Immunofluorescence of total NDRG1 (green) and phosphorylated NDRG1 (Thr346) (red) in myelinating Schwann cells. In the peripheral nerve from an Alaskan malamute homozygous for the wild type *NDRG1* allele (**a-d**), strong pNDRG1 signal is present in the abaxonal cytoplasm. In comparison, in the nerve from the *NDRG1*$^{mut/mut}$ Alaskan malamute (**e-h**), there is no pNDRG1 signal (**f**). In the magnified images, the adaxonal and abaxonal cytoplasm is indicated by arrowheads and arrows, respectively

transferred to polyvinylidene fluoride (PVDF) membranes (GE Healthcare, Little Chalfont, United Kingdom). The membranes were blocked with 5% non-fat milk in TBS-Tween for 90 min at room temperature and incubated with primary antibodies diluted in blocking buffer overnight at 4 °C. Thereafter, the membranes were washed and incubated for 90 min in 1% non-fat milk containing alkaline phosphatase-conjugated anti-mouse IgG (dilution 1/4000, Thermo Fisher Scientific) or anti-rabbit IgG (dilution 1/4000, GE Healthcare). The membrane was developed using EFC™ substrate (GE Healthcare) and visualized with Typhoon 9200 (Amersham Bioscience, GE Healthcare).

Immunoprecipitation from peripheral nerve lysate was performed with Dynabeads® Protein G (Novex, Life Technologies, Thermo Fisher Scientific) according to the manufacturer's instructions. Three μg of anti-NDRG1 antibody (catalog number HPA006881, Sigma-Aldrich, Merck) was used for the precipitation. Western blotting was subsequently performed as previously described with another anti-NDRG1 antibody (catalog number WH0010397, Sigma-Aldrich, Merck).

Immunohistochemistry

Sections of 3–4 μm were placed on glass slides (Superfrost Plus®, Menzel Gläser, Thermo Fisher Scientific) and

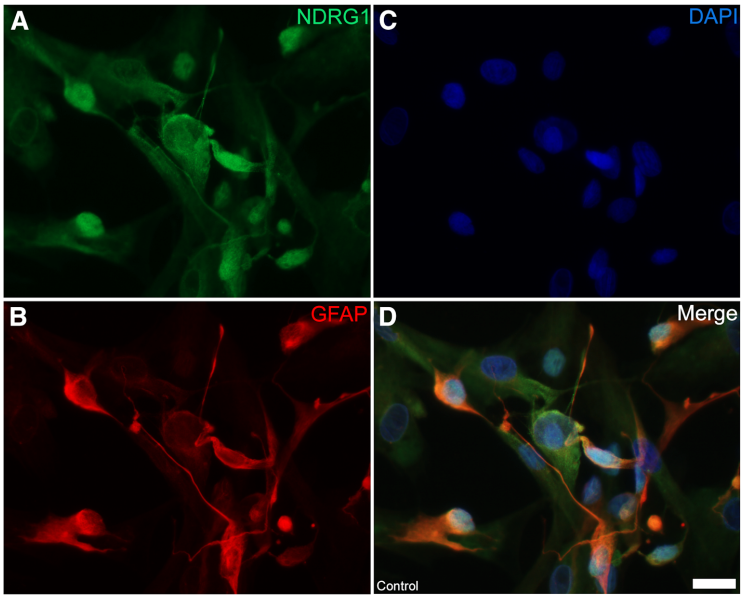

Fig. 10 Expression of NDRG1 in cultured Schwann cells (**a-d**). Total NDRG1 (green) is present both in the cytoplasm and the nucleus of the immature, GFAP-positive Schwann cells (red). The Schwann cells have a characteristic spindle shape and a stronger NDRG1-expression than the GFAP-negative fibroblasts. Bar 20 μm

stored at 4 °C until staining. The slides were deparaffinized in xylene and rehydrated through a descending alcohol series. Sections were washed in PBS for 5 min, twice between each step, except before incubation with the primary antibody. For all antibodies except anti-Iba1, antigen retrieval was performed by heating the slides for 15 min in citrate buffer (0.01 M, pH 6.0) in a Lab Vision™ PT Module (Thermo Fisher Scientific). For anti-Iba1, the slides were incubated with trypsin (1 mg/mL) in Tris HCl-buffer (0.1 M, pH 8.0) with 0.1% $CaCl_2$ for 40 min at 37 °C. Endogenous peroxidase activity was blocked with 3% H_2O_2 in methanol for 10 min. Non-specific antibody binding was blocked by incubating the slides for 30 min in 5% bovine serum albumin (BSA) with 2% normal serum from the same species as the secondary antibody. The sections were incubated with three different primary antibodies against NDRG1, diluted in 1% BSA for 60 min at concentrations summarized in Table 3. To optimize the signal intensity and signal-to-noise ratio, a modified protocol was used for the rabbit polyclonal anti-NDRG1 antibody; the slides were blocked with 1% normal serum in PBS, the primary antibody was diluted in PBS, while the secondary antibody was diluted in PBS with 2% normal serum.

Next, the sections were incubated with biotinylated secondary antibodies (dilution 1/50, catalog number BA-9200, BA-9500 and BA-1000, Vector Laboratories, California, United States) diluted in 1% BSA for 30 min. The sections were subsequently incubated with Vectastain Elite ABC reagent (Vectastain Elite ABC Kit, Vector Laboratories) for 30 min and then with ImmPact AEC Peroxidase Substrate (catalog number SK-4205, Vector Laboratories) for 3 min. In analyses where Iba1 was included, secondary antibodies conjugated to horseradish peroxidase-labeled polymer and AEC + -substrate from the EnVision+ kit (catalog number K4009, Dako) were used. The sections were counterstained with hematoxylin and mounted with Aquatex (Merck, Darmstadt, Germany). Sections where the primary antibodies were omitted were used as negative controls. For each tissue, samples from at least two individuals were included in the analysis. Micrographs were taken using an Axio Imager 2 microscope equipped with an Axiocam 506 color camera (Zeiss, Oberkochen, Germany).

Immunofluorescence on paraffin sections of peripheral nerves

Peripheral nerves were fixed and processed as described previously. Antigen retrieval was performed by heating the slides in citrate buffer (0.01 M, pH 6.0) in a microwave. The temperature in the solution was held at 92 °C for 5 min, thereafter the slides were kept in the hot

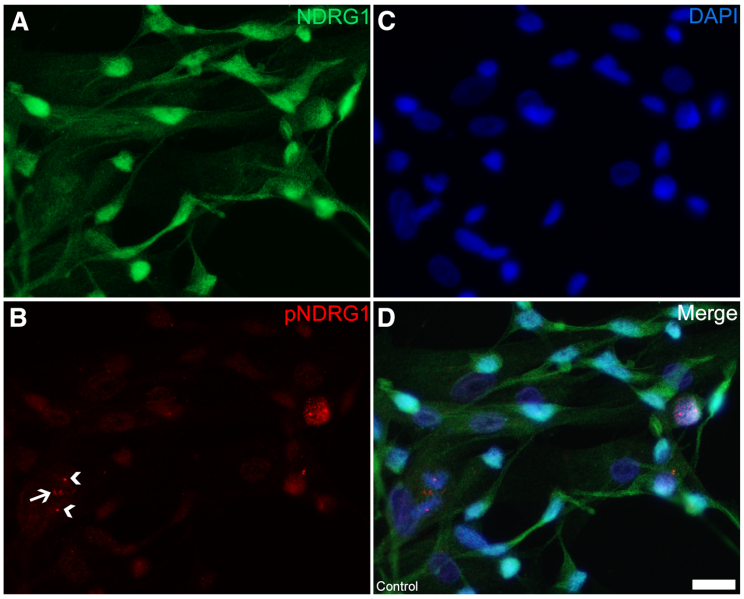

Fig. 11 Expression of total NDRG1 and phosphorylated NDRG1 (Thr346) in cultured Schwann cells (**a-d**). While total NDRG1 (green) is present both in the cytoplasm and nucleus, pNDRG1 (red) localizes to the nucleus as well as two centrosome-like structures (arrowheads) and a midbody in a mitosis (arrow). Bar 20 μm

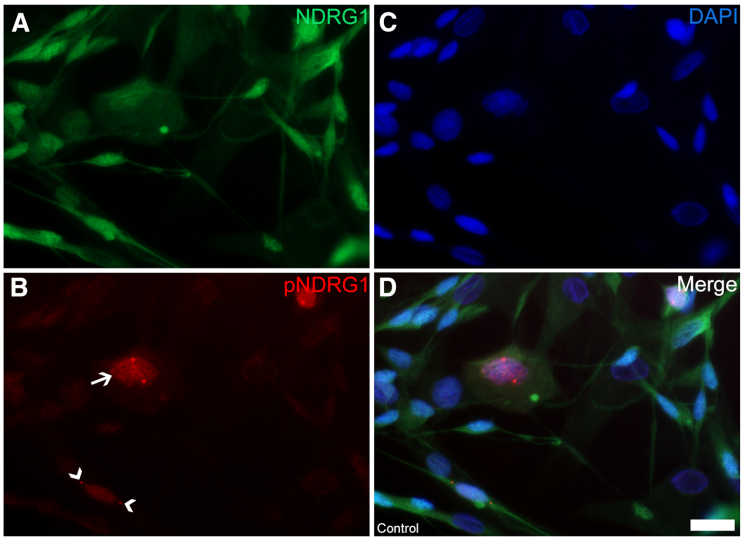

Fig. 12 Expression of total NDRG1 (green) and pNDRG1 (Thr346) (red) in cultured Schwann cells (**a-d**). In some of the cells, there was a granular nuclear signal (arrow) (**b**). Even though the distinct, punctate structures were overlaying the nucleus in many instances, they are actually located in the cytoplasm (arrowheads) (**b**). Bar 20 μm

Table 2 Signalment of the individuals included in the analyses of NDRG1 in canine tissues and cells

Breed	Age	Gender	Analysis
Spitz dog	3 weeks	Female	IHC
Norwegian Lundehund	2 months	Male	WB
Labrador retriever	8 months	Female	IHC
French Bulldog	6 years	Male	IHC
Alaskan malamute	7 years	Male	IHC
Norwegian Elkhound	7 years	Male	IHC, IF
Alaskan malamute	8 years	Female	IHC, IF, Schwann cell culture, WB
Alaskan malamute	11 years	Female	IHC
Gordon setter	12 years	Female	IHC
Pointer	12 years	Male	WB
English Springer Spaniel	14 years	Male	IHC
Alaskan malamute, homozygous for *Gly98Val* mutation	10 years	Female	IHC, IF

IHC Immunohistochemistry, *IF* Immunofluorescence, *WB* Western blot

solution for another 15 min before being rinsed in PBS. Non-specific antibody activity was blocked by incubating the slides for 30 min in 5% BSA with 2% normal serum from the same species as the secondary antibody. The sections were incubated with primary antibodies diluted in 1% BSA for 60 min at concentrations summarized in Table 3. The slides were rinsed three times for 5 min in PBS and incubated in secondary antibodies diluted in 1% BSA for 30 min. The secondary antibodies used were goat anti-mouse IgG Alexa Fluor 488 (dilution 1/400, catalog number A-11029, Invitrogen, Thermo Fisher Scientific) and goat anti-rabbit IgG Alexa Fluor 594 (dilution 1/400, catalog number A-11006, Invitrogen, Thermo Fisher Scientific). The slides were rinsed three times for 5 min in PBS and mounted with ProLong Gold Antifade Mountant with 4′,6 diamidino-2-phenyl indole (DAPI; Molecular Probes, Thermo Fisher Scientific). Slides where the primary antibodies were omitted were used as negative controls. Micrographs were taken using an Axio Imager 2 microscope equipped with an Axiocam 506 mono camera (Zeiss).

Schwann cell cultures

A primary Schwann cell culture from a control dog was established as previously described [34]. Briefly, an approximately 5 cm long whole trunk biopsy of the common fibular nerve was sampled shortly after pentobarbital-euthanasia of a dog. Immediately, the epineurium was removed and the fibers teased apart. Thereafter, the fibers were subjected to enzymatic digestion by 0.25% dispase and 0.05% type I collagenase in Dulbecco's Modified Eagle Medium (DMEM). For expansion of the cell cultures, complete medium (high glucose-DMEM supplemented with 10% FBS, 1% GlutaMAX, 1% penicillin/streptomycin, 25 μg/mL gentamicin, 10 nM neuregulin and 2 μM forskolin) was used. For cryopreservation, the cells were trypsinated, resuspended in complete medium,

Table 3 Antibodies and dilutions used in the analyses of NDRG1 in canine tissues and cells

Name	Catalog number	Producer	Dilutions		
			IHC	IF	WB
Monoclonal anti-NDRG1 antibody produced in mouse	WH0010397	Sigma-Aldrich, Merck, Darmstadt, Germany	1/2000	1/2000	1/2000
Polyclonal anti-NDRG1 antibody produced in goat	PA5–18109	Invitrogen, Thermo Fisher Scientific	1/750	NA	NA
Polyclonal anti-NDRG1 antibody produced in rabbit	HPA006881	Sigma-Aldrich, Merck	1/100	1/100	1/1000
Monoclonal phospho-specific anti-NDRG1 (Thr346) produced in rabbit	5482	Cell Signaling Technology, Leiden, Netherlands	NA	1/500	1/1000
Monoclonal phospho-specific anti-NDRG1 (Ser330) produced in rabbit	ab124713	Abcam, Cambridge, United Kingdom	NA	1/75	1/10000
Anti-glial fibrillary acidic protein	Z0334	Dako, California, United States	1/500	1/500	NA
Anti-Iba1	019–19,741	Fujifilm Wako Chemicals, Neuss, Germany	1/250	NA	NA

IHC Immunohistochemistry, *IF* Immunofluorescence, *WB* Western blot, *NA* Not analyzed

centrifugated and frozen in Recovery Cell Culture Freezing Medium.

Immunolabeling of cultured Schwann cells

The cell cultures were grown in eight well-glass chambered slides in complete medium. The cells were rinsed twice in PBS, fixed in 2% paraformaldehyde for 10 min at room temperature, rinsed in PBS three times for 1 min, permeabilized with 0.2% Triton X-100 in PBS and rinsed in PBS three times for 1 min. The cells were incubated 30 min in a blocking solution consisting of 2% BSA, 0.2% TWEEN 20, 7% glycerol and 2% goat serum. Thereafter, the cells were incubated with primary antibodies diluted in blocking solution for 60 min at room temperature at concentrations summarized in Table 3. The cells were rinsed three times for 1 min in PBS and incubated with secondary antibodies for 30 min. The secondary antibodies and mounting medium were the same as used for immunofluorescence on paraffin sections. Wells where the primary antibodies were omitted were used as negative controls.

Abbreviations

BSA: Bovine serum albumin; CMT4D: Charcot-Marie-Tooth type 4D; Cys49: Cysteine at amino acid position 49; DMEM: Dulbecco's Modified Eagle Medium; EMT: Epithelial-mesenchymal transition; GFAP: Glial fibrillary acidic protein 1; Gly50: Glycine at amino acid position 50; *Gly98Val*: Glycin to valine substitution at amino acid position 98; Iba1: Ionized calcium binding adaptor molecule 1; IF: Immunofluorescence; IHC: Immunohistochemistry; LDL: Low-density lipoprotein; MAP: Microtubule-associated proteins; MTOC: Microtubule-organizing center; *NDRG1*: *N-myc downstream regulated gene 1*; PBS: Phosphate-buffered saline; PI3K: Phosphoinositide 3-kinase; pNDRG1: Phosphorylated NDRG1; PVDF: Polyvinylidene fluoride; SDS: Sodium dodecyl sulfate; Ser330: Serine at amino acid position 330; Sgk1: Serum and glucocorticoid-regulated kinase 1; TBS: Tris-buffered saline; Thr346: Threonine at amino acid position 346; WB: Western blotting

Acknowledgements

The authors thank Dr. Natalia D. Andersen, Miami, for very useful help in our effort to establish the primary Schwann cell cultures. The authors acknowledge Dr. Lucy Robertson for proofreading the manuscript. The authors would also like to thank Mari Katharina Aas Ådland, Soheir Al Taoyl, Sigbjørn Lunner, Laila Aune, Rory Flack, Veronika Stabell and Tore Engen for all practical help during the study.

Funding

This study was financed by Agria och SKK Forskningsfond (grant number N2015–0016). The funding body did not have any role in the design of the study, collection, analysis, interpretation of data or in writing the manuscript.

Availability of data and materials

The data supporting the conclusions is contained within the manuscript. Any additional data are available from the corresponding author on reasonable request.

Author's contributions

FSS, MAT, AE, GG, KP, KM, KHJ designed the experiments. FSS, AE, MAT, GG, KP, LCH, KHJ performed the experiments. FSS, AE, MAT, GG, KP, KM, KHJ analyzed the data. FSS, AE, MAT, GG, KHJ wrote the paper. All authors read and approved the final manuscript.

Ethics approval and consent to participate

Pathologists at the Norwegian University of Life Sciences collected samples from dogs during routine post mortem examination of privately owned dogs euthanized by intravenous pentobarbital injection at the University Animal Hospital. Control dogs were euthanized of reasons unrelated to this study. Written consent for euthanasia, post mortem examination and tissue sampling, were given by the dog owners, in accordance with institutional guidelines. A specific permission for the study was not required from the Norwegian Food Safety Authority because all the samples were retrieved from the archive of the pathology laboratory.

Consent for publication

Not applicable.

Competing interests

The authors declare that they have no competing interests.

Publisher's Note

Author details

[1]Department of Companion Animal Clinical Sciences, Norwegian University of Life Sciences, Oslo, Norway. [2]Department of Basic Sciences and Aquatic Medicine, Norwegian University of Life Sciences, Oslo, Norway. [3]Department of Biosciences, University of Oslo, Oslo, Norway. [4]Section of Clinical & Comparative Neuropathology, Centre for Clinical Veterinary Medicine, Ludwig-Maximilians-Universität, Munich, Germany. [5]Department of Plant Sciences, Norwegian University of Life Sciences, Ås, Norway.

Received: 12 October 2018 Accepted: 16 April 2019
Published online: 27 April 2019

References

1. Kokame K, Kato H, Miyata T. Homocysteine-respondent genes in vascular endothelial cells identified by differential display analysis. GRP78/BiP and novel genes. J Biol Chem. 1996;271(47):29659–65.
2. van Belzen N, Dinjens WN, Diesveld MP, Groen NA, van der Made AC, Nozawa Y, Vlietstra R, Trapman J, Bosman FT. A novel gene which is up-regulated during colon epithelial cell differentiation and down-regulated in colorectal neoplasms. Lab Investig. 1997;77(1):85–92.
3. Kalaydjieva L, Gresham D, Gooding R, Heather L, Baas F, de Jonge R, Blechschmidt K, Angelicheva D, Chandler D, Worsley P, et al. N-myc downstream-regulated gene 1 is mutated in hereditary motor and sensory neuropathy-Lom. Am J Hum Genet. 2000;67(1):47–58.
4. Drogemuller C, Becker D, Kessler B, Kemter E, Tetens J, Jurina K, Jaderlund KH, Flagstad A, Perloski M, Lindblad-Toh K, et al. A deletion in the N-myc downstream regulated gene 1 (NDRG1) gene in greyhounds with polyneuropathy. PLoS One. 2010;5(6):e11258.
5. Bruun CS, Jaderlund KH, Berendt M, Jensen KB, Spodsberg EH, Gredal H, Shelton GD, Mickelson JR, Minor KM, Lohi H, et al. A Gly98Val mutation in the N-Myc downstream regulated gene 1 (NDRG1) in Alaskan malamutes with polyneuropathy. PLoS One. 2013;8(2):e54547.
6. Lachat P, Shaw P, Gebhard S, van Belzen N, Chaubert P, Bosman FT. Expression of NDRG1, a differentiation-related gene, in human tissues. Histochem Cell Biol. 2002;118(5):399–408.
7. Berger P, Sirkowski EE, Scherer SS, Suter U. Expression analysis of the N-Myc downstream-regulated gene 1 indicates that myelinating Schwann cells are the primary disease target in hereditary motor and sensory neuropathy-Lom. Neurobiol Dis. 2004;17(2):290–9.
8. Patzig J, Jahn O, Tenzer S, Wichert SP, de Monasterio-Schrader P, Rosfa S, Kuharev J, Yan K, Bormuth I, Bremer J, et al. Quantitative and integrative proteome analysis of peripheral nerve myelin identifies novel myelin proteins and candidate neuropathy loci. J Neurosci. 2011;31(45):16369–86.
9. Sharma A, Mendonca J, Ying J, Kim HS, Verdone JE, Zarif JC, Carducci M, Hammers H, Pienta KJ, Kachhap S. The prostate metastasis suppressor gene NDRG1 differentially regulates cell motility and invasion. Mol Oncol. 2017;11(6):655–69.
10. Bandyopadhyay S, Pai SK, Hirota S, Hosobe S, Tsukada T, Miura K, Takano Y, Saito K, Commes T, Piquemal D, et al. PTEN up-regulates the tumor metastasis suppressor gene Drg-1 in prostate and breast cancer. Cancer Res. 2004;64(21):7655–60.
11. Bandyopadhyay S, Pai SK, Gross SC, Hirota S, Hosobe S, Miura K, Saito K, Commes T, Hayashi S, Watabe M, et al. The Drg-1 gene suppresses tumor metastasis in prostate cancer. Cancer Res. 2003;63(8):1731–6.

12. Bandyopadhyay S, Pai SK, Hirota S, Hosobe S, Takano Y, Saito K, Piquemal D, Commes T, Watabe M, Gross SC, et al. Role of the putative tumor metastasis suppressor gene Drg-1 in breast cancer progression. Oncogene. 2004;23(33):5675–81.
13. Mao Z, Sun J, Feng B, Ma J, Zang L, Dong F, Zhang D, Zheng M. The metastasis suppressor, N-myc downregulated gene 1 (NDRG1), is a prognostic biomarker for human colorectal cancer. PLoS One. 2013;8(7):e68206.
14. Mi L, Zhu F, Yang X, Lu J, Zheng Y, Zhao Q, Wen X, Lu A, Wang M, Zheng M, et al. The metastatic suppressor NDRG1 inhibits EMT, migration and invasion through interaction and promotion of caveolin-1 ubiquitylation in human colorectal cancer cells. Oncogene. 2017;36(30):4323–35.
15. Askautrud HA, Gjernes E, Gunnes G, Sletten M, Ross DT, Borresen-Dale AL, Iversen N, Tranulis MA, Frengen E. Global gene expression analysis reveals a link between NDRG1 and vesicle transport. PLoS One. 2014;9(1):e87268.
16. Kachhap SK, Faith D, Qian DZ, Shabbeer S, Galloway NL, Pili R, Denmeade SR, DeMarzo AM, Carducci MA. The N-Myc down regulated Gene1 (NDRG1) is a Rab4a effector involved in vesicular recycling of E-cadherin. PLoS One. 2007;2(9):e844.
17. Pietiainen V, Vassilev B, Blom T, Wang W, Nelson J, Bittman R, Back N, Zelcer N, Ikonen E. NDRG1 functions in LDL receptor trafficking by regulating endosomal recycling and degradation. J Cell Sci. 2013;126(Pt 17):3961–71.
18. Ghalayini Mohammad K, Dong Q, Richardson Des R, Assinder Stephen J. Proteolytic cleavage and truncation of NDRG1 in human prostate cancer cells, but not normal prostate epithelial cells. Biosci Rep. 2013;33(3):e00042.
19. Lee JE, Kim JH. SUMO modification regulates the protein stability of NDRG1. Biochem Biophys Res Commun. 2015;459(1):161–5.
20. Heller BA, Ghidinelli M, Voelkl J, Einheber S, Smith R, Grund E, Morahan G, Chandler D, Kalaydjieva L, Giancotti F, et al. Functionally distinct PI 3-kinase pathways regulate myelination in the peripheral nervous system. J Cell Biol. 2014;204(7):1219–36.
21. McCaig C, Potter L, Abramczyk O, Murray JT. Phosphorylation of NDRG1 is temporally and spatially controlled during the cell cycle. Biochem Biophys Res Commun. 2011;411(2):227–34.
22. Park KC, Menezes SV, Kalinowski DS, Sahni S, Jansson PJ, Kovacevic Z, Richardson DR. Identification of differential phosphorylation and sub-cellular localization of the metastasis suppressor, NDRG1. Biochim Biophys Acta. 2018;1864(8):2644-2663.
23. Echaniz-Laguna A, Degos B, Bonnet C, Latour P, Hamadouche T, Levy N, Leheup B. NDRG1-linked Charcot-Marie-tooth disease (CMT4D) with central nervous system involvement. Neuromuscul Disord. 2007;17(2):163–8.
24. King RH, Chandler D, Lopaticki S, Huang D, Blake J, Muddle JR, Kilpatrick T, Nourallah M, Miyata T, Okuda T, et al. Ndrg1 in development and maintenance of the myelin sheath. Neurobiol Dis. 2011;42(3):368–80.
25. Sun J, Zhang D, Bae DH, Sahni S, Jansson P, Zheng Y, Zhao Q, Yue F, Zheng M, Kovacevic Z, et al. Metastasis suppressor, NDRG1, mediates its activity through signaling pathways and molecular motors. Carcinogenesis. 2013;34(9):1943–54.
26. Croessmann S, Wong HY, Zabransky DJ, Chu D, Mendonca J, Sharma A, Mohseni M, Rosen DM, Scharpf RB, Cidado J, et al. NDRG1 links p53 with proliferation-mediated centrosome homeostasis and genome stability. Proc Natl Acad Sci U S A. 2015;112(37):11583–8.
27. Kim KT, Ongusaha PP, Hong YK, Kurdistani SK, Nakamura M, Lu KP, Lee SW. Function of Drg1/Rit42 in p53-dependent mitotic spindle checkpoint. J Biol Chem. 2004;279(37):38597–602.
28. Manandhar G, Simerly C, Schatten G. Highly degenerated distal centrioles in rhesus and human spermatozoa. Hum Reprod. 2000;15(2):256–63.
29. Bellett G, Carter JM, Keynton J, Goldspink D, James C, Moss DK, Mogensen MM. Microtubule plus-end and minus-end capture at adherens junctions is involved in the assembly of apico-basal arrays in polarised epithelial cells. Cell Motil Cytoskeleton. 2009;66(10):893–908.
30. Zhou Y, Yang S, Mao T, et al. MAPanalyzer: a novel online tool for analyzing microtubule-associated proteins. Database. 2015;2015:article ID bav108. https://doi.org/10.1093/database/bav108.
31. Melotte V, Qu X, Ongenaert M, van Criekinge W, de Bruine AP, Baldwin HS, van Engeland M. The N-myc downstream regulated gene (NDRG) family: diverse functions, multiple applications. FASEB J. 2010;24(11):4153–66.
32. Shi XH, Larkin JC, Chen B, Sadovsky Y. The expression and localization of N-myc downstream-regulated gene 1 in human trophoblasts. PLoS One. 2013;8(9):e75473.
33. Hirata K, Masuda K, Morikawa W, He JW, Kuraoka A, Kuwano M, Kawabuchi M. N-myc downstream-regulated gene 1 expression in injured sciatic nerves. Glia. 2004;47(4):325–34.
34. Andersen ND, Srinivas S, Piñero G, Monje PV. A rapid and versatile method for the isolation, purification and cryogenic storage of Schwann cells from adult rodent nerves. Sci Rep. 2016;6:31781.

Paper II

Manuscript

Impaired NDRG1 functions in Schwann cells cause demyelinating neuropathy with focally folded myelin in a dog model of Charcot-Marie-Tooth type 4D

Fredrik S. Skedsmo[a], Arild Espenes[b], Michael A. Tranulis[b], Kaspar Matiasek[c], Gjermund Gunnes[b], Inge Bjerkås[b], Lars Moe[a], Susan Skogtvedt Røed[b], Mette Berendt[d], Merete Fredholm[e], Cecilia Rohdin[f, g], G. Diane Shelton[h], Per Bruheim[i], Marit H. Stafsnes[i], Zdenka Bartosova[i], Lene C. Hermansen[j], Øyvind Stigen[a], Karin H. Jäderlund[a*].

[a]Department of Companion Animal Clinical Sciences, Faculty of Veterinary Medicine, Norwegian University of Life Sciences, Ullevålsveien 72, 0454 Oslo,

[b]Department of Preclinical Sciences and Pathology, Faculty of Veterinary Medicine, Norwegian University of Life Sciences, Ullevålsveien 72, 0454 Oslo, Norway.

[c]Section of Clinical & Comparative Neuropathology, Centre for Clinical Veterinary Medicine, Ludwig-Maximilians-Universität, Veterinärstr. 13, D-80539 Munich, Germany

[d]Department of Veterinary Clinical Sciences, Faculty of Health and Medical Sciences, University of Copenhagen, Dyrlægevej 16, 1870 Frederiksberg C, Denmark.

[e]Department of Veterinary and Animal Sciences, Faculty of Health and Medical Sciences, University of Copenhagen, Grønnegårdsvej 2, 1870 Frederiksberg C, Denmark.

[f]Department of Clinical Sciences, Swedish University of Agricultural Sciences, Ultunaalléen 5A, 756 51 Uppsala, Sweden.

[g]Anicura Albano Small Animal Hospital, Rinkebyvägen 21, 182 36 Danderyd, Sweden.

[h]Department of Pathology, School of Medicine, University of California San Diego, 9500 Gilman Drive, La Jolla, California 92093-0709, United States of America.

[i]Department of Biotechnology and Food Science, Faculty of Natural Sciences, Norwegian University of Science and Technology, Sem Sælands vei 6, 7034 Trondheim, Norway.

[j]Department of Plant Sciences, Faculty of Biosciences, Norwegian University of Life Sciences, Universitetstunet 3, 1433 Ås, Norway

***Corresponding author: Karin Hultin Jäderlund, Karinhultin.jaderlund@nmbu.no, tel +4767232323.**

Abstract

Mutations in the *N-myc downstream-regulated gene 1* (*NDRG1*) cause degenerative polyneuropathy in ways that are poorly understood. We have investigated Alaskan Malamute dogs with neuropathy caused by a missense mutation in *NDRG1*. In affected animals, nerve levels of NDRG1 protein were reduced by more than 70% ($P < 0.03$) despite normal mRNA transcript levels. Nerve fibers were thinly myelinated, axonal loss was pronounced and teased fiber preparations showed both demyelination and remyelination. Inclusions of filamentous material containing actin, were present as early lesions in adaxonal Schwann cell cytoplasm and Schmidt-Lanterman clefts. This condition strongly resembles human Charcot-Marie-Tooth type 4D (CMT4D). However, the focally folded myelin with adaxonal infoldings segregating the axon found in this study are ultrastructural changes not previously described in CMT4D. Furthermore, lipidomic analysis revealed a profound loss of peripheral nerve lipids. Our data suggest that the low levels of mutant NDRG1 is insufficient to support Schwann cells in maintaining myelin homeostasis.

Keywords

Alaskan Malamute, canine, CMT, Greyhound, N-myc downstream-regulated gene 1, polyneuropathy.

1. Introduction

Degenerative neuropathies caused by mutations in *N-myc downstream-regulated gene 1* (*NDRG1*) are reported from humans, classified as Charcot-Marie-Tooth type 4D (CMT4D) (1), Greyhound show dogs (2) and Alaskan Malamute dogs (3). Cases of Alaskan Malamute polyneuropathy (AMP) were first described in Norway in the 1980's (4) and the disease was believed eradicated due to breeding programs, but re-

emerged in Scandinavia several decades later (3). We have previously described that AMP is inherited in an autosomal recessive manner and associated with a missense mutation in *NDRG1* causing a glycine to valine substitution (p.Gly98Val) in the NDRG1 protein (3). Clinically, the disease is slowly progressive and characterized by tetraparesis, pelvic limb ataxia, exercise intolerance and inspiratory stridor with onset of clinical signs in adolescence (3-5).

The NDRG1 protein is not specific for peripheral nerves and is detected in a wide variety of human, rodent and dog tissues with the highest levels in epithelial cells and myelinating glial cells (6-8). Still, how *NDRG1* mutations lead to neuropathies without clinical signs from other body systems, as well as the specific function of NDRG1 in the peripheral nervous system, are not clear (8, 9). The protein is functionally diverse being involved in several cellular processes, such as vesicular transport (10-12), microtubule dynamics (13), centrosome homeostasis (14) and lipid metabolism (15, 16). The posttranslational processing of NDRG1 is complex and tissue- and cell-specific (7). Notably, in myelinating Schwann cells high levels of phosphorylated NDRG1 localizes to the abaxonal cytoplasm and outer parts of the Schmidt-Lanterman clefts (7, 17). In addition to its role in neuropathies, the NDRG1 protein is also reported to be involved in carcinogenesis (18), metastasis suppression (19) and counteracts epithelial-mesenchymal transition (20).

Charcot-Marie-Tooth disease (CMT) denominates the most frequent forms of inherited neuropathies in humans. This is a heterogeneous group of diseases, further classified into subtypes based on clinical and pathological phenotype, mode of inheritance, nerve conduction velocity and causative gene (21). The CMT4 subgroup includes demyelinating neuropathies with autosomal recessive inheritance (22). One of them,

CMT4D, also known as Hereditary motor and sensory neuropathy-Lom (HMSNL), is a primary demyelinating neuropathy with onion bulb formation, accumulation of pleomorphic material in the Schwann cell cytoplasm and secondary axonal loss (23). In contrast, the *NDRG1*-associated polyneuropathy of Greyhound show dogs was reportedly dominated by axonal changes (2), while descriptions from Alaskan Malamutes are differing (3, 4). However, in-depth studies of nerves from affected Alaskan Malamute dogs have not previously been performed.

Naturally occurring neuropathies in dogs are increasingly recognized as models for human neuropathies (24, 25). As opposed to experimental rodents, dogs naturally develop similar diseases to humans. Dogs also have a larger body size and a life-expectancy that is more comparable to this species. Furthermore, dogs share environmental conditions and lifestyle with humans. Together this makes them excellent translational disease models (2). The fact that dogs can be investigated with sophisticated standardized neurological and electrophysiological tests is a further advantage, as it allows for a detailed characterization of the disease phenotype .

The aim of this study was to describe in detail the morphology, including ultrastructural changes, of AMP nerves and discuss these changes in relation to the cell biology of NDRG1 in general and, in particular, in Schwann cells, as well as in relation to the overall clinical presentation. Furthermore, studying Alaskan Malamutes with a *NDRG1* mutation is relevant to understand more about the involvement of NDRG1 in human diseases.

2. Materials and methods

2.1 Animals

Nineteen privately owned pure-bred Alaskan Malamute dogs (14 affected dogs and 5 controls free from clinical signs of polyneuropathy) were included in the study (summarized in Table 1, more detailed information is provided in Supplementary Table A.1). Sixteen out of nineteen were genotyped for the *NDRG1*-allele using the TaqMan assay described by Bruun and coworkers (3); Twelve dogs (*n*=12) were classified as homozygous mutants (mut/mut) and four dogs were homozygous wild type (wt/wt) (*n*=4). Whether genotyped or not, all affected dogs (*n*=14) were closely related to each other and presented with neurological signs classically associated with AMP. All samples for the study were collected by veterinarians after written consent from the dog owners. No ethics committee approval was required as all samples were taken as part of the standard diagnostic procedures, in vivo (*n*=7) and/or postmortem (*n*=15), and the investigation did not interfere or impede other tests. Information regarding sex, age at sampling, results from electrodiagnostic testing (electromyography (EMG) and motor nerve conduction velocity (MNCV)), and long-term clinical course was collected from the medical records.

Table 1
Overview of Alaskan Malamute dogs included in the study

Case number and sex	Age (years) at sampling	Control number and sex	Age (years) at sampling
1 Female	6	1 Female	8
2 Male	8	2 Female	11
3 Female	3, 4, 9	3 Male	12
4 Female	2, 6**	4 Male	7
5 Female	1, 3	5 Male*	13
6 Male	2		
7 Female	1		
8 Female	1		
9 Female	2		
10 Male*	5		
11 Male*	2		
12 Male	1		
13 Male	6		
14 Female	6		

* All dogs were genotyped except case 10, case 11 and control 5, due to technical problems with DNA extraction from paraffin-embedded material.
** Only muscle biopsies.
Note: All cases except case 1 and 2 were included in (5). Furthermore, case 3, 5 and 6 were included in (3).

2.2 Tissue sampling

Biopsies from the common fibular nerve and the cranial tibial, biceps femoris and gastrocnemius muscles were taken under general anesthesia as part of the diagnostic workup. Formalin-fixed and fresh samples were shipped to diagnostic laboratories for evaluation. Unfixed biopsies were evaluated cryohistologically. Fixed nerve biopsies were resin-embedded and evaluated in semithin sections (1 µm), while fixed muscle biopsies were paraffin-embedded and routinely stained with hematoxylin and eosin. A standard panel of histochemical stains and reactions were used for the cryosections (26).

Postmortem examinations were carried out shortly after pentobarbital-euthanasia. Samples for immunohistochemistry and immunofluorescence were fixed in 10% buffered formalin and subsequently paraffin-embedded. Samples for Western blotting and RT-qPCR were snap frozen in isopentane, transferred to liquid nitrogen and stored at -80 °C until analysis. Samples for electron microscopy and nerve fiber teasing were gently separated into individual fascicles and fixed in 2.5% glutaraldehyde in Sorensen's phosphate buffer (0.1 M, pH 7.4) for 4 hours at room temperature. In individual dogs, nerve samples were prepared from one or more of the following sites: Tibial nerve (*n*=7), recurrent laryngeal nerve (*n*=5), sciatic nerve (*n*=7), ulnar nerve (*n*=4), obturator nerve (*n*=5), common fibular nerve (*n*=13), superficial radial nerve (*n*=6), facial nerve (*n*=1), hypoglossal nerve (*n*=4), vagosympathetic trunk (*n*=3), femoral nerve (*n*=1), brachial plexus (*n*=1), ventral lumbar nerve root (*n*=1) and thoracic nerve root (*n*=1). In addition, a routine postmortem examination was performed, including sampling from cranial tibial, biceps femoris and gastrocnemius muscles.

2.3 Western blotting

Nerve samples from four *NDRG1*$^{mut/mut}$ and four *NDRG1*$^{wt/wt}$ Alaskan Malamutes were thawed, and the epineurial fat removed. The samples were lysed in homogenizing buffer (Tris HCl 50 mM, NaCl 150 mM, EDTA 1 mM, DOC 0.25%, NP40 1%) supplemented with protease inhibitor cocktail (Roche complete, Roche Holding AG, Basel, Switzerland) and anti-phosphatase (Halt™ Phosphatase Inhibitor Cocktail, Thermo Fisher Scientific, Massachusetts, USA). Protein concentrations were measured using Protein assay (Bio-Rad, Hercules, California, USA).

Twenty-five µg protein from the samples were separated by sodium dodecyl sulfate (SDS) polyacrylamide gel electrophoresis (12% Criterion™ XT-Bis-Tris, Bio-Rad), and transferred to polyvinylidene fluoride (PVDF) membrane (GE Healthcare, Little Chalfont, United Kingdom). The membrane was blocked with 5% non-fat milk in TBS-Tween for 90 minutes at room temperature and incubated with primary antibodies diluted in blocking buffer overnight at 4 °C. Thereafter, the membrane was washed and incubated for 90 minutes in 1% non-fat milk containing Alkaline Phosphatase-conjugated anti-mouse IgG (dilution 1/4000, Thermo Fisher Scientific) or anti-rabbit IgG (dilution 1/4000, GE Healthcare). The membrane was developed using EFC™ substrate (GE Healthcare) and visualized with Typhoon 9200 (Amersham Bioscience, GE Healthcare).

Protein transfer efficiency and protein loading were assessed by staining total protein on the PVDF membranes by SYPRO® Ruby Protein Blot Stain (Molecular Probes, Thermo Fisher Scientific). Band signals were quantified with ImageQuant TL (GE Healthcare) and statistical analyses performed with a non-parametric test (Mann Whitney U-test) in GraphPad Prism (GraphPad Software, San Diego, California, USA).

2.4 RT-qPCR

Nerve tissue from four *NDRG1*$^{mut/mut}$ and four *NDRG1*$^{wt/wt}$ Alaskan Malamutes was homogenized in Trizol (Thermo Fisher Scientific) using a Mixer mill 301 (Retsch, Haan, Germany) with stainless steel beads (∅ 3 mm, Qiagen, Hilden, Germany), in cycles of 2 min at 25 Hz with 1 min cooling on ice in between. Total RNA was extracted following the Trizol protocol for samples with high fat content, and further purified with a Rneasy Plus minikit (Qiagen), according to the manufacturer's protocol.

RNA was quantified by an Epoch Microplate Spectrophotometer with Take3 plate (BioTek Instruments Inc, Vermont, USA). The procedure robustly yielded RNA of good quality, which was confirmed by analysis of a sub-set of samples (RIN-values > 5) with an Agilent Bioanalyzer and an RNA 6000 Nano Kit (Agilent Technologies, Santa Clara, California, USA). Total RNA was stored at -80 °C.

cDNA was synthesized using SuperScript III Reverse Transcriptase, RNase Out, dNTP mix and Random Primers (all from Invitrogen, Thermo Fisher Scientific), under these conditions: 5 min at 65 °C, >1 min on ice, 5 min at 25 °C, 1 h at 50 °C and 15 min at 70 °C.

qPCR was performed with LightCycler 480 Sybr Green I Master mix (Roche) and cDNA corresponding to 2.5 ng RNA. The following primers were used: caNDRG1-F2 (TGAACAACCCCGAGATGGTG), caNDRG1-R2 (CCCGGAGATCTTGGATGCAG), caGAPDH-1F (GTATGATTCTACCCACGGCAAAT) and caGAPDH-1R (GATGGACTTCCCGTTGATGACAA). Samples were run in quadruplets in a total volume of 20 µl. The LightCycler 96 System (Roche) was run under the following conditions; 5 min at 95 °C, 40 cycles of 10 sec at 95 °C, 10 sec at 60 °C, and then 10 sec at 72 °C; and melting curve with 5 sec at 95 °C, 1 min at 65 °C and 97 °C.

Relative expression levels were calculated using the Relative Standard Curve method with standard curves obtained from a random sample, and *NDRG1* expression was normalized to *GAPDH*. Statistics (Mann Whitney U-test) were performed in GraphPad Prism.

2.5 Processing for transmission electron microscopy and nerve fiber teasing

Fixed samples were transferred to phosphate buffer and stored at 4 °C until processing. 2 mm long pieces were cut from the fascicles, post-fixed in 1% osmium tetroxide at 4 °C, dehydrated by an ascending acetone series and embedded in epoxy. Sections were cut using a diamond knife (Diatome, Hatfield, Pennsylvania, USA) on a Leica EM UC 6 ultramicrotome (Leica, Wetzlar, Germany). Semithin (0.5 µm) sections were stained with toluidine blue and safranin-O, and evaluated light microscopically using a Zeiss Axio Imager 2 microscope equipped with an Axiocam 506 color camera (Zeiss, Oberkochen, Germany). Ultrathin (70 nm) sections were picked up on formvar/carbon-coated slot grids, contrasted with uranyl acetate and lead citrate, and studied using a Fei Morgagni 268 transmission electron microscope (FEI, Oregon, USA) equipped with an Olympus Veleta CCD camera and iTEM software (Olympus, Tokyo, Japan). For nerve fiber teasing, fixed nerve fascicles were post-fixed in 2% osmium tetroxide at room temperature, washed in phosphate buffer, immersed in glycerol and teased under a dissection microscope.

2.6 Antibodies

Details about the antibodies used in the analyses are specified in Table 2.

Table 2
Antibodies and dilutions used in the analyses

Name	Catalog number	Producer	Dilutions		
			IF	IHC	WB
Anti-NDRG1	WH0010397	Sigma-Aldrich, Merck, Darmstadt, Germany	1/2000	NA	1/2000
Phospho-specific anti-NDRG1 (Thr346)	5482	Cell Signaling Technology, Leiden, Netherlands	NA	NA	1/1000
Anti-neurofilament 200	064H-4809 (batch number)	Sigma-Aldrich, Merck, Darmstadt, Germany	1/400	NA	NA
Anti-beta actin	MA1-140	Invitrogen, Thermo Fisher Scientific, Massachusetts, USA	1/2000	NA	NA
Anti-CD3	A-0452	Dako, California, USA	NA	1/500	NA
Anti-CD79	NB100-64347	Novus Biologicals, Colorado, USA	NA	1/750	NA
Anti-Iba1	019-19741	Fujifilm Wako Chemicals, Neuss, Germany	NA	1/250	NA

IF = Immunofluorescence, IHC = Immunohistochemistry, WB = Western blotting, NA = Not analyzed

2.7 Immunofluorescence

Sections of 3-4 μm from formalin-fixed and paraffin-embedded tissues were placed on glass slides (Superfrost Plus®, Menzel Gläser, Thermo Fisher Scientific) and stored at 4 °C until staining. The slides were deparaffinized in xylene and rehydrated through a descending alcohol series. Antigen retrieval was performed by heating the slides in citrate buffer (0.01 M, pH 6.0) in a microwave. The temperature in the solution was held at 92 °C degrees for 5 minutes, thereafter the slides were kept in the hot solution for another 15 minutes before being rinsed in phosphate-buffered saline (PBS). Non-specific antibody activity was blocked by incubating the slides for 30 minutes in 5% bovine serum albumin (BSA) with 2% normal serum from the same species as the

secondary antibody. The sections were incubated with primary antibodies diluted in blocking buffer for 60 minutes at concentrations summarized in Table 2. The slides were rinsed three times for 5 minutes in PBS and incubated in secondary antibodies diluted in PBS for 30 minutes. The secondary antibodies used were goat anti-mouse IgG Alexa Fluor 488 (dilution 1/400, catalog number A-11029, Invitrogen, Thermo Fisher Scientific) and goat anti-rabbit IgG Alexa Fluor 594 (dilution 1/400, catalog number A-11006, Invitrogen, Thermo Fisher Scientific). The slides were rinsed three times for 5 minutes in PBS and mounted with ProLong Gold Antifade Mountant with 4',6 diamidino-2-phenyl indole (DAPI; Molecular Probes, Thermo Fisher Scientific). Slides, where the primary antibodies were omitted, were used as negative controls. Micrographs were taken using an Axio Imager 2 microscope equipped with an Axiocam 506 mono camera (Zeiss).

2.8 Immunohistochemistry

Sections of 3-4 μm were placed on glass slides (Superfrost Plus®) and stored at 4 °C until staining. The slides were deparaffinized in xylene and rehydrated through a descending alcohol series. Between steps, sections were washed twice in PBS for 5 min, except before incubation with primary antibodies. For anti-Iba1, the slides were incubated with trypsin (1 mg/mL) in Tris HCl (0.1 M, pH 8 with 0.1% $CaCl_2$) for 40 min at 37 °C before inhibition of endogenous peroxidase activity. For anti-CD3 and anti-CD79, antigen retrieval was performed by heating the slides in Tris/EDTA (pH 9.1) in a microwave before inhibition. The temperature in the solution was held at 92 °C degrees for 5 min, thereafter the slides were kept in the hot solution for another 5 min before the procedure was repeated. Endogenous peroxidase was inhibited with 3%

H_2O_2 in methanol for 10 min. Non-specific antibody binding was blocked by incubating the slides for 20 min in 5% BSA with 2% goat serum. The sections were incubated for 60 min with primary antibodies, diluted in 1% BSA at dilutions indicated in Table 2. Next, the sections were incubated with secondary antibodies conjugated to horseradish peroxidase-labelled polymer from the EnVision kit (catalogue number K4009, Dako) for 30 min, and developed with AEC-substrate for 5 min. The sections were counterstained with haematoxylin and mounted with Aquatex (Merck, Darmstadt, Germany). Slides, where the primary antibodies were omitted, were used as negative controls. The sections were evaluated independently by two different observers (FSS and AE), and labelling was concealed prior to assessment.

2.9 Morphometry

Images from semithin sections of n. fibularis communis (*n*=8) or n. tibialis (*n*=3) were evaluated by Image-Pro Plus (Media Cybernetics, Rockville, Maryland, USA). By using the segmentation tool in the computer software, the area of the nerve fibers and axons were measured. Thereafter, the diameters of these were derived from the area of a circle of equivalent area, as reported to be the method of choice (27), and the g-ratios calculated. Graphs were produced in GraphPad Prism. An example of the image analysis is provided in Supplementary Fig B.2.

2.10 Extraction of lipids from peripheral nerves

Lipid extraction from nerves and chromatographic analysis were performed as previously described (28). Lipids from nerve tissue were extracted using the solvent system based on the Folch method (29). A Precellys®24 bead homogenizer equipped with a Cryolys temperature controller (All Bertin Technologies SAS, Montigny-Le-Bretonneux, France) was used to disrupt and homogenize the tissue for lipid extraction. Nerve tissue (50 mg) was homogenized with zirconium oxide beads (0.5 ± 0.01 g, ∅ 1.4 mm) in 500 µL of a cold mixture of chloroform/methanol (2:1, v/v). The tissue was kept frozen during cutting and weighing. Final rounds (5-10) of bead-beating for 30 sec at 6500 rpm, with an intermediate 15 sec pause between rounds, were performed. Another 500 µL of a cold mixture of chloroform/methanol (2:1, v/v) was added to the sample and the tube was shaken for 10 min using a thermoshaker (Thermal shake lite, VWR) and phase separation was induced by adding 200 µL of 20 mM acetic acid. After 10 min of shaking (1500 rpm, 16 °C), tubes were centrifuged for 6 min at maximum speed (13400 rpm) using a small centrifuge (MiniSpin, Eppendorf, Hamburg, Germany). A volume of 400 µl of the chloroform layer (lower) was collected and the sample re-extracted with 500 µl of a cold mixture of chloroform/methanol/water (86:14:1, v/v), vortexed and centrifuged as above. From the lower layer, 650 µl was collected and pooled with the first extract. The resulting extract was filtered through a syringe filter with GHP membrane, 0.2 µm, ∅ 13 mm (Acrodisc®, Pall Laboratory, Port Washington, New York, USA) and kept in a dark glass vial with a PTFE-lined lid and kept at -20 °C until analysis with ultra-performance convergence chromatography tandem mass spectrometry (UPC^2-MS/MS). Dichloromethane was used as diluent for lipid extracts.

2.11 Chromatographic analysis of lipids

A lipid profile analysis was performed using an UPC^2® separation system coupled to a hybrid quadrupole orthogonal time-of-flight mass spectrometer SYNAPT G2-S HDMS (Waters, Milford, Massachusetts, USA). A previously described analytical method (30) was adopted and modified, as described in (28). The mass spectrometer was operated in MS^E mode and the collision energy ramped from 20 to 30 eV for positive ion mode and from 20 to 35 eV for negative ion mode. Data were acquired over the mass range of 50–1200 Da and the resolution of the mass spectrometer was 20000. Both positive and negative ion electrospray ionization modes were applied. MS tuning parameters were set as follows: capillary voltages 3.0 kV and -2.5 kV for positive and negative ionization modes, respectively; source temperature 150 °C; the sampling cone 40 V; source offset 60 V; desolvation temperature 500 °C; cone gas flow 50 L/h; desolvation gas flow 850 L/h; nebulizer gas pressure 4 bar. Leucine enkephalin was used as the lock mass. Data were collected using the MassLynx 4.1 (Waters Corporation) software. Raw data were processed using a Progenesis QI software (Nonlinear Dynamics, Waters) with an in-built LipidBlast database (31) and LipidMaps database (32) for lipid identification. Identification of a lipid compound is based on the following main characteristics: retention time of the appropriate lipid class, accurate mass (ppm error <5), isotope pattern similarity (>80%), and fragmentation pattern. The lipid nomenclature and shorthand notation described by LIPID MAPS (33) and Liebisch G. et al (34) , were followed.

Further, the data were filtered using an in-house developed script collecting total abundances for each individual lipid class. Experimentally determined response

factors (Rf) from external standard dilution series, were used for correction of raw abundances to show semi-quantitative composition of lipid classes in the studied samples.

3. Results

3.1 Long-term clinical course and electrodiagnostic examination

Four of the 14 affected dogs were euthanized, at the owner's request, in conjunction with the diagnosis of AMP. Ten of the affected dogs were allowed to survive this disease stage and were followed up (median 44 months, range 12-100 months) by repeated examinations or contact with clinicians in the research group. In three of these 10 dogs, the clinical signs gradually progressed until euthanasia. In one other dog, the clinical signs progressed in the two years following diagnosis, but the dog was subsequently lost to follow up. In the remaining six dogs followed up, both the gait abnormalities and the exercise intolerance slowly improved during the months after nadir and then stabilized. However, none of the dogs returned to normal and the inspiratory stridor persisted. At a later stage (at the age of 3 and 6 years, respectively), two affected dogs presented with regurgitation due to development of megaoesophagus (Fig. 1), and were then euthanized. Eleven of the 14 affected dogs were subjected to postmortem examination and autopsy confirmed megaoesophagus in three dogs (including the two dogs with regurgitation).

MNCV in the fibular (*n*=4, mean 23.13 m/s, SD 14.24, reference 79.8±1.9 (35)) and ulnar nerves (*n*=10, mean 37.5 m/s, SD 12.73, reference 58.9±1 (35)) were decreased in all the examined dogs (Supplementary Table A.1). In two dogs, MNCV could not be determined as no compound muscle action potential (CMAP) was produced by

stimulation. EMG revealed spontaneous activity with fibrillation potentials and positive sharp waves in several muscles in all dogs tested (*n*=10). In two dogs, repeated MNCV measurements were performed. For case three, the MNCV in the ulnar nerve was 30, 40 and 56.3 m/s at the age of three, eight and nine years, respectively. Furthermore, the MNCV in the fibular nerve was 31.4 m/s at the age of three years, but not possible to measure at the age of nine. For case four, the MNCV in the fibular nerve was 29 m/s and 26.9 m/s at the age of two and five years, respectively.

3.2 Levels of NDRG1 protein and mRNA

Nerves from affected dogs had reduced NDRG1 protein levels compared to controls (Figs. 2A, C). The intensity of the 42 kDa band, corresponding to the full length protein, as well as the bands with molecular weights between 32 and 40 kDa, were reduced by approximately 70% in the *NDRG1*$^{mut/mut}$ dogs (*P*=0.029). Additionally, there was a significant reduction in signal intensity from the band corresponding to NDRG1 phosphorylated at residue Thr346 (pNDRG1) in this group of dogs (*P*=0.029, Figs. 2B, C).

In contrast, the mRNA levels in nerves of *NDRG1*$^{mut/mut}$ dogs were not significantly different from the controls (*P*=0.2, Fig. 2D).

3.3 Pathology

3.3.1 Teased nerve fibers

In nerves from affected dogs examined by nerve fiber teasing, internodal lengths and myelin thickness varied (Fig. 3). Demyelinated segments and short internodes with

reduced myelin thickness (intercalated internodes), consistent with remyelination, were present. The changes had a multifocal distribution, and severely affected internodes intermingled with internodes without observable changes. This distribution is typical for a demyelinating disease (36, 37). In some cases, paranodal retraction and widening of the nodal gap were evident. Focal thickenings of the nerve fibers were present, mostly internodally, occasionally close to the Schwann cell perikaryon (Fig. 3d), but paranodal localization was also observed. At this level, it was not possible to ascertain whether the swellings derived from the axon, the Schwann cell or both. Wallerian-like axonal degeneration with fragmentation of the myelin sheath was observed in only a few fibers (not shown).

3.3.2 Light microscopy

Nerves from *NDRG1*$^{mut/mut}$ Alaskan Malamutes exhibited a reduction in the density of nerve fibers (Fig. 4A), especially large myelinated fibers. The loss of nerve fibers was accompanied by a concurrent increase in endoneurial connective tissue. These changes varied inter- and intraindividually from only mild affection to severe loss of nerve fibers with concomitant fibrosis. As shown morphometrically for the common fibular nerve, there was a shift in the distribution of myelinated nerve fibers towards smaller diameter fibers (Fig. 4B). As the same shift was observed in axonal diameter-frequency histograms, this shift is probably caused by a combination of loss of large myelinated fibers and reduced myelin thickness. While the fibular nerves from the *NDRG1*$^{wt/wt}$ Alaskan Malamutes had the expected bimodal diameter distribution of myelinated fibers (38), the distribution in nerves from some of the cases approached unimodality (for example case four). For case three and five, biopsies taken at different ages

allowed assessment of a potential disease progression. The investigations showed a shift towards thinner fibers at greater age.

When nerves were studied at higher magnification, many of the remaining fibers had thin myelin sheaths in relation to the axonal size (Figs. 5E-G), in agreement with results from the study of teased fibers and our finding that the g-ratios of the *NDRG1*$^{mut/mut}$ Alaskan Malamutes were shifted towards higher values compared to the control (Supplementary Fig. B.1). Presumptive regenerative clusters were observed in a minority of the nerves (Fig. 5E). Swollen nerve fibers were present in the nerves from the *NDRG1*$^{mut/mut}$ Alaskan Malamutes (Figs. 5F, G) and studied more closely at the ultrastructural level (see subsection 3.3.3).

Lesions were observed at a similar degree in both proximal (for example nerve roots and sciatic nerves) and distal nerve segments (such as tibial, fibular and recurrent laryngeal nerves), long (for example recurrent laryngeal nerve) and short nerves (obturator nerve), and involved both mixed and purely sensory nerves (superficial radial nerve).

In skeletal muscle, angular atrophy of myofibers (varying from scattered singular to small and large groups) were present (Fig. 5A). The angular atrophied fibers were of both fiber types as shown by the ATPase reaction (Fig. 5B). The normal mosaic pattern of muscle fiber types was regionally absent in some cases with fiber type grouping, supporting attempts at reinnervation (Fig. 5B).

3.3.3 Ultrastructural pathology

The ultrastructural examination confirmed the presence of thinly myelinated nerve fibers and real onion bulbs, as the cells present in these structures had a basal lamina, and therefore represent supernumerary Schwann cells (Fig. 6A). Onion bulbs and thinly myelinated nerve fibers suggest repeated episodes of demyelination and remyelination. Macrophages with intracytoplasmic vacuoles were present around demyelinated nerve fibers and also observed intratubary (not shown). The presence of Iba1+-macrophages in the endoneurium was confirmed by immunohistochemistry (see subsection 3.3.5).

A frequent finding was accumulation of filamentous material in the cytoplasm of myelinating Schwann cells. This material was observed in the adaxonal Schwann cell cytoplasm (Fig. 6B) or in the inner part of dilated Schmidt-Lanterman clefts (Figs. 6C, D). Occasionally, the Schmidt-Lanterman clefts were disrupted and then associated with dyscompacted myelin sheaths mixed with a pleomorphic, coarsely granular osmiophilic material (Figs. 6E, F) dispersed between the sheets. This morphologically heterogenous material probably consists of a mixture of the aforementioned filamentous material and lipids from myelin degradation as it intermingled with fragments of periodically structured lamellae (39).

Focally folded myelin was often observed. In some instances, it involved the whole thickness of the myelin sheath, causing redundant myelin loops internal (Fig. 7A) or external to the myelin sheath (Figs. 7C, D). Occasionally, myelin sheaths lacking axons were found (Fig. 7B). Additionally, infoldings derived from the inner part of the myelin sheaths were present (Figs 7E, F). The folds evolved from the Schmidt-Lanterman clefts (Figs 7C, D, F) and occasionally seemed to subdivide the axon into pockets (Fig. 7F, higher magnification in 8A). This resulted in several axonal structures enclosed by

the same myelin sheath, separated by thin myelin septa derived from the adaxonal part of the sheath (Figs. 6E, 7F, 8A-F). These findings were supported by immunofluorescence, showing the presence of several neurofilament-positive axonal structures within one NDRG1-positive Schwann cell (Fig. 8B). Degenerating organelles were present in the myelin-enclosed axonal pockets (Figs. 8A-8D) and in adjacent axon segments (Figs. 8E-F), suggestive of disrupted axonal transport and early axonal degeneration. Despite an overall increase in nerve fiber diameter, the diameter of the axon was often reduced and the axonal outline distorted in the segments with focally folded myelin, seemingly compressed by the myelin infoldings and adaxonal Schwann cell material (Figs. 8E, F).

3.3.4 Immunofluorescence

As structures resembling Hirano bodies, containing actin and actin-related proteins (40), have been described in the Schwann cell cytoplasm of rodents with *NDRG1* mutations (9), immunofluorescence was performed on paraffin sections with antibodies against β-actin and neurofilament. In nerves from the *NDRG1*$^{mut/mut}$ Alaskan Malamutes, β-actin-positive aggregates were present focally in myelinating Schwann cells (Fig. 9). More specifically, the β-actin signal was present in thin strands and occasionally formed circular or semi-circular structures. The diameter of the neurofilament-positive axon was reduced in these areas, but axonal swellings were present in adjacent segments. Occasionally, the actin-positive material surrounded small axonal structures only coupled to the main axonal structure through thin connections.

3.3.5 Immunohistochemistry

Infiltration and/or proliferation of macrophages, T- and B-lymphocytes in the nerves were investigated with antibodies against Iba1, CD3 and CD79, respectively. While increased numbers of Iba1+ cells in the endoneurium were observed in *NDRG1*$^{mut/mut}$ Alaskan Malamutes compared to *NDRG1*$^{wt/wt}$, no difference between the genotypes was observed for CD3 and CD79 (not shown).

3.4 Lipid analysis

Analysis of peripheral nerve lipid composition revealed decreases in hexosylceramides (HexCer), sphingomyelins (SM) and phospholipids (PC, PE), while cholesteryl esters (CE) and triacylglycerols (TG) were increased in the relative lipid class distribution in the *NDRG1*$^{mut/mut}$ Alaskan Malamutes (Fig. 10 and Table 3) compared to *NDRG1*$^{wt/wt}$.

Table 3
Relative lipid class distribution in peripheral nerves from Alaskan Malamute polyneuropathy cases (*NDRG1*$^{mut/mut}$) and controls (*NDRG1*$^{wt/wt}$)

Lipid class	*NDRG1*$^{wt/wt}$		*NDRG1*$^{mut/mut}$	
	Mean %	SD	Mean %	SD
MG	0.79	0.47	0.88	0.83
DG	2.29	0.65	1.97	1.09
TG	55.31	11.54	78.01	12.41
HexCer	3.70	1.33	0.99	0.49
HexCer(OH)	1.33	0.43	0.37	0.17
CE	2.85	1.57	5.53	4.81
PC	6.31	1.51	3.30	1.44
FC	0.20	0.06	0.09	0.06
SM	21.73	4.77	5.99	3.04
LPC	0.05	0.02	0.06	0.02
PE	5.43	1.72	2.81	1.66
Total	100		100	

MG = Monoacylglycerols, DG = Diacylglycerols, TG = Triacylglycerols, HexCer = Hexosylceramides, , CE = Cholesteryl esters, PC =Phosphatidylcholines, FC = Free Cholesterol, SM = Sphingomyelins, LPC = Lysophosphatidylcholines, PE = Phosphatidylethanolamines.

4. Discussion

In this paper we clarify features of the *NDRG1*-associated polyneuropathy of Alaskan Malamute that have not previously been reported. By Western blotting, we show that the affected dogs have a significant reduction of NDRG1 protein in the nerves, although NDRG1 mRNA levels were not reduced. The accumulation of filamentous material in the adaxonal cytoplasm of Schwann cells and in dilated Schmidt-Lanterman clefts, and the prominent myelin outfoldings and infoldings, sometimes dividing the axon, are all changes likely reflecting a dyshomeostasis of the Schwann cell and its ability to maintain the myelin sheath. The result is demyelination, remyelination and, finally, axonal loss, with infiltration of macrophages. Lipid analysis showed that the

pathological lesions in nerves of the affected Alaskan Malamutes were associated with distinct changes in the lipid composition.

When dealing with neuropathies, the differentiation between a primary demyelinating and a primary axonal disease is important, not only in search for the etiology, but also when trying to elucidate the functions of a deficient protein involved or the mechanisms leading to nerve damage. However, in many neuropathies it can be challenging to identify which part of the axon-glia axis is the primary target. Secondary axonal degeneration is known to occur in demyelinating neuropathies (41, 42) and axonal disease can cause secondary demyelination (43). In human CMT4D patients, demyelinating changes are found in childhood, but rapidly followed by axonal loss (9, 44) and severe clinical signs (44, 45). The disease in mice with *Ndrg1* mutations, however, was mainly characterized by demyelination, with axonal loss being less pronounced (9). The changes observed in the nerves of affected Alaskan Malamutes in this study indicate a demyelinating disease with remyelination, characteristic axonal changes and eventually loss, resembling descriptions from humans and rodents with *NDRG1* mutations (9, 23, 45, 46). This contrasts with previous reports from dogs (2, 3). In a study of Greyhounds lacking NDRG1 (2), and in a previous report on the same AMP as presented here (3), it was concluded that the disease was predominantly axonal or mixed due to the presence of degenerative axonal changes in segments without concurrent myelin abnormalities. However, in the Greyhounds, thinly myelinated (i.e. remyelinated) nerve fibers, dyscompaction of the adaxonal myelin sheath and granulofilamentous inclusions in the adaxonal Schwann cell cytoplasm were also observed (2). Thus, the changes in nerves of humans, rodents and dogs with NDRG1 abnormalities share certain similarities, and AMP is indeed a new model for

human CMT4D, replicating both the demyelination and secondary axonal changes, in both motor and sensory nerve fibers, present in the human disease (23, 46).

Furthermore, the demyelinating features of the disease and previously reported localization of canine NDRG1 (7), indicate that the Schwann cells are primarily affected in AMP. The onset of clinical signs coincides with a period of intense body growth where the internodal length increases massively (9) as the largest fibers in the adult dog have internodes up to 2 mm in length (47). The clinical improvement in gait abnormalities and exercise intolerance in adulthood in most of the dogs, suggests that the NDRG1 protein is particularly important during this growth period. However, NDRG1 is also vital to maintain the myelin sheath in adult dogs, emphasized by active changes observed in the nerves and additional clinical signs (such as megaoesophagus) showing up later in life. A progressive polyneuropathy is described in human CMT4D patients with gait disturbance in their first decade, upper limb involvement in their second and sensorineural deafness in their third decade of life (44). Disease progression in adulthood in affected Alaskan Malamutes was documented in nerve biopsies from a few dogs, including morphometric analyses of semi-thin nerve sections. Results from electrodiagnostic examinations were in agreement with a polyneuropathy involving motor nerve fibers, however repeated examinations of a few dogs during follow up showed contradictory results regarding progression or not.

The filamentous material present in the adaxonal cytoplasm and inner part of the Schmidt-Lanterman cleft resembles inclusion material reported from the same location in nerves of human patients and rodent models with *NDRG1* mutations (9, 23, 45, 46). In humans with CMT, this material is seemingly specific for the 4D subtype

(46, 48), however, to the best of our knowledge, the content of the material has not been ascertained. From studies in rodent models, the inclusions have been proposed to represent Hirano bodies based on morphological criteria (9), but in human CMT4D nerves, a similar material did not have the structured morphology of true Hirano bodies (23). Hirano bodies are described as paracrystalline inclusions consisting of sheets of parallel actin filaments with a diameter of approximately 6-10 nm (40). The filamentous material observed in the nerves of affected Alaskan Malamutes lacked the paracrystalline structure reported from rodents (9, 49), but otherwise resembles the inclusion material reported from humans and rodents by its ultrastructural morphology and localization. Furthermore, we demonstrate its richness in actin by immunofluorescence. As the material was present in nerve fibers without other morphological changes, we consider this an early step in the sequence of events leading to demyelination and subsequently axonal degeneration and loss.

The apparent division of the axon into several axonal pockets regionally within one myelin sheath is not reported in CMT4D (9, 23, 45, 46, 50-52), but is described from neuropathic Greyhounds lacking NDRG1 (2). This condition seems to be characterized by intrusion of the Schwann cell into the axon and, thus, represents focal hypermyelination, frequently associated with the Schmidt-Lanterman clefts. Focally folded myelin is described from several neuropathies caused by mutations in genes encoding phosphoinositide-associated proteins such as *MTMR2* and *MTMR13* (CMT4B) (53, 54), *Pten* (55) and *FRABIN* (CMT4H) (56). The folds usually arise from Schmidt-Lanterman clefts and paranodes (53, 55, 56), which are considered the main sites of myelin addition (55, 56). The myelinating Schwann cell is a highly polarized cell type, with abaxonal and adaxonal regions (57) interconnected by Schmidt-Lanterman clefts (43, 58). Specific phosphoinositides are associated with the different membrane

domains in the Schwann cell (59). The spatial and temporal regulation of these phosphoinositides are important as they recruit different effector molecules (60) and participate in specific signaling pathways (61). A possible explanation for the occurrence of myelin folds in the aforementioned neuropathies, and the AMP presented here, is dysregulated phosphoinositide levels in non-compact myelin leading to abnormal signaling (56), uncontrolled membrane growth (55) and focal hypermyelination. Consistent with this, ectopic insertion of phosphatidylinositol 3,4,5-trisphosphate (PtdIns(3,4,5)P_3) in the apical domain of epithelial cells causes phosphoinositide-dependent recruitment of Rho GTPase activators, resulting in actin-rich membrane protrusions (61). Furthermore, deranged PtdIns(3,4,5)P_3 levels in the apical-like adaxonal domain and Schmidt-Lanterman clefts of myelinating Schwann cells were suggested to cause actin-rich membrane protrusions progressing to myelin fold formation in a *Pten* mutant (55).

As NDRG1 participates in recycling of endosomes to the plasma membrane (11, 12) and in this process is recruited by binding to a specific phosphoinositide (phosphatidylinositol 4-phosphate) in the Golgi (11), impaired trafficking of vesicles resulting in improper maintenance of distinct membrane domains is a possible mechanism for the changes present in AMP nerves. Interestingly, depletion of phosphatidylinositol 4-phosphate from the plasma membrane of myelinating Schwann cells caused rearrangement of the actin cytoskeleton in mouse nerves with formation of actin aggregates and myelin outfoldings (62), suggesting that proper membrane composition of this phosphoinositide is important for the structure of the actin cytoskeleton and to avoid focal hypermyelination. Thus, we suggest that reduced NDRG1 activity in Schwann cells of affected Alaskan Malamutes causes focal

hypermyelination, and that the actin aggregates observed in the Schmidt-Lanterman clefts of AMP nerves are associated with an early stage in the uncontrolled membrane growth ultimately leading to formation of myelin folds (55) with secondary disruption of axonal transport and axonal degeneration. The axonal degeneration might be caused by "demyelinative internal strangulation", as observed in hereditary neuropathy with pressure palsies (21, 63). Next, the myelin sheaths without axons can either represent nerve fibers where the axon has been obliterated by this process, or, hyperactive, aberrant myelination.

We have previously shown that phosphorylated NDRG1 preferentially localized to the abaxonal cytoplasm and outer aspects of the Schmidt-Lanterman clefts in myelinating Schwann cells of normal dogs by immunofluorescence, while no pNDRG1 signal was observed in an affected Alaskan Malamute (7). Phosphorylated NDRG1 (Thr346) has been suggested to participate in termination of myelination, as loss of serum glucocorticoid kinase 1 (Sgk1), with less pNDRG1 as a sequel, caused hypermyelination in mice (17). We did not observe decreased g-ratios in the *NDRG1*$^{mut/mut}$ Alaskan Malamutes, as would be expected in a condition with diffuse hypermyelination. However, in conditions with focal hypermyelination, a reduced g-ratio may not be found (56), as most cross-sections of nerves with focally folded myelin will be represented in a semithin section by a nerve segment with normal myelination. Further studies are needed to investigate whether the NDRG1 mutation disrupts signaling in the Schwann cells by affecting the phosphorylation of the protein, either directly or indirectly, eventually resulting in the focal hypermyelination observed.

Analysis of peripheral nerve lipid composition revealed several differences between the genotype groups. Alterations caused by loss of myelin and axons in the neuropathic Alaskan Malamutes are expected. These include reduction in the levels of sphingomyelins, cholesterol and glycolipids, and increased levels of cholesteryl esters and free fatty acids (64). In line with this, hexosylceramides and sphingomyelins were decreased, while cholesteryl esters were increased, in the relative lipid distribution in nerves of *NDRG1*$^{mut/mut}$ dogs compared to controls. Unspecific changes caused by demyelination in the nerves precludes interpretation of changes specifically related to loss of NDRG1 function. Nevertheless, the increased levels of cholesteryl esters in the affected Alaskan Malamutes resemble reports from cell culture studies where NDRG1 has been silenced, resulting in aberrant formation of lipid droplets (15, 16). In contrast, defective vesicular recycling of the low-density lipoprotein receptor (LDLR) caused a reduction in cholesteryl esters in epithelial cell lacking NDRG1 (12). Thus, a specific contribution to the observed differences in lipid composition from loss of NDRG1 function in vesicular formation or trafficking, cannot be ruled out, but needs further investigation.

The Western blots showed that the affected Alaskan Malamutes did not have a total lack of NDRG1, but the expression of the 42 kDa full length protein was significantly reduced. In contrast, Greyhounds with *NDRG1*-associated neuropathy were reported to have a total NDRG1-deficiency (2), just as in humans with CMT4D caused by a nonsense mutation (9). The difference between the affected Alaskan Malamutes and Greyhounds is comparable to the difference between the two mouse models used in studies of *NDRG1*-associated neuropathies; while the *stretcher* mice had a complete lack of normal NDRG1, the *NDRG1* knock-out mice expressed low levels of the protein and had a less severe phenotype than the former (9). Consequently, the molecular

difference between the affected Alaskan Malamutes and the Greyhounds might explain the differing phenotype, such as earlier age of onset and more rapid progression to axonal degeneration in the Greyhounds. Missense mutations can impair the normal function of NDRG1 *in vitro* (65). Whether this is also the case for the p.Gly98Val mutation needs further investigations. However, based on the clinical course, we consider it likely that the mutant protein in the Alaskan Malamutes has at least some functionality, meaning that the affected Alaskan Malamutes represent a model with incomplete loss of NDRG1 function.

While nerves from the *NDRG1*$^{wt/wt}$ Alaskan Malamutes had a strong expression of phosphorylated NDRG1 (Thr346), the levels were significantly reduced in the *NDRG1*$^{mut/mut}$ dogs. As the phosphorylated fraction of NDRG1 seemingly was reduced to the same extent as total NDRG1, there did not seem to be any compensatory increase in the phosphorylation of the protein. Unlike the protein levels, the levels of NDRG1 mRNA in the nerves were similar between the two genotypes. This suggests that the reduced NDRG1 levels were not caused by degradation of the transcript, but rather protein degradation or reduced translation, in contrast to the reports from neuropathic Greyhounds (2).

In conclusion, Alaskan Malamutes with *NDRG1* mutation is a unique spontaneous animal model with incomplete loss of NDRG1 function, demonstrating a more protracted disease course compared to models with total lack of NDRG1. By detailed morphological investigations, we have gained insight into changes specifically related to NDRG1; accumulation of actin in the adaxonal cytoplasm and initial turn of Schmidt-Lanterman cleft, formation of myelin folds, demyelination and axonal loss.

Acknowledgements

The authors thank Mari Katharina Aas Ådland for technical assistance. We are also grateful to all dog owners and veterinarians who have contributed with information, and all colleagues that have assisted us in the sampling procedures.

Funding sources

The study was financed by Agria och SKK Forskningsfond (grant number N2015-0016).

Declarations of interest

None

References

1. Kalaydjieva L, Gresham D, Gooding R, Heather L, Baas F, de Jonge R, et al. N-myc downstream-regulated gene 1 is mutated in hereditary motor and sensory neuropathy-Lom. Am J Hum Genet. 2000;67(1):47-58.
2. Drogemuller C, Becker D, Kessler B, Kemter E, Tetens J, Jurina K, et al. A deletion in the N-myc downstream regulated gene 1 (NDRG1) gene in Greyhounds with polyneuropathy. PLoS One. 2010;5(6):e11258.
3. Bruun CS, Jaderlund KH, Berendt M, Jensen KB, Spodsberg EH, Gredal H, et al. A Gly98Val mutation in the N-Myc downstream regulated gene 1 (NDRG1) in Alaskan Malamutes with polyneuropathy. PLoS One. 2013;8(2):e54547.
4. Moe L. Hereditary polyneuropathy of Alaskan malamutes. In: Kirk R, Bonagura J, editors. Kirks Current Veterinary Therapy. XI ed. St. Louis, Missouri: Saunders 1992. p. 1038-9.
5. Jäderlund KH, Rohdin C, Berendt M, Stigen Ø, Fredholm M, Espenes A, et al. Re-emergence of hereditary polyneuropathy in Scandinavian Alaskan malamute dogs—old enemy or new entity? A case series. Acta Vet Scand. 2017;59(1):26.
6. Lachat P, Shaw P, Gebhard S, van Belzen N, Chaubert P, Bosman FT. Expression of NDRG1, a differentiation-related gene, in human tissues. Histochem Cell Biol. 2002;118(5):399-408.

7. Skedsmo FS, Tranulis MA, Espenes A, Prydz K, Matiasek K, Gunnes G, et al. Cell and context-dependent sorting of neuropathy-associated protein NDRG1 – insights from canine tissues and primary Schwann cell cultures. BMC Vet Res. 2019;15(1):121.
8. Berger P, Sirkowski EE, Scherer SS, Suter U. Expression analysis of the N-Myc downstream-regulated gene 1 indicates that myelinating Schwann cells are the primary disease target in hereditary motor and sensory neuropathy-Lom. Neurobiol Dis. 2004;17(2):290-9.
9. King RH, Chandler D, Lopaticki S, Huang D, Blake J, Muddle JR, et al. Ndrg1 in development and maintenance of the myelin sheath. Neurobiol Dis. 2011;42(3):368-80.
10. Askautrud HA, Gjernes E, Gunnes G, Sletten M, Ross DT, Borresen-Dale AL, et al. Global gene expression analysis reveals a link between NDRG1 and vesicle transport. PLoS One. 2014;9(1):e87268.
11. Kachhap SK, Faith D, Qian DZ, Shabbeer S, Galloway NL, Pili R, et al. The N-Myc down regulated Gene1 (NDRG1) Is a Rab4a effector involved in vesicular recycling of E-cadherin. PLoS One. 2007;2(9):e844.
12. Pietiainen V, Vassilev B, Blom T, Wang W, Nelson J, Bittman R, et al. NDRG1 functions in LDL receptor trafficking by regulating endosomal recycling and degradation. J Cell Sci. 2013;126(Pt 17):3961-71.
13. Kim KT, Ongusaha PP, Hong YK, Kurdistani SK, Nakamura M, Lu KP, et al. Function of Drg1/Rit42 in p53-dependent mitotic spindle checkpoint. J Biol Chem. 2004;279(37):38597-602.
14. Croessmann S, Wong HY, Zabransky DJ, Chu D, Mendonca J, Sharma A, et al. NDRG1 links p53 with proliferation-mediated centrosome homeostasis and genome stability. Proc Natl Acad Sci U S A. 2015;112(37):11583-8.
15. Schweitzer CJ, Zhang F, Boyer A, Valdez K, Cam M, Liang TJ. N-Myc Downstream-Regulated Gene 1 Restricts Hepatitis C Virus Propagation by Regulating Lipid Droplet Biogenesis and Viral Assembly. J Virol. 2018;92(2):e01166-17.
16. Sevinsky CJ, Khan F, Kokabee L, Darehshouri A, Maddipati KR, Conklin DS. NDRG1 regulates neutral lipid metabolism in breast cancer cells. Breast Cancer Res. 2018;20(1):55.
17. Heller BA, Ghidinelli M, Voelkl J, Einheber S, Smith R, Grund E, et al. Functionally distinct PI 3-kinase pathways regulate myelination in the peripheral nervous system. J Cell Biol. 2014;204(7):1219-36.
18. Mao XY, Fan CF, Wei J, Liu C, Zheng HC, Yao F, et al. Increased N-myc downstream-regulated gene 1 expression is associated with breast atypia-to-carcinoma progression. Tumour Biol. 2011;32(6):1271-6.
19. Bandyopadhyay S, Pai SK, Gross SC, Hirota S, Hosobe S, Miura K, et al. The Drg-1 gene suppresses tumor metastasis in prostate cancer. Cancer Res. 2003;63(8):1731-6.
20. Mi L, Zhu F, Yang X, Lu J, Zheng Y, Zhao Q, et al. The metastatic suppressor NDRG1 inhibits EMT, migration and invasion through interaction and promotion of caveolin-1 ubiquitylation in human colorectal cancer cells. Oncogene. 2017;36(30):4323-35.
21. Bilbao JM, Schmidt RE. Genetically Determined Neuropathies. Biopsy Diagnosis of Peripheral Neuropathy. Cham: Springer International Publishing; 2015. p. 375-428.
22. Mathis S, Goizet C, Tazir M, Magdelaine C, Lia AS, Magy L, et al. Charcot-Marie-Tooth diseases: an update and some new proposals for the classification. J Med Genet. 2015;52(10):681-90.
23. King RH, Tournev I, Colomer J, Merlini L, Kalaydjieva L, Thomas PK. Ultrastructural changes in peripheral nerve in hereditary motor and sensory neuropathy-Lom. Neuropathol Appl Neurobiol. 1999;25(4):306-12.
24. Matiasek K, Drogemuller C. Charcot-Marie-Tooth disease: inherited neuropathies revisited. Vet J. 2011;188(3):254-5.
25. Correard S, Plassais J, Lagoutte L, Botherel N, Thibaud J-L, Hédan B, et al. Canine neuropathies: powerful spontaneous models for human hereditary sensory neuropathies. Hum Genet. 2019;138(455).

26. Shelton GD, Humphries N. What is the Complete Muscle Profile? : UC San Diego School of Medicine; 2017 [Available from: http://vetneuromuscular.ucsd.edu/CompleteMuscleProfile.html.
27. Dyck PJ, J. K, Lais A, Lofgren EP, Stevens JC. Pathologic alterations of the peripheral nervous system of humans. In: Dyck PJ, Thomas PK, Lambert EH, Bunge R, editors. Peripheral neuropathy. vol. 1. 2nd ed. Philadelphia: WB Saunders; 1984. p. 790-3.
28. Skedsmo FS, Malachin G, Våge DI, Hammervold MM, Salvesen Ø, Ersdal C, et al. Demyelinating polyneuropathy in goats lacking prion protein. FASEB J. [Epub ahead of print 13.12.19].
29. Folch J, Lees M, Sloane Stanley G. A simple method for the isolation and purification of total lipides from animal tissues. J Biol Chem. 1957;226(1):497-509.
30. Lisa M, Holcapek M. High-throughput and comprehensive lipidomic analysis using ultrahigh-performance supercritical fluid chromatography-mass spectrometry. Anal Chem. 2015;87(14):7187-95.
31. Kind T, Liu K-H, Yup Lee D, DeFelice B, Meissen JK, Fiehn O. LipidBlast - in-silico tandem mass spectrometry database for lipid identification. Nature methods. 2013;10(8):755-8.
32. Fahy E, Sud M, Cotter D, Subramaniam S. LIPID MAPS online tools for lipid research. Nucleic Acids Res. 2007;35(Supplement):W606-W12.
33. Fahy E, Subramaniam S, Murphy RC, Nishijima M, Raetz CR, Shimizu T, et al. Update of the LIPID MAPS comprehensive classification system for lipids. J Lipid Res. 2009;50(Supplement):S9-S14.
34. Liebisch G, Vizcaíno JA, Köfeler H, Trötzmüller M, Griffiths WJ, Schmitz G, et al. Shorthand notation for lipid structures derived from mass spectrometry. J Lipid Res. 2013;54(6):1523-30.
35. Walker TL, Redding RW, Braund KG. Motor nerve conduction velocity and latency in the dog. Am J Vet Res. 1979;40(10):1433-9.
36. Weller RO, Cervós-Navarro J. General Pathology of Peripheral Nerves. Pathology of Peripheral Nerves. London: Butterworths; 1977. p. 61-89.
37. Summers BA, Cummings JF, DeLahunta A. Diseases of the Peripheral Nervous System. Veterinary Neuropathology. St. Louis, Mo: Mosby; 1995. p. 402-501.
38. Braund KG, McGuire JA, Lincoln CE. Age-related changes in peripheral nerves of the dog. II. A morphologic and morphometric study of cross-sectional nerve. Vet Pathol. 1982;19(4):379-98.
39. Lassmann H, Ammerer HP, Kulnig W. Ultrastructural sequence of myelin degradation. Acta Neuropathol. 1978;44(2):91-102.
40. Galloway PG, Perry G, Gambetti P. Hirano body filaments contain actin and actin-associated proteins. J Neuropathol Exp Neurol. 1987;46(2):185-99.
41. Pareyson D, Scaioli V, Laura M. Clinical and electrophysiological aspects of Charcot-Marie-Tooth disease. Neuromolecular Med. 2006;8(1-2):3-22.
42. Hanemann CO, Gabreels-Festen AA. Secondary axon atrophy and neurological dysfunction in demyelinating neuropathies. Curr Opin Neurol. 2002;15(5):611-5.
43. Bilbao JM, Schmidt RE. Schwann Cells and Myelin in the Peripheral Nervous System. Biopsy Diagnosis of Peripheral Neuropathy. Cham: Springer International Publishing; 2015. p. 85-109.
44. Kalaydjieva L, Nikolova A, Turnev I, Petrova J, Hristova A, Ishpekova B, et al. Hereditary motor and sensory neuropathy--Lom, a novel demyelinating neuropathy associated with deafness in gypsies. Clinical, electrophysiological and nerve biopsy findings. Brain. 1998;121 (Pt 3):399-408.
45. Baethmann M, Göhlich-Ratmann G, Schröder JM, Kalaydjieva L, Voit T. HMSNL in a 13-year-old Bulgarian girl. Neuromuscul Disord. 1998;8(2):90-4.
46. Ricard E, Mathis S, Magdelaine C, Delisle MB, Magy L, Funalot B, et al. CMT4D (NDRG1 mutation): genotype-phenotype correlations. J Peripher Nerv Syst. 2013;18(3):261-5.

47. Friede RL, Bischhausen R. The precise geometry of large internodes. J Neurol Sci. 1980;48(3):367-81.
48. Tazir M, Hamadouche T, Nouioua S, Mathis S, Vallat J-M. Hereditary motor and sensory neuropathies or Charcot–Marie–Tooth diseases: An update. J Neurol Sci. 2014;347(1):14-22.
49. Schochet SS, Jr., McCormick WF. Ultrastructure of Hirano bodies. Acta Neuropathol. 1972;21(1):50-60.
50. Luigetti M, Taroni F, Milani M, Del Grande A, Romano A, Bisogni G, et al. Clinical, electrophysiological and pathological findings in a patient with Charcot-Marie-Tooth disease 4D caused by the NDRG1 Lom mutation. J Neurol Sci. 2014;345(1-2):271-3.
51. Butinar D, Zidar J, Leonardis L, Popovic M, Kalaydjieva L, Angelicheva D, et al. Hereditary auditory, vestibular, motor, and sensory neuropathy in a Slovenian Roma (Gypsy) kindred. Ann Neurol. 1999;46(1):36-44.
52. Colomer J, Iturriaga C, Kalaydjieva L, Angelicheva D, King RHM, Thomas PK. Hereditary Motor and Sensory Neuropathy-Lom (HMSNL) in a Spanish family: clinical, electrophysiological, pathological and genetic studies. Neuromuscul Disord. 2000;10(8):578-83.
53. Bolino A, Bolis A, Previtali SC, Dina G, Bussini S, Dati G, et al. Disruption of Mtmr2 produces CMT4B1-like neuropathy with myelin outfolding and impaired spermatogenesis. J Cell Biol. 2004;167(4):711-21.
54. Robinson DC, Mammel AE, Logan AM, Larson AA, Schmidt EJ, Condon AF, et al. An In Vitro Model of Charcot-Marie-Tooth Disease Type 4B2 Provides Insight Into the Roles of MTMR13 and MTMR2 in Schwann Cell Myelination. ASN Neuro. 2018;10.
55. Goebbels S, Oltrogge JH, Wolfer S, Wieser GL, Nientiedt T, Pieper A, et al. Genetic disruption of Pten in a novel mouse model of tomaculous neuropathy. EMBO Mol Med. 2012;4(6):486-99.
56. Horn M, Baumann R, Pereira JA, Sidiropoulos PN, Somandin C, Welzl H, et al. Myelin is dependent on the Charcot-Marie-Tooth Type 4H disease culprit protein FRABIN/FGD4 in Schwann cells. Brain. 2012;135(Pt 12):3567-83.
57. Tricaud N. Myelinating Schwann Cell Polarity and Mechanically-Driven Myelin Sheath Elongation. Front Cell Neurosci. 2017;11:414.
58. Hall SM, Williams PL. Studies on the 'Incisures' of Schmidt and Lanterman. J Cell Sci. 1970;6(3):767-91.
59. Pereira JA, Lebrun-Julien F, Suter U. Molecular mechanisms regulating myelination in the peripheral nervous system. Trends Neurosci. 2012;35(2):123-34.
60. Jean S, Kiger AA. Coordination between RAB GTPase and phosphoinositide regulation and functions. Nat Rev Mol Cell Biol. 2012;13(7):463-70.
61. Gassama-Diagne A, Yu W, ter Beest M, Martin-Belmonte F, Kierbel A, Engel J, et al. Phosphatidylinositol-3,4,5-trisphosphate regulates the formation of the basolateral plasma membrane in epithelial cells. Nat Cell Biol. 2006;8(9):963-70.
62. Alvarez-Prats A, Bjelobaba I, Aldworth Z, Baba T, Abebe D, Kim YJ, et al. Schwann-Cell-Specific Deletion of Phosphatidylinositol 4-Kinase Alpha Causes Aberrant Myelination. Cell Rep. 2018;23(10):2881-90.
63. Dyck PJ, Dyck PJB, Engelstad J. Pathologic Alterations of Nerves. In: Dyck PJ, Thomas PK, editors. Peripheral Neuropathy. 4th ed. Philadelphia: W.B. Saunders; 2005. p. 733-829.
64. Yao JK. Lipid Composition of Normal and Degenerating Nerve. In: Dyck PJ, Thomas PK, Lambert EH, Bunge R, editors. Peripheral neuropathy. vol. 1. 2nd ed. Philadelphia: WB Saunders; 1984. p. 510-30.
65. Li LX, Liu GL, Liu ZJ, Lu C, Wu ZY. Identification and functional characterization of two missense mutations in NDRG1 associated with Charcot-Marie-Tooth disease type 4D. Hum Mutat. 2017;38(11):1569-78.

Figure 1

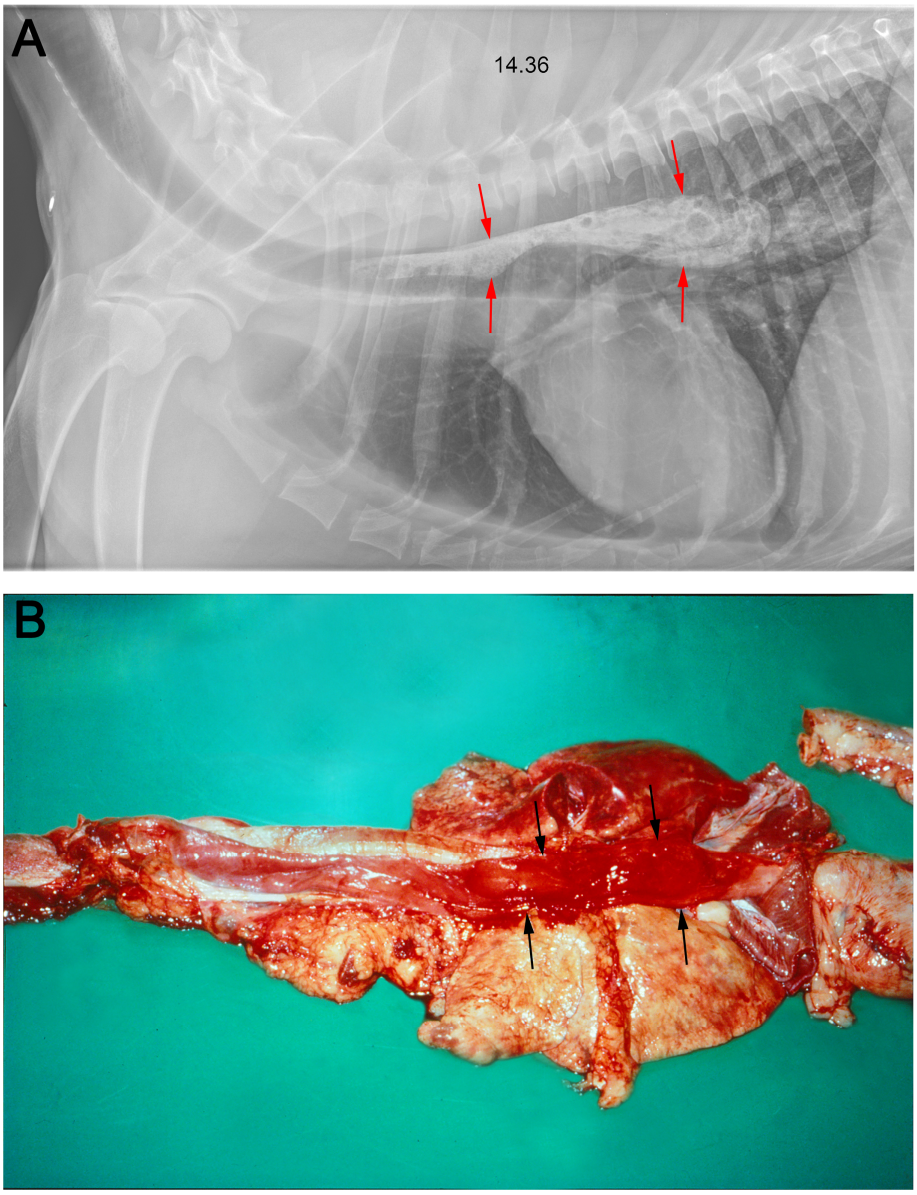

Figure 1. **A.** Radiograph of case 5 that developed megaesophagus at the age of 3-4 years. Retention of barium sulphate in dilated part of oesophagus (red arrows). **B.** Photograph illustrating megaesophagus (black arrows) in case 14.

Figure 2

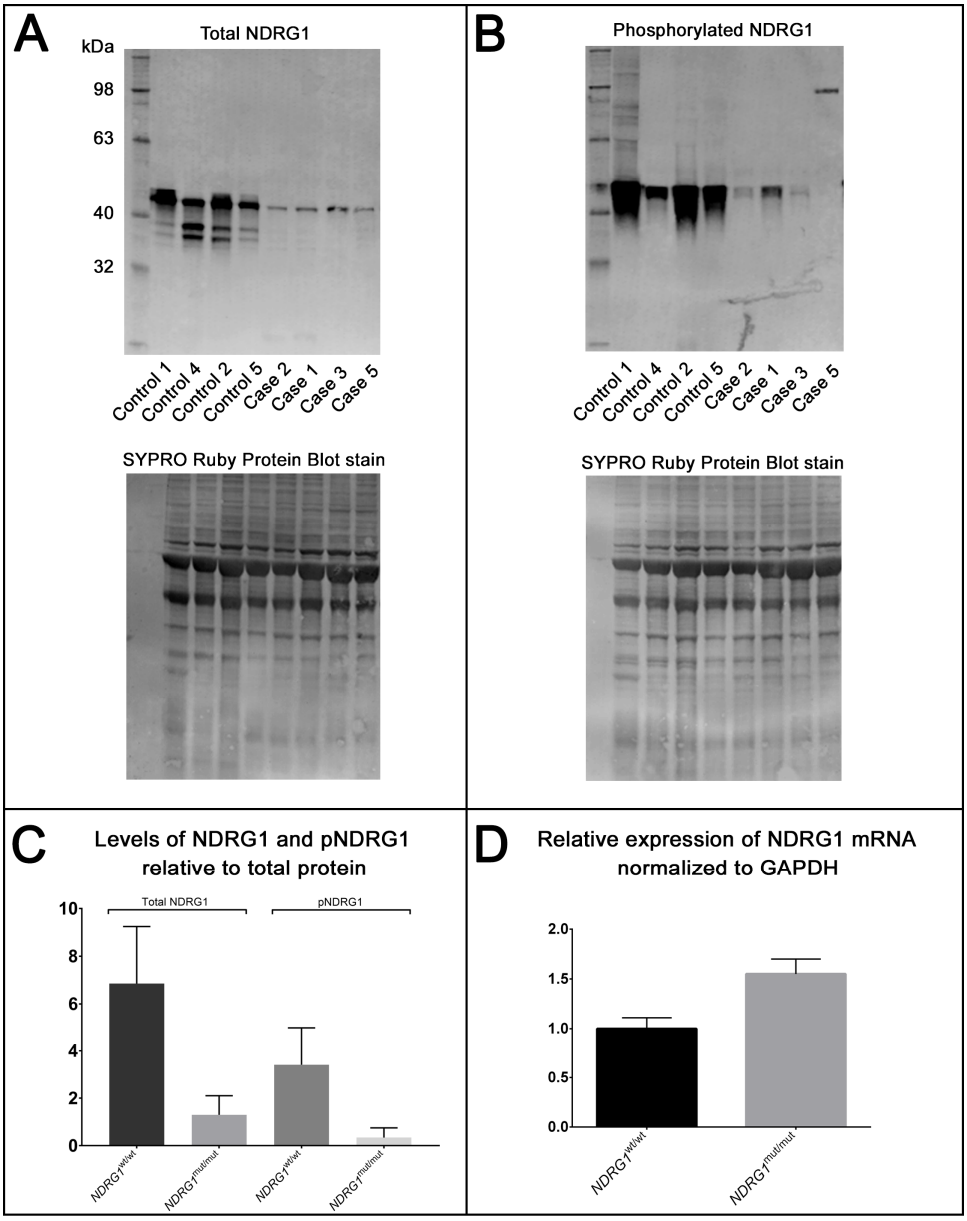
A
Total NDRG1
kDa
98
63
40
32
Control 1
Control 4
Control 2
Control 5
Case 2
Case 1
Case 3
Case 5
SYPRO Ruby Protein Blot stain
B
Phosphorylated NDRG1
Control 1
Control 4
Control 2
Control 5
Case 2
Case 1
Case 3
Case 5
SYPRO Ruby Protein Blot stain
C
Levels of NDRG1 and pNDRG1 relative to total protein
Total NDRG1
pNDRG1
10
8
6
4
2
0
NDRG1wt/wt
NDRG1mut/mut
NDRG1wt/wt
NDRG1mut/mut
D
Relative expression of NDRG1 mRNA normalized to GAPDH
2.0
1.5
1.0
0.5
0.0
NDRG1wt/wt
NDRG1mut/mut

Figure 2. **A, B.** Western blot of nerve lysate from Alaskan Malamutes with antibodies against NDRG1 (**A**) and phospho-NDRG1 (**B**). **C.** Semiquantification of NDRG1 protein in nerve lysates based on band intensity in Western blot (mean+SD). There is a significant reduction in the levels of both total NDRG1 (P=0.029) and pNDRG1 (P=0.029) in NDRG1$^{mut/mut}$ Alaskan Malamutes compared to controls. **D.** Relative expression of NDRG1 mRNA in nerve samples (mean+SD). The difference between the groups was not significant (P=0.2).

Figure 3

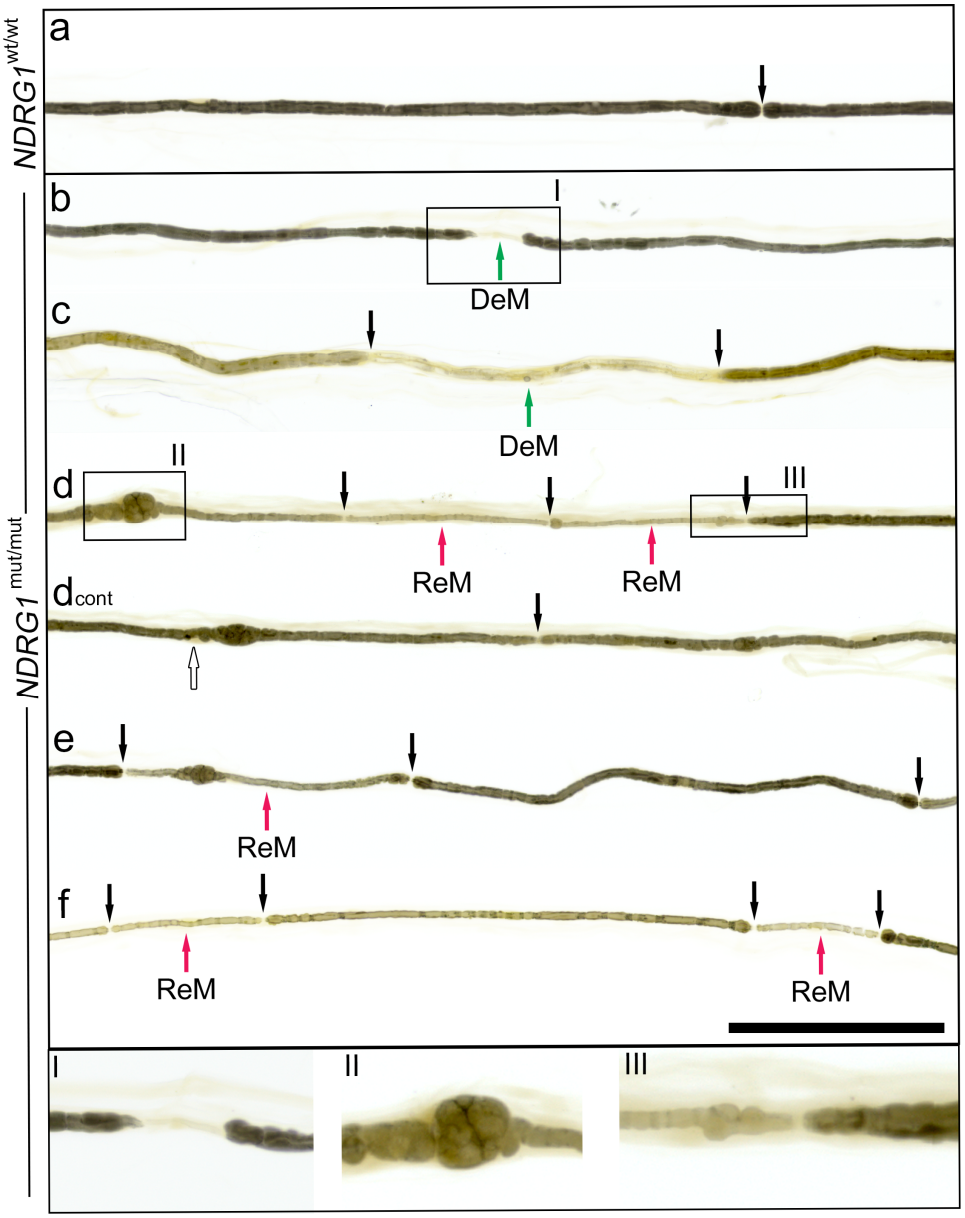
NDRG1wt/wt
NDRG1mut/mut
a
b
I
DeM
c
DeM
II
d
III
ReM
ReM
dcont
e
ReM
f
ReM
ReM
I
II
III

Figure 3. Teased nerve fibers, representative examples from the common fibular and tibial nerves of a control (**a**) and cases (**b-f**). Boxes indicated by roman numerals are magnified in the lower part of the figure. In fibers from cases, paranodal (**b**, magnified in **I**) and segmental demyelination (**c**) were present. Focal thickenings of the nerve fiber were observed internodally (**d**, **e**, magnified in **II**), occasionally close to the Schwann cell nucleus (**d**, white arrow). Short and thinly myelinated internodes, consistent with remyelination, intermingled with longer internodes with thicker myelin sheath (**d-f**, magnified in **III**). Nodes of Ranvier are indicated by black arrows. DeM = Demyelinated segment. ReM = Remyelinated segment. Bar 200 µm.

Figure 4

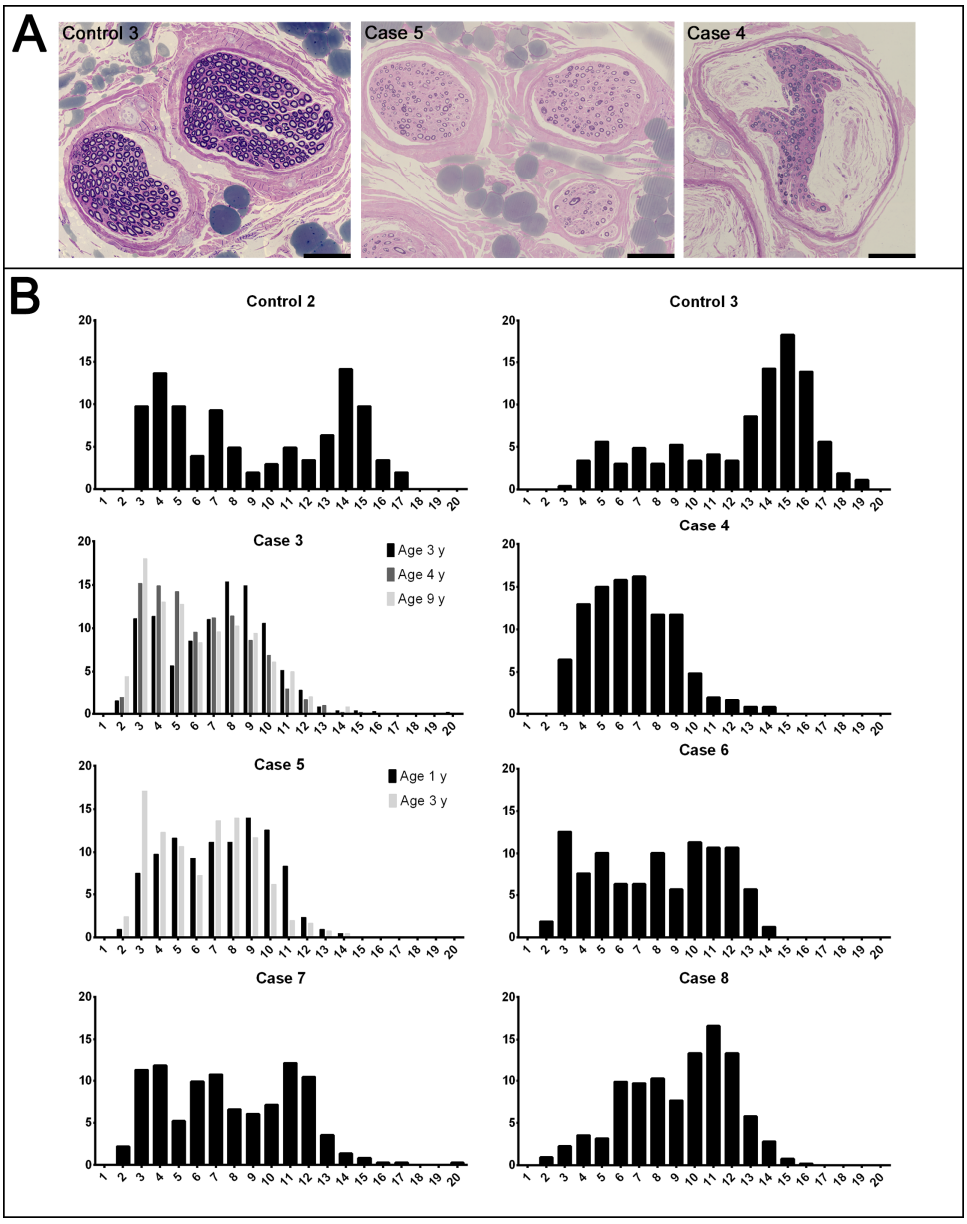
A
Control 3
Case 5
Case 4
B
Control 2
Control 3
Case 3
Age 3 y
Age 4 y
Age 9 y
Case 4
Case 5
Age 1 y
Age 3 y
Case 6
Case 7
Case 8

Figure 4. A. Comparison of semithin sections from the common fibular nerves of controls and cases at low magnification. Note the reduction of large myelinated fibres in the cases. The prominent Renaut bodies observed in case 4 are not typical findings in affected dogs. Bar 100 µm. **B**. Myelinated fibre diameter-frequency histograms. Note the shift in the distribution of myelinated fibres in the cases. For case 3 and 5, morphometrical comparison of biopsies taken at different ages is included in the histogram. Y-axis: Percentage of myelinated fibers. X-axis: Diameter of myelinated fibers in µm.

Figure 5

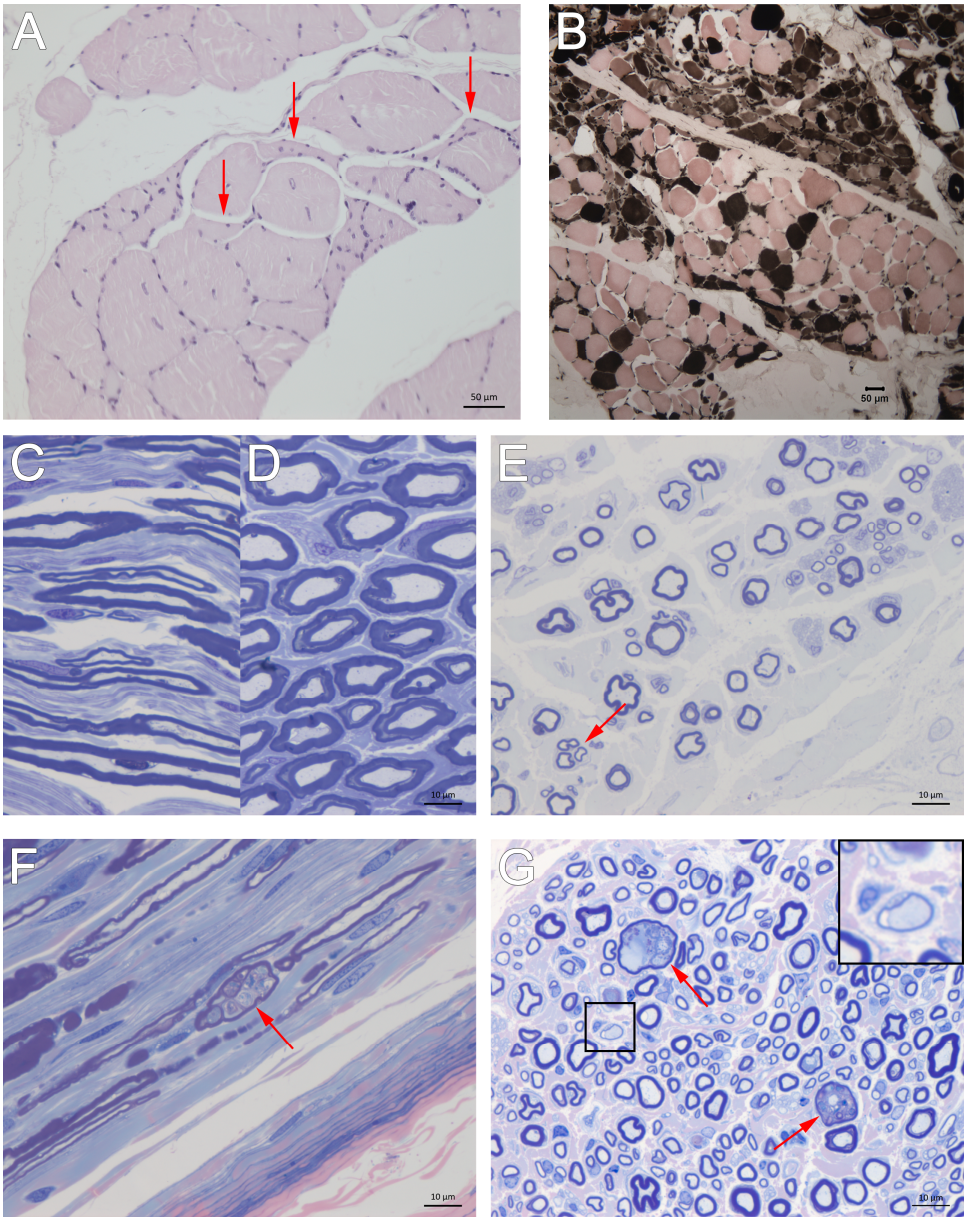

Figure 5. Skeletal muscle (**A, B**) and nerves (**C-G**) from affected (**A, B, E-G**) and control (**C, D**) Alaskan Malamutes. **A**. Scattered and small groups of angular, atrophic myofibers (arrows) in the gastrocnemius muscle. **B**. Fiber type grouping in the gastrocnemius muscle. Type 1 muscle fibers are dark, while type 2 are pale. **C, D**. Nerve from a control Alaskan Malamute. **E**. Axonal loss and thinly myelinated (remyelinating) fibers in nerve from affected Alaskan Malamute. A regenerative fiber cluster is indicated by red arrow. **F, G**. Focal swelling of nerve fibers (red arrows) is seen in both longitudinal (**F**) and transverse (**G**) sections. A myelinated fiber with very thin myelin sheath is highlighted (box and inset) in **G**. Stained with hematoxylin and eosin (**A**), Myofibrillar ATPase reaction at pH 4.3 (**B**), toluidine (**C-E**), toluidine and safranin-O (**F, G**).

Figure 6

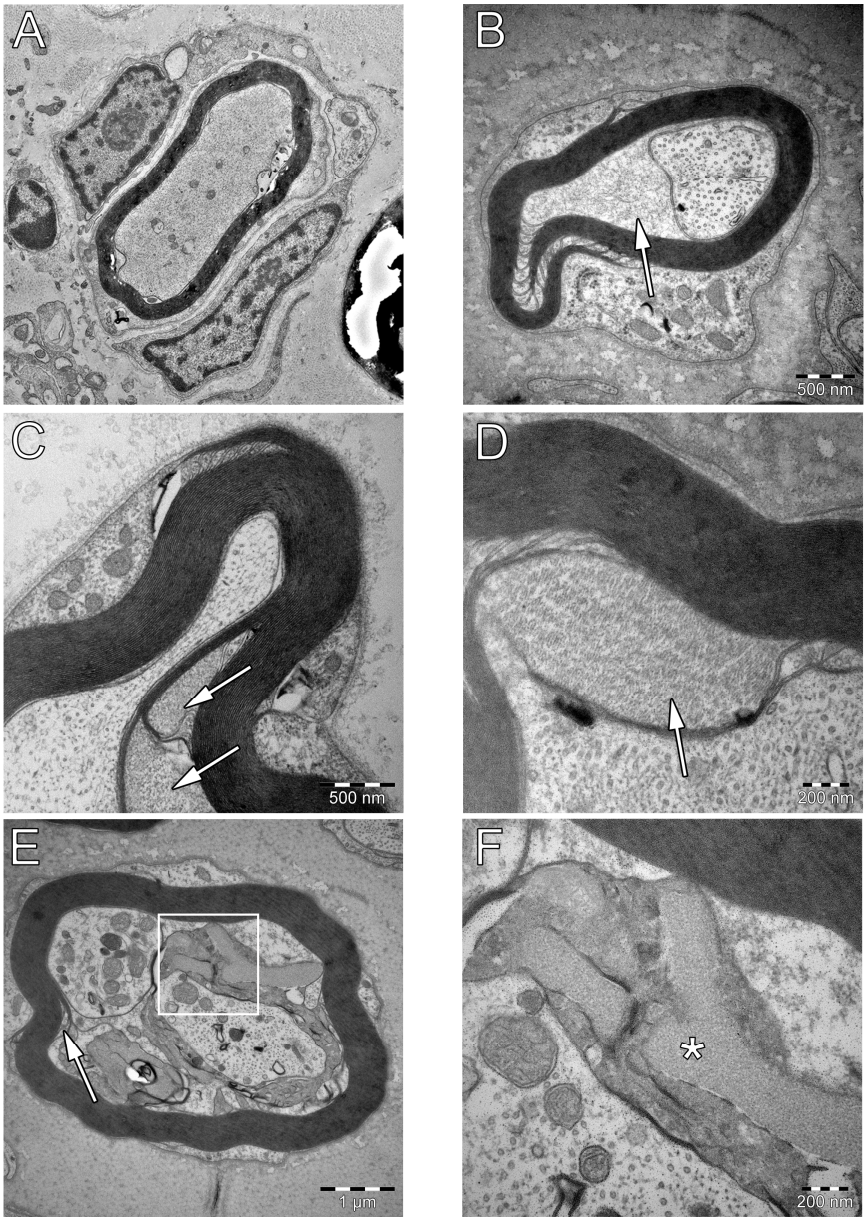

Figure 6. Electron micrographs of nerves from affected Alaskan Malamutes, transverse sections. **A**. Thinly myelinated nerve fiber in the center of a small onion bulb. Bar not available. **B-D**. Accumulation of filamentous material in the adaxonal cytoplasm (**B**) or in the inner part of distended Schmidt-Lanterman clefts (**C, D**). **E, F** (white box magnified in **F**) Disrupted Schmidt-Lanterman cleft (arrow in **E**) with coarsely granular material (asterisk in **F**) between dyscompacted myelin lamellae from the inner part of the myelin sheath. Note the two axonal structures within the myelin sheath in **E**, both with aggregates of mitochondria.

Figure 7

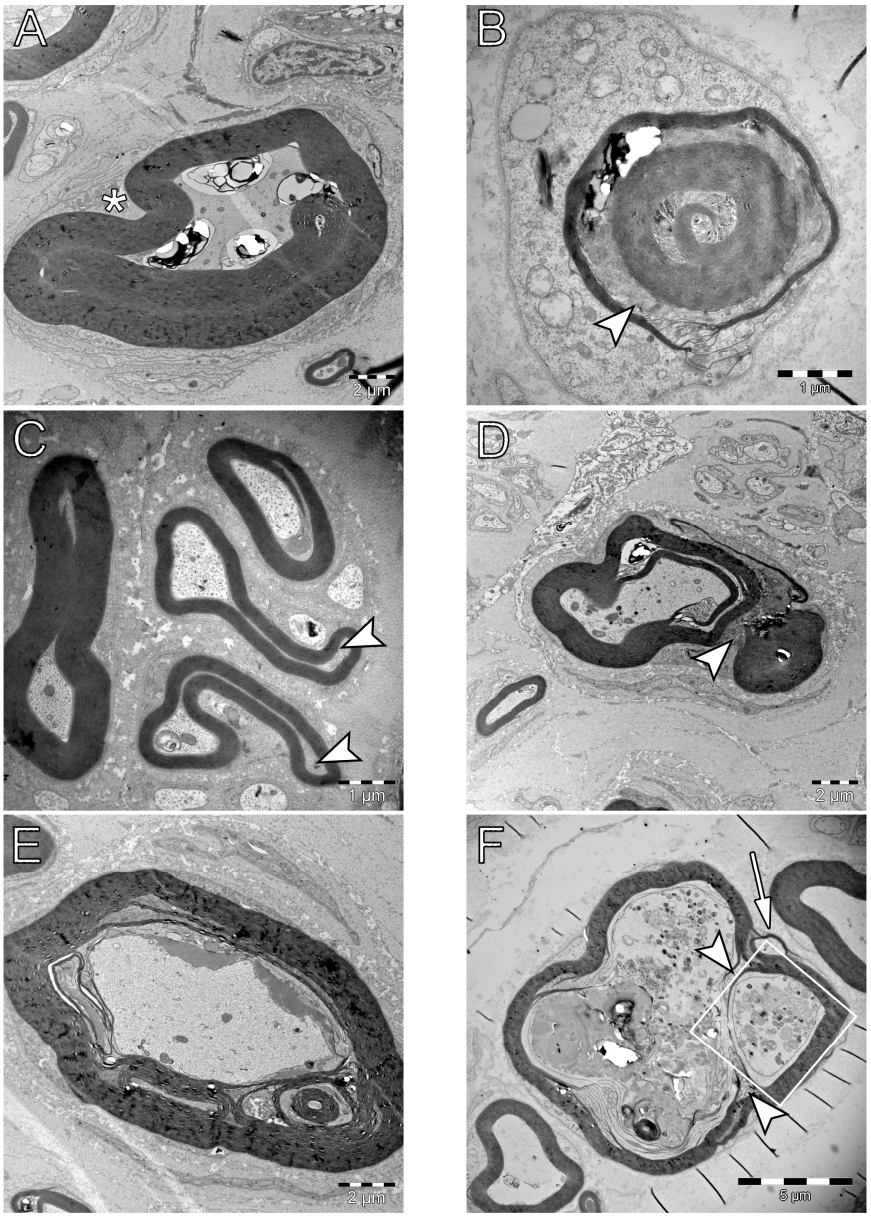

Figure 7. Electron micrographs of nerves from affected Alaskan Malamutes, transverse sections. Infoldings (**A, B, E, F**) and outfoldings (**C, D**) of the myelin sheath, originating from the paranodal region (**A**, asterisk shows aggregates of mitochondria in the abaxonal cytoplasm, characteristic of this region) or Schmidt-Lanterman clefts (arrow heads in **B, C, D, F**). The folds can either involve the whole thickness of the myelin sheath (**A, C, D**) or only some of the lamellae (**E, F**). In **B**, no axon is observed inside the myelin sheath. In **F**, the infoldings seemingly divide the axon into several structures. Note the outfolding originating from the abaxonal part of the Schmidt-Lanterman cleft in **F** (arrow). White frame magnified in **8A**.

Figure 8

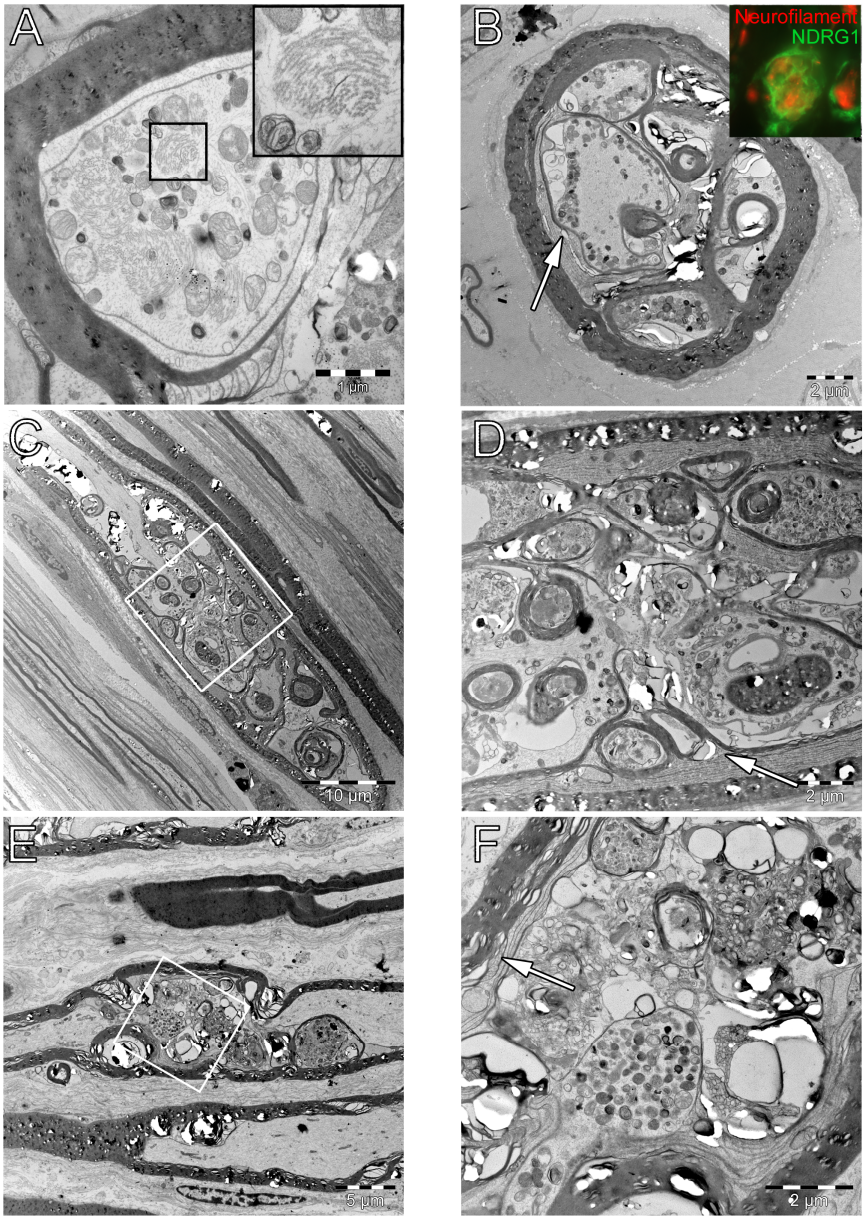

Figure 8. Electron micrographs of nerves from affected Alaskan Malamutes. Transverse (**A, B**) and longitudinal (**C-F**). Myelin infoldings, often derived from the Schmidt-Lanterman clefts (**A**, lower magnification in **7F**), divide the axon into pockets, resulting in the appearance of several axonal structures within one myelin sheath in transverse sections (**B**). The identity of these structures were confirmed by immunofluorescence (inset in **B**). The axonal structures contain accumulations of organelles, including degenerating mitochondria (**A-F**) and aggregates of neurofilaments (**A**, magnified in inset), consistent with early axonal degeneration. The focal distribution of changes are shown in **E**, magnified in **F**. Arrows (**B, D, F**) indicate dyscompacted myelin.

Figure 9

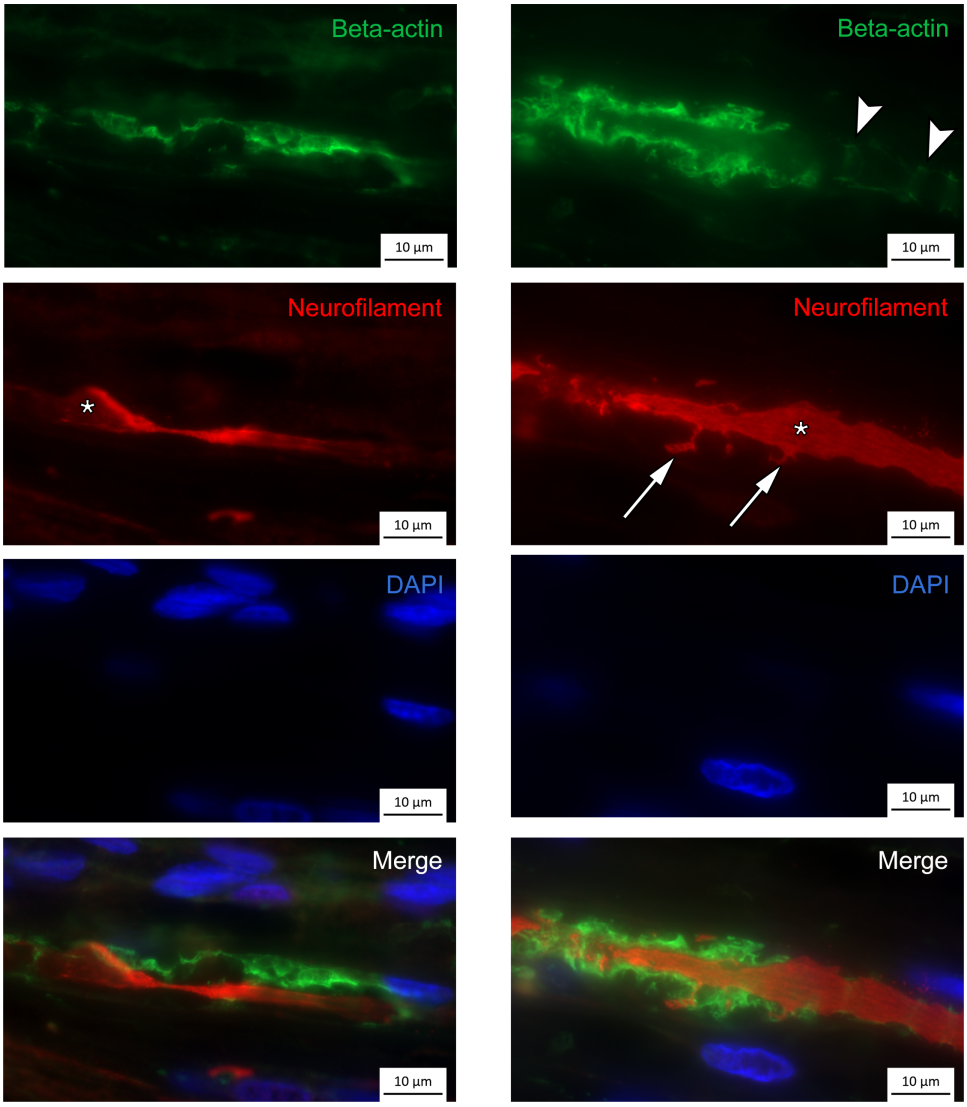
Beta-actin
10 µm
Beta-actin
10 µm
Neurofilament
*
10 µm
Neurofilament
*
10 µm
DAPI
10 µm
DAPI
10 µm
Merge
10 µm
Merge
10 µm

Figure 9. Immunofluorescence on nerve section from case 5 with antibodies against beta-actin (green) and neurofilament (red), two different nerve fibers are shown. Nuclei are stained with DAPI (blue). Aggregates of actin are present in the nerves of affected Alaskan Malamutes. Note the difference between the aggregates and the sparse amount of actin normally present in the Schmidt-Lanterman clefts (arrowheads). Although the axonal diameter was reduced in the areas with aggregates, the axon was swollen adjacent to these segments (asterisk). Note the small axonal structures within the actin-positive areas only coupled to the main axon through thin connections (arrows).

Figure 10

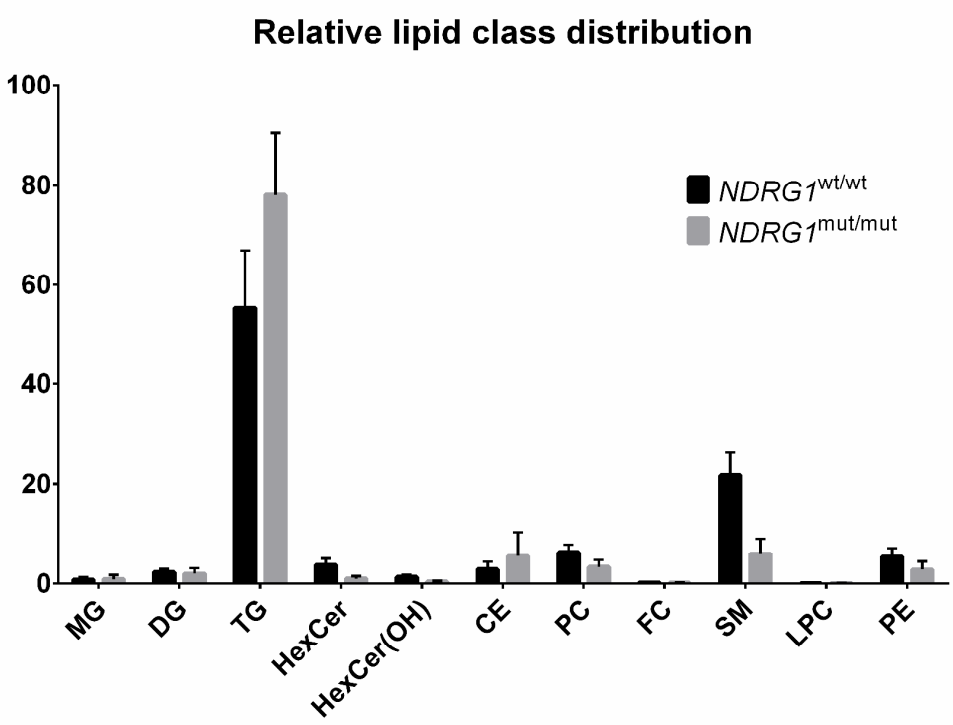

Figure 10. Ultra-performance convergence chromatography tandem mass spectrometry (UPC²-MS/MS) analysis of nerve lipid composition. Relative lipid class distribution (mean+SD). While hexosylceramides, sphingomyelins and phospholipids were decreased in the affected dogs, triacylglycerols and cholesteryl esters were increased. See Table 3 in text for abbreviations.

Supplementary Table A.1: Detailed information about Alaskan Malamutes and analyses included in the study

Number	Genotype	Sex	Age at sampling (years)	Biopsy (B), postmortem (P)	Analysis												
					WB	qRT-PCR	IHC (Iba1, CD18, CD3, CD79)	IF (NDRG1/ neurofilament)	IF (beta-actin/ neurofilament)	Muscle biopsy	Nerve fiber teasing	Semithin	Morpho-metry	TEM	MNCV	EMG	Lipidomics
Case no 1	mut/mut	Female	6	B, P	N7	N4	N1		N1	x	N1, N2, N7	N1, N2, N3, N4, N5, N7, N8, N9, N10, N14	N1	N7, N9, N14			N4, N12
Case no 2	mut/mut	Male	8	P	N7	N1	N7	N4	N7	x	N1	N1, N2, N6, N8, N9	N1	N6, N9			
Case no 3	mut/mut	Female	3, 4, 9	B, P	N7	N1+N10	N1	N1		x	N1, N2, N4, N7, N9	N1, N2, N3, N4, N5, N6, N7, N8, N9, N10	N7	N3, N4, N9, N10	x	x	N4, N5
Case no 4	mut/mut	Female	2, 6	B						x	N7	N7	N7		x	x	
Case no 5	mut/mut	Female	1, 3	B, P	N7	N1	N7	N4	N7	x		N7, N8	N7		x	x	N4, N5+N6
Case no 6	mut/mut	Male	2	P						x		N1, N2, N4, N7, N8	N7		x	x	
Case no 7	mut/mut	Female	1	B						x		N7	N7		x	x	
Case no 8	mut/mut	Female	1	P						x		N5, N7	N7				
Case no 9	mut/mut	Female	2	P										N13, N15	x	x	
Case no 10	*	Male	5	P								N6		N6, N11	x	x	
Case no 11	*	Male	2	B										N7	x	x	
Case no 12	mut/mut	Male	1	P										N1	x	x	
Case no 13	mut/mut	Male	6	P										N6	x	x	
Case no 14	mut/mut	Female	6	P													
Control no 1	wt/wt	Female	8	P	N6	N8	N1	N1, N4	N1	x	N1	N1, N2, N3, N4, N6, N7, N8, N9, N10	N1				N4, N5
Control no 2	wt/wt	Female	11	P	N7	N7	N7	N4	N7	x	N5, N7	N5, N7	N7				N4, N5
Control no 3	wt/wt	Male	12	B						x		N7	N7				
Control no 4	wt/wt	Male	7	P	N1	N6											N5, N6
Control no 5	*	Male	13	P	N7	N4											

*All dogs were genotyped except case 10, case 11 and control 5, due to technical problems with DNA extraction from paraffin-embedded material.

Abbreviation	Nerve
N1	N. tibialis
N2	N. laryngeus recurrens, sin
N3	N. laryngeus recurrens, dex
N4	N. ischiadicus
N5	N. ulnaris
N6	N. obturatorius, sin
N7	N. fibularis communis
N8	N. radialis superficialis

Abbreviation	Nerve
N9	N. hypoglossus
N10	Truncus vagosympaticus
N11	N. femoralis
N12	Plexus brachialis
N13	Ventral lumbar nerve root
N14	N. facialis
N15	Thoracal nerve root

Supplementary Figure B.1

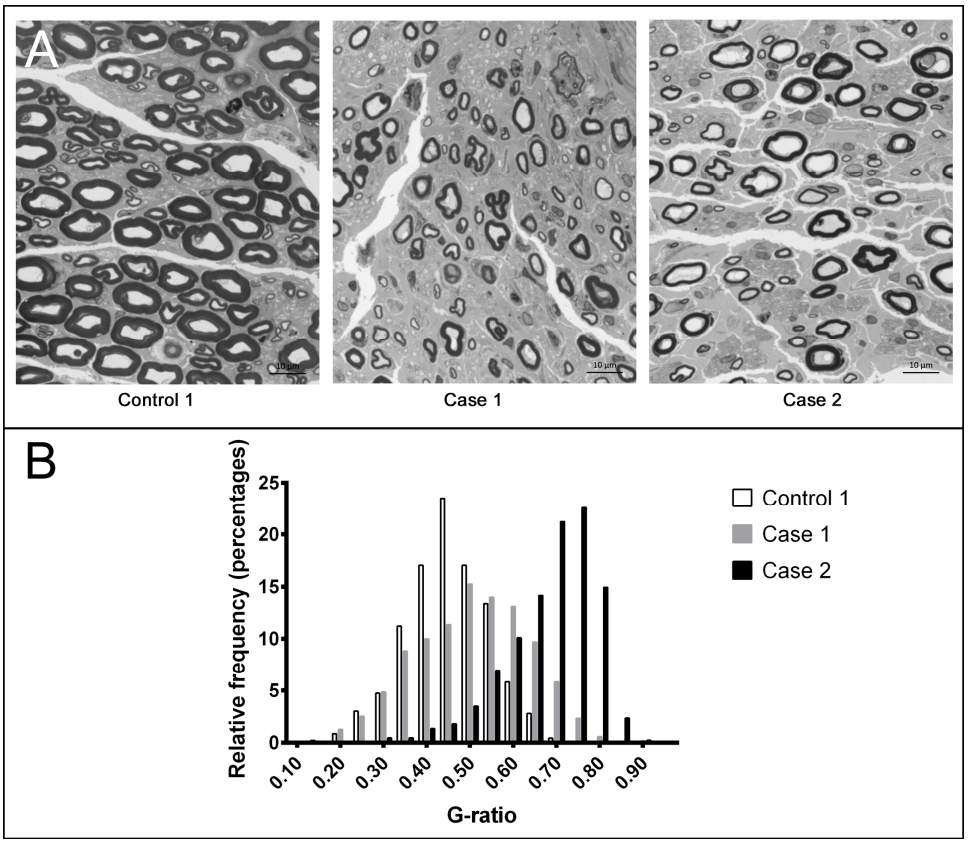

Supplementary Figure B.1. A. Semithin sections from the tibial nerves of control and affected Alaskan Malamutes. Note the thinly myelinated fibres in the cases. **B**. G-ratio-frequency histogram. The distribution is shifted towards higher g-ratios in the cases.

Supplementary Figure B.2

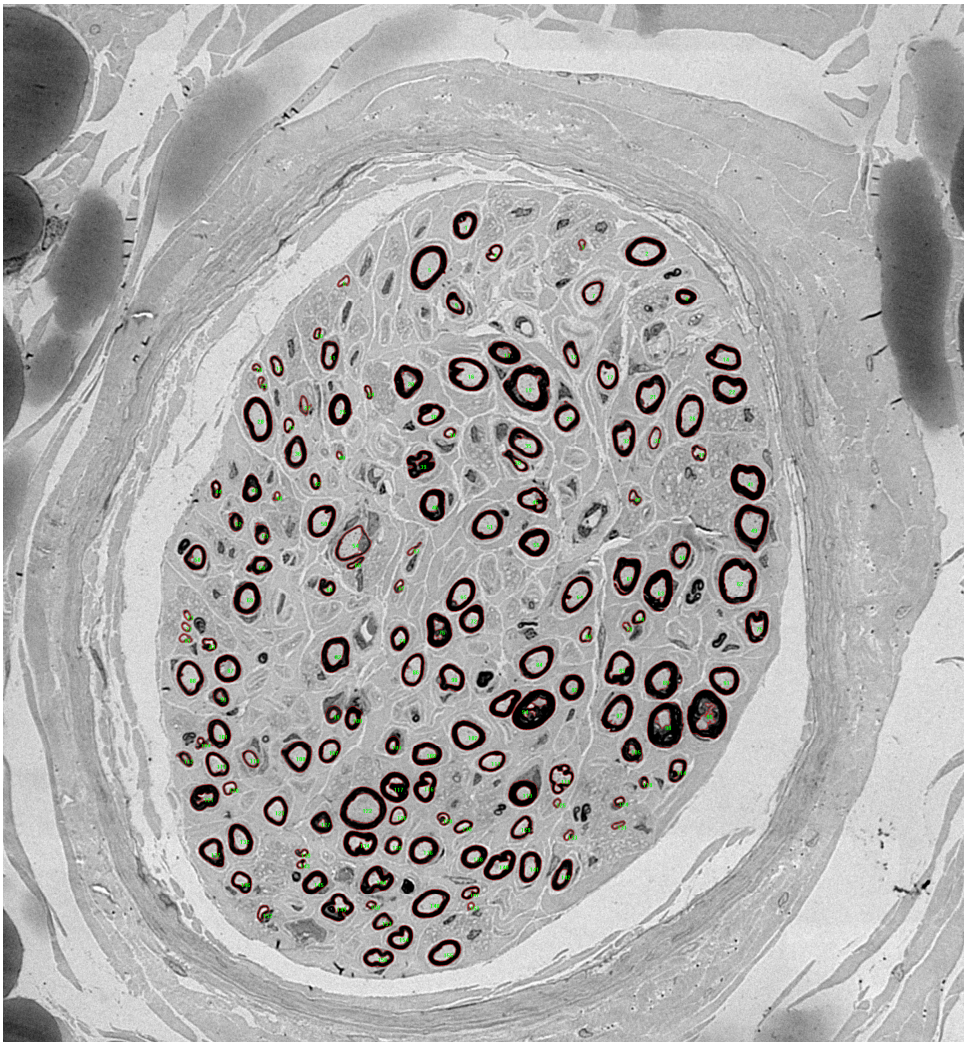

Supplementary Figure B.2. Semithin section from the common fibular nerve of an affected Alaskan Malamute. Example of morphometric measurement. Red outlines show measured objects and the number of the counted object is indicated in green.

Paper III

Received: 23 October 2019 | Revised: 27 November 2019 | Accepted: 27 November 2019

DOI: 10.1096/fj.201902588R

RESEARCH ARTICLE

THE FASEB JOURNAL

Demyelinating polyneuropathy in goats lacking prion protein

Fredrik S. Skedsmo[1] | Giulia Malachin[2] | Dag Inge Våge[3] | Mie Marie Hammervold[3] | Øyvind Salvesen[4] | Cecilie Ersdal[4] | Birgit Ranheim[4] | Marit H. Stafsnes[5] | Zdenka Bartosova[5] | Per Bruheim[5] | Karin H. Jäderlund[1] | Kaspar Matiasek[6] | Arild Espenes[2] | Michael A. Tranulis[2]

[1]Department of Companion Animal Clinical Sciences, Faculty of Veterinary Medicine, Norwegian University of Life Sciences, Oslo, Norway

[2]Department of Basic Sciences and Aquatic Medicine, Faculty of Veterinary Medicine, Norwegian University of Life Sciences, Oslo, Norway

[3]Centre for Integrative Genetics (CIGENE), Department of Animal and Aquacultural Sciences, Faculty of Biosciences, Norwegian University of Life Sciences, Ås, Norway

[4]Department of Production Animal Clinical Sciences, Faculty of Veterinary Medicine, Norwegian University of Life Sciences, Oslo, Norway

[5]Department of Biotechnology and Food Science, Faculty of Natural Sciences, Norwegian University of Science and Technology, Trondheim, Norway

[6]Section of Clinical & Comparative Neuropathology, Centre for Clinical Veterinary Medicine, Ludwig-Maximilians-Universität, Munich, Germany

Correspondence
Michael A. Tranulis, Department of Basic Sciences and Aquatic Medicine, Faculty of Veterinary Medicine, Norwegian University of Life Sciences, Ullevålsveien 72, Oslo 0454, Norway.
Email: Michael.Tranulis@nmbu.no

Abstract

Studies in mice with ablation of *Prnp*, the gene that encodes the cellular prion protein (PrP^C), have led to the hypothesis that PrP^C is important for peripheral nerve myelin maintenance. Here, we have used a nontransgenic animal model to put this idea to the test; namely, goats that, due to a naturally occurring nonsense mutation, lack PrP^C. Teased nerve fiber preparation revealed a demyelinating pathology in goats without PrP^C. Affected nerves were invaded by macrophages and T cells and displayed vacuolated fibers, shrunken axons, and onion bulbs. Peripheral nerve lipid composition was similar in young goats with or without PrP^C, but markedly different between corresponding groups of adult goats, reflecting the progressive nature of the neuropathy. This is the first report of a subclinical demyelinating polyneuropathy caused by loss of PrP^C function in a nontransgenic mammal.

KEYWORDS

lipidomic, myelin, neuropathy, PRNP haplotype

Abbreviations: AI bucks, Selected bucks used in artificial insemination (AI) in the Norwegian goat population; BSA, Bovine serum albumin; HexCer, Hexosyl ceramides; MAF, Minimal allele frequency; PBS, Phosphate-buffered saline; $PRNP^{Ter/Ter}$, Goats homozygous for nonsense mutation in *PRNP*; PrP^{Sc}, Misfolded prion protein; PrPC, Cellular prion protein; *Prnp*, *PRNP*, Gene encoding the cellular prion protein; SNP, Single-nucleotide polymorphism; TBST, Tris-buffered saline-Tween.

Fredrik S. Skedsmo and Giulia Malachin joint first authors.

Funding information
The Research Council of Norway, Grant/ Award Number: 227386/E40

1 | INTRODUCTION

Prion diseases are rare, invariably fatal, neurodegenerative conditions in which pathognomonic misfolded prion protein (PrP^{Sc}) aggregates appear in the central nervous system of affected humans and animals.[1] The misfolded PrP^{Sc} conformers stem from physiological cellular prion protein (PrP^{C}), which, in an incompletely understood process, is converted to PrP^{Sc} through physical interaction between the two conformational states of PrP. Transgenic mice without endogenous PrP^{C} cannot develop prion disease.[2,3] Thus, neuronal PrP^{C} is the obligatory molecule for prion disease progression and hence is the prime target for interventions.

Several lines of transgenic mice with ablation of gene encoding the cellular prion protein *(Prnp)* have been generated (hereafter referred to as $Prnp^{-/-}$), and only minor abnormalities were initially observed under resting conditions.[3-8] However, Nishida and coworkers reported white matter vacuolation, demyelination, and a loss of large myelinated fibers in peripheral nerves in several $Prnp^{-/-}$ lines of mice, and proposed that PrP^{C} serves important roles in myelin formation and/or maintenance in both the central and peripheral nervous system.[9] After a period of relative neglect, the topic of PrP^{C} and myelin health has recently been revisited in a series of investigations involving several experimental designs and $Prnp^{-/-}$ mouse lines.[10] The current view is that axonal PrP^{C} contributes to preserve Schwann cell myelin quality. Specifically, PrP^{C}-derived peptides, liberated from axons through controlled proteolysis, diffuse to Schwann cell receptors and thereby stimulate myelin maintenance.[11] Absence of such signalling gradually leads to demyelination and remyelination in response.

Different from inbred laboratory mice, dairy goats, and humans have a high degree of genetic variation. By comparing *PRNP* haplotypes with and without the $PRNP^{Ter}$ nonsense mutation, we find that the region affected by genetic hitchhiking is surprisingly short, covering less than 1% of genes encoded by chromosome 13. Like $Prnp^{-/-}$ mice, goats without PrP^{C} develop a mild demyelinating neuropathy, demonstrating that PrP^{C} functions in myelin maintenance are highly conserved and probably translates to other mammals, including humans.

2 | MATERIALS AND METHODS

2.1 | Animals and ethics

Animal experiments and tissue sampling were performed in compliance with the ethical guidelines and approved by the Norwegian Animal Research Authority (FOTS ID 7860, 5826), with reference to the Norwegian regulations on animal experimentation. All goats were of the Norwegian Dairy Goat Breed, recruited from a research facility at the Norwegian University of Life Sciences and housed together in a farmhouse environment.

For morphological analyses, electrophysiology and lipidomics, a total of 24 goats were used, of which 10 were homozygous for the wild type *PRNP* allele and 14 were homozygous for the mutated *PRNP* allele (hereafter called $PRNP^{+/+}$ and $PRNP^{Ter/Ter}$, respectively). Genomic DNA

TABLE 1 Antibodies and dilutions used in the analyses

Name	Catalogue No.	Producer	Dilutions IHC	IF	WB
Anti-Iba1	019-19741	Fujifilm Wako Chemicals, Neuss, Germany	1/250	NA	NA
Anti-CD3	A-0452	Dako, California, United States	1/500	NA	NA
Anti-PrP 6H4	01-010	Prionics, Zürich, Switzerland	NA	1/500	NA
Anti-PrP P4	R8007	Ridascreen Biopharm, Darmstadt, Germany	NA	NA	1/100
Anti-Neurofilament 200	064H-4809	Sigma-Aldrich, Merck, Darmstadt, Germany	NA	1/400	NA

Abbreviations: NA = Not analyzed. IHC immunohistochemistry, IF immunofluorescence, WB western blot.

sampled for haplotype analysis is specified below. A detailed overview of goats used, according to age groups and analyses, is given in Supplementary Table 1.

2.2 | Tissue sampling

Tissues were collected immediately after euthanasia. Samples for immunohistochemistry were fixed in 10% neutral buffered formalin and then embedded in paraffin. For western blot, samples were snap frozen in isopentane, transferred to liquid nitrogen, and stored at −80°C. Whole-trunk samples of peripheral nerves were gently separated into fascicles and fixed in 2.5% glutaraldehyde in Soerensen's phosphate buffer (0.1 M, pH 7.4) for 4 hours at room temperature and then overnight at 4°C.

2.3 | Immunohistochemistry

Sections of 3-4 μm were placed on glass slides (Superfrost Plus®, Menzel Gläser, Thermo Fisher Scientific, Massachusetts, United States) and stored at 4°C until staining. The slides were deparaffinized in xylene and rehydrated through a descending alcohol series. Between steps, sections were washed twice in phosphate-buffered saline (PBS) for 5 minutes. For anti-Iba1, the slides were incubated with trypsin (1 mg/mL) in Tris HCl (0.1 M, pH 8 with 0.1% $CaCl_2$) for 40 min at 37°C before inhibition of endogenous peroxidase. For anti-CD3, antigen retrieval was performed by heating the slides in Tris/EDTA (pH 9.1) in a microwave before inhibition. The temperature in the solution was held at 92°C degrees for 5 min, thereafter the slides were kept in the hot solution for another 5 min before the procedure was repeated. Endogenous peroxidase was inhibited with 3% H_2O_2 in methanol for 10 minutes. Nonspecific antibody binding was blocked by incubating the slides for 20 minutes in 5% bovine serum albumin (BSA) with 2% goat serum. The sections were incubated for 60 min with primary antibodies, diluted in 1% BSA at dilutions indicated in Table 1. Next, the sections were incubated with secondary antibodies conjugated to horseradish peroxidase-labelled polymer from the EnVision+ kit (catalogue number K4009, Dako, California, United States) for 30 minutes, and developed with AEC+-substrate for 5 minutes. The sections were counterstained with hematoxylin and mounted with Aquatex (Merck, Darmstadt, Germany). Sections for which the primary antibodies were omitted were used as negative controls. Micrographs were taken using Axio Imager 2 microscope, equipped with an Axiocam 506 color camera (Zeiss, Oberkochen, Germany). The level of immune cell influx in peripheral nerves was scored from zero to three (0 = negative, 1 = low, 2 = moderate, and 3 = high) by two independent observers and an average was calculated. Slide-labels were concealed prior to scoring.

2.4 | Immunofluorescence

Cryostat sections of 8 μm were placed on glass slides (Superfrost Plus) and stored at −80°C until staining. After thawing, slides were fixed in formal-calcium (4% formaldehyde, 1% calcium chloride, pH 7.44) for 15 minutes. Blocking was performed for 30 minutes in 5% BSA with 2% goat serum followed by incubation with primary antibodies overnight at 4°C, diluted in blocking solution at dilutions specified in Table 1. Slides were incubated with secondary antibodies, goat anti-mouse IgG1 Alexa Fluor 488 and goat anti-rabbit IgG Alexa Fluor 594 (both from Invitrogen, Thermo Fisher Scientific), diluted in PBS for 45 minutes. The slides were mounted with ProLong Gold Antifade Mountant with 4′,6 diamidino-2-phenyl indole (DAPI; Molecular Probes, Thermo Fisher Scientific). Micrographs were taken using Axio Imager 2 microscope, equipped with an Axiocam 506 mono camera (Zeiss).

2.5 | Western blot

Peripheral nerves were lysed in homogenizer buffer (Tris HCl 50 μM, NaCl 150 mM, EDTA 1mM, DOC 0.25%, NP40 1%), supplemented with protease inhibitor cocktail (Complete, Roche, Merck), after removal of the connective tissue. Protein concentration was measured with the Protein assay (Bio-Rad, Hercules, California, USA). Total proteins (80 μg) were deglycosylated with PNGase-F, according to manufacturer's instructions (New England Biolabs, Ipswich, Massachusetts, United States). One hundred and thirty micrograms of total proteins and 80 μg of the deglycosylated samples were separated on SDS-Page (12% Bio-Rad) and blotted on PVDF membrane (GE Healthcare, Little Chalfont, United Kingdom). After protein transfer, gels were stained with Coomassie blue (Invitrogen, Thermo Fisher Scientific). Membranes were blocked in 5% dry milk in Tris-buffered saline-Tween (TBST), and probed with primary antibody Anti-PrP P4, diluted as indicated in Table 1. Secondary anti-mouse antibody conjugated with alkaline phosphatases was used for the detection. The signal was developed with Enhanced chemiluminescence (ECF) reagent (GE Healthcare) and Typhoon 9200 (Amersham Bioscience, GE Healthcare).

2.6 | Processing of peripheral nerves for morphological assessment

About 1-2 mm pieces were cut from the nerve fascicles, postfixed in 1% osmium tetroxide at 4°C, and transferred to washing buffer. The samples were dehydrated through an ascending acetone series and embedded in epoxy (Electron Microscopy Sciences, Hatfield, Pennsylvania, United States). Semi-thin (0.5 μm) sections were stained with toluidine blue and safranin-O, and evaluated by light microscopy using a

Zeiss Axio Imager 2 microscope equipped with an Axiocam 506 color camera. Ultra-thin (70 nm) sections were contrasted with uranyl acetate and lead citrate, and studied using a FEI Morgagni 268 transmission electron microscope (FEI, Hillsboro, Oregon, United States) equipped with an Olympus Veleta CCD camera. In the semi-thin sections, the number of nuclei per 0.5 mm^2 from each individual was quantified independently by two observers.

For nerve fiber teasing, 1 cm pieces of fixed nerve fascicles were postfixed in 2% osmium tetroxide at room temperature for 1 hours, washed in phosphate buffer, immersed in glycerol and separated under a dissection microscope. A total of 489 teased nerve fibers were studied; 313 from goats homozygous for nonsense mutation in *PRNP* (*PRNP*$^{Ter/Ter}$) goats and 176 from *PRNP*$^{+/+}$ goats. The percentage of fibers with evidence of demyelination and/or remyelination (internodes with reduced length and myelin thickness) was scored blindly by two independent observers.

For morphometric analysis, semi-thin sections were analyzed with Image-Pro Plus software (Media cybernetics, Maryland, USA). The area of the myelin sheaths and axons were measured and used to calculate the respective diameters as previously described.[12] *G*-ratio was then calculated as the ratio between axonal diameter and fiber diameter.

2.7 | Extraction of lipids from peripheral nerves

Mass spectrometry grade water and chloroform (reagent Ph. Eur.) stabilized with 0.6% of ethanol were purchased from VWR International (Radnor, Pennsylvania, United States). Methanol (LC-MS grade) was obtained from Merck. Ammonium acetate (for mass spectrometry, 98%) was purchased from Honeywell International Inc (Charlotte, North Carolina, United States).

Lipids from goat nerve tissue were extracted using the solvent system based on the Folch method.[13] A Precellys®24 bead homogenizer equipped with a Cryolys temperature controller (All Bertin Technologies SAS, Montigny-Le-Bretonneux, France) was used to disrupt and homogenize the tissue for lipid extraction. Nerve tissue (50 mg) was homogenized with zirconium oxide beads (0.5 ± 0.01 g, Ø 1.4 mm) in 500 µL of a cold mixture of chloroform/methanol (2:1, v/v). The tissue was kept frozen during cutting and weighing. Final rounds$^{5\text{-}10}$ of bead-beating for 30 seconds at 6500 rpm, with an intermediate 15 seconds pause between rounds were performed. Another 500 µL of a cold mixture of chloroform/methanol (2:1, v/v) was added to the sample and the tube was shaken for 10 minutes using a thermoshaker (Thermal shake lite, VWR) and phase separation was induced by adding 200 µL of 20 mM acetic acid. After 10 minutes of shaking (1500 rpm, 16°C), tubes were centrifuged for 6 minutes at maximum speed (13 400 rpm) using a small centrifuge (MiniSpin, Eppendorf, Hamburg, Germany). A volume of 400 µL of the chloroform layer (lower) was collected and the sample re-extracted with 500 µL of a cold mixture of chloroform/methanol/water (86:14:1, v/v), vortexed and centrifuged as above. From the lower layer, 650 µL was collected and pooled with the first extract. The resulting extract was filtered through a syringe filter with GHP membrane (0.2 µm, Ø 13 mm, Acrodisc®, Pall Laboratory, Port Washington, New York, United States) and kept at −20°C until analysis with ultra-performance convergence chromatography tandem mass spectrometry (UPC^2-MS/MS). Dichloromethane was used as diluent for lipid extracts.

2.8 | Chromatographic analysis of lipids

A lipid profile analysis was performed using an UPC^2® separation system coupled to a hybrid quadrupole orthogonal time-of-flight mass spectrometer SYNAPT G2-S HDMS (Waters, Milford, Massachusetts, United States). A previously described analytical method[14] was adopted and modified. The column was protected with a VanGuard pre-column (BEH 2.1 × 5 mm) and temperature of the column was 50°C. The gradient of the modifier used was set as follows: 0 minutes, 1%; 4.0 minutes, 30%;^{6} 4.4 minutes, 50%;^{2} 6.25 minutes, 50%;^{1} 7.25 minutes, 50%;^{6} 7.35 minutes, 1%^{6}, 8.50 minutes, 1%.

The mass spectrometer was operated in MS^E mode and the collision energy ramped from 20 to 30 eV for positive ion mode and from 20 to 35 eV for negative ion mode. Data were acquired over the mass range of 50-1200 Da and the resolution of the mass spectrometer was 20 000. Both positive and negative ion electrospray ionization modes were applied. MS tuning parameters were set as follows: capillary voltages 3.0 kV and −2.5 kV for positive and negative ionization modes, respectively; source temperature 150°C; the sampling cone 40V; source offset 60V; desolvation temperature 500°C; cone gas flow 50 L/h; desolvation gas flow 850 L/h; nebulizer gas pressure 4 bar. Leucine enkephalin was used as the lock mass. Identification of a lipid compound is based on the following main characteristics: retention time of the appropriate lipid class, accurate mass (ppm error <5), isotope pattern similarity (>80%), and fragmentation pattern. The lipid nomenclature and shorthand notation described by LIPID MAPS[15] and Liebisch G. et al,[16] were followed.

2.9 | Haplotype analysis

A total of 48 goats, either heterozygous (n = 27) or homozygous (n = 21), were used for the haplotype analysis (henceforth referred to as *PRNP*$^{+/Ter}$ and *PRNP*$^{Ter/Ter}$ respectively). A previously acquired Illumina 50K SNP(single-nucleotide polymorphism) dataset of 48 AI bucks (born 2009-2012)

from the Norwegian goat breeding system was used as a reference population. Among the 48 bucks, 41 were wild type ($PRNP^{+/+}$), and 7 were heterozygous, while none were homozygous $PRNP^{Ter/Ter}$. The goats were genotyped by the Illumina 50K SNP (single-nucleotide polymorphism) chip. The genotyping was carried out by Neogen Ltd, Scotland, UK.

After initial filtering for quality of the *PRNP*-groups, the final number of markers were 49 277. Two individuals (one $PRNP^{+/Ter}$ and one $PRNP^{Ter/Ter}$) were removed due to low call rate. The 48 AI bucks previously genotyped with the same SNPs array were left with 49 124 markers after identical quality filtering. Comparing these two datasets after filtering, 47 847 markers were present in both datasets. These two datasets were merged into one common file, containing 94 individuals and the 47 847 markers.

SNP (single-nucleotide polymorphism) positions were updated to the ARS1 assembly version. The minor allele frequencies (MAF) for all SNPs on chromosome 13 were calculated using the PLINK −freq function. This analysis was done for the three genotype classes separately ($PRNP^{+/+}$, $PRNP^{+/Ter}$ and $PRNP^{Ter/Ter}$). The seven heterozygous AI bucks were included in the $PRNP^{+/Ter}$ group. In addition, the average MAF of all chromosomes were estimated for the same genotype classes.

2.10 | Electrophysiological recordings and clinical examination

All electrophysiological recordings were conducted in the same rooms as the goats were housed. The goats were placed in a small pen and restrained using a halter and rope. The experimental session was conducted on the thoracic limb in every animal. Self-adhesive surface stimulation electrodes (Neuroline 70010-K/C/12, AMBU, Copenhagen, Denmark) were attached to the skin overlaying the lateral digital nerves after shaving and washing with ether and ethanol. Recording needle electrodes (Aiglette 019200 REF:S46-638, Technomed, Netherlands) were placed in the ipsilateral deltoid muscle, and a reference electrode (Natus Ref 019-409100, Middleton, Wisconsin, United States) was placed on the back of the goat. Flexible leads were connected to the electrodes and resistance of each electrode pair was checked to be below 3 kΩ.

Stimulations and recordings were performed using Cephalon Natus Viking Quest (Cephalon, Aalborg, Denmark). Stimulation started at 1 mA and increments were in steps of 0.5 mA. Reactions to the stimulation were assessed and scored according to the following descriptors: 0 = no reaction; 1 = weak muscle contraction of the deltoid muscle; 2 = muscle contraction of the deltoid muscle and a short withdrawal reflex; 3 = definite withdrawal reflex and muscle contractions in the flank; 4 = distinct and repeated withdrawal reflex accompanied by responses in other body parts (head, neck, contralateral leg); 5 = distinct and repeated withdrawal reflex accompanied with a whole body response.

A standard single stimulus consisted of a train-of-five 1 ms constant current pulses delivered at 200 Hz. The electromyography (EMG) activity in the deltoid muscle was recorded from 100 ms before to 300 ms after each stimulus. Reflex amplitude was calculated as the root-mean square (RMS) of the EMG burst activity following stimulation. To be considered a reflex response, the EMG burst following the electrical stimulation had to have a RMS amplitude of at least 30 μV, with a minimal duration of 20 ms. Latency was defined as the time (ms) from the stimulus to the onset of the EMG deflection. The lowest stimulation intensity eliciting an EMG response combined with a behavioral reaction score > 2 was used when latency was measured.

$PRNP^{Ter/Ter}$ goats were subjected to clinical, including basic neurological, examination.

2.11 | Statistical analysis

Data were processed using GraphPad Prism. For statistical comparison of two groups ($PRNP^{+/+}$ and $PRNP^{Ter/Ter}$) for demyelinated fibers, number of nuclei in semi-thin sections and *g*-ratio we performed unpaired *t*-tests.

For haplotype analysis, the following filtering parameters were used; call rate > 90% both for individual markers and per animal, maf > 1% and hwe *P* value > 1e-5, using the PLINK 2.0 software (−geno, −mind, −maf, and −hwe).[17]

Mass chromatogram raw data were processed using Progenesis QI software (Nonlinear Dynamics, Waters) with in-built LipidBlast[18] and LipidMaps databases[19] for lipid identification. Lipid classification was based on defined retention time windows and experimentally obtained response factors.[20] Only lipid species within the defined lipid class retention time windows were retained for analysis and interpretation (Supplementary Table 4). Further, the processed data were exported for multivariate analysis using a freely available statistical tool MetaboAnalyst.[21] The data were normalized and auto-scaled before they were subjected to principal component analysis (PCA) and hierarchical clustering analysis (heatmap).

3 | RESULTS

3.1 | Morphological and immunohistochemical analyses of peripheral nerves

Teased fibers from the tibial nerve of the $PRNP^{Ter/Ter}$ goats (Figure 1 and 2A) had interposed, short internodes with

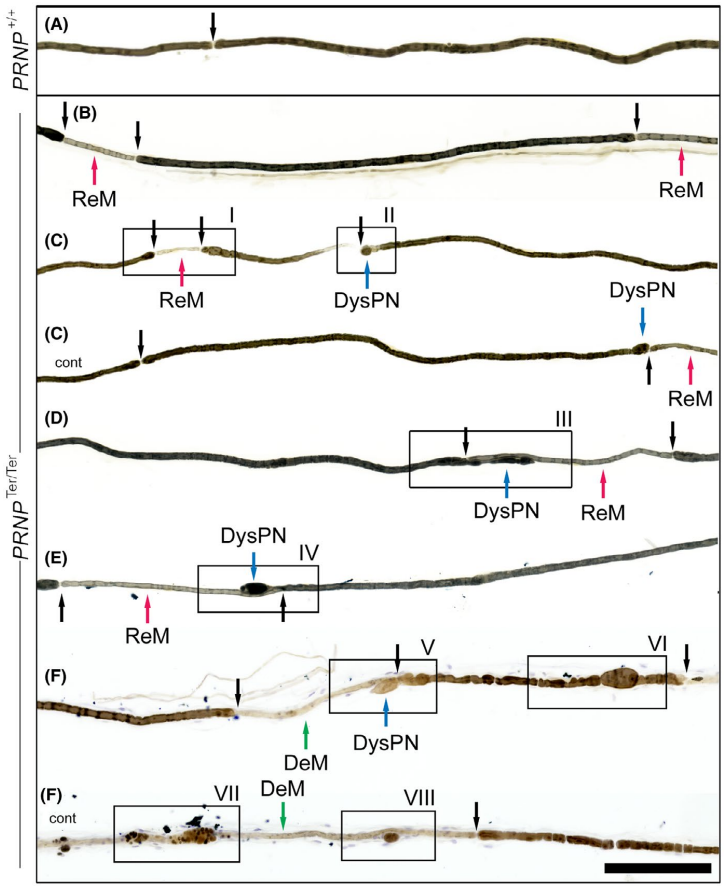

FIGURE 1 Teased nerve fibers. A, Nerve fiber from normal goat (*PRNP*$^{+/+}$); the thickness of the myelin is similar on both sides of the node of Ranvier (black arrow). B-F, Nerve fibers from *PRNP*$^{Ter/Ter}$ goats. Short internodes with reduced myelin thickness (intercalated internodes, red arrows) between (C, D, E) or at both sides (B) of longer internodes with normal myelin thickness. The intercalated internodes are associated with the presence of dysmorphic paranodes (blue arrows) (C-E). Active segmental demyelination (green arrows) with myelin degradation products along the demyelinated axon, and accompanied by cellular infiltrates (F). Black arrows = Nodes of Ranvier, ReM = Remyelinated segments, DeM = Demyelinating segments, DysPN = Dysmorphic paranodes. Black boxes and Roman numerals refer to segments shown at higher magnification in Figure 2. Bar 200 µm. Staining: Osmium tetroxide with (F) or without (A-E) hematoxylin

reduced myelin thickness, consistent with remyelination,[22] wide-spread multifocally. These segments intermingled with internodes of normal length and myelin thickness. More specifically, the remyelinated segments were frequently found as intercalated internodes at both sides of a longer internode with a thicker myelin sheath. The paranodes of the latter were often dysmorphic, with changes ranging from swollen paranodes to protrusions of the myelin sheath stretching for 100-200 µm along the intercalated internodes. Series of short, thinly myelinated internodes were also observed. Actively demyelinating segments with osmiophilic balls consisting of myelin debris[12] were accompanied by cellular infiltrates, but such segments were infrequently observed (Figure 1F). The *PRNP*$^{Ter/Ter}$ goats had an increased percentage of fibers ($P = .0001$), with evidence of demyelination and/or remyelination, compared with age-matched controls (Figure 2B). The changes in the 8 months old goats were less pronounced, but morphologically similar to those in adult (3-7 years) goats.

Semi-thin sections confirmed these morphological alterations (Figure 3), with the presence of thin myelin sheaths and onion bulbs (Figure 3E,G). Onion bulbs consist of concentrically arranged Schwann cell processes, and suggest repeated demyelination and remyelination. Vacuolated and thickened fibers were occasionally seen in the nerves of the *PRNP*$^{Ter/Ter}$ goats. These fibers presented with interlamellar myelin splitting (Figure 3D), thin myelin and/or hypertrophy of the Schwann cell adaxonal cytoplasm, often in combination with axonal shrinkage (Figure 3G). Diminished axonal diameters without other pathological features were present, but difficult to interpret, as apparent axonal retraction from the myelin sheath can be found artifactual. Paranodal outfoldings were identified in longitudinal sections (Figure 3H). The splitting of the myelin sheath in the *PRNP*$^{Ter/Ter}$ goats must be distinguished from the very prominent Schmidt-Lanterman clefts seen in both groups (Figure 3C).

Moreover, an increased number of mononuclear cells were observed evenly distributed in the endoneurial connective tissue of the *PRNP*$^{Ter/Ter}$ goats (Figure 3F, $P = .0267$). To investigate these cells, we stained nerve sections with antibodies against Iba1 (macrophages) and

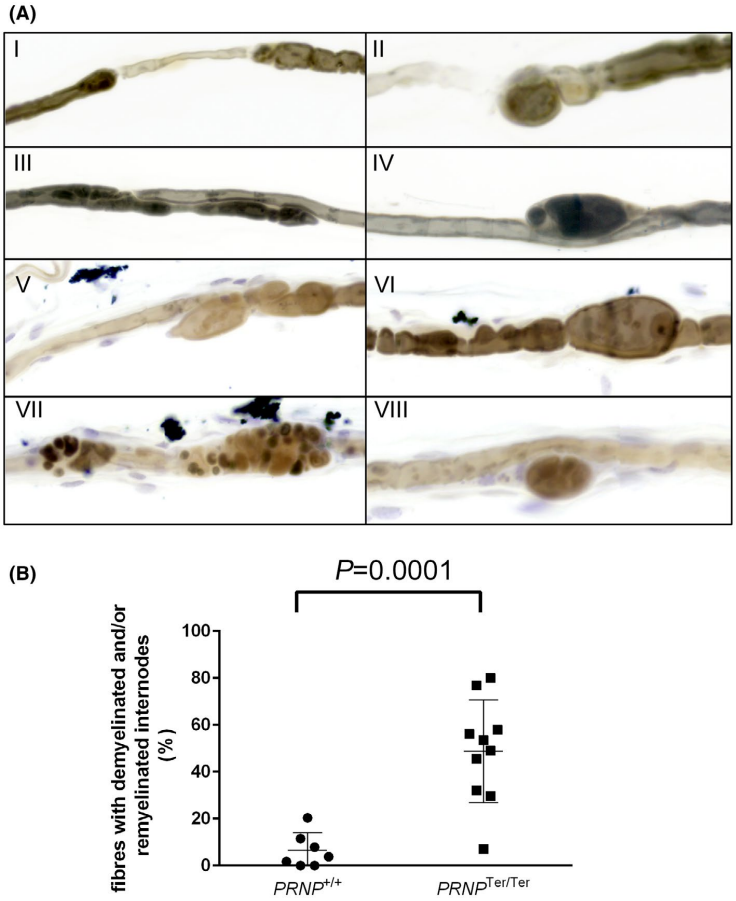

FIGURE 2 A, Higher magnification of changes in teased nerve fibers marked by black boxes in Figure 1. Intercalated, thinly myelinated and short internodes, indicative of paranodal demyelination and subsequent remyelination (I-IV). The paranodal pathology ranged from swollen paranodes (II) to outfoldings along the intercalated internode (III-V). Cellular infiltrates were visible along demyelinating segments (VI). Active demyelination in an internode exhibiting highly irregular myelin sheath with myelin degradation products and cellular infiltrates present along the demyelinating segment (VII, VIII). B, In *PRNP*$^{Ter/Ter}$ goats there were significantly more fibers with evidence of demyelination or remyelination than in normal goats

CD3 (T lymphocytes). This showed that both the number of macrophages (Figure 4A,B) and T lymphocytes (Figure 4C,D) were increased in the endoneurium of adult goats lacking PrP^{C}.

At the ultrastructural level, *PRNP*$^{Ter/Ter}$ fibers with myelin splitting proved to be fibers with intramyelinic edema (Figure 5A). The myelin splitting occurred at the intraperiod line (not shown), separating the outer aspects of the Schwann cell plasma membrane, thereby focally increasing the extracellular volume in the myelin sheath. In the fibers with swelling within the adaxonal and/or abaxonal Schwann cell cytoplasm, the edematous spaces contained vesicular structures, probably swollen organelles (Figures 5B and 6B,D). The corresponding axons were shrunken, with an increased density of neurofilaments (Figure 5B,C) and, occasionally, other organelles, suggesting compression[23] (Figure 5C). Myelinated fibers with thin myelin sheaths surrounded by supernumerary Schwann cells, recognized by the presence of a basal lamina, were present (Figure 5C). Cells without basal lamina, probably representing the Iba1- or CD3-positive cells demonstrated by immunohistochemistry, were observed around some of the nerve fibers (Figure 5D). Neither of these were observed to penetrate the basal lamina of the Schwann cell, nor did we observe such cells between the myelin sheath and axon. Less frequently, severely dysmorphic organelles were present in the adaxonal Schwann cell cytoplasm (Figure 5E). No changes were detected in unmyelinated C-fibers of Remak clusters (Figure 5F).

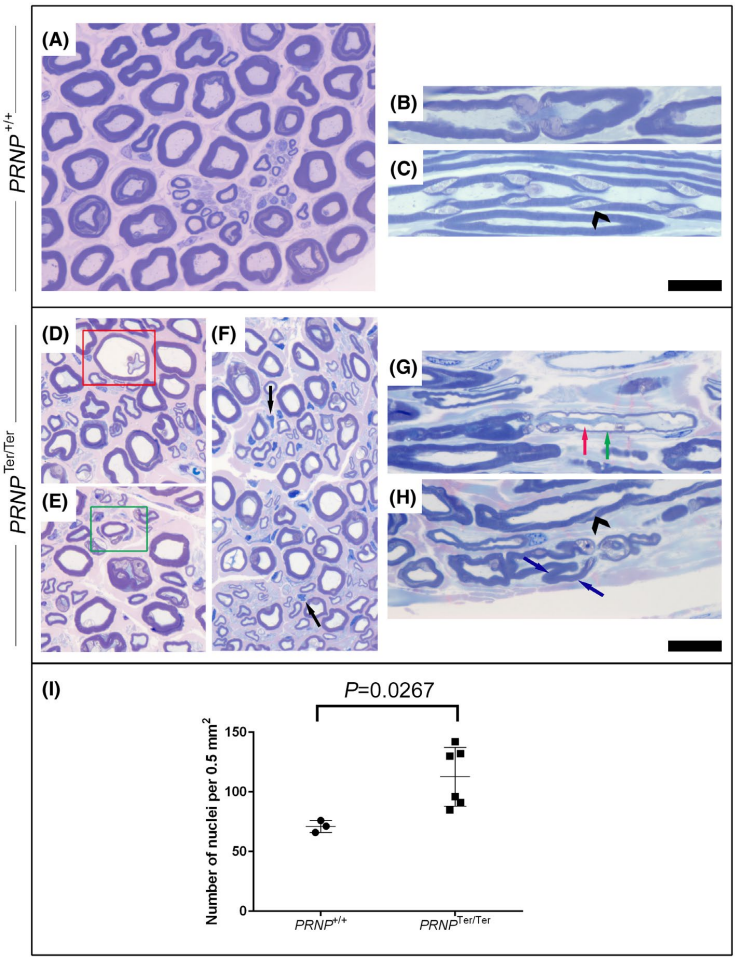

FIGURE 3 Toluidine blue- and safranin O-stained cross and longitudinal semi-thin sections of tibial nerves of *PRNP*$^{+/+}$ A-C, and *PRNP*$^{Ter/Ter}$ (D-H) goats. (C, H) Prominent Schmidt-Lanterman clefts were visible in both groups (arrowheads). D, Vacuolated fibers (red frame) were present in the nerves from the *PRNP*$^{Ter/Ter}$ goats; a fiber with severe myelin splitting and a shrunken axon centrally is shown in a red frame—compare with Figure 5A. E, A green frame shows an onion bulb. F, An increased number of cell nuclei (two examples are indicated by black arrows) was present in the nerves from the *PRNP*$^{Ter/Ter}$ goats. G, A remyelinated nerve fiber (green arrow) with swelling of the adaxonal Schwann cell cytoplasm (red arrow) is present next to an internode with normal myelin thickness. H, A paranodal outfolding (blue arrows) is visible next to a node of Ranvier. Bar 20 μm. I, Quantification of nuclei in semi-thin sections demonstrated increased number of cells in *PRNP*$^{Ter/Ter}$ goats

3.2 | Nerve fiber diameter distribution

We investigated nerve fiber distribution in *PRNP*$^{+/+}$ and *PRNP*$^{Ter/Ter}$ goats, and observed a lower percentage of large fibers in the latter group (Figure 7A). To compare myelin thickness between the groups, we calculated the *g*-ratio (axonal diameter/total fiber diameter) in cross sections of the tibial nerve. Nerve fibers from *PRNP*$^{Ter/Ter}$ goats had a higher *g*-ratio ($P = .0139$) than *PRNP*$^{+/+}$ goats (Figure 7B), particularly prominent in large myelinated fibers.

3.3 | Peripheral nerve lipid composition

Analysis of the peripheral nerve lipid composition was performed with UPC2-MS/MS technology enabling both high resolution detection of individual lipid species and a semi-quantitative estimation of lipid class distribution in the extracts.[20] Principal component analysis revealed a predominantly age-dependent difference of the global lipid profiles with adult goats (more than 1 year old) clustering separately from young goats (Figure 8A). However, a clear

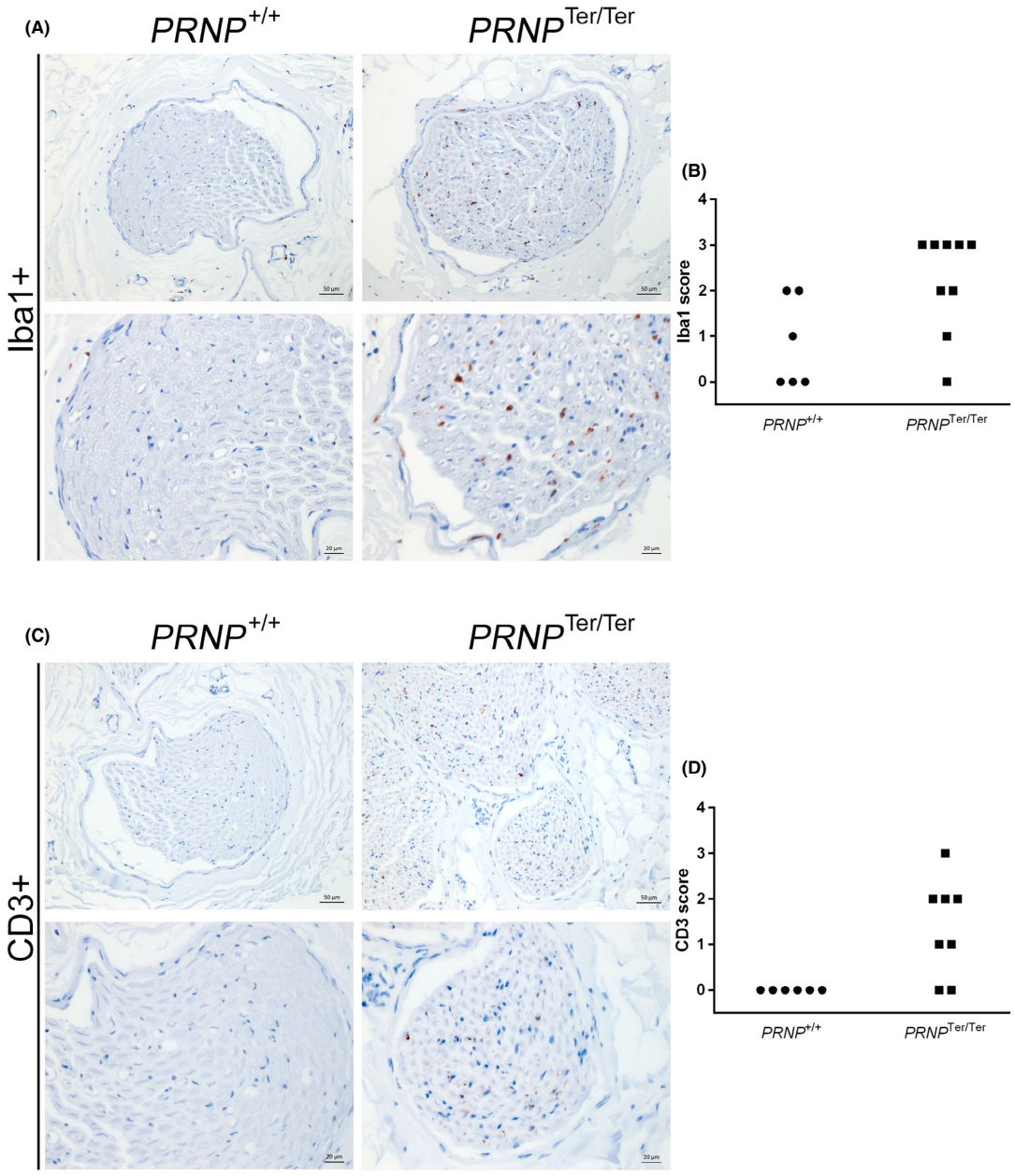

FIGURE 4 Immunostaining of Iba1+ (A) and CD3+ (C) cells in peripheral nerve cross sections. An increased level of Iba1+ cells in the endoneurium of *PRNP*$^{Ter/Ter}$ goats when compared to *PRNP*$^{+/+}$ indicates macrophage infiltration and/or proliferation in the former group. Endoneurial CD3+ lymphocytes are present in the *PRNP*$^{Ter/Ter}$ goats. In the *PRNP*$^{+/+}$ group, no signal was observed from the endoneurium. Quantification of the staining level was performed for both Iba1 (B) and CD3 (D), confirming increased staining in *PRNP*$^{Ter/Ter}$ goats

enrichment of hexosyl ceramides (HexCer) was observed among the lipids significantly changed within the adult groups. While only 13% of lipid species accounting for only 5% of summed abundance in the whole lipidome is significantly changed, 42% lipid species (44 out of 105 species) and 30% in summed abundance is significantly changed in

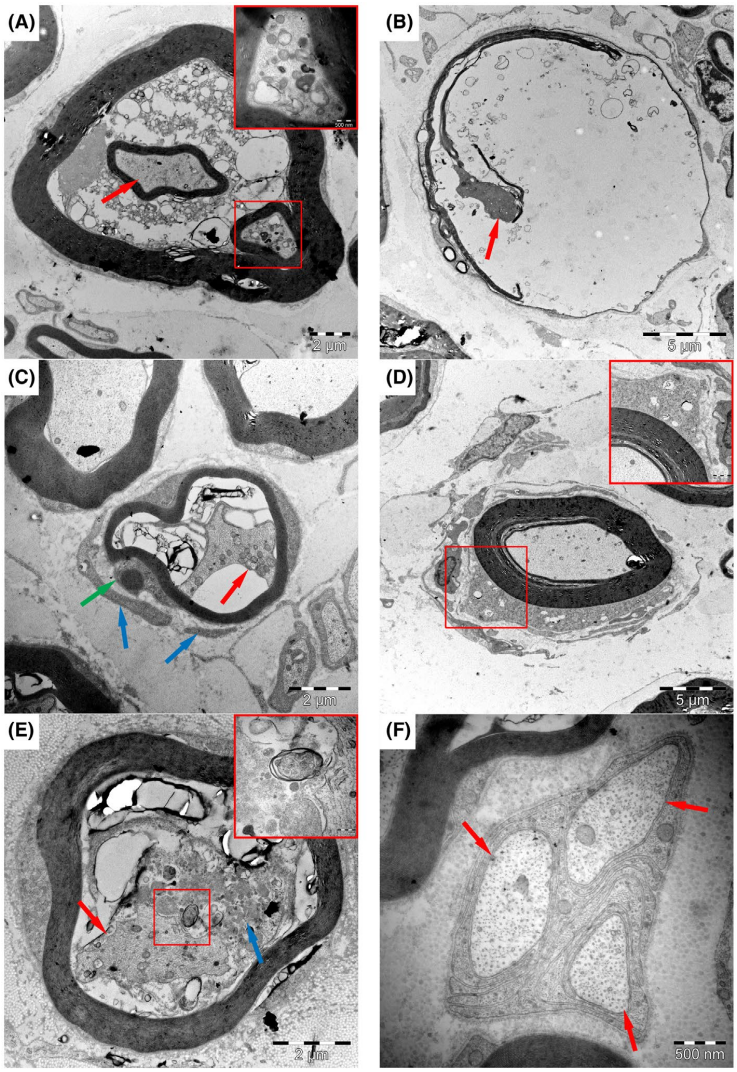

FIGURE 5 Ultrastructural changes in nerves from *PRNP*$^{Ter/Ter}$ goats. A, Myelin splitting and accumulation of vesicles. A shrunken axon (red arrow) is present in the middle of the image, while a myelin fold surrounds a cytoplasmic space with accumulation of mitochondria (red frame, magnified in inset). B, A severely swollen nerve fiber with a shrunken axon (red arrow). Only remnants of the myelin sheath are present. Vesicular structures are visible in the vacuolated space. C, An axon with abnormally thin myelin sheath is surrounded by supernumerary Schwann cell processes in a small onion bulb. The cytoplasm of the myelinating Schwann cell is indicated by green arrow, while the supernumerary Schwann cell is shown with blue arrows. The axon is shrunken and has increased densities of neurofilaments and mitochondria (red arrow). D, Cellular infiltrates next to a myelinated fiber with prominent rough endoplasmic reticulum in the Schwann cell. E, Dysmorphic organelles (red frame, magnified in inset) in the adaxonal Schwann cell cytoplasm (blue arrow). Shrunken axon (red arrow). F, No changes were detected in unmyelinated fibers (red arrows) of a Remak bundle

the HexCer lipid class for the adult goats (Figure 8B). A closer inspection of the 18 most abundant species constituting 95% of the total abundance of the HexCer group revealed a global downregulation of HexCer of the *PRNP*$^{Ter/Ter}$ goats compared to the adult controls (Figure 8C). There were individual differences, that is, goats 1, 2, 3, and 5 are down in all HexCer lipids, while goats 4 and 6 still have a more scattered abundance profile, probably reflecting that the demyelination has reached different stages among the *PRNP*$^{Ter/Ter}$ goats.

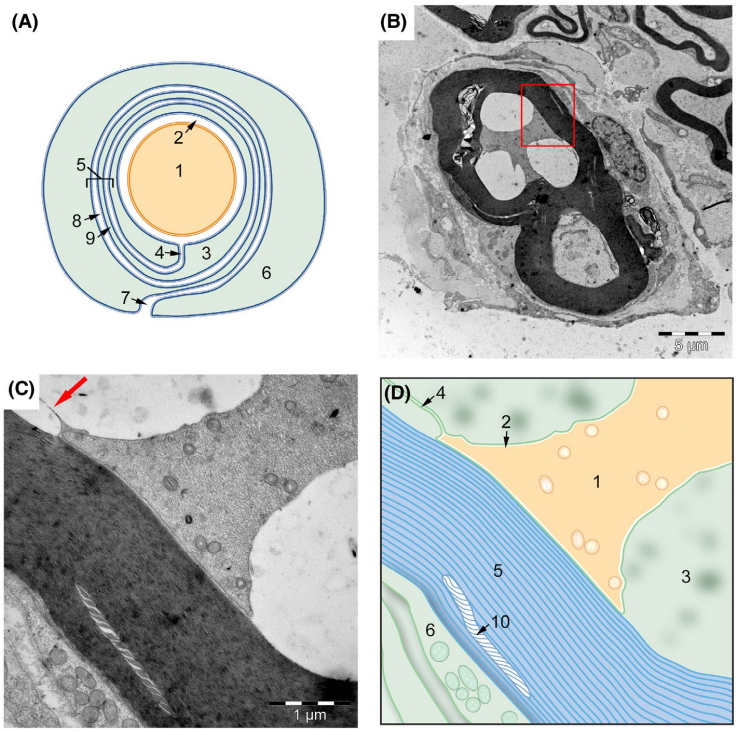

FIGURE 6 A, Schematic representation of a myelinated fiber. B, A myelinated nerve fiber with swelling of the adaxonal Schwann cell cytoplasm (red frame in b, magnified in C, Note the presence of vesicular structures in the adaxonal Schwann cell cytoplasm. The inner mesaxon is indicated by the red arrow. D, Schematic representation of c. 1 = Axon, 2 = Periaxonal space, 3 = Adaxonal Schwann cell cytoplasm, 4 = Inner mesaxon, 5 = Compact myelin, 6 = Abaxonal Schwann cell cytoplasm, 7 = Outer mesaxon, 8 = Intraperiod line, 9 = Major dense line, and 10 = Schmidt-Lanterman cleft

3.4 | Genomic analysis

The average minor allele frequency across the 29 autosomes showed strong similarity between the AI bucks (n = 41) and the group of individuals heterozygous (n = 33) for the *PRNP*^{Ter} allele. The goats homozygous for the *PRNP*^{Ter} allele (n = 20) had a lower MAF across all chromosomes, reflecting their increased relatedness relative to the general goat population. As expected, these homozygous goats also showed a significant drop in MAF at chromosome 13, on which *PRNP* resides, indicating an extended homozygosity surrounding the *PRNP* locus (Figure 9A).

A more detailed analysis of chromosome 13 was achieved by plotting the average MAF of a sliding window of 5 SNPs across the chromosome. Only noncarriers and homozygous *PRNP*$^{Ter/Ter}$ goats were plotted (Figure 9B,C). These data show that 58 consecutive SNPs in the region from 44.97 MB to 47.45 MB are completely homozygous, delineating the minimum shared haplotype between the homozygous individuals in our study. The *PRNP* gene is located in the region 46.45-46.47 Mb on goat chromosome 13, almost in the middle of the homozygous region. Whereas the homozygous region constitutes approximately 2.5 MB of genomic DNA, the region spanning from 43.7 to approximately 50.0 MB (6.3 Mb of genomic DNA) showed a reduced MAF compared with the rest of chromosome 13. This means that genes located in this wider region (43.7-50.0 MB) have increased linkage to the *PRNP*^{Ter} allele, while genes in the core region (44.97-47.45 Mb) are completely linked to the *PRNP*^{Ter} variant in the investigated population. In Supplementary Table 2, genes located in the core flanking region are given.

3.5 | Detection of PrP^{C} in peripheral nerves

Immunofluorescence analysis of PrP^{C} (Mab 6H4) in longitudinal and cross-sections of peripheral nerves (Figure 10) demonstrated that *PRNP*$^{+/+}$ goats showed a strong PrP^{C} expression in Schwann cells and myelin sheaths. Axons

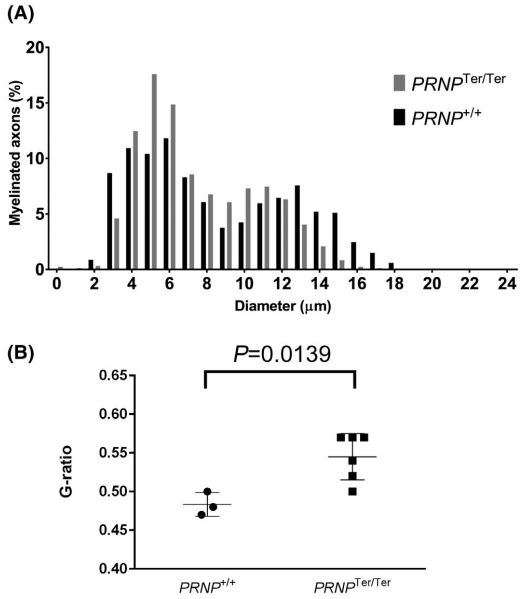

FIGURE 7 Fiber diameter frequency distribution in $PRNP^{+/+}$ and $PRNP^{Ter/Ter}$ A, goats illustrates a bimodal distribution in both genotypes and a loss of large diameter fibers in the $PRNP^{Ter/Ter}$ group. B, Nerve fibers of $PRNP^{Ter/Ter}$ goats showed a higher *g*-ratio (axonal diameter/fiber diameter), corresponding to a higher percentage of thinly myelinated fibers

appeared negative, but levels could be below the detection limit of the method used. As expected, PrP^C was not present in $PRNP^{Ter/Ter}$ goats. (Figure 11), western blot analysis confirmed PrP^C presence in $PRNP^{+/+}$ goats. Glycosylated full-length PrP^C is visible; moreover, after deglycosylation with PNGase-F, full length appeared at 27 kDa. A second band, with an approximate molecular mass of 22 kDa, could represent a C-terminal truncated form of PrP^C.

3.6 | Electrophysiology and clinical examination

Electrophysiological recordings are summarized in Supplementary Table 3. No significant differences in terms of latency were noted. No neurological deficits were observed in goats clinically examined.

4 | DISCUSSION

Over the past 7 years (from 2012), we have studied a total of nearly 50 homozygous $PRNP^{Ter/Ter}$ goats, both genders represented. Most have been young, but a few were more than 5 years old, and thus "aged" after husbandry standards. Although, no major physiological disturbances were apparent at rest, when subjected to acute endotoxin challenge, young (7 months) homozygous $PRNP^{Ter/Ter}$ goats displayed more profound sickness behavior[24] and increased inflammatory lung damage than normal goats.[25]

In the current study, analysis of peripheral nerves from goats, 8 months-7 years of age, revealed the presence of thinly myelinated internodes intermingled with internodes of normal myelin thickness, together with an increased variability in internodal length. These results suggest the presence of demyelinating neuropathy. These patterns of changes are in line with abnormalities observed at around 10 weeks of age in mice lacking the prion protein.[8-10] Axonal and not Schwann-cell restricted PrP^C expression completely prevented peripheral neuropathy in these mice, although some disease features were partly reversed after Schwann cell PrP^C expression.[10] Focally folded myelin was observed in the paranodal areas of the nerves of $Prnp^{-/-}$ mice.[10] Although paranodal demyelination is an early and unspecific sign of demyelination, the presence of intercalated internodes at both sides of a longer internode, as well as the severely dysmorphic paranodes in the $PRNP^{Ter/Ter}$ goats, could be due to a function for PrP^C in paranodal and juxtaparanodal fiber segments, in particular membrane junctions. In some nonneural tissues, like the gastrointestinal tract[26] and lungs,[27] PrP^C expression has been associated with stability of desmosomes, adherens junctions, and tight junctions. As the paranodal regions are stabilized by autotypic tight junctions,[28] one possibility is that in the absence of PrP^C, these are slightly destabilized, leading to paranodal outfoldings. Furthermore, disrupted axoglial junctions have been shown to cause ion channel dispersion with accumulation of potassium between the axon and Schwann cell, eliciting swelling of the Schwann cell and remodeling of the myelin,[29] a phenomenon that fits with the observed pathology in the nerves from $PRNP^{Ter/Ter}$ goats.

No clinical manifestations or electrophysiological aberrations were detected in $PRNP^{Ter/Ter}$ goats up to 7 years old. In $Prnp^{-/-}$ mice, reduced performance was noted in two out of three tests for neuromuscular function and nerve conduction velocity was also reduced, most pronounced at older age.[10]In this study, the oldest homozygous $PRNP^{Ter/Ter}$ goat was close to 7 years and appeared neurologically normal. However, goats can reach 15 years, so a seven-year-old goat is probably "middle-aged."

The pathophysiological significance of the elevated number of Iba1+ macrophages in the endoneurium of PrP-deficient goats needs further study. For instance, the macrophages appear to be evenly distributed throughout the endoneurium, and not, as in $Prnp^{-/-}$ mice, located to digestive chambers,[10] which are sites of myelin degradation. This raises the intriguing possibility that macrophage infiltration in goats precedes demyelination. To clarify

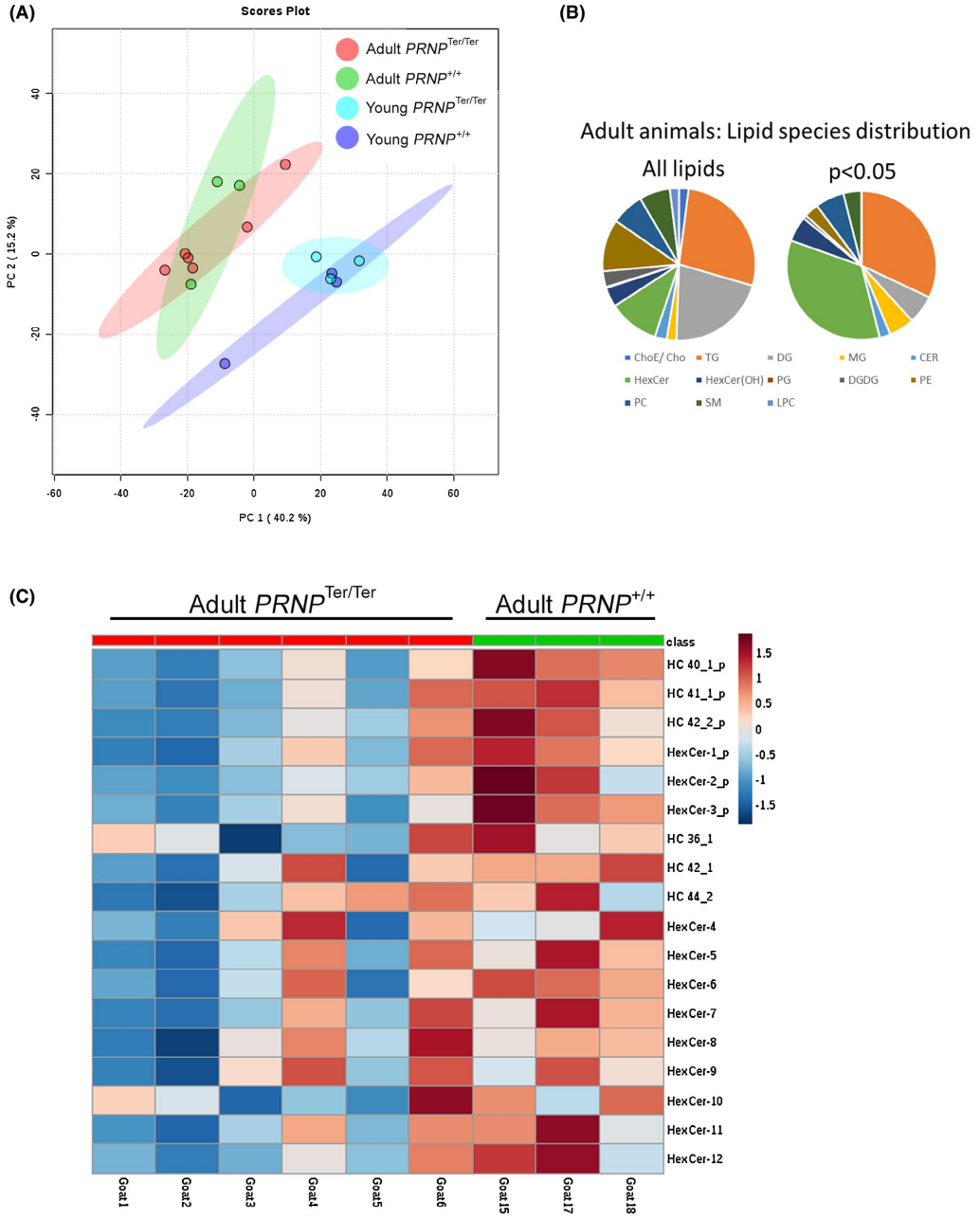

FIGURE 8 UPC^2-MS/MS analysis of peripheral nerve lipid composition. A, Principal component analysis (PCA) shows a clustering of animals according to age. B, Almost 1000 lipid species were retained after removal of noise and retention time filtering, and 128 of those were significantly changed between the two adult groups (*t*-test, $P < .05$). Of the 13 lipid classes (see Supplementary Table S4 for names), the hexosyl ceramides are enriched among the significantly changed (right panel in b and Supplementary Table S4). C, Nonordered heatmap presentation of the 18 most abundant HexCer lipids (top 6 with $P < .05$). Six of the lipids were tentatively identified with LipidMaps

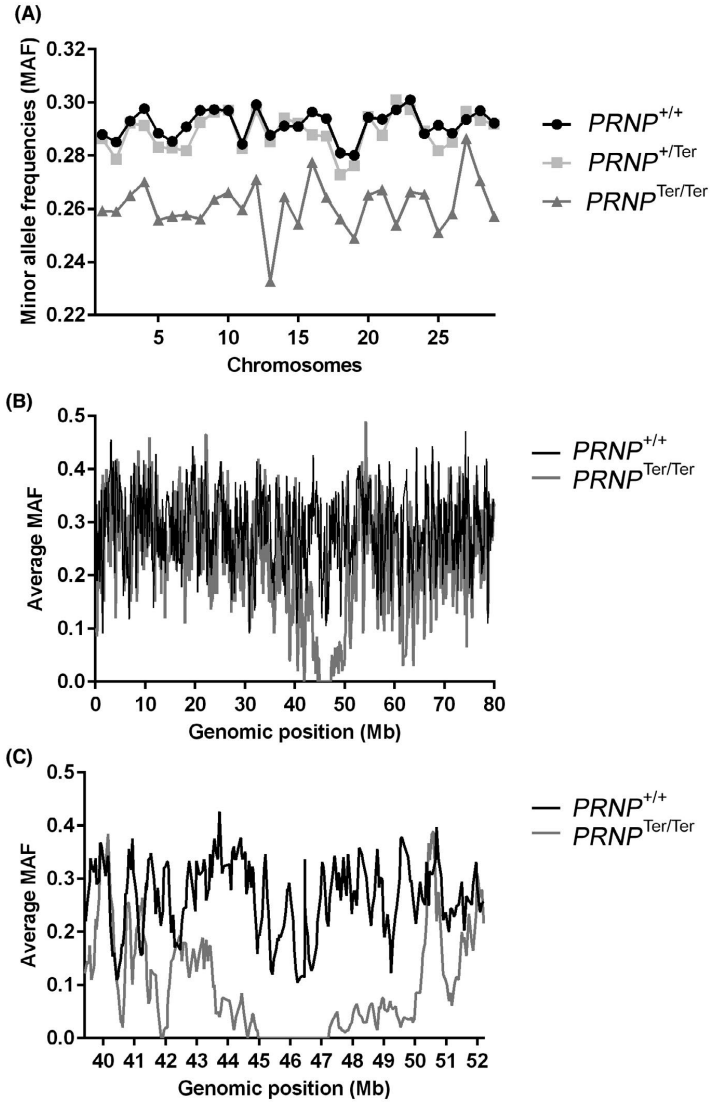

FIGURE 9 Haplotype analysis of goats. A, The figure illustrates the average minor allele frequencies (MAF) of all 29 autosomes, in *PRNP*$^{+/+}$, *PRNP*$^{+/Ter}$, and *PRNP*$^{Ter/Ter}$ goats. Chromosome numbers are on the x-axis and MAF-frequency on the y-axis. B, The graph shows the average MAF of a sliding window of 5 sequential SNPs across chromosome 13. For clarity, only *PRNP*$^{+/+}$ and *PRNP*$^{Ter/Ter}$ goats are included. Figure C, is zoomed in at the region surrounding the *PRNP* gene. Positions in mega bases (MB) on the x-axis and average MAF-frequency (of 5 sequential SNPS) on the y-axis

this, studies of nerves from younger goats are necessary. However, no increase in Iba1+ macrophages has been observed in the choroid plexus of goats without PrP^{C},[24] arguing that a pathological process in the peripheral nerves provides the chemoattractant clues for macrophage influx. Interestingly, we did not detect macrophages penetrating the basal lamina of Schwann cells; as reported in macrophage-mediated demyelination,[30,31] and observed in *Prnp*$^{-/-}$ mice.

Additionally, T lymphocytes infiltrating the goat endoneurium were detected. In mice, demyelination appeared independent of lymphocytes, since crossing *Prnp*$^{-/-}$ mice with recombinase-1 ablated mice *Rag1*$^{-/-}$ that are devoid of functional B and T lymphocytes, did not affect the pathogenesis. Although, polyneuropathies are heterogeneous with respect to clinical manifestations and pathogenic mechanisms, dysregulated immune responses that trigger or aggravate the conditions are a frequent commonality. Given that a mild, but distinct, systemic immunological imbalance has been observed in goats without PrP^{C},[24,25,32] it cannot be ruled out that this also affects the immunological homeostasis of peripheral nerves and that this can underlie, or possibly aggravate, what appears to be a primary demyelinating condition.

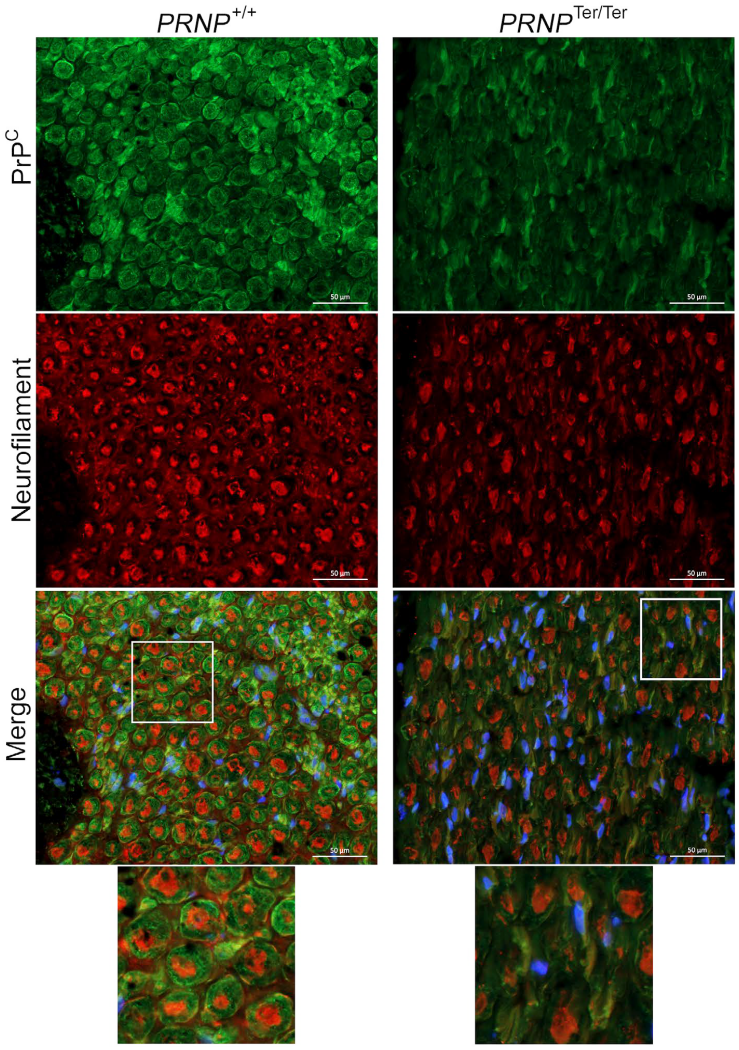

FIGURE 10 Localization of PrP^C in peripheral nerves. Immunofluorescence analysis of peripheral nerves in *PRNP*$^{+/+}$ (left) and *PRNP*$^{Ter/Ter}$ (right). PrP^C (green) is present in Schwann cells and compact myelin (magnification 40x, scale bars 50 µm.). Axonal neurofilament is stained red. White frames are magnified in the lower part of the figure

A contribution to myelin degeneration could arise from perturbation in lipid composition.[33] In goat nerves, we found that the lipid composition changes with age irrespective of *PRNP* genotype. Whereas no major differences due to genotypes were detected in young goats, changes in lipid composition between genotypes were evident in adults. Not all the lipid components differentially present were identified, but decreases in HexCer were noted. These lipids include galactosylceramides and glucosylceramides, and are among the sphingolipids. Mice lacking fatty acid 2-hydroxylase (FA2H), an enzyme involved in the synthesis of 2-hydroxylated sphingolipids, develop normally up to early adulthood, then develop degeneration in the spinal cord and lesions in the peripheral nerves, indicating that FA2H is necessary for myelin maintenance.[34] Glycosphingolipids are not essential for the synthesis of compact myelin, but are required for stability and maintenance of myelin into old age.[33] Whether or not PrP^C is involved in sphingolipid metabolism remains to be clarified.

Taken together, our results provide strong support for a PrP^C function in peripheral nerve myelin maintenance. Further studies that clarify the mechanisms by which PrP^C can affect myelin maintenance are needed. In vitro studies

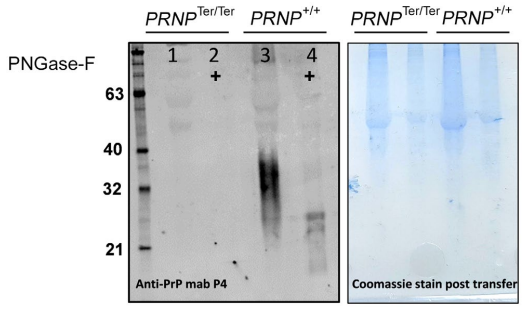

FIGURE 11 Western blot analysis of peripheral nerves. Glycosylated full-length PrP^C is detected in $PRNP^{+/+}$ goats. After deglycosylation with PNGase-F full length PrP^C is visible, together with a C-terminal fragment. No PrP^C was detected in $PRNP^{Ter/Ter}$ goats. On the right, Coomassie stain was used to verify equal protein loading between lanes

have shown that part of the amino-terminal flexible tail of PrP^C is released by proteolysis from axons and diffuses to a G protein-coupled receptor (Gpr126/Adgrg6), increasing cAMP levels in myelinating Schwann cells.[11] The binding of the flexible tail of PrP^C to Gpr126 has also been confirmed in vivo,[11] although the effect of Gpr126 on myelin maintenance has been questioned.[35]

Our genomic analysis of the *PRNP*-region at chromosome 13 shows that the invariant $PRNP^{Ter}$ haplotype only spans 2.5 Mb, which constitutes approximately 3% of the chromosome and less than 1% of the proteins encoded by chromosome 13. Thus, the haplotype containing the $PRNP^{Ter}$ allele are short compared with those observed in some of the $Prnp^{-/-}$ lines of mice.[36] Taken together, data from transgenic mice and the nontransgenic goat model presented here, demonstrate that PrP^C has a conserved role in myelin maintenance in mammals.

ACKNOWLEDGMENTS

The authors acknowledge Lucy Robertson for proofreading the manuscript, and Mari Katharina Aas Ådland for technical assistance.

CONFLICT OF INTERESTS

The authors declare that they have no conflicts of interests.

AUTHOR CONTRIBUTIONS

F.S. Skedsmo, G. Malachin, A. Espenes, and M.A. Tranulis designed the research. F.S. Skedsmo, G. Malachin, D.I. Våge, M.M. Hammervold, Ø. Salvesen, C. Ersdal, B. Ranheim, M.H. Stafsnes, Z. Bartosova, A. Espenes, and M.A. Tranulis performed the experiments. F.S. Skedsmo, G. Malachin, D.I. Våge, M.M. Hammervold, Ø. Salvesen, C. Ersdal, B. Ranheim, M.H. Stafsnes, Z. Bartosova, P. Bruheim, K.H. Jäderlund, K. Matiasek, A. Espenes, and M.A. Tranulis analyzed the data and wrote the paper.

REFERENCES

1. Prusiner SB. Molecular biology of prion diseases. *Science*. 1991;252:1515-1522.
2. Büeler H, Aguzzi A, Sailer A, et al. Mice devoid of PrP are resistant to scrapie. *Cell*. 1993;73:1339-1347.
3. Manson J, Clarke A, Hooper M, Aitchison L, McConnell I, Hope J. 129/Ola mice carrying a null mutation in PrP that abolishes mRNA production are developmentally normal. *Mol Neurobiol*. 1994;8:121-127.
4. Büeler H, Fischer M, Lang Y, et al. Normal development and behaviour of mice lacking the neuronal cell-surface PrP protein. *Nature*. 1992;356:577-582.
5. Sakaguchi S, Katamine S, Nishida N, et al. Loss of cerebellar Purkinje cells in aged mice homozygous for a disrupted PrP gene. *Nature*. 1996;380:528.
6. Moore RC, Redhead NJ, Selfridge J, Hope J, Manson JC, Melton DW. Double replacement gene targeting for the production of a series of mouse strains with different prion protein gene alterations. *Nat Biotechnol*. 1995;13:999.
7. Rossi D, Cozzio A, Flechsig E, et al. Onset of ataxia and Purkinje cell loss in PrP null mice inversely correlated with Dpl level in brain. *EMBO J*. 2001;20:694-702.
8. Nuvolone M, Hermann M, Sorce S, et al. Strictly co-isogenic C57BL/6J-$Prnp^{-/-}$ mice: a rigorous resource for prion science. *J Exp Med*. 2016;213:313-327.
9. Nishida N, Tremblay P, Sugimoto T, et al. A mouse prion protein transgene rescues mice deficient for the prion protein gene from purkinje cell degeneration and demyelination. *Lab Invest; A J Tech Methods Pathol*. 1999;79:689-697.
10. Bremer J, Baumann F, Tiberi C, et al. Axonal prion protein is required for peripheral myelin maintenance. *Nat Neurosci*. 2010;13:310-318.
11. Küffer A, Lakkaraju AKK, Mogha A, et al. The prion protein is an agonistic ligand of the G protein-coupled receptor Adgrg6. *Nature*. 2016;536:464.
12. Dyck PJ, Karnes J, Lais A, Lofgren EP, Stevens JC. Pathologic alterations of the peripheral nervous system of humans. In: Dyck PJ, Thomas PK, Lambert EH, Bunge R, eds. *Peripheral Neuropathy*. Vol 1. Philadelphia: WB Saunders; 1984:790-793.
13. Folch J, Lees M, Sloane Stanley G. A simple method for the isolation and purification of total lipides from animal tissues. *J Biol Chem*. 1957;226:497-509.
14. Lisa M, Holcapek M. High-throughput and comprehensive lipidomic analysis using ultrahigh-performance supercritical fluid chromatography-mass spectrometry. *Anal Chem*. 2015;87:7187-7195.
15. Fahy E, Subramaniam S, Murphy RC, et al. Update of the LIPID MAPS comprehensive classification system for lipids. *J Lipid Res*. 2009;50:S9-S14.
16. Liebisch G, Vizcaíno JA, Köfeler H, et al. Shorthand notation for lipid structures derived from mass spectrometry. *J Lipid Res*. 2013;54:1523-1530.
17. Purcell S, Neale B, Todd-Brown K, et al. PLINK: a tool set for whole-genome association and population-based linkage analyses. *Am J Human Genet*. 2007;81:559-575.

18. Kind T, Liu K-H, Yup Lee D, DeFelice B, Meissen JK, Fiehn O. LipidBlast - in-silico tandem mass spectrometry database for lipid identification. *Nat Methods*. 2013;10:755-758.
19. Fahy E, Sud M, Cotter D, Subramaniam S. LIPID MAPS online tools for lipid research. *Nucleic Acids Res*. 2007;35:W606-W612.
20. Holcapek M, Cifkova E, Cervena B, Lisa M, Vostalova J, Galuszka J. Determination of nonpolar and polar lipid classes in human plasma, erythrocytes and plasma lipoprotein fractions using ultrahigh-performance liquid chromatography-mass spectrometry. *J Chromatogr A*. 2015;1377:85-91.
21. Chong J, Soufan O, Li C, et al. MetaboAnalyst 4.0: towards more transparent and integrative metabolomics analysis. *Nucleic Acids Res*. 2018;46:W486-W494.
22. Weller RO, Cervós-Navarro J. General pathology of peripheral nerves. In: Weller RO, Cervós-NavarroJ, eds. *Pathology of Peripheral Nerves*. London: Butterworths; 1977:61-89.
23. Mizisin AP, Shelton GD, Wagner S, Rusbridge C, Powell HC. Myelin splitting, Schwann cell injury and demyelination in feline diabetic neuropathy. *Acta Neuropathol*. 1998;95:171-174.
24. Salvesen Ø, Reiten MR, Espenes A, Bakkebo MK, Tranulis MA, Ersdal C. LPS-induced systemic inflammation reveals an immunomodulatory role for the prion protein at the blood-brain interface. *J Neuroinflammation*. 2017;14:106.
25. Salvesen Ø, Reiten MR, Kamstra JH, et al. Goats without prion protein display enhanced proinflammatory pulmonary signaling and extracellular matrix remodeling upon systemic lipopolysaccharide challenge. *Front Immunol*. 2017;8:1722.
26. Petit CSV, Besnier L, Morel E, Rousset M, Thenet S. Roles of the cellular prion protein in the regulation of cell-cell junctions and barrier function. *Tissue Barriers*. 2013;1:e24377-e24377.
27. Kouadri A, El Khatib M, Cormenier J, et al. Involvement of the prion protein in the protection of the human bronchial epithelial barrier against oxidative stress. *Antioxid Redox Signal*. 2019;31(1):59–74.
28. Poliak S, Matlis S, Ullmer C, Scherer SS, Peles E. Distinct claudins and associated PDZ proteins form different autotypic tight junctions in myelinating Schwann cells. *J Cell Biol*. 2002;159:361-372.
29. Rodionova NN, Allakhverdiev ES, Maksimov GV. Study of myelin structure changes during the nerve fibers demyelination. *PLoS ONE*. 2017;12:e0185170.
30. Brechenmacher C, Vital C, Deminiere C, et al. Guillain-Barré syndrome: an ultrastructural study of peripheral nerve in 65 patients. *Clin Neuropathol*. 1987;6:19-24.
31. Prineas JW. Pathology of the Guillain-Barré syndrome. *Ann Neurol*. 1981;9(Suppl):6-19.
32. Malachin G, Reiten MR, Salvesen Ø, et al. Loss of prion protein induces a primed state of type I interferon-responsive genes. *PLoS ONE*. 2017;12:e0179881.
33. Schmitt S, Castelvetri LC, Simons M. Metabolism and functions of lipids in myelin. *Biochimica et Biophysica Acta (BBA)-Mol Cell Biol Lipids*. 2015;1851:999-1005.
34. Zöller I, Meixner M, Hartmann D, et al. Absence of 2-hydroxylated sphingolipids is compatible with normal neural development but causes late-onset axon and myelin sheath degeneration. *J Neurosci* 2008;28:9741-9754.
35. Mogha A, Harty BL, Carlin D, et al. Gpr126/Adgrg6 has Schwann cell autonomous and nonautonomous functions in peripheral nerve injury and repair. *J Neurosci*. 2016;36:12351-12367.
36. Nuvolone M, Kana V, Hutter G, et al. SIRPalpha polymorphisms, but not the prion protein, control phagocytosis of apoptotic cells. *J Exp Med*. 2013;210:2539-2552.

SUPPORTING INFORMATION

Additional supporting information may be found online in the Supporting Information section.

How to cite this article: Skedsmo FS, Malachin G, Inge Våge D, et al. Demyelinating polyneuropathy in Goats lacking Prion Protein. *The FASEB Journal*. 2020;00:1–17. https://doi.org/10.1096/fj.201902588R

ISBN: 978-82-575-1691-8
ISSN: 1894-6402

Norwegian University
of Life Sciences

Postboks 5003
NO-1432 Ås, Norway
+47 67 23 00 00
www.nmbu.no

107810 / ANDVORDGRAFISK.NO